(5)

CH2M HILL DOCUMENT RELEASE FORM

(1) Document Number: RPP-RPT-28963	**(2) Revision Number:** 0	**(3) Effective Date:** Issue Date	
(4) Document Type: ☐ Digital Image ☐ Hard copy ☒ PDF ☐ Video	**(a) Number of pages (including the DRF) or number of digital images** 208		
(5) Release Type ☒ New ☐ Cancel	☐ Page Change	☐ Complete Revision	
(6) Document Title: Hanford Double-Shell Tank Thermal and Seismic Project - Dytran Analysis of Seismically Induced Fluid-Structure Interaction in a Hanford Double-Shell Primary Tank			
(7) Change/Release Description: The "Double-Shell Tank (DST) Integrity Project – DST Thermal and Seismic Analysis" is in support of Tri-Party Agreement Milestone M-48-14.			
(8) Change Justification: N/A			

(9) Associated Structure, System, and Component (SSC) and Building Number:	**(a) Structure Location:** 200E/200W	**(c) Building Number:** 241-AP, AN, AY, AZ, AW, and SY	
	(b) System Designator: WST	**(d) Equipment ID Number (EIN):** All DST tanks	

(10) Impacted Documents:	**(a) Document Type**	**(b) Document Number**	**(c) Document Revision**
	N/A	N/A	N/A

(11) Approvals:

(a) Author (Print/Sign): TC Mackey T.C. Mackey	**Date:** 3/14/06
(b) Responsible Manager (Print/Sign): C. Defigh-Price C. Defigh-Price	**Date:** 3/14/06
(c) Reviewer (Optional, Print/Sign):	**Date:**
(d) Reviewer (Optional, Print/Sign):	**Date:**

(12) Distribution:

(a) Name	(b) MSIN	(a) Name	(b) MSIN
HS Berman			
KD Boomer			
C Defigh-Price			
GP Duncan			
JH Huber			
TC Mackey			
DJ Washenfelder			

Release Stamp

DATE: MAR 17 2006
STA: 4
HANFORD RELEASE
ID: 2

(13) Clearance	**(a) Cleared for Public Release** ☒ Yes ☐ No	**(b) Restricted Information?** ☐ Yes ☒ No	**(c) Restriction Type:**
(14) Clearance Review (Print/Sign): GE. Bratton G.E. Bratton		**Date:** 3/14/06	

Hanford Double-Shell Tank Thermal and Seismic Project - Dytran Analysis of Seismically Induced Fluid-Structure Interaction in a Hanford Double-Shell Primary Tank

TC Mackey
CH2M Hill, Hanford Group, Inc.
Richland, WA 99352

U.S. Department of Energy Contract DE-AC27-99RL14047

EDT/ECN: DRF UC:
Cost Center: Charge Code:
B&R Code: Total Pages: 208

Key Words:
Double-Shell Tank, Tank, Integrity Project, Thermal, Seismic, TPA, M-48-14.

Abstract:
The overall scope of the project is to complete an up-to-date comprehensive analysis of record of the DST System at Hanford. The "Double-Shell Tank (DST) Integrity Project - DST Thermal and Seismic Analysis" is in support of Tri-Party Agreement Milestone M-48-14.

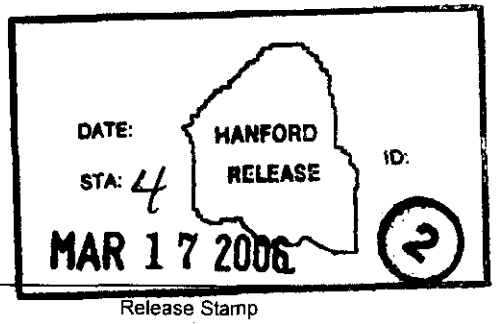

LE Bratton 3/14/06
Release Approval Date

Release Stamp

Approved For Public Release

RPP-RPT-28963, Rev. 0

PNNL-15704
Limited Distribution

Pacific Northwest
National Laboratory
Operated by Battelle for the
U.S. Department of Energy

Hanford Thermal and Seismic Project—Dytran Analysis of Seismically Induced Fluid-Structure Interaction on a Hanford Double-Shell Primary Tank

M. W. Rinker
F. G. Abatt

January 2006

Prepared for the U.S. Department of Energy
under Contract DE-AC05-76RL01830

DISCLAIMER

PACIFIC NORTHWEST NATIONAL LABORATORY
operated by
BATTELLE
for the
UNITED STATES DEPARTMENT OF ENERGY
under Contract DE-AC05-76RL01830

Acknowledgments

The Double-Shell Tank Thermal and Seismic Project has been funded at PNNL for the past three and a half years by DOE and CH2M HILL. There has been a tremendous amount of work and progress made by many people from many organizations in order to get to this point.

In particular, one of the greatest challenges of this project has been the seismic analysis of the double-shell tanks. The project team would like to acknowledge the dedicated effort by M&D Professional Services technical staff in completing this work.

It is also important to acknowledge, that while this report has a PNNL cover on it, all of this work was completed by George Abatt, one of the senior technical staff at M&D.

This page intentionally left blank.

Dytran Benchmark Analysis of Seismically Induced Fluid-Structure Interaction in a Hanford Double Shell Primary Tank

F.G. Abatt

February 2006

Prepared by
M&D Professional Services, Inc.
for
Pacific Northwest National Laboratory

Prepared by F.G. Abatt 2/1/06
F.G. Abatt

M&D PROFESSIONAL SERVICES INCORPORATED

This page intentionally left blank.

Executive Summary

M&D Professional Services, Inc. (M&D) is under subcontract to Pacific Northwest National Laboratories (PNNL) to perform seismic analysis of the Hanford Site Double-Shell Tanks (DSTs) in support of a project entitled *Double-Shell Tank (DST) Integrity Project - DST Thermal and Seismic Analyses*. The overall scope of the project is to complete an up-to-date comprehensive analysis of record of the DST System at Hanford in support of Tri-Party Agreement Milestone M-48-14. The work described herein was performed in support of the seismic analysis of the DSTs. The thermal and operating loads analysis of the DSTs is documented in Rinker et al. (2004).

The overall seismic analysis of the DSTs is being performed with the general-purpose finite element code ANSYS[1]. The global model used for the seismic analysis of the DSTs includes the DST structure, the contained waste, and the surrounding soil. The seismic analysis of the DSTs must address the fluid-structure interaction behavior and sloshing response of the primary tank and contained liquid. ANSYS has demonstrated capabilities for structural analysis, but has more limited capabilities for fluid-structure interaction analysis.

The purpose of this study is to demonstrate the capabilities and investigate the limitations of the finite element code MSC.Dytran[2] for performing a dynamic fluid-structure interaction analysis of the primary tank and contained waste. To this end, the Dytran solutions are benchmarked against theoretical solutions appearing in BNL 1995, when such theoretical solutions exist. When theoretical solutions were not available, comparisons were made to theoretical solutions to similar problems, and to the results from ANSYS simulations.

Both rigid tank and flexible tank configurations were analyzed with Dytran. The response parameters of interest that are evaluated in this study are the total hydrodynamic reaction forces, the impulsive and convective mode frequencies, the waste pressures, and slosh heights. To a limited extent, primary tank stresses are also reported.

The capabilities and limitations of ANSYS for performing a fluid-structure interaction analysis of the primary tank and contained waste were explored in a parallel investigation and documented in a companion report (Carpenter and Abatt [2006]). The results of this study were used in conjunction with the results of the global ANSYS analysis reported in Carpenter et al. (2006) and the parallel ANSYS fluid-structure interaction analysis to help determine if a more refined sub-model of the primary tank is necessary to capture the important fluid-structure interaction effects in the tank and if so, how to best utilize a refined sub-model of the primary tank.

The results of this study demonstrate that Dytran has the capability to perform fluid-structure interaction analysis of a primary tank subjected to seismic loading. With the

[1] ANSYS is a registered trademark of ANSYS Inc.
[2] MSC.Dytran is a registered trademark of MSC.Software Corporation

exception of some isolated peak pressures and to a lesser extent peak stresses, the results agreed very well with theoretical solutions.

The benchmarking study documented in Carpenter and Abatt (2006) showed that the ANSYS model used in that study captured much of the fluid-structure interaction (FSI) behavior, but did have limitations for predicting the convective response of the waste. While Dytran appears to have stronger capabilities for the analysis of the FSI behavior in the primary tank, it is more practical to use ANSYS for the global evaluation of the tank. Thus, Dytran served the purpose of helping to identify limitations in the ANSYS FSI analysis so that those limitations can be addressed in the structural evaluation of the primary tank.

CONTENTS

1.0 INTRODUCTON 1
1.1 DISCUSSION 2
1.2 SUMMARY 7
1.3 CONCLUSIONS 9
2.0 MODEL DESCRIPTION 11
2.1 MODEL GEOMETRY 12
2.2 MATERIAL PROPERTIES AND ELEMENT TYPES 20
2.3 BOUNDARY CONDITIONS 21
2.4 INITIAL CONDITIONS 21
2.5 SEISMIC INPUT 22
3.0 RIGID DYTRAN MODEL AT 422 INCH WASTE LEVEL 30
3.1 Hydrodynamic Forces 30
3.1.1 Horizontal Excitation 31
3.1.2 Vertical Excitation 33
3.2 Waste Pressures 35
3.2.1 Horizontal Excitation Run at Absolute Pressure 35
3.2.2 Vertical Excitation 41
3.3 SLOSH HEIGHT RESULTS 46
4.0 RIGID TANK MODEL AT 460 INCH WASTE LEVEL 48
4.1 HYDRODYNAMIC FORCES 48
4.1.1 Horizontal Excitation at Absolute Pressure 48
4.1.2 Vertical Excitation at Absolute Pressure 50
4.2 WASTE PRESSURES 51
4.2.1 Horizontal Excitation Run at Absolute Pressure 51
4.2.2 Vertical Excitation Run at Absolute Pressure 57
4.3 SLOSH HEIGHT RESULTS 63
5.0 FLEXIBLE TANK DYTRAN MODEL AT 422 INCH WASTE LEVEL 65
5.1 DAMPING IMPLEMENTATION AND CALIBRATION 65
5.2 Hydrodynamic Forces 67
5.2.1 Horizontal Excitation 67
5.2.2 Vertical Excitation 81
5.3 Waste Pressures 84
5.3.1 Horizontal Excitation Run at Absolute Pressure 84
5.3.2 Wall and Base Pressures Due to Vertical Excitation Run at Absolute Pressure 93
5.4 MAXIMUM SLOSH HEIGHT RESULTS 99
5.5 ELEMENT STRESSES 101
5.5.1 Horizontal Excitation Run at Absolute Pressure 102
6.0 FLEXIBLE TANK DYTRAN MODEL AT 460 INCH WASTE LEVEL 105
6.1 HYDRODYNAMIC FORCES 105
6.1.1 Horizontal Excitation Run at Absolute Pressure 105
6.1.2 Vertical Excitation Run at Absolute Pressure 108
6.2 WASTE PRESSURES 109
6.2.1 Horizontal Excitation Run at Absolute Pressure 110

6.2.2 Wall and Base Pressures Due to Vertical Excitation Run at Absolute Pressure 116
6.3 MAXIMUM SLOSH HEIGHT RESULTS 123
6.4 ELEMENT STRESSES 124
6.4.1 Horizontal Excitation Run at Absolute Pressure 124
6.4.2 Vertical Excitation Run at Absolute Pressure 127
7.0 ANSYS to DYTRAN COMPARISONS 131
7.1 FREQUENCIES AND SLOSH HEIGHTS 131
7.2 HYDRODYNAMIC FORCES 131
7.3 WASTE PRESSURES 135
7.4 ELEMENT STRESSES 138
8.0 REFERENCES 142

APPENDIX A Description of Input and Results Files
APPENDIX B Theoretical Solutions

LIST OF FIGURES

Figure 2-1. AY Primary Tank Dimensions 13
Figure 2-2. Plot of Primary Tank and Base 14
Figure 2-3. Plot of Tank and Waste at 422 in. Waste Level 15
Figure 2-4. Plot of Tank and Waste at 460 in. Waste Level 15
Figure 2-5. Top View of Model Showing the Angular Locations of Fluid Elements at Which Pressures Were Monitored. 16
Figure 2-6. Waste Element Numbering for Element Sets "Plusx_els"," Minusx_els", and Cent_press". 17
Figure 2-7. Waste Element Numbering for Element Sets "Press_45" and Plusz_els". 18
Figure 2-8. Shell Element Numbering for Tank Wall Stress Results at θ=0 and θ=90°. 19
Figure 2-9. Shell Element Numbering for Tank Wall Stress Results at θ=45° and θ=180°. 19
Figure 2-10. Section Plot of Flexible Primary Tank 20
Figure 2-11. ANSYS Composite Tank Model Detail 23
Figure 2-12. Excavated Soil Model Detail for Global ANSYS Model. 23
Figure 2-13. Far-Field Soil Model Detail for Global ANSYS Model. 24
Figure 2-14. Tank With Hinged Top Boundary Condition per BNL 1995. 24
Figure 2-15. Horizontal Acceleration Time History Output from ANSYS Model. 25
Figure 2-16. Vertical Acceleration Time History Output from ANSYS Model 26
Figure 2-17. Velocity Time Histories Output from ANSYS Model 26
Figure 2-18. Displacement Time Histories Output from ANSYS Model. 27
Figure 2-19. 4% Damped Response Spectra for Acceleration Time Histories Extracted from ANSYS Model. 27
Figure 2-20. Comparison of Horizontal Dome Apex Response Spectra at Different Damping Values 28
Figure 2-21. Comparison of Horizontal Dome Apex Response Spectra at Different Damping Values for Low Frequencies. 29
Figure 3-1. Coupling Surface Reaction Forces for the Rigid Tank at 422 in. Waste Level Under Horizontal Seismic Input. 32
Figure 3-2. Horizontal Coupling Surface Reaction Force for the Rigid Tank at 422 in. Waste Level Under Horizontal Seismic Input. 32
Figure 3-3. Horizontal Coupling Surface Reaction Force for Rigid Tank at 422 in. Waste Level Under Horizontal Seismic Excitation – Convective Response 33
Figure 3-4. Coupling Surface Reaction Forces for Rigid Tank at 422 in. Waste Level Under Vertical Seismic Input 34
Figure 3-5. Vertical Coupling Surface Reaction Force for Rigid Tank at 422 in. Waste Level Under Vertical Seismic Input. 34
Figure 3-6. Waste Pressure Time Histories for the Rigid Tank With 422 in. of Waste Under Horizontal Excitation at θ=0 Run at Absolute Pressure. 37
Figure 3-7. Selected Waste Pressure Time Histories for the Rigid Tank With 422 in. of Waste Under Horizontal Excitation at θ=0 Run at Absolute Pressure. 37
Figure 3-8. Waste Pressure Time Histories for the Rigid Tank With 422 in. of Waste Under Horizontal Excitation at θ=45° Run at Absolute Pressure 38

Figure 3-9. Waste Pressure Time Histories for the Rigid Tank With 422 in. of Waste Under Horizontal Excitation at θ=90° Run at Absolute Pressure. 38
Figure 3-10. Maximum and Minimum Waste Pressures vs. Normalized Height from Tank Bottom for Horizontal Excitation at θ=0 Run at Absolute Pressure. 39
Figure 3-11. Maximum and Minimum Waste Pressures vs. Normalized Height from Tank Bottom for Horizontal Excitation at θ=45° Run at Absolute Pressure. 40
Figure 3-12. Maximum and Minimum Waste Pressures vs. Normalized Height from Tank Bottom for Horizontal Excitation at θ=90° Run at Absolute Pressure. 40
Figure 3-13. Waste Pressure Time Histories for the Rigid Tank With 422 in. of Waste Under Vertical Excitation at θ=0 Run at Absolute Pressure. 42
Figure 3-14. Waste Pressure Time Histories for the Rigid Tank With 422 in. of Waste Under Vertical Excitation at θ=45° Run at Absolute Pressure. 42
Figure 3-15. Waste Pressure Time Histories for the Rigid Tank With 422 in. of Waste Under Vertical Excitation at θ=90° Run at Absolute Pressure. 43
Figure 3-16. Pressure Time History for Bottom Center Waste Element for the Rigid Tank at the 422 in. Waste Level and Vertical Excitation Run at Absolute Pressure. 44
Figure 3-17. Maximum and Minimum Waste Pressures vs. Normalized Height from Tank Bottom for Vertical Excitation of Rigid Tank at 422 in. Waste Level and θ=0 Run at Absolute Pressure 45
Figure 3-18. Maximum and Minimum Waste Pressures vs. Normalized Height from Tank Bottom for Vertical Excitation of Rigid Tank at 422 in. Waste Level and θ=45° Run at Absolute Pressure 45
Figure 3-19. Maximum and Minimum Waste Pressures vs. Normalized Height from Tank Bottom for Vertical Excitation of Rigid Tank at 422 in. Waste Level and θ=90° Run at Absolute Pressure 46
Figure 3-20. Maximum Slosh Height Time History Over All Waste Elements for Horizontal Excitation. 47
Figure 4-1. Coupling Surface Reaction Forces at the 460 in. Waste Level for the Rigid Tank Under Horizontal Seismic Excitation. 49
Figure 4-2. Horizontal Coupling Surface Reaction Force for Rigid Tank at 460 in. Waste Level Under Horizontal Seismic Excitation. 49
Figure 4-3. Horizontal Coupling Surface Reaction Force for Rigid Tank at 460 in. Waste Level Under Horizontal Seismic Excitation – Convective Response 50
Figure 4-4. Vertical Coupling Surface Reaction Force for Rigid Tank at 460 in. Waste Level Under Vertical Seismic Excitation. 51
Figure 4-5. Waste Pressure Time Histories for the Rigid Tank With 460 in. of Waste Under Horizontal Excitation at θ=0 Run at Absolute Pressure. 53
Figure 4-6. Selected Waste Pressure Time Histories for the Rigid Tank With 460 in. of Waste Under Horizontal Excitation at θ=0 Run at Absolute Pressure. 53
Figure 4-7. Waste Pressure Time Histories for the Rigid Tank With 460 in. of Waste Under Horizontal Excitation at θ=45° Run at Absolute Pressure. 54
Figure 4-8. Selected Waste Pressure Time Histories for the Rigid Tank With 460 in. of Waste Under Horizontal Excitation at θ=45° Run at Absolute Pressure 54
Figure 4-9. Waste Pressure Time Histories for the Rigid Tank With 460 in. of Waste Under Horizontal Excitation at θ=90° Run at Absolute Pressure. 55

Figure 4-10. Maximum and Minimum Waste Pressures vs. Normalized Height from Tank Bottom for Horizontal Excitation of Rigid Tank at 460 in. Waste Level and θ=0 Run at Absolute Pressure. 56
Figure 4-11. Maximum and Minimum Waste Pressures vs. Normalized Height from Tank Bottom for Horizontal Excitation of Rigid Tank at 460 in. Waste Level and θ=45° Run at Absolute Pressure. 56
Figure 4-12. Maximum and Minimum Waste Pressures vs. Normalized Height from Tank Bottom for Horizontal Excitation of Rigid Tank at 460 in. Waste Level and θ=90° Run at Absolute Pressure. 57
Figure 4-13. Waste Pressure Time Histories for the Rigid Tank With 460 in. of Waste Under Vertical Excitation at θ=0 Run at Absolute Pressure. 58
Figure 4-14. Selected Waste Pressure Time Histories for the Rigid Tank With 460 in. of Waste Under Vertical Excitation at θ=0 Run at Absolute Pressure. 58
Figure 4-15. Waste Pressure Time Histories for the Rigid Tank With 460 in. of Waste Under Vertical Excitation at θ=45° Run at Absolute Pressure. 59
Figure 4-16. Selected Waste Pressure Time Histories for the Rigid Tank With 460 in. of Waste Under Vertical Excitation at θ=45° Run at Absolute Pressure. 59
Figure 4-17. Waste Pressure Time Histories for the Rigid Tank With 460 in. of Waste Under Vertical Excitation at θ=90° Run at Absolute Pressure. 60
Figure 4-18. Selected Waste Pressure Time Histories for the Rigid Tank With 460 in. of Waste Under Vertical Excitation at θ=90° Run at Absolute Pressure. 60
Figure 4-19. Pressure Time History for Bottom Center Waste Element for the Rigid Tank at the 460 in. Waste Level and Vertical Excitation Run at Absolute Pressure. 61
Figure 4-20. Maximum and Minimum Waste Pressures vs. Normalized Height from Tank Bottom for Vertical Excitation of Rigid Tank at 460 in. Waste Level and θ=0 Run at Absolute Pressure 61
Figure 4-21. Maximum and Minimum Waste Pressures vs. Normalized Height from Tank Bottom for Vertical Excitation of Rigid Tank at 460 in. Waste Level and θ=45° Run at Absolute Pressure 62
Figure 4-22. Maximum and Minimum Waste Pressures vs. Normalized Height from Tank Bottom for Vertical Excitation of Rigid Tank at 460 in. Waste Level and θ=90° Run at Absolute Pressure 63
Figure 4-23. Maximum Slosh Height Time History Over All Waste Elements for Horizontal Excitation of the Rigid Tank at the 460 in. Waste Level. 64
Figure 4-24. Plot of Waste Free Surface Under Gravity Loading Only for the Rigid Tank at the 460 in. Waste Level 64
Figure 5-1. Coupling Surface Reaction Forces for the Flexible Tank Under Horizontal Seismic Input at Gage Pressure– Case 1 69
Figure 5-2. Coupling Surface Reaction Forces for the Flexible Tank Under Horizontal Seismic Input at Gage Pressure During the Initial Free Vibration Phase – Case 1. 70
Figure 5-3. Mid-Wall Hoop Stress for Flexible Tank at Gage Pressure and θ=0 – Case 1. 70
Figure 5-4. Coupling Surface Reaction Forces at the 422 in. Waste Level for the Flexible Tank at Gage Pressure Under Horizontal Seismic Input During the Initial Free Vibration Phase – Case 2a (alpha=0.08). 71

Figure 5-5. Coupling Surface Reaction Forces at the 422 in. Waste Level for the Flexible Tank at Gage Pressure Under Horizontal Seismic Input – Case 2a (alpha=0.08). 72
Figure 5-6, Coupling Surface Reaction Forces at the 422 in. Waste Level for the Flexible Tank at Gage Pressure Under Horizontal Seismic Input During the Initial Free Vibration Phase – Case 2b (alpha=0.04). 73
Figure 5-7. Coupling Surface Reaction Forces at the 422 in. Waste Level for the Flexible Tank at Gage Pressure Under Horizontal Seismic Input – Case 2b (alpha=0.04). 73
Figure 5-8. Coupling Surface Reaction Forces at the 422 in. Waste Level for the Flexible Tank at Gage Pressure Under Horizontal Seismic Input During the Initial Free Vibration Phase – Case 2c (alpha=0.02). 75
Figure 5-9. Coupling Surface Reaction Forces at the 422 in. Waste Level for the Flexible Tank at Gage Pressure Under Horizontal Seismic Input – Case 2c (alpha=0.02). 75
Figure 5-10. Coupling Surface Reaction Forces at the 422 in. Waste Level for the Flexible Tank at Gage Pressure Under Horizontal Seismic Input During the Final Free Vibration Phase – Case 2c (alpha=0.02). 76
Figure 5-11. Coupling Surface Reaction Forces at the 422 in. Waste Level for the Flexible Tank at Absolute Pressure Under Horizontal Seismic Input During the Initial Free Vibration Phase – Case 2c (alpha=0.02). 76
Figure 5-12. Horizontal Coupling Surface Reaction Force at the 422 in. Waste Level for the Flexible Tank at Absolute Pressure Under Horizontal Seismic Input – Case 2c (alpha=0.02). 77
Figure 5-13. Coupling Surface Reaction Forces at the 422 in. Waste Level for the Flexible Tank at Absolute Pressure Under Horizontal Seismic Input During the Final Free Vibration Phase – Case 2c (alpha=0.02). 77
Figure 5-14. Coupling Surface Reaction Forces at the 422 in. Waste Level for the Flexible Tank at Gage Pressure Under Horizontal Seismic Input During the Initial Free Vibration Phase – Case 2d (alpha=0.01). 78
Figure 5-15. Coupling Surface Reaction Forces at the 422 in. Waste Level for the Flexible Tank at Gage Pressure Under Horizontal Seismic Input – Case 2d (alpha=0.01). 79
Figure 5-16. Coupling Surface Reaction Forces at the 422 in. Waste Level for the Flexible Tank at Gage Pressure Under Horizontal Seismic Input During the Final Free Vibration Phase – Case 2d (alpha=0.01). 79
Figure 5-17. Coupling Surface Reaction Forces for the Flexible Tank at Gage Pressure Under Horizontal Seismic Input – Case 3 80
Figure 5-18. Coupling Surface Reaction Forces for the Flexible Tank at Gage Pressure Under Horizontal Seismic Input from 23.0 to 25.0 s – Case 3 81
Figure 5-19. Coupling Surface Reaction Forces for the Flexible Tank at Gage Pressure Under Vertical Seismic Input – Case 2c. 82
Figure 5-20. Coupling Surface Reaction Forces for the Flexible Tank at Gage Pressure Under Vertical Seismic Input – Case 3 83
Figure 5-21. Coupling Surface Reaction Forces for the Flexible Tank at Absolute Pressure Under Vertical Seismic Input – Case 2c. 84
Figure 5-22. Waste Pressures Time Histories for the Flexible Tank at the 422 in. Waste Level for Horizontal Excitation at θ=0, Case 2c (alpha=0.02) Run at Absolute Pressure. 86

Figure 5-23. Selected Element Pressure Time Histories for the Flexible Tank at the 422 in. Waste Level for Horizontal Excitation at θ=0, Case 2c (alpha=0.02) Run at Absolute Pressure 87
Figure 5-24. Waste Pressures Time Histories for the Flexible Tank at the 422 in. Waste Level for Horizontal Excitation at θ=45, Case 2c (alpha=0.02) Run at Absolute Pressure. 87
Figure 5-25. Selected Element Pressure Time Histories for the Flexible Tank at the 422 in. Waste Level for Horizontal Excitation at θ=45, Case 2c (alpha=0.02) Run at Absolute Pressure 88
Figure 5-26. Waste Pressures Time Histories for the Flexible Tank at the 422 in. Waste Level for Horizontal Excitation at θ=90, Case 2c (alpha=0.02) Run at Absolute Pressure. 88
Figure 5-27. Selected Element Pressure Time Histories for the Flexible Tank at the 422 in. Waste Level for Horizontal Excitation at θ=90, Case 2c (alpha=0.02) Run at Absolute Pressure 89
Figure 5-28. Comparison of Waste Pressures in the Flexible Tank at the 422 in. Waste Level at Absolute and Gage Pressure for Selected Elements at θ=0. 90
Figure 5-29. Comparison of Waste Pressures in the Flexible Tank at the 422 in. Waste Level at Absolute and Gage Pressure for Selected Elements at θ=45° 90
Figure 5-30. Comparison of Waste Pressures in the Flexible Tank at the 422 in. Waste Level at Absolute and Gage Pressure for Selected Elements at θ=90° 91
Figure 5-31. Maximum and Minimum Waste Pressures vs. Normalized Height from Tank Bottom for the Flexible Tank at the 422 in. Waste Level Under Horizontal Excitation for α=0.02 and θ=0. 92
Figure 5-32. Maximum and Minimum Waste Pressures vs. Normalized Height from Tank Bottom for the Flexible Tank at the 422 in. Waste Level Under Horizontal Excitation for α=0.02 and θ=45°. 92
Figure 5-33. Maximum and Minimum Waste Pressures vs. Normalized Height from Tank Bottom for the Flexible Tank at the 422 in. Waste Level Under Horizontal Excitation for α=0.02 and θ=90°. 93
Figure 5-34. Waste Pressure Time Histories for the Flexible Tank at the 422 in. Waste Level for Vertical Excitation Run at Absolute Pressure for θ=0 and alpha=0.02. 95
Figure 5-35. Selected Waste Pressure Time Histories for the Flexible Tank at the 422 in. Waste Level for Vertical Excitation Case 2c (alpha=0.02) Run at Absolute Pressure..... 96
Figure 5-36. Selected Waste Pressure Time Histories for the Flexible Tank at the 422 in. Waste Level for Vertical Excitation Case 2c (alpha=0.02) Run at Absolute Pressure – Time 0 to 3 s 96
Figure 5-37. Maximum and Minimum Waste Pressures vs. Normalized Height from Tank Bottom for the Flexible Tank at the 422 in. Waste Level Under Vertical Excitation at θ=0 and α=0. 02 97
Figure 5-38. Comparison of Waste Pressure to Tank Wall Hoop Stress for the Flexible Tank at the 422 in. Waste Level and Vertical Excitation at Absolute Pressure Near the Tank Bottom at θ=0. 97
Figure 5-39. Maximum and Minimum Waste Pressures vs. Normalized Height from Tank Bottom for the Flexible Tank at the 422 in. Waste Level Under Vertical Excitation at θ=45° and α=0.02. 98

Figure 5-40. Maximum and Minimum Waste Pressures vs. Normalized Height from Tank Bottom for the Flexible Tank at the 422 in. Waste Level at Absolute Pressure with θ=90° and α=0. 02 98
Figure 5-41. Pressure Time History for Bottom Center Waste Element for 422 in. Waste Level and Vertical Excitation at Absolute Pressure and alpha=0.02 99
Figure 5-42. Comparison of Maximum Slosh Height Time-Histories for the Flexible Tank at the 422 in. Waste Level and α=0.02. 100
Figure 5-43. Dependence of the Maximum Slosh Height on the Damping Parameter α 100
Figure 5-44. Mid-Plane Hoop Stress for the Flexible Tank at the 422 in. Waste Level at θ=0 and alpha=0.02 Run at Absolute Pressure. 102
Figure 5-45. Mid-Plane Hoop Stress for the Flexible Tank at the 422 in. Waste Level at θ=45° and alpha=0.02 Run at Absolute Pressure. 103
Figure 5-46. Mid-Plane Hoop Stress for the Flexible Tank at the 422 in. Waste Level at θ=90° and alpha=0.02 Run at Absolute Pressure. 103
Figure 5-47. Comparison of Mid-Plane Hoop Stress in Tank Wall Element 433 to pr/t for Waste Element 6108 at Wall Mid-Height and θ =0. 104
Figure 5-48. Comparison of Mid-Plane Hoop Stress at Absolute and Gage Pressure for Selected Elements at θ =90°. 104
Figure 6-1. Coupling Surface Reaction Forces at the 460 in. Waste Level for the Flexible Tank Under Horizontal Seismic Input During the Initial Free Vibration Phase – (alpha=0.02). 106
Figure 6-2. Coupling Surface Reaction Forces at the 460 in. Waste Level for the Flexible Tank Under Horizontal Seismic Input – (alpha=0.02) 107
Figure 6-3. Coupling Surface Reaction Forces at the 460 in. Waste Level for the Flexible Tank Under Horizontal Seismic Input During the Final Free Vibration Phase – alpha=0.02 107
Figure 6-4. Comparison of the Horizontal Coupling Surface Reaction Force for the 460 and 422 in. Waste Levels During the Final Free Vibration Period – alpha=0.02 108
Figure 6-5. Vertical Coupling Surface Reaction Force at the 460 in Waste Level for the Flexible Tank Under Vertical Seismic Input. 109
Figure 6-6. Waste Pressures Time Histories for the Flexible Tank at the 460 in. Waste Level for Horizontal Excitation at θ=0 and alpha=0.02 Run at Absolute Pressure. 111
Figure 6-7. Selected Element Pressure Time Histories for the Flexible Tank at the 460 in. Waste Level for Horizontal Excitation at θ=0 and alpha=0.02 Run at Absolute Pressure. 112
Figure 6-8. Waste Pressures Time Histories for the Flexible Tank at the 460 in. Waste Level for Horizontal Excitation at θ=45 and alpha=0.02 Run at Absolute Pressure. 112
Figure 6-9. Selected Element Pressure Time Histories for the Flexible Tank at the 460 in. Waste Level for Horizontal Excitation at θ=45 and alpha=0.02 Run at Absolute Pressure. 113
Figure 6-10. Waste Pressures Time Histories for the Flexible Tank at the 460 in. Waste Level for Horizontal Excitation at θ=90 and alpha=0.02 Run at Absolute Pressure. 113
Figure 6-11. Maximum and Minimum Waste Pressures vs. Normalized Height from Tank Bottom for the Flexible Tank Under Horizontal Excitation at the 460 in. Waste Level at θ=0 and α=0.02. 114

Figure 6-12. Maximum and Minimum Waste Pressures vs. Normalized Height from Tank Bottom for the Flexible Tank Under Horizontal Excitation at the 460 in. Waste Level at θ=45° and α=0.02. 115
Figure 6-13. Maximum and Minimum Waste Pressures vs. Normalized Height from Tank Bottom for the Flexible Tank Under Horizontal Excitation at the 460 in. Waste Level at θ=90° and α=0.02. 115
Figure 6-14. Waste Pressure Time Histories for the Flexible Tank at the 460 in. Waste Level for Vertical Excitation at θ=0 and α=0.02. 117
Figure 6-15. Selected Element Waste Pressure for the Flexible Tank at the 460 in. Waste Level for Vertical Excitation at θ=0 and α=0.02. 118
Figure 6-16. Selected Element Waste Pressures for the Flexible Tank at the 460 in. Waste Level for Vertical Excitation at θ=0 and α=0.02 – Time 0 to 3 s. 118
Figure 6-17. Waste Pressure Time Histories for the Flexible Tank at the 460 in. Waste Level for Vertical Excitation at θ=45° and α=0.02. 119
Figure 6-18. Selected Element Waste Pressure for the Flexible Tank at the 460 in. Waste Level for Vertical Excitation at θ=45° and α=0.02. 119
Figure 6-19. Waste Pressure Time Histories for the Flexible Tank at the 460 in. Waste Level for Vertical Excitation at θ=90° and α=0.02. 120
Figure 6-20. Selected Element Waste Pressure for the Flexible Tank at the 460 in. Waste Level for Vertical Excitation at θ=90° and α=0.02. 120
Figure 6-21. Maximum and Minimum Waste Pressures vs. Normalized Waste Height from Tank Bottom for 460 in. Waste Level for Vertical Excitation at θ=0 and α=0.02. 121
Figure 6-22. Maximum and Minimum Waste Pressures vs. Normalized Waste Height from Tank Bottom for 460 in. Waste Level for Vertical Excitation at θ=45° and α=0.02. 121
Figure 6-23. Maximum and Minimum Waste Pressures vs. Normalized Waste Height from Tank Bottom for 460 in. Waste Level for Vertical Excitation at θ=90° and α=0.02. 122
Figure 6-24. Pressure Time History for Bottom Center Waste Element for 460 in. Waste Level and Vertical Excitation for α=0.02. 122
Figure 6-25. Maximum Slosh Height Time-History for the Flexible Tank at the 460 in. Waste Level for α=0.02. 123
Figure 6-26. Mid-Plane Hoop Stress for the Flexible Tank at the 460 in. Waste Level at θ=0 and alpha=0.02 Run at Absolute Pressure. 124
Figure 6-27. Mid-Plane Hoop Stress for the Flexible Tank at the 460 in. Waste Level at θ=45° and alpha=0.02 Run at Absolute Pressure. 125
Figure 6-28. Mid-Plane Hoop Stress for the Flexible Tank at the 460 in. Waste Level at θ=90° and alpha=0.02 Run at Absolute Pressure. 125
Figure 6-29. Comparison of Waste Pressure to Tank Wall Hoop Stress for the Flexible Tank at the 460 in. Waste Level at Absolute Pressure for Waste Element 9753 and Tank Wall Element 406 Near the Free Surface at θ=0. 126
Figure 6-30. Comparison of Waste Pressure to Tank Wall Hoop Stress for the Flexible Tank at the 422 in. Waste Level at Absolute Pressure for Waste Element 9024 and Tank Wall Element 431 Near the Free Surface at θ=0. 127
Figure 6-31. Mid-Plane Hoop Stress for the Flexible Tank at the 460 in. Waste Level for Vertical Excitation at θ=0 and alpha=0.02 Run at Absolute Pressure. 128

Figure 6-32. Mid-Plane Hoop Stress for the Flexible Tank at the 460 in. Waste Level for Vertical Excitation at θ=45° and alpha=0.02 Run at Absolute Pressure. 128
Figure 6-33. Mid-Plane Hoop Stress for the Flexible Tank at the 460 in. Waste Level for Vertical Excitation at θ=90° and alpha=0.02 Run at Absolute Pressure. 129
Figure 6-34. Comparison of Waste Pressure to Tank Wall Hoop Stress for the Flexible Tank at the 460 in. Waste Level Under Vertical Excitation at Absolute Pressure Near the Free Surface at θ=45° 130
Figure 6-35. Comparison of Waste Pressure to Tank Wall Hoop Stress for the Flexible Tank at the 460 in. Waste Level Under Vertical Excitation at Absolute Pressure Near the Free Surface at θ=90° 130
Figure 7-1. Comparison of ANSYS and Dytran Total Horizontal Reaction Forces for the Flexible Tank at the 422 in. Waste Level Under Horizontal Seismic Excitation. 133
Figure 7-2. Comparison of ANSYS and Dytran Total Vertical Reaction Forces for the Flexible Tank at the 422 in. Waste Level Under Vertical Seismic Excitation. 133
Figure 7-3. Comparison of ANSYS and Dytran Total Horizontal Reaction Forces for the Flexible Tank at the 460 in. Waste Level Under Horizontal Seismic Excitation. 134
Figure 7-4. Comparison of ANSYS and Dytran Total Vertical Reaction Forces for the Flexible Tank at the 460 in. Waste Level Under Vertical Seismic Excitation. 134
Figure 7-5. Comparison of ANSYS and Dytran Waste Pressures for the Flexible Tank at the 422 in. Waste Level Under Horizontal Excitation – Waste Elements Near Tank Top and Bottom at θ=0 136
Figure 7-6. Comparison of ANSYS and Dytran Waste Pressures for the Flexible Tank at the 422 in. Waste Level Under Horizontal Excitation – Waste Elements at Elevation 292 in. Above Tank Bottom at θ=0. 136
Figure 7-7. Comparison of ANSYS and Dytran Waste Pressures for the Flexible Tank at the 460 in. Waste Level Under Horizontal Excitation – Waste Elements Near Tank Top and Bottom at θ=0 137
Figure 7-8. Comparison of ANSYS and Dytran Waste Pressures for the Flexible Tank at the 460 in. Waste Level Under Horizontal Excitation – Waste Elements at Elevation 292 in. Above Tank Bottom at θ=0. 137
Figure 7-9. Comparison of ANSYS and Dytran Mid-Plane Hoop Stress at Primary Tank Wall Element Near the Waste Free Surface for the Flexible Tank at the 422 in. Waste Level for Horizontal Excitation and θ=0. 139
Figure 7-10. Comparison of ANSYS and Dytran Mid-Plane Hoop Stress at an Elevation of 292 in. from the Tank Bottom for the Flexible Tank at the 422 in. Waste Level for Horizontal Excitation and θ=0. 139
Figure 7-11. Comparison of ANSYS and Dytran Mid-Plane Hoop Stress at Primary Tank Wall Element Near the Tank Bottom for the Flexible Tank at the 422 in. Waste Level for Horizontal Excitation and θ=0. 140
Figure 7-12. Comparison of ANSYS and Dytran Mid-Plane Hoop Stress at Primary Tank Wall Element Near the Waste Free Surface for the Flexible Tank at the 460 in. Waste Level for Horizontal Excitation and θ=0. 140
Figure 7-13. Comparison of ANSYS and Dytran Mid-Plane Hoop Stress at an Elevation of 292 in. from the Tank Bottom for the Flexible Tank at the 460 in. Waste Level for Horizontal Excitation and θ=0. 141

Figure 7-14. Comparison of ANSYS and Dytran Mid-Plane Hoop Stress at Primary Tank Wall Element Near the Tank Bottom for the Flexible Tank at the 460 in. Waste Level for Horizontal Excitation and θ=0. 141

LIST OF TABLES

Table 1-1. Summary of Frequencies and Maximum Slosh Heights 8
Table 1-2. Summary of Global Reaction Forces. 9
Table 3-1. Expected Hydrostatic Pressure of Waste Elements 30
Table 3-2. Theoretical Maximum Waste Pressures for Horizontal Excitation in the Rigid Tank at 422 in. Waste Level for Elements at θ=0 Run at Absolute Pressure. 36
Table 3-3. Theoretical Maximum Waste Pressures for Horizontal Excitation in the Rigid Tank at 422 in. Waste Level for Elements at θ=45° Run at Absolute Pressure. 36
Table 3-4. Theoretical Maximum Wall Pressures for Vertical Excitation in the Rigid Tank at 422 in. Waste Level. 41
Table 4-1. Theoretical Maximum Absolute Waste Pressures for Horizontal Excitation in the Rigid Open Top Tank at 460 in. Waste Level for Elements at θ=0 52
Table 4-2. Theoretical Maximum Absolute Waste Pressures for Horizontal Excitation in the Rigid Open Top Tank at 460 in. Waste Level for Elements at θ=45°. 52
Table 5-1. Theoretical Maximum Absolute Waste Pressures for Horizontal Excitation in the Flexible Tank at 422 in. Waste Level for Elements at θ=0. 85
Table 5-2. Theoretical Maximum Absolute Waste Pressures for Horizontal Excitation in the Flexible Tank at 422 in. Waste Level for Elements at θ=45°. 85
Table 5-3. Theoretical Maximum Absolute Wall Pressures for Vertical Excitation in at the 422 in. Waste Level. 94
Table 6-1. Theoretical Maximum Absolute Waste Pressures for Horizontal Excitation in the Flexible Open Top Tank at 460 in. Waste Level for Elements at θ=0. 110
Table 6-2. Theoretical Maximum Absolute Waste Pressures for Horizontal Excitation in the Flexible Open Top Tank at 460 in. Waste Level for Elements at θ=45. 110
Table 6-3. Theoretical Maximum Absolute Wall Pressures for Vertical Excitation of an Open Top Tank at the 460 in. Waste Level. 116
Table 7-1. Comparison of ANSYS and Dytran Frequencies and Maximum Slosh Heights. 131
Table 7-2. Summary of Centroidal Elevations for ANSYS and Dytran Selected Waste Elements at θ=0. 135
Table 7-3. Summary of Centroidal Elevations for Tank Wall Elements at θ=0. 138

1.0 INTRODUCTON

M&D Professional Services, Inc. (M&D) is under subcontract to Pacific Northwest National Laboratories (PNNL) to perform seismic analysis of the Hanford Site Double-Shell Tanks (DSTs) in support of a project entitled *Double-Shell Tank (DST) Integrity Project - DST Thermal and Seismic Analyses*. The overall scope of the project is to complete an updated analysis of record of the DST System at Hanford. The work described herein was performed in support of the seismic analysis of DSTs. The seismic analysis of the DSTs is part of an overall project to provide an up-to-date comprehensive analysis of record for the tanks.

The overall seismic analysis of the DSTs is being performed with the general-purpose finite element code ANSYS[3]. The overall model used for the seismic analysis of the DSTs includes the DST structure, the contained waste, and the surrounding soil. The seismic analysis of the DSTs must address the fluid-structure interaction behavior and sloshing response of the primary tank and contained liquid. ANSYS has demonstrated capabilities for structural analysis, but has more limited capabilities for fluid-structure interaction analysis.

The purpose of this study is to demonstrate the capabilities and investigate the limitations of Dytran for performing a dynamic fluid-structure interaction analysis of the primary tank and contained waste. The explicit code MSC.Dytran[4] was developed to analyze fluid-structure interaction problems. MSC.Dytran resulted from a unification of Dyna-3D and the Pisces code, in which the latter was developed specifically for the analysis of fluid-structure interaction problems. The Dytran solutions are benchmarked against theoretical solutions appearing in BNL 1995, when such theoretical solutions exist. When theoretical solutions were not available, comparisons were made to theoretical solutions to similar problems, and to the results from ANSYS simulations.

The capabilities and limitations of ANSYS for performing a fluid-structure interaction analysis of the primary tank and contained waste were explored in a parallel investigation and documented in a companion report (Carpenter and Abatt [2006]). The results of this study will be used in conjunction with the results of the global ANSYS analysis documented in Carpenter et al. (2006) and the parallel ANSYS fluid-structure interaction analysis to help determine if a more refined sub-model of the primary tank is necessary to capture the important fluid-structure interaction (FSI) effects in the tank and if so, how to best analyze a refined sub-model of the primary tank.

Both rigid tank and flexible tank configurations were analyzed with Dytran. Numerous cases of damping or dynamic relaxation were studied to determine the best way to implement damping in Dytran for the flexible tank problems. The options available are to introduce dynamic relaxation solely as a means to obtain a stable solution to the initial gravity loading, and then remove it from the problem and run seismic loading without

[3] ANSYS is a registered trademark of ANSYS Inc.
[4] MSC.Dytran is a registered trademark of MSC.Software Corporation.

damping, or to keep the dynamic relaxation parameter constant throughout the problem. The first method is probably the more typical use of dynamic relaxation in Dytran. The second method requires calibrating the dynamic relaxation coefficient by iteration and comparison to known solutions.

The response parameters of interest that are evaluated in this study are the total hydrodynamic reaction forces, the impulsive and convective mode frequencies, the waste pressures, and slosh heights. To a limited extent, primary tank stresses are also reported.

1.1 DISCUSSION

The earlier Dytran runs performed were run at gage rather than absolute pressure for the simple reason that stable solutions were easier to obtain using gage pressure. However, it was recognized from the beginning of the study that it would be preferable to perform the analyses at absolute pressure. Running at absolute pressure eliminates any potential problems that can arise when dynamic pressures exceed static pressures, and total pressures become negative, at least in theory.

Eventually, stable solutions were achieved in most instances running at absolute pressure, and the focus of the discussion and results in the body of the report will be on the absolute pressure results. In a few places, results of gage pressure runs are shown alongside results from absolute pressure runs to illustrate some differences in the solutions.

Hand in hand with the discussion of running the problem at absolute or gage pressure is the subject of how to best implement damping into the solution to achieve the desired effective damping. It turned out that solution stability depended both on whether the problem was run at absolute or gage pressure, and, in the case of flexible wall tanks, how damping was introduced into the problem. Typically, damping is introduced into a Dytran analysis through the use of dynamic relaxation parameters that are intended to aid in finding the steady-state part of a dynamic solution to a transient loading. The dynamic relaxation factors available in Dytran are introduced directly into the central difference integration scheme of the equations of motion. The tie to overall system damping is loose, especially for complex systems. Thus, using dynamic relaxation to produce a target effective damping in a complex system becomes a matter of trial and error. For these reasons, dynamic relaxation is normally introduced to achieve a steady-state response to a transient loading (e.g. gravity), and then is removed for the remainder of the problem. It is not typically used to achieve a desired effective damping in a complex system such as a DST.

Several implementations of damping or dynamic relaxation were investigated. The first attempt at utilizing dynamic relaxation was made by introducing a constant dynamic relaxation value throughout the complete analysis based on a guideline given in the Dytran Theory Manual (MSC 2005a). This resulted in the system being significantly

under-damped to the point that it was difficult to achieve a steady-state solution to gravity loading.

The second attempt (referred to as Case 3 later in the report) was the more traditional approach of introducing a much larger dynamic relaxation factor during the initial gravity loading, and then removing the damping for the remainder of the problem that consisted of the seismic transient and an ensuing free vibration phase. This approach resulted in good agreement with the theoretical value of the total horizontal hydrodynamic reaction force when the problem was run at gage pressure, but had the deficiency that a stable solution was not achieved when the problem was run at absolute pressure.

The final approach was to use a constant dynamic relaxation factor throughout the whole problem and to calibrate the value based on trial and error. The value that was finally selected was much larger than that suggested in the Dytran Theory Manual, but somewhat less than was used in the more traditional approach. This approach had the desired outcome that it produced stable solutions at absolute pressure and gave good agreement with theoretical solutions.

The four tank configurations investigated were a rigid tank with a waste level of 422 in., a rigid tank with a waste level of 460 in., a flexible wall tank with a waste level of 422 in., and a flexible wall tank with a waste level of 460 in. The 422 in. waste level is intended to represent a baseline waste level for the Hanford DSTs, while the 460 in. waste level represents a higher level being proposed to increase the capacity of the Hanford AP DSTs. Each of the four configurations was subjected to horizontal and vertical seismic excitation as separate cases.

For the rigid tank configurations, dynamic relaxation was not necessary, but the bulk viscosities were assigned non-default values to help achieve stable solutions. The response parameters investigated for the rigid tanks were the total hydrodynamic force components, the convective frequency, the waste pressures, and the slosh height. The analyses of the flexible wall tanks used the dynamic relaxation schemes described above, and the response parameters were those for the rigid tanks plus impulsive frequencies and element stresses.

The solution for the rigid tank at the 422 in. level was compared to the theoretical solution for an open top rigid tank with a hinged top boundary condition (although the boundary condition is irrelevant for a rigid tank). The peak hydrodynamic forces and the convective frequency closely matched theoretical predictions, although the convective component of the horizontal hydrodynamic force was somewhat lower than expected. The waste pressures and pressure distributions also matched well to theoretical values, except for a few isolated peaks in the pressure time histories. Such isolated peaks were present to some degree in all of the simulations and will be discussed further below. The maximum slosh height was 7% greater than predicted by theory.

Theoretical solutions are not available at the 460 in. waste level because of the interaction between the waste and the dome curvature. However, comparisons were made to the

corresponding solution for a tank at the 460 in. waste level with vertical walls, and open top, and a hinged top boundary condition.

The simulation for the rigid tank at the 460 in. waste level showed that the total peak horizontal reaction force agreed with that predicted by the theoretical solution for an open top tank with a 460 in. waste level, and the total peak vertical reaction force was slightly higher than predicted by the open top theoretical solution. The convective component of the horizontal reaction force was low indicating that the presence of the dome acts to inhibit the convective response. The fundamental convective frequency matches that for the open top tank, but the reaction time history for the convective response shows some high frequency content that was not present at the 422 in. waste level.

The waste pressures are generally as predicted for the open top tank, but isolated peaks exist in the pressure time histories, especially for elements near the elevation of the waste free surface. More such isolated pressure peaks were evident in the simulation at the 460 in. waste level than at the 422 in waste level. The maximum slosh height was 86% of that predicted for the open top tank.

The total horizontal reaction force for the flexible wall tank at the 422 in. waste level was 96% of the theoretical value, while the total vertical reaction force was 20% greater than predicted by theory. The response showed a breathing mode[5] frequency of 6 Hz and an impulsive mode frequency of slightly less than 7 Hz – both in good agreement with theoretical predictions. The fundamental convective frequency was 0.19 Hz, also in agreement with theory. Based on the decay of the total horizontal reaction force during the final free vibration phase, the effective damping associated with the convective response is approximately 1% of critical damping.

The waste pressures due to horizontal excitation show generally good agreement with theory, but as with the other solutions, isolated peaks that are not predicted by theory exist in the pressure time histories. The peaks are more prevalent in elements closer to the waste surface. The pressures associated with vertical excitation of the tank also show general agreement with theory and contain a few isolated peak pressures. Both the pressure and hoop stress time histories show a gradual drift down over time toward the end of solution. The maximum slosh height of 24.5 in. calculated by Dytran is 3% greater than the theoretical value.

The Dytran analysis of the flexible wall tank at the 460 in. waste level showed that the total horizontal reaction force was as predicted by the open top theory, and the total vertical reaction force was 6% greater than the theoretical value. *That is, according to the Dytran model, the peak horizontal hydrodynamic force is essentially the same as predicted for the open top tank, and any interaction of the fluid with the dome has not significantly changed the peak force from that predicted for an open top tank.* The breathing mode frequency was 5.5 Hz, and the impulsive frequency was 6.5 Hz, both in

[5] The breathing mode is the axisymmetric vibratory mode associated with volumetric expansion and contraction of the cylinder. It is the fundamental mode for the transient response of the model to gravity loading.

agreement with open top theory, and both approximately ½ Hz less than for the 422 in. waste level. The fundamental convective frequency is 0.2 Hz, as expected from the theory.

As was the case for the rigid tank at the 460 in. waste level, the convective component of the total horizontal reaction force is less than predicted for an open top tank, and less than was observed for the flexible tank at the 422 in. waste level. Once again, it appears that the dome curvature inhibits the convective response.

The waste pressure responses for horizontal and vertical seismic input both showed isolated peaks that were similar to those seen for the rigid tank at the 460 in. waste level. In the case of vertical input, both pressures and hoop stresses showed a slight downward drift over time. The tank wall hoop stresses from horizontal seismic input are as expected and generally do not reflect the isolated spikes in waste pressures. Hoop stresses in tank wall elements near the free surface that are caused by vertical excitation appear to be only loosely correlated to the waste pressures of adjacent waste elements. The hoop stresses show a few isolated spikes, but the spikes do not appear well correlated with the more frequent spikes in the waste pressures. The maximum slosh height was 20 in. or 82% of the value predicted for an open top tank.

The interpretation of isolated peaks in the waste pressure time histories that occurred in all four analysis configurations warrants discussion. The fundamental issue is whether the peaks are physically real or whether they are numerical noise in the Dytran solution. To some degree, the question is irrelevant, or at least ill-posed, since ultimately the interest is in performing a stress analysis on the primary tank, and the behavior of the stress time histories is not the same as the pressure time histories. It appears that the primary tank structure acts to filter out at least some of the localized high (and low) waste pressures.

However, although the waste pressure time histories are of less importance than the stress time histories for the structural assessment of the primary tank, it is still informative to look closely at the waste pressure behavior. The positive and negative spikes in the waste pressure time histories occurred in all four analyses and for both horizontal and vertical excitation. The spikes occurred at both the top and bottom of the waste, and occurred during the seismic excitation, and afterwards during the unforced vibration phase when the seismic excitation was not present. The spikes were more prevalent at the higher waste level, but still occurred at the lower waste level.

The frequency of output for the pressure time histories was 10 ms – the same as the frequency of the seismic input. The isolated peaks typically occurred at one output point at a time meaning that the duration of a peak on the pressure time history output files was 20 ms. There is some evidence to suggest that the pressure spikes are real and are due to impact pressures generated by waves impacting the boundary of the structure. Such phenomena were observed in experiments reported by Kurihara et al. (1992) for liquid sloshing in flat roofed tanks. The fact that the pressure spikes occur more frequently at

the higher liquid level where interaction with the dome curvature is important is consistent with the observations for the flat roofed tanks.

On the other hand, the manifestation of the spikes in the pressure time histories also showed behavior that suggests that the spikes may be numerical in origin. For instance, some spikes occur in waste elements near the bottom of the tank and some spikes occurred during the second free vibration phase of the analysis after the seismic input was terminated. These observations make it seem less plausible that the pressure spikes are real. Moreover, if the highest isolated peak pressures are disregarded, the agreement between the computer simulations and the theoretical solutions (for exact solutions at the 422 in. waste level) improves markedly. Indeed, it is likely that excellent agreement between the simulations and theory would result either by filtering the pressure time histories via post-processing, or re-running the simulations using the technique of bulk scaling in which the bulk modulus of the liquid is reduced, thereby providing a natural filtering mechanism for the high-frequency pressure response.

Although it is not clear whether the pressure spikes are physical or numerical in origin, the most important aspect of the response is the stress in the primary tank. As noted above, most of the high-frequency peaks in the pressures do not show up in the stress response. In a few instances, similar peaks do show up in the stress time histories, but the stress magnitudes are low enough to not cause concern.

Further investigation of the phenomenon could include re-running the simulations and requesting the pressure time histories at a higher frequency to better characterize the nature of the response, and to run a simulation of a tank with vertical walls and no fluid-structure interaction with the dome. The analyses at the 422 in. liquid level nearly satisfy this condition, but not exactly, since the free surface of the waste will have very mild interaction with the dome. If high frequency pressure spikes still showed up in this situation, it is more likely that the peaks are numerical in origin.

Some unexpected behavior was noted in the slosh height time histories at the 460 in. waste level. Specifically, maximum waste free surface heights of nearly 10 in. were recorded during the initial gravity loading of the structure before seismic excitation commenced. Investigation of the deformed shape of the waste showed that the initial change in the waste free surface height under gravity loading was due an axisymmetric increase in the waste free surface near the tank boundary that had the appearance of a meniscus. This effect was attributed to either a limitation of the post-processing routine used to calculate the maximum waste free surface height, or else a limitation caused by lack of sufficient resolution in the model discretization. Nonetheless, the maximum slosh heights recorded for these analyses did appear reasonable relative to theoretical predictions.

Section 7.0 of this report contains direct comparisons between the results from the flexible tank ANSYS models reported in Carpenter and Abatt (2006) and the flexible tank Dytran models described in this report. Both codes predict frequencies that agree well with theoretical values, although the Dytran predictions are generally closer to

expected values than the ANSYS predictions. Comparison of the reaction forces from the ANSYS and Dytran models showed that the responses from the models are similar with ANSYS generally being conservative relative to Dytran, and both codes generally showing good agreement with theoretical predictions. At the 422 in. waste level, the ANSYS reaction forces were slightly greater than the reaction force predicted by Dytran for both horizontal and vertical seismic input. At the 460 in. waste level, the horizontal reaction force predicted by ANSYS is the same as predicted by theory and essentially the same as predicted by Dytran. In the case of the vertical reaction forces, somewhat higher peaks are predicted by Dytran than ANSYS. In particular, since the loads into the j-bolts connecting the primary tank to the concrete dome are driven by the overall forces on the primary tank, it appears that a global ANSYS model is sufficient for analysis of the j-bolts and that any sub-model of the primary tank need not contain the j-bolts.

Comparison of a limited set of waste pressures due to horizontal excitation from ANSYS and Dytran showed that at the 422 in. waste level, the waste pressures were very similar near the bottom of the tank. In the middle and upper portions of the waste, the ANSYS solution showed more of a convective response than the Dytran solution. At the 460 in. waste level, the peak pressures near the bottom of the waste are higher in Dytran than in ANSYS. Near the top of the waste, the responses are similar, with ANSYS predicting somewhat higher pressures. The appearance of a convective response in ANSYS is less evident at the higher waste level. At an elevation of 292 in. up from the tank bottom, the pressure predictions are very similar, with the ANSYS response being slightly higher.

Finally, comparisons were made between membrane hoop stress predictions for the models. It is difficult to draw conclusions from these comparisons because of differences in modeling techniques, mesh resolution in the tank wall, mesh resolution near the tank knuckle, and differences in the elevation of the tank wall element centroids. The two models do give very similar results for membrane hoop stress at the middle elevation of 292 in. up from the tank bottom, with the ANSYS results being slightly higher than the Dytran results. A couple of interesting observations on the hoop stresses are that whereas the convective response was more apparent in the waste pressures predicted by ANSYS near the free surface at the 422 in. waste level, this response is more apparent in the Dytran hoop stress predictions at that elevation. Also, the convective response that was observed from ANSYS in the waste pressure time history at 292 in. above the tank bottom at the 422 in. waste level is not readily apparent in the hoop stress time history.

1.2 SUMMARY

The purpose of this study was to demonstrate the capabilities and investigate the limitations of Dytran for performing a fluid-structure interaction (FSI) analysis of the primary tank and contained waste. The results of this study were used in conjunction with the results of the global ANSYS analysis (Carpenter et al. [2006]) and the parallel ANSYS FSI analysis (Carpenter and Abatt [2006]) to help determine if a more refined sub-model of the primary tank is necessary to capture the important fluid-structure interaction effects in the tank and if so, how to best utilize a refined sub-model of the primary tank.

The results of this study demonstrate that Dytran has the capability to perform FSI analysis of a primary tank subjected to seismic loading. With the exception of some isolated peak pressures and to a lesser extent peak stresses, the results agreed very well with theoretical solutions as shown in Table 1-1 and Table 1-2.

The results of the ANSYS FSI benchmark analysis documented in Carpenter and Abatt (2006) showed that the ANSYS model was suitable for predicting the global response of the tank and contained waste and was capable of adequately predicting waste pressures in a large portion of the waste. However, the ANSYS model did not accurately capture the waste pressures near the free surface due to the convective response, nor did the model give accurate predictions of maximum slosh heights.

While Dytran appears to have stronger capabilities for the analysis of the FSI behavior in the primary tank, it is more practical to use ANSYS for the global evaluation of the tank. Thus, Dytran served the purpose of helping to identify limitations in the ANSYS FSI analysis so that those limitations can be addressed in the structural evaluation of the primary tank.

Due to the limitations identified in the ANSYS model for predicting the convective response of the waste, the evaluation of primary tank stresses near the waste free surface should be supplemented by results from an ANSYS sub-model of the primary tank that incorporates pressures from theoretical solutions or from Dytran solutions. However, the primary tank is expected to have low demand to capacity ratios in the upper wall.

Table 1-1. Summary of Frequencies and Maximum Slosh Heights

Configuration	First Convective Mode Frequency (Hz)		Impulsive Mode Frequency (Hz)		Breathing Mode Frequency (Hz)		Maximum Slosh Height (in)	
	Theory	Dytran	Theory	Dytran	Theory	Dytran	Theory	Dytran
Rigid 422	0.19	0.19	Rigid	Rigid	Rigid	Rigid	23.7	25.4
Rigid 460[1]	0.2	0.2	Rigid	Rigid	Rigid	Rigid	24.5	21.1
Flexible 422	0.19	0.19	7.0	6.85	6.1	6.0	23.7	24.5
Flexible 460[1]	0.2	0.2	6.5	6.4	5.5	5.5	24.5	20.1

[1]Theoretical solutions for the 460 in. waste level are based on an open tank with vertical walls and a hinged top boundary condition.

Table 1-2. Summary of Global Reaction Forces.

Configuration	Peak Horizontal Reaction Force (lbf)		Peak Vertical Reaction Force (lbf)	
	Theory	Dytran	Theory[2]	Dytran[2]
Rigid 422	2.42×10^6	2.45×10^6	1.96×10^6	2.15×10^6
Rigid 460[1]	3.0×10^6	3.02×10^6	2.3×10^6	3.1×10^6
Flexible 422	7.56×10^6	7.25×10^6	5.24×10^6	6.3×10^6
Flexible 460[1]	1.03×10^7	1.02×10^7	4.54×10^6	5.98×10^6

[1]Theoretical solutions for the 460 in. waste level are based on an open tank with vertical walls and a hinged top boundary condition.
[2]Values shown are the dynamic components of the vertical reaction forces exclusive of the waste weight.

1.3 CONCLUSIONS

1. The results of the Dytran analyses of the rigid and flexible wall tanks at the 422 in. waste level generally agree well with known theoretical solutions.
2. Although theoretical solutions for a domed tank with the static liquid level near the dome as in the 460 in. waste level simulation do not exist, the results of Dytran analyses of the rigid and flexible wall tanks at the 460 in. waste level appear reasonable and show many similarities to solutions for an open top tank with a hinged top boundary condition.
3. The peak horizontal reaction force for the both the rigid and flexible tanks at the 460 in. waste level under horizontal seismic excitation agree with the theoretical predictions for the corresponding open top tanks. *That is, any interaction of the fluid with the dome during the simulations at the 460 in. waste level has not significantly changed the peak force from that theoretically predicted for the corresponding open top tanks.*
4. Dytran appears capable of providing a realistic fluid-structure interaction-analysis of a primary tank and contained waste. However, the features and configurations of a Dytran model should be compatible with the strengths of the program.
5. All solutions showed instances of isolated high-frequency spikes in the pressure time histories that deviate from theoretical solutions.
6. Such high-frequency pressure spikes typically did not show up as stress spikes in the primary tank, since the tank structure evidently acts as a natural mechanical filter. In the few instances where higher spikes appeared in stress time histories, the magnitudes of the stresses were low enough to not cause concern.
7. It is preferable to analyze the problem at absolute rather than gage pressure, but it was more difficult to get stable solutions using absolute pressure.
8. The implementation of dynamic relaxation or damping can have a significant affect on solution stability and solution accuracy.
9. Once the dynamic relaxation parameter was properly calibrated, a single value worked well for all cases. That is, a single value appeared to work well for both waste heights, for horizontal and vertical excitation, and for predicting total hydrodynamic reaction forces, pressures, and slosh heights.

10. Although the damping was calibrated based on response decay during an initial free oscillation phase and peak responses during forced motion, critical damping values for the convective response in a final free oscillation phase were in the range of 1% or less.
11. The convective component of the total reaction force is small relative to the total reaction force. That is, the total reaction force is dominated by the impulsive response.
12. The Dytran model has better capabilities than the ANSYS model for predicting slosh heights, and for predicting waste pressures and tank stresses near the free surface of the waste.
13. Based on good agreement between ANSYS, Dytran, and theoretical solutions for reaction forces, a global ANSYS model is sufficient for analysis of the j-bolts and any sub-model of the primary tank need not contain the j-bolts.

2.0 MODEL DESCRIPTION

A simplified model of a Hanford Double Shell Tank (DST) was created using the 2005 version of MSC.Patran[6], and was analyzed using the Dytran 2006 Development Version. The verification and validation of the software on the local computer platform is documented in M&D (2005). The purpose of the analysis was to investigate the fluid-structure interaction behavior for several tank structural configurations, liquid levels, loadings, and damping implementations. Results from theoretical solutions are presented and summarized for each of the cases in the body of the report. The details of the theoretical solutions are not included in the body of the report, but instead are included in Appendix B.

The two structural configurations studied include a completely rigid primary tank, and a primary tank with a rigid dome and base, but with flexible walls. All Dytran models are full three-dimensional (3D) representations of the tanks. Simulations were performed for both the 422 and 460 in. waste levels. Applied loads include gravity loading and seismic loading, with seismic loading applied in the horizontal and vertical directions as separate load cases.

The first configuration studied was a completely rigid tank with a waste depth of 422 in. This case is intended to simulate the response of a rigid tank with vertical walls without significant fluid interaction with the dome. The second case was a completely rigid tank with a waste depth of 460 in. At the 460 in. waste level, significant fluid-structure interaction occurs in the dome under seismic excitation. This configuration does not have a theoretical solution, but it is useful as a comparison to the solution for the flexible tank at the 460 in. waste level.

In the third case, the walls of the tank were flexible, and the waste depth was 422 in. This case is intended to simulate the response of a tank with flexible vertical walls without significant fluid interaction with the dome. The fourth configuration studied was a flexible wall tank with a waste depth of 460 in. In the case of the flexible wall models, the material properties and wall thickness were based on the AY tank configuration, though the model was simplified to have a uniform wall thickness to allow more direct comparisons with theoretical solutions. All four configurations were run for horizontal and vertical seismic excitation independently. The solutions to the first and third configurations at the 422 in. waste level were compared to theoretical solutions from BNL 1995. The results from the second and fourth configurations at the 460 in. waste depth were compared to the first and third cases as well as to theoretical solution to similar configurations, but no closed form solutions exist for the actual configurations.

The rigid tank configuration was run without damping other than the artificial viscosities inherent in the Dytran program. The artificial viscosities implemented in Dytran are referred to as the linear (BULKL) and quadratic (BULKQ) bulk viscosities. The bulk viscosities act to control the formation of shock waves by introducing viscosity to the

[6] MSC.Patran is a registered trademark of MSC.Software Corporation.

bulk straining of the fluid. Trial and error showed that increased bulk viscosity coefficients relative to the default values were necessary to achieve stable solutions, at least in some cases. As a result of the trail and error investigation, all results reported were run with the linear and quadratic bulk viscosity parameters set to 0.2 and 1.1, respectively. The default values for the bulk viscosity coefficients are 0 for the linear coefficient and 1.0 for the quadratic coefficient.

2.1 MODEL GEOMETRY

The tank model geometry was based on the AY tank configuration shown in Hanford Drawing No. H-2-64449. The primary tank has a 450 in. radius and the height of the vertical wall is 424 in. The dome apex is 561.5 in. above the bottom of the tank. The models were run using waste depths of 422 in. and 460 in. An excerpt from Drawing No. H-2-64449 is shown as Figure 2-1.

Figure 2-1. AY Primary Tank Dimensions

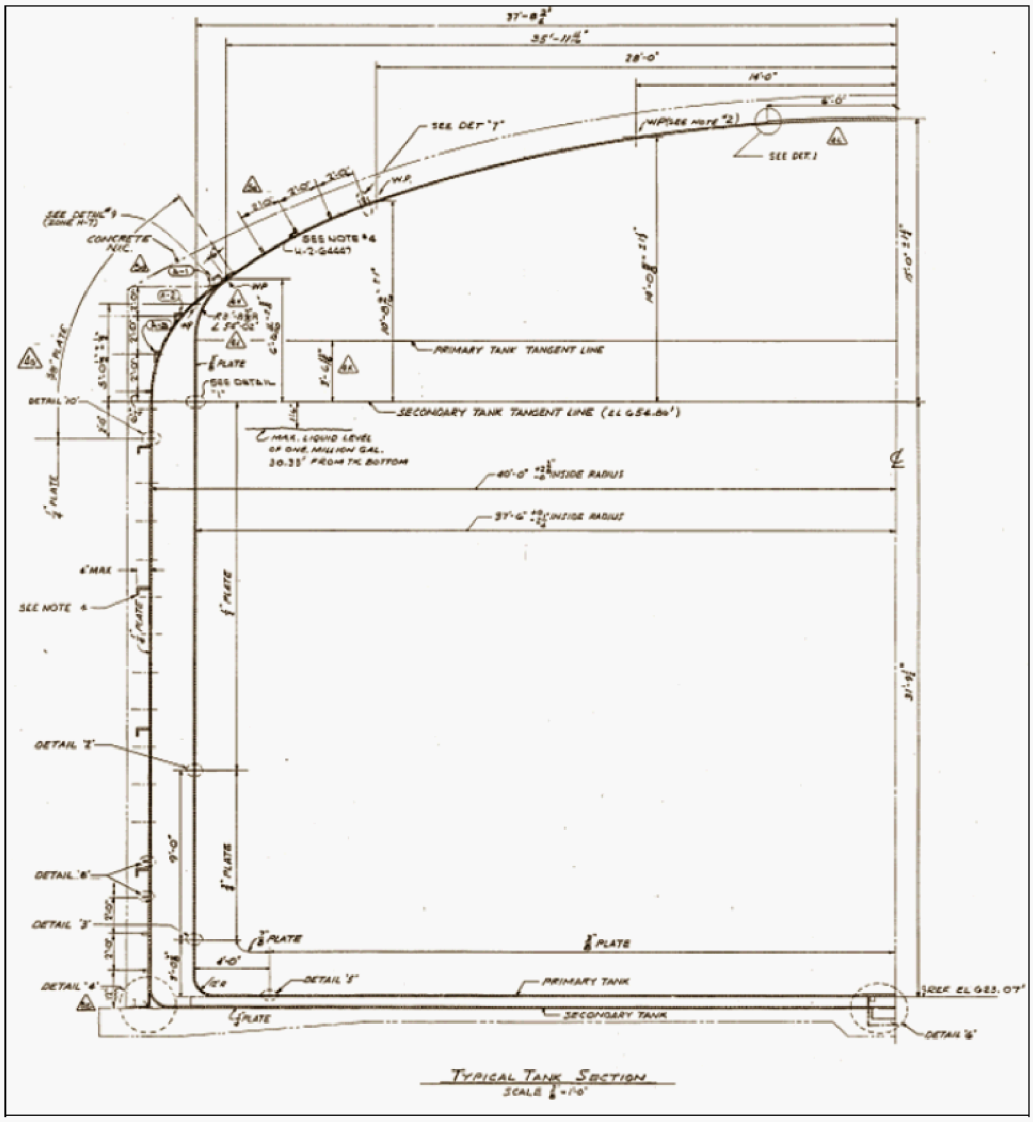

In the full three-dimensional Dytran model, the bottom of the primary tank is supported vertically by a fixed rigid base plate in contact with the tank bottom as shown in Figure 2-2. The purpose of the base plate is to provide the vertical support to the bottom of the primary tank model that is provided by the insulating concrete in the actual tank.

A notable difference between the Dytran model and the actual tank as shown in Figure 2-2 is that the junction between the vertical wall and the tank bottom is modeled as a right angle. Consequently, the details of the tank lower knuckle region and its support by the insulating concrete have not been captured by this simplified model.

Figure 2-2. Plot of Primary Tank and Base

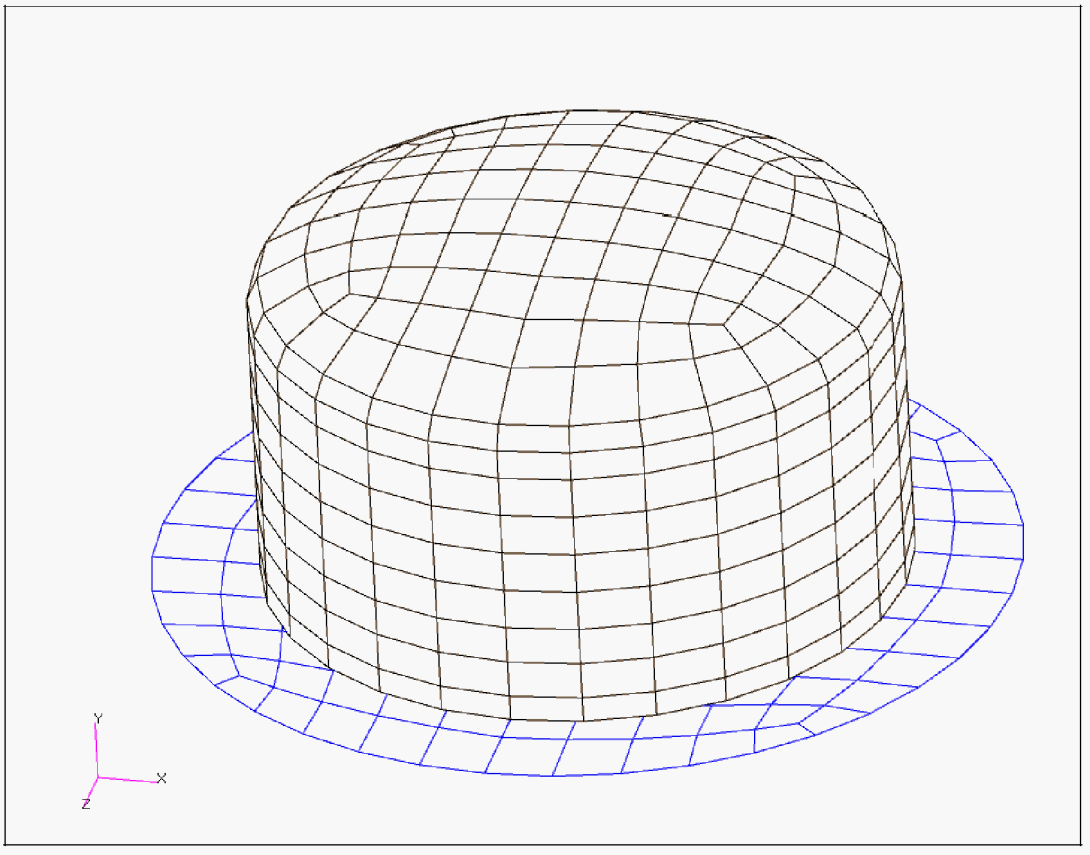

The relative height of the waste to the tank for the 422 and 460 in. waste levels is shown in Figure 2-3 and Figure 2-4, respectively. The tank floor and walls form what is known as a Dytran coupling surface with the water. The coupling surface allows the Eulerian waste mesh to interact with the Lagrangian structural mesh, and although the Eulerian mesh extends beyond the tank boundary, all the fluid dynamics occurs inside the tank.

Figure 2-3. Plot of Tank and Waste at 422 in. Waste Level

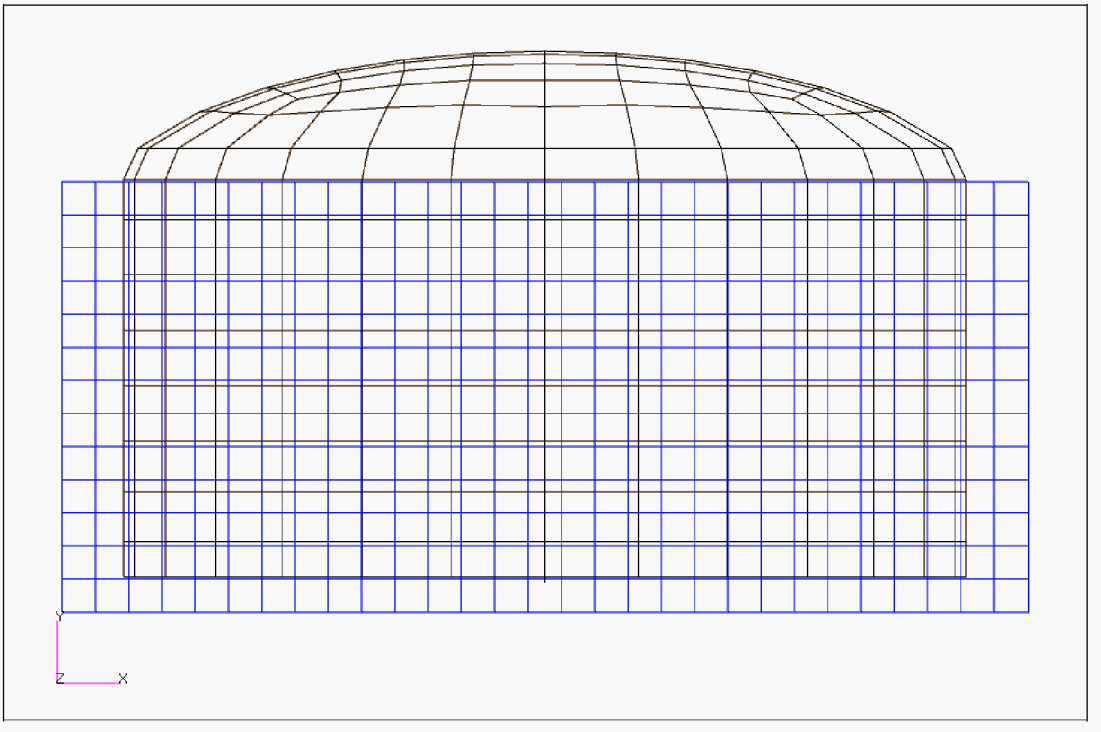

Figure 2-4. Plot of Tank and Waste at 460 in. Waste Level

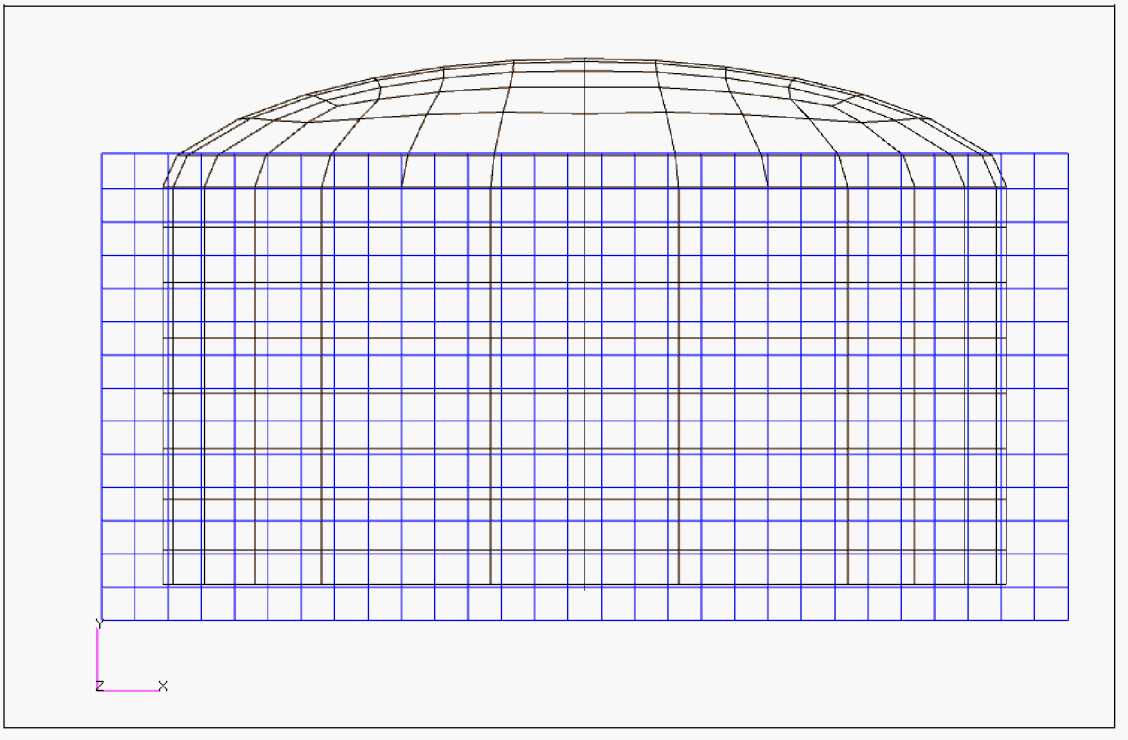

Dynamic waste pressures are a function of depth, angular location and radial location of the fluid element. Waste pressures were extracted from five sets of fluid elements

throughout the tank as shown in Figure 2-5. The element set "plusx_els" is located near the tank wall in the positive x-direction (θ=0) in the plane of the seismic excitation. Note that the angle θ is measured from the positive x-axis to the positive z-axis to describe the angular position of elements in the model. Element sets "press_45" and "plusz_els" are located near the tank wall at 45° (approximately) and 90° from the excitation direction. Element set "minusx_els" is near the tank wall in the negative x-direction, and the set "cent_press" is near the center of the tank at a radial location of approximately zero. Figure 2-6 and Figure 2-7 show the waste element numbering for four element sets described above. In Figure 2-6, the center pressure elements are in the middle, the plusx_els" are on the right, and the "minusx_els" are on the left. In Figure 2-7, the set "press_45" is on the right, and the set plusz_els" is on the left.

Figure 2-5. Top View of Model Showing the Angular Locations of Fluid Elements at Which Pressures Were Monitored.

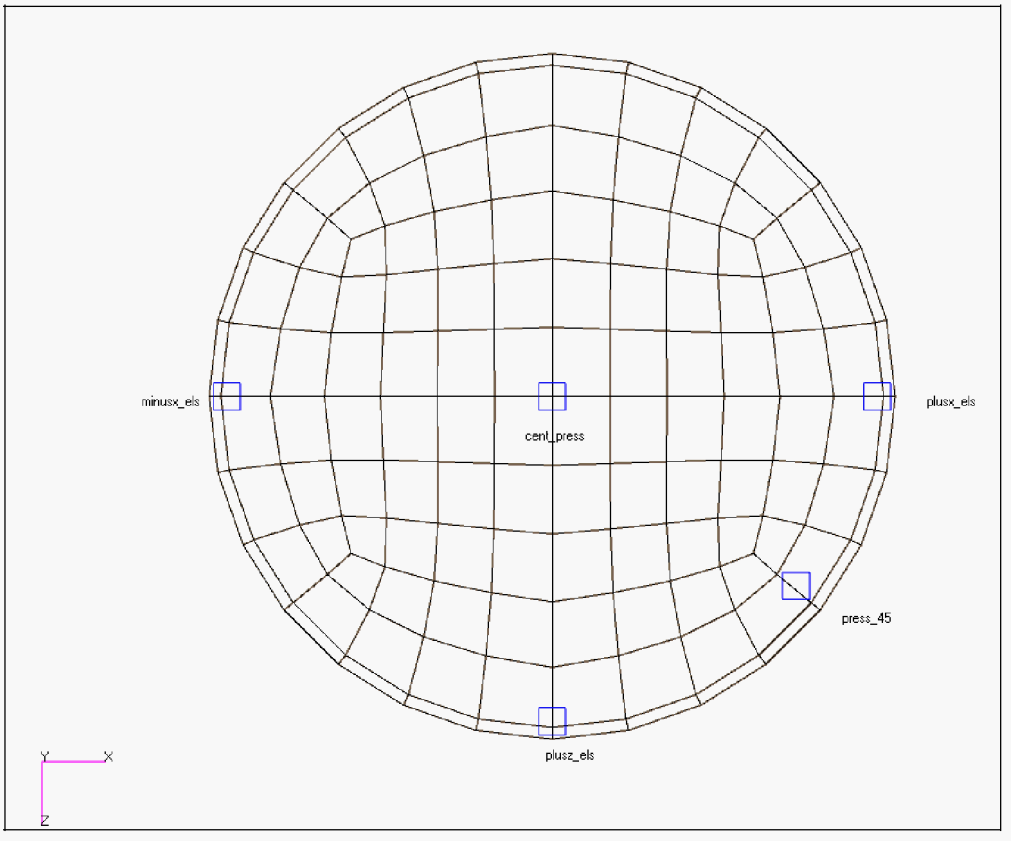

Figure 2-6. Waste Element Numbering for Element Sets "Plusx_els"," Minusx_els", and Cent_press".

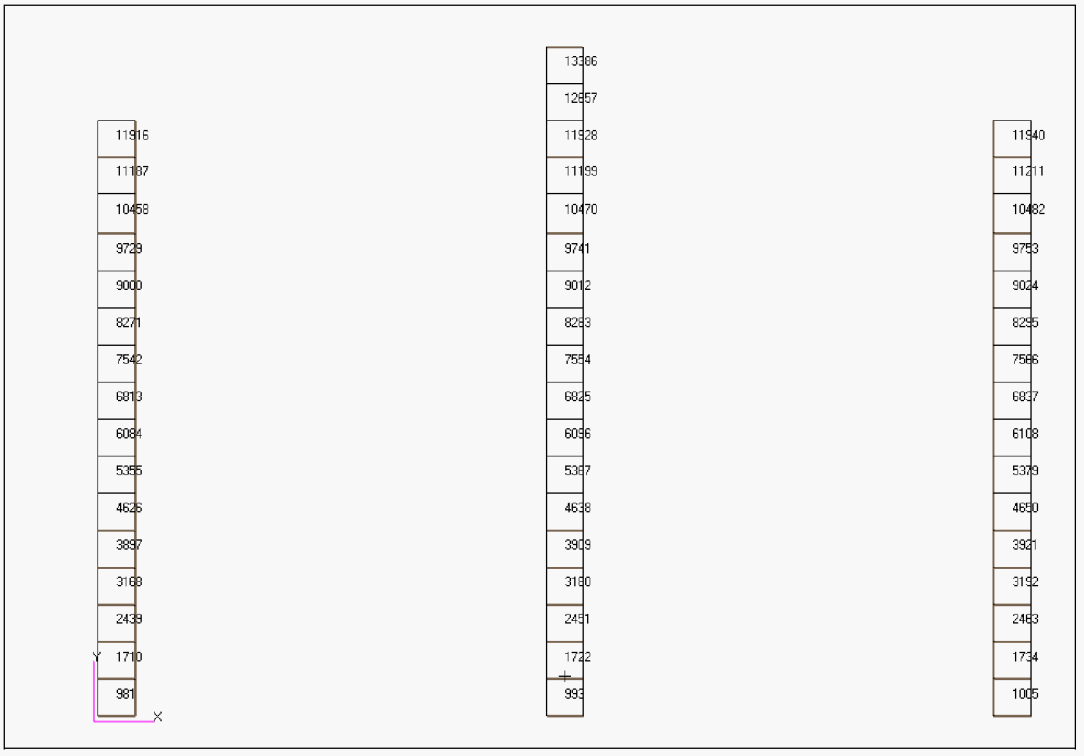

Figure 2-7. Waste Element Numbering for Element Sets "Press_45" and Plusz_els".

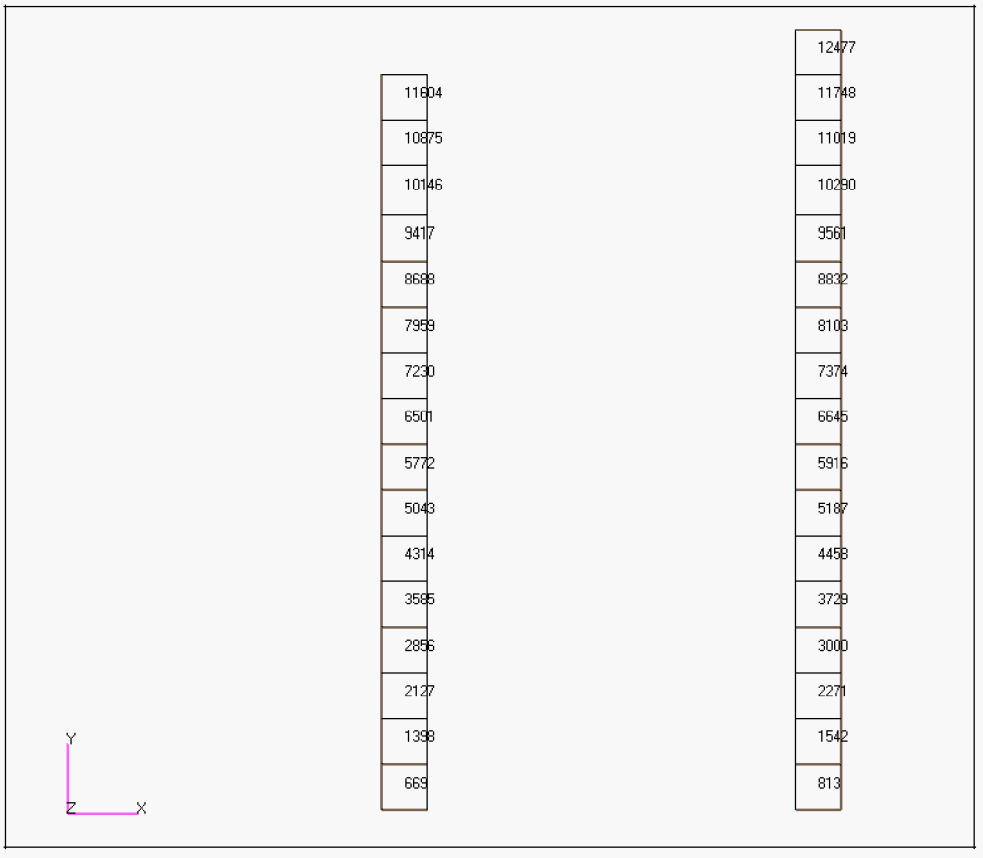

In the case of the flexible wall model, tank wall stresses were extracted at angular locations of θ=0, 45, 90, and 180°. The shell element numbering for the θ=0 and θ=90° sets is shown in Figure 2-8, with the elements at θ=0 and on the right, and the elements at θ=90° on the left. The numbering for the θ=45° and θ=180° sets is shown in Figure 2-9, with the elements at θ=45° and on the right, and the elements at θ=180° on the left.

Figure 2-8. Shell Element Numbering for Tank Wall Stress Results at θ=0 and θ=90°.

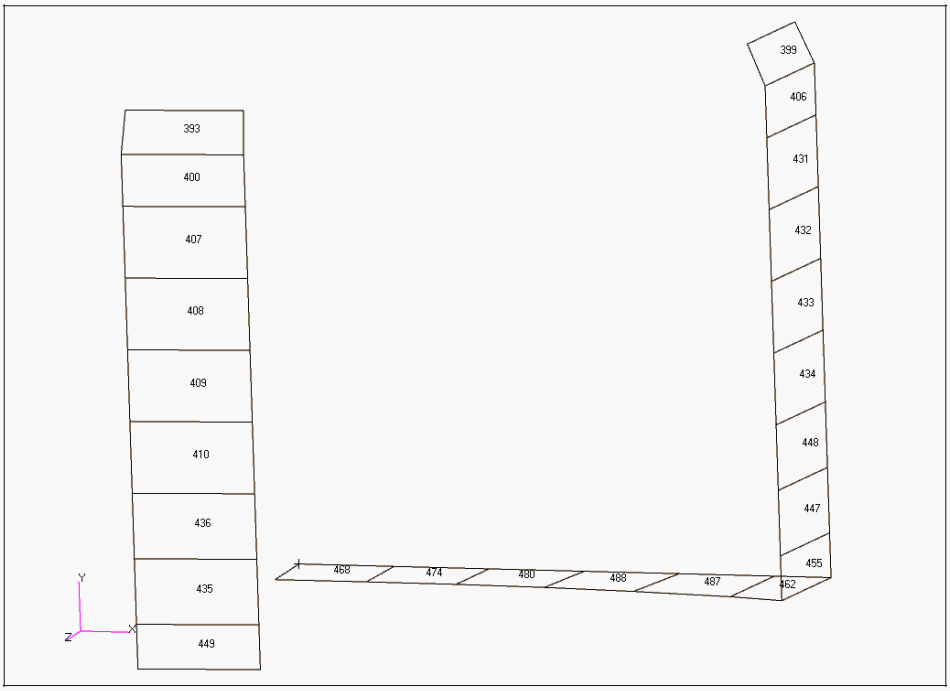

Figure 2-9. Shell Element Numbering for Tank Wall Stress Results at θ=45° and θ=180°.

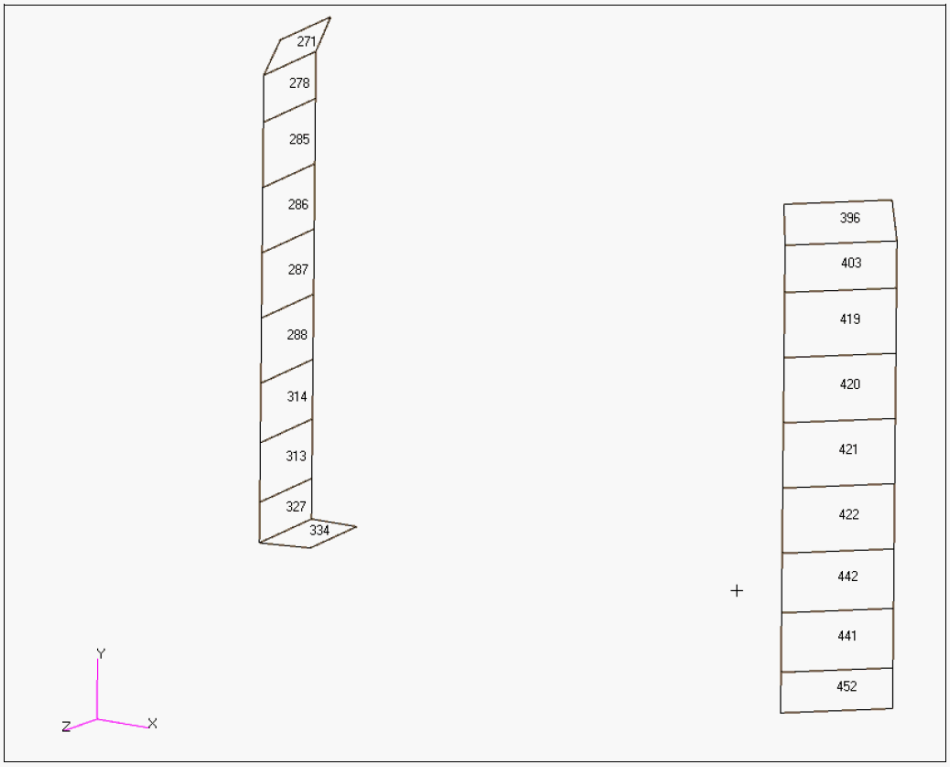

2.2 MATERIAL PROPERTIES AND ELEMENT TYPES

The tank was modeled in Dytran using CQUAD4 shell elements. In the case of the rigid tank, the complete tank was modeled as a rigid body using the "MATRIG" command. The mass of the tank was much larger than the mass of the waste to faithfully reflect the applied seismic motion.

In the case of the flexible wall tank, the elastic modulus, Poisson's ratio, and specific weight of the steel walls were set to 29 x 10^6 lbf/in^2, 0.3, and 0.284 lbf/in^3, respectively. The tank wall was assigned a thickness of 0.65 in. which is the approximate average thickness of the lower 2/3 of the AY tank wall. The uniform wall thickness was introduced to simplify the benchmarking model – it is not used for any analysis of record of the primary tank.

For the flexible wall tank, the dome was kept rigid above the primary tank tangent line, and the central portion of the primary tank bottom was also kept rigid. The outer ring of elements in the primary tank bottom was flexible, and was assigned normal steel properties. Both of the rigid regions were assigned artificially high mass density as in the completely rigid case. A section plot of the flexible tank configuration is presented in Figure 2-10 with the rigid elements shown in black, and the deformable elements shown in blue.

Figure 2-10. Section Plot of Flexible Primary Tank

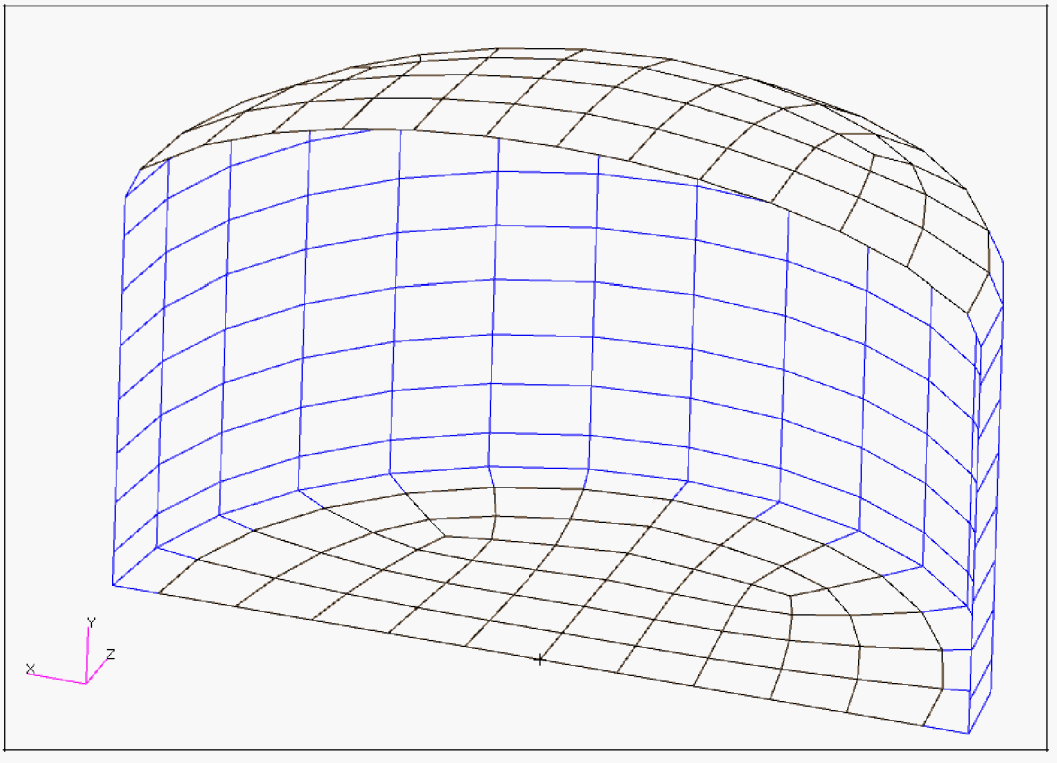

The waste and air in the dome space were modeled using 8-node CHEXA Eulerian solid elements. Because two fluids are present, the Eulerian elements were assigned multi-material hydrodynamic material properties (MMHYDRO). Both the air and the waste were modeled as homogeneous, inviscid, fluids.

The waste was modeled using a polynomial equation of state (EOSPOL) that requires the initial mass density and the bulk modulus of the fluid as input. The initial density of the waste was set to 1.59 x 10^{-4} lbf-s^2/in^4 (specific gravity=1.7) for the 422 in. waste level models and it was set to 1.71 x 10^{-4} lbf-s^2/in^4 (specific gravity=1.83) for the 460 in. waste level models. The bulk modulus of the waste was set to 305,000 lbf/in^2, which is a typical bulk modulus for water. The results are expected to be insensitive to the value of the bulk modulus since fluid compressibility is not critical to the response in this problem. Although the bulk modulus of water is realistic for this problem, scaling the bulk modulus down over several orders of magnitude can be an effective solution technique to reduce computer run time without unduly affecting the solution of problems where compressibility is not critical.

The air was modeled using the gamma law equation of state (EOSGAM), where the pressure is a function of the density ρ, the specific internal energy per unit mass e, and the ideal gas ratio of specific heats γ via $p = (\gamma - 1)\rho e$. The mass density of air is 1.167 x 10^{-7} lbf-s^2/in^4, and the ratio of constant-pressure specific heat to constant-volume specific heat is 1.4. The specific internal energy per unit mass of the air was set to 3.15 x 10^8 in^2/s^2 for the absolute pressure simulations, and zero for gage pressure simulations. The internal energy for the absolute pressure simulations corresponds to an air pressure of 14.7 lbf/in^2.

2.3 BOUNDARY CONDITIONS

In the case of horizontal seismic excitation, the rigid regions were free in the x-direction, and fixed in the other five degrees-of-freedom. For vertical excitation, the rigid regions were free in the vertical direction, and fixed in the other five degrees-of-freedom.

The Dytran general coupling algorithm was used to allow the Eulerian waste mesh to interact with the Lagrangian structural mesh. The problem was set up to take advantage of the "fast coupling" option in Dytran.

2.4 INITIAL CONDITIONS

Generally, it is preferable to run at absolute pressure to avoid any difficulties associated with dynamic pressures exceeding static pressures and total pressures becoming negative.

Earlier in the project, runs were performed at gage pressure simply because it was more difficult to achieve stable solutions when running at absolute pressure. For the most part, those issues were resolved, and stable solutions are now achieved using either method in

most cases. For the remainder of the report, the emphasis will be on absolute pressure results.

The results from the absolute pressure runs are presented in the body of the report. Selected results are included in the body of the report that show the comparison between absolute and gage pressure results. The results from other gage pressure runs are included as background information in electronic format on the accompanying DVD, however, those results do not have a direct bearing on the analysis.

The changes required to run at absolute pressure are to set the atmospheric pressure to 14.7 lbf/in^2 in the parameters section of the input file, and set the specific internal energy per unit mass of the air to 3.15 x 10^8 in^2/s^2 according to the gamma law equation of state

$$e = \frac{p}{(\gamma - 1)\rho}.$$

As a convenience, a balancing pressure of 14.7 lbf/in^2 was applied to the outside of the tank using the Dytran COUOPT command (MSC 2005b) to keep the tank stresses in terms of gage pressures.

2.5 SEISMIC INPUT

The seismic time histories used to excite the tank model were output from a more complete linear ANSYS model of the DST and surrounding soil shown in Figure 2-11, Figure 2-12, and Figure 2-13. The horizontal time history was taken from the dome apex of the ANSYS model, and the vertical time history was taken from the haunch region 90° from the direction of horizontal excitation to minimize rocking effects. The ANSYS model was subjected to simultaneous horizontal and vertical seismic excitation in the absence of gravity. The seismic input for the ANSYS model was applied at the base of the far-field soil shown in Figure 2-13. The extracted time histories consisted of 2,048 points defined at 0.01 s intervals giving seismic records with durations of 20.48 s.

Figure 2-11. ANSYS Composite Tank Model Detail

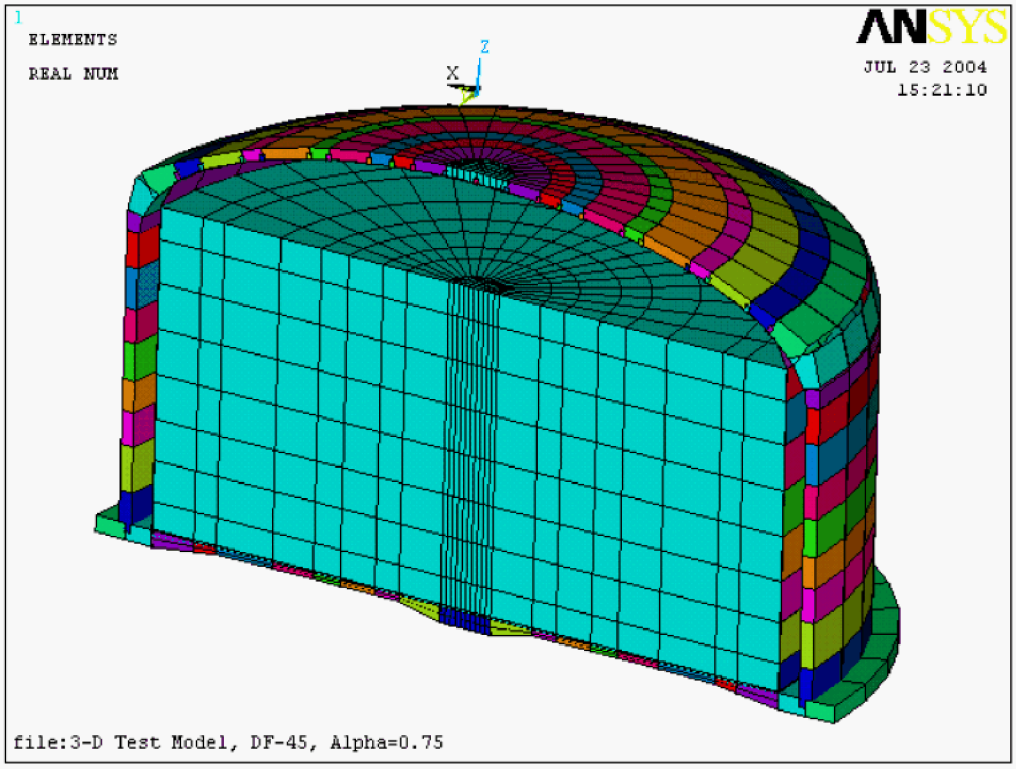

Figure 2-12. Excavated Soil Model Detail for Global ANSYS Model.

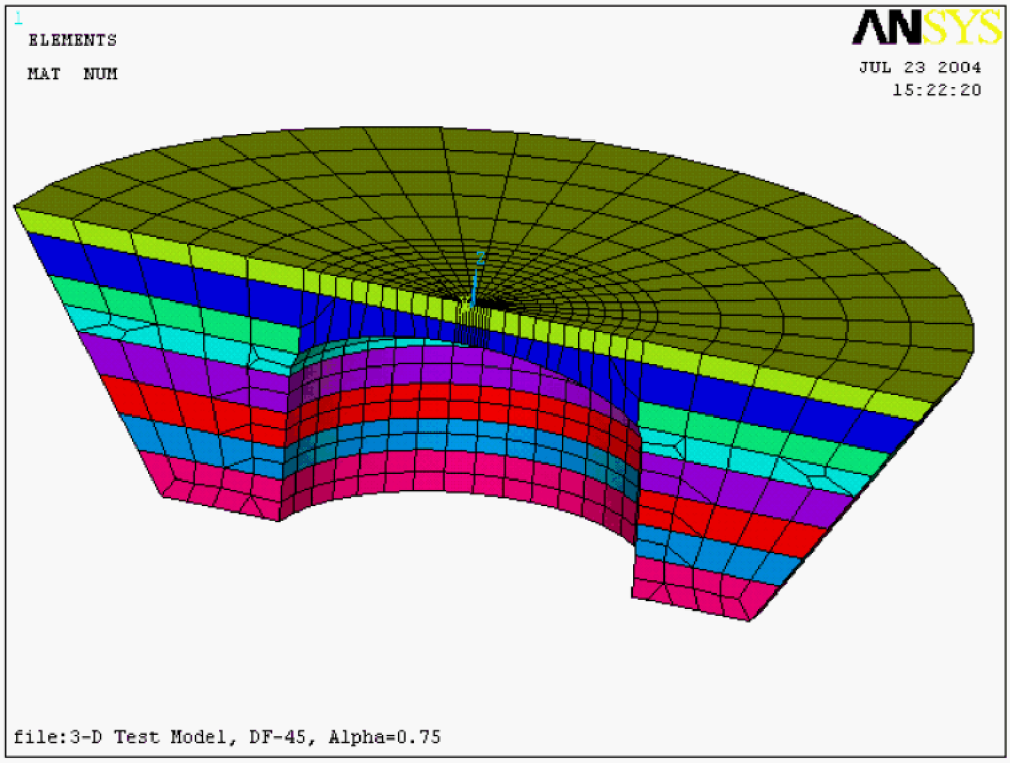

Figure 2-13. Far-Field Soil Model Detail for Global ANSYS Model.

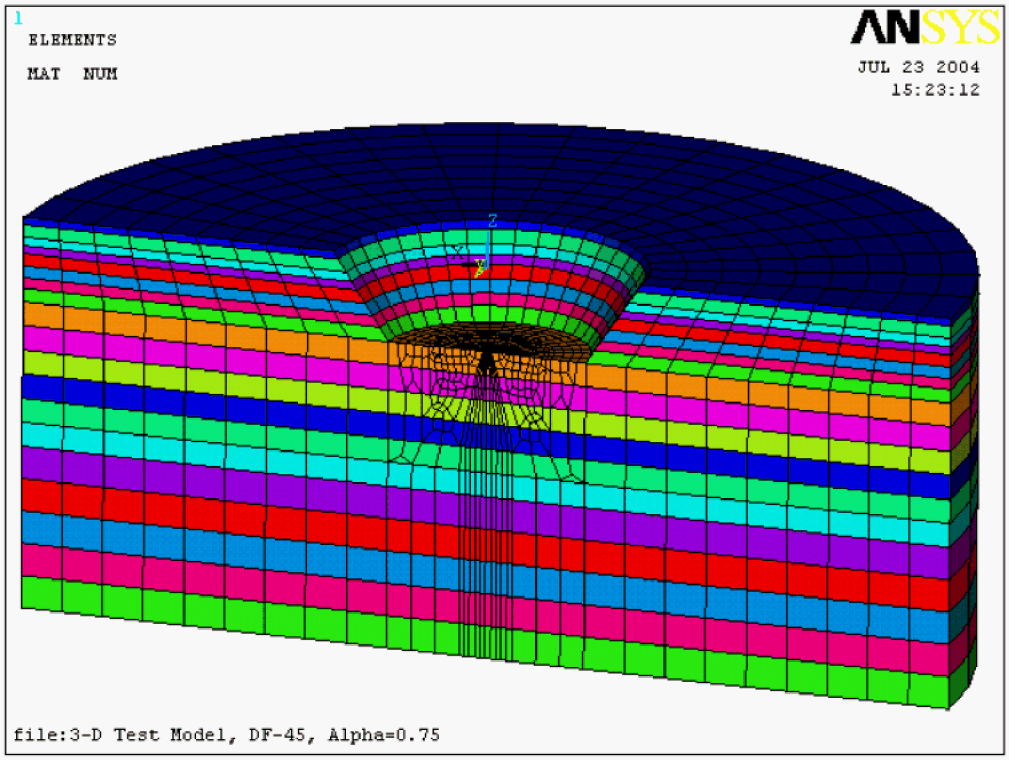

For the completely rigid tank, the whole tank was subjected to the seismic motion. In the flexible tank configuration, the rigid dome and rigid central portion of the tank bottom were subjected to the same input simultaneously. This represents the hinged top boundary condition discussed in BNL 1995 and shown in Figure 2-14.

Figure 2-14. Tank With Hinged Top Boundary Condition per BNL 1995.

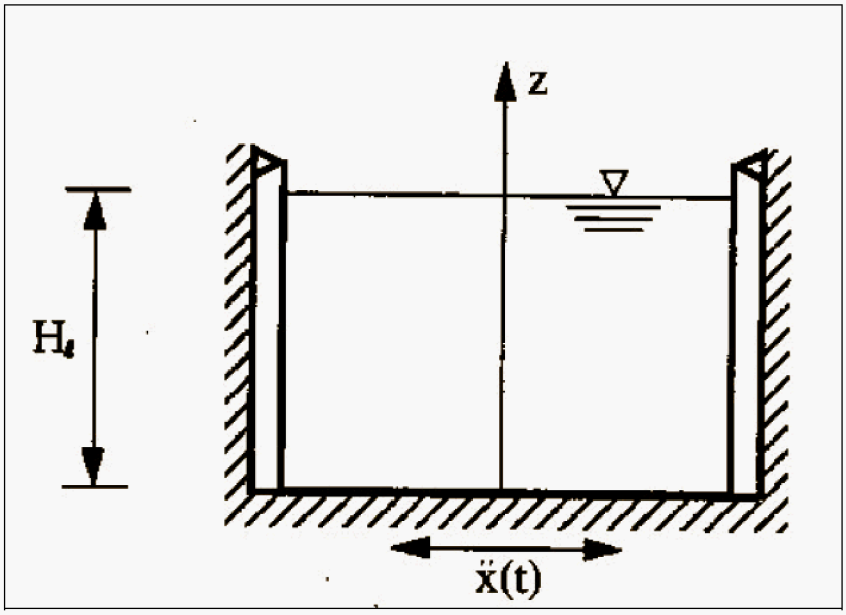

In the case of horizontal (x-direction) excitation, the seismic time histories were applied to both the rigid and flexible tank Dytran models as body force accelerations per unit mass on the nodes of the rigid portions of the tank that have artificially high mass. The vertical seismic time history was applied as a velocity time history to the rigid portions of the tank. The reason that the vertical input was applied as a velocity rather than an acceleration time history is that this approach prevents having to exactly balance the vertical gravity load with the vertical acceleration time history, thus preventing any vertical drift.

The horizontal acceleration, vertical acceleration, and the velocity and displacement time histories for horizontal and vertical input are shown in Figure 2-15, Figure 2-16, Figure 2-17, and Figure 2-18, respectively. The 4% damped response spectra for the horizontal and vertical time histories are shown in Figure 2-19. A comparison of horizontal response spectra at damping values of 0.5% and 4%, is shown in Figure 2-20 and Figure 2-21, respectively. The plots in Figure 2-21 show that the spectral acceleration near the first convective frequency of approximately 0.2 Hz is 20% greater at 0.5% damping than at 4% damping. That is, in this range of damping values, the convective response is not highly sensitive to damping. The spectra for 0.5% and 4% critical damping are of particular interest because these are the target effective damping for the convective and impulsive response of the tank and waste according to DOE-STD-1020-2002.

Figure 2-15. Horizontal Acceleration Time History Output from ANSYS Model.

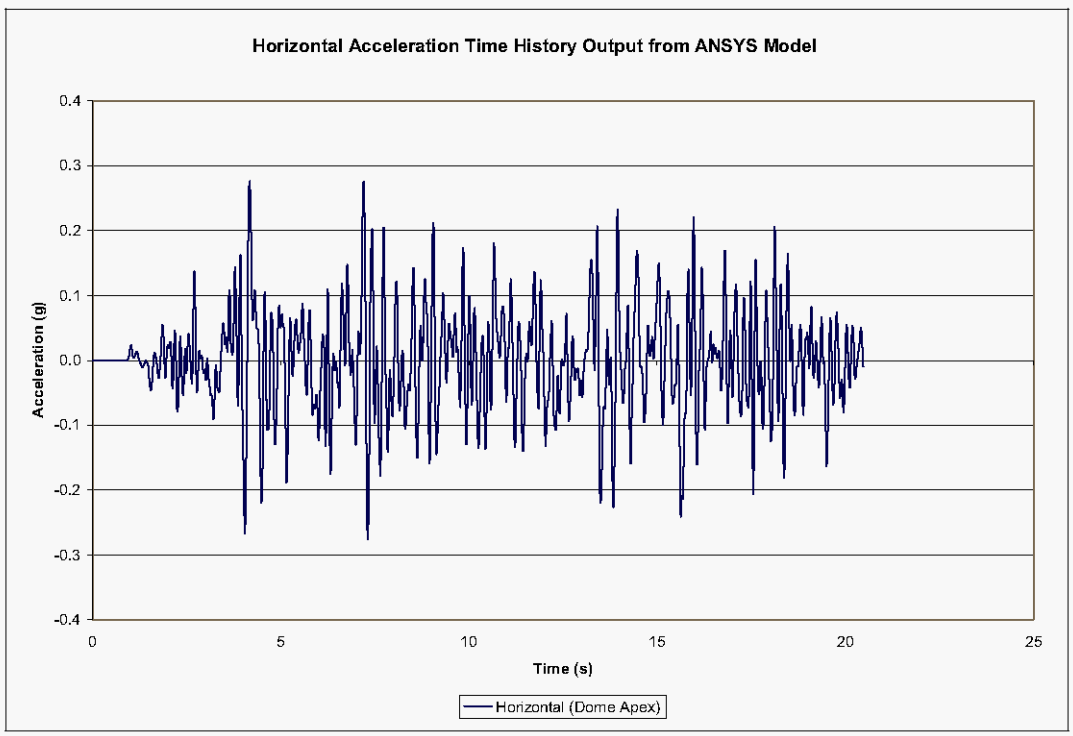

Figure 2-16. Vertical Acceleration Time History Output from ANSYS Model.

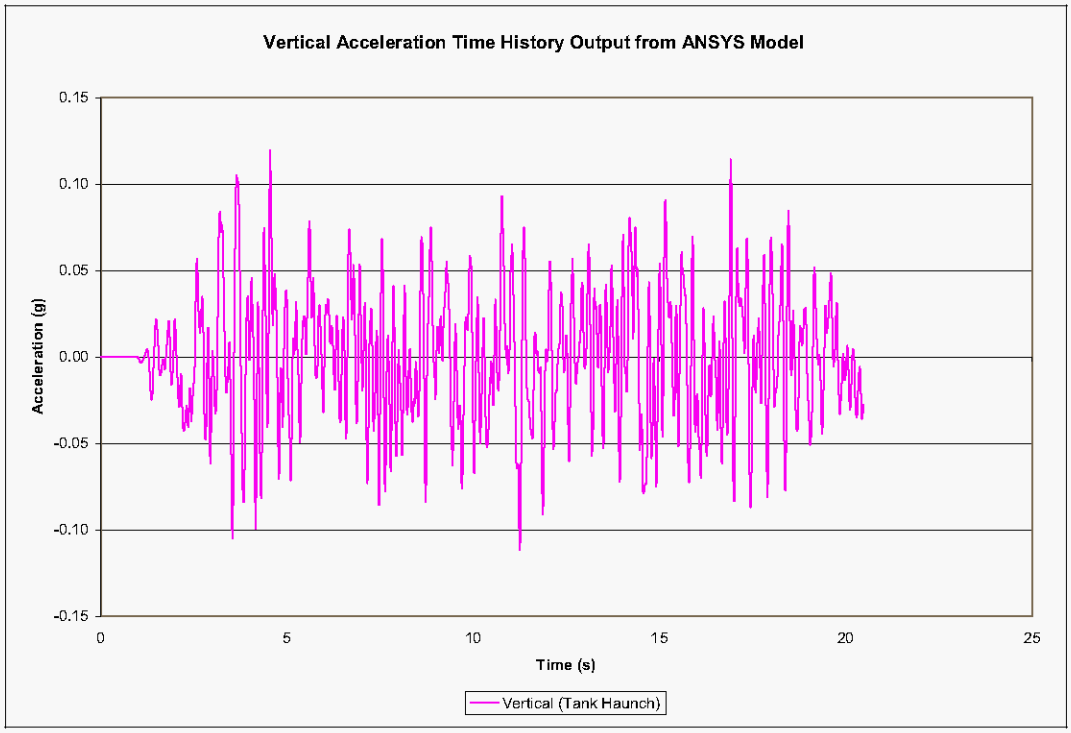

Figure 2-17. Velocity Time Histories Output from ANSYS Model.

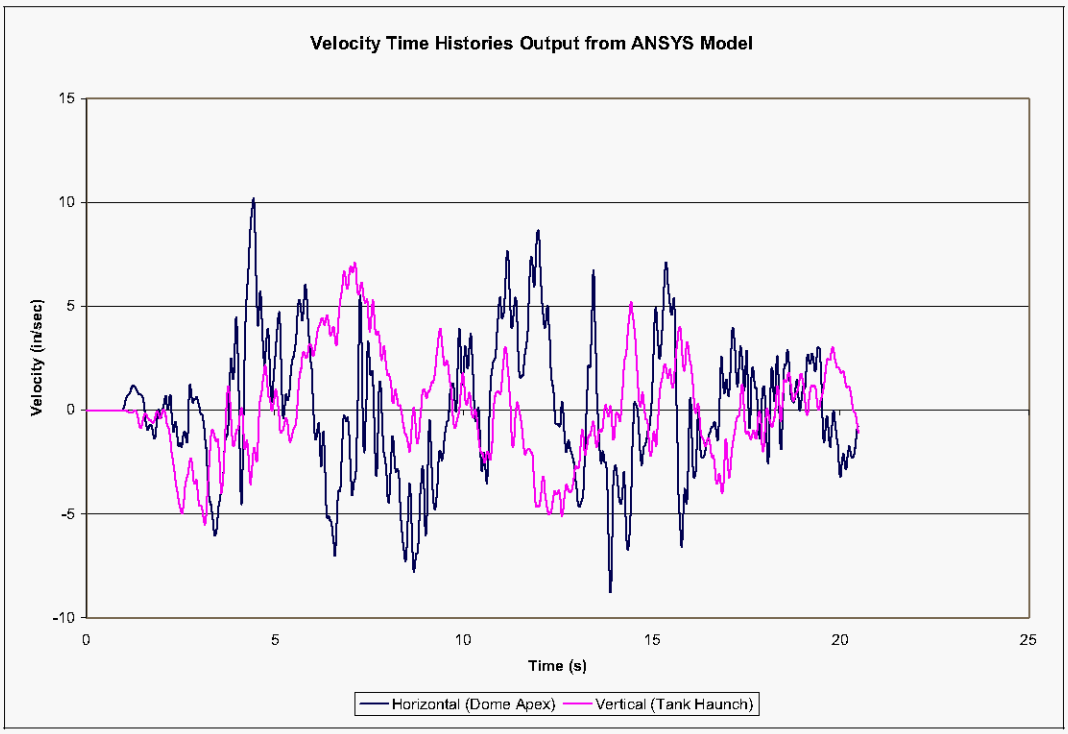

Figure 2-18. Displacement Time Histories Output from ANSYS Model.

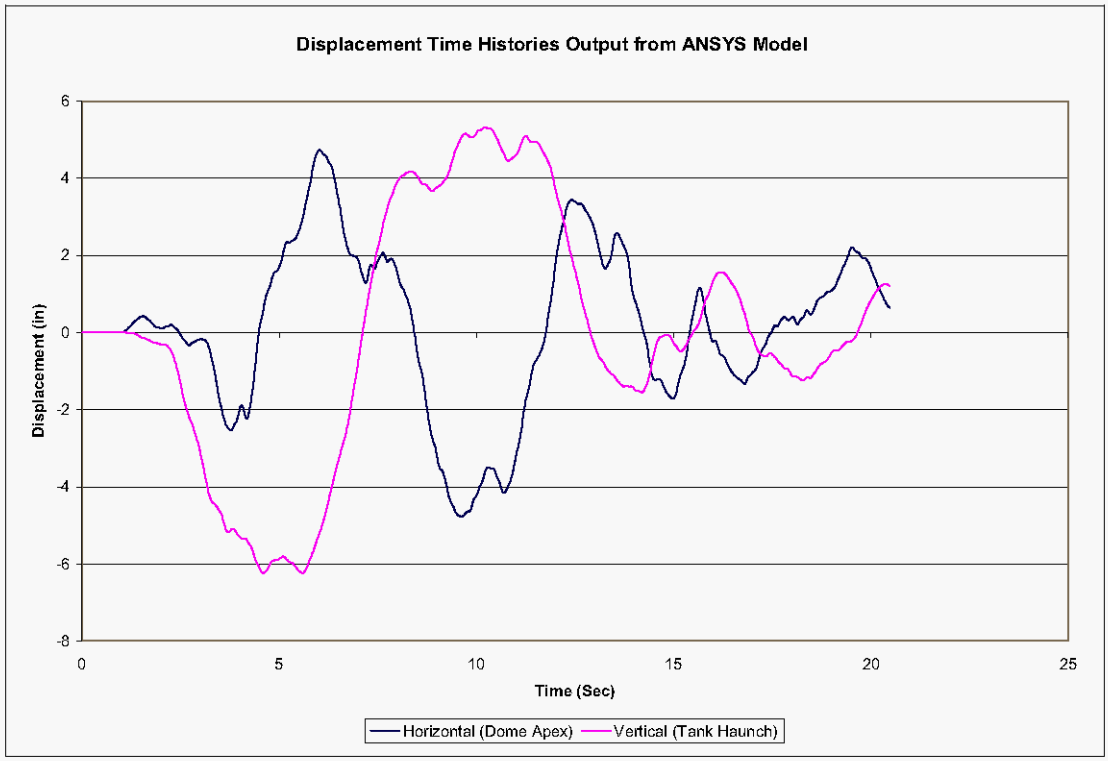

Figure 2-19. 4% Damped Response Spectra for Acceleration Time Histories Extracted from ANSYS Model.

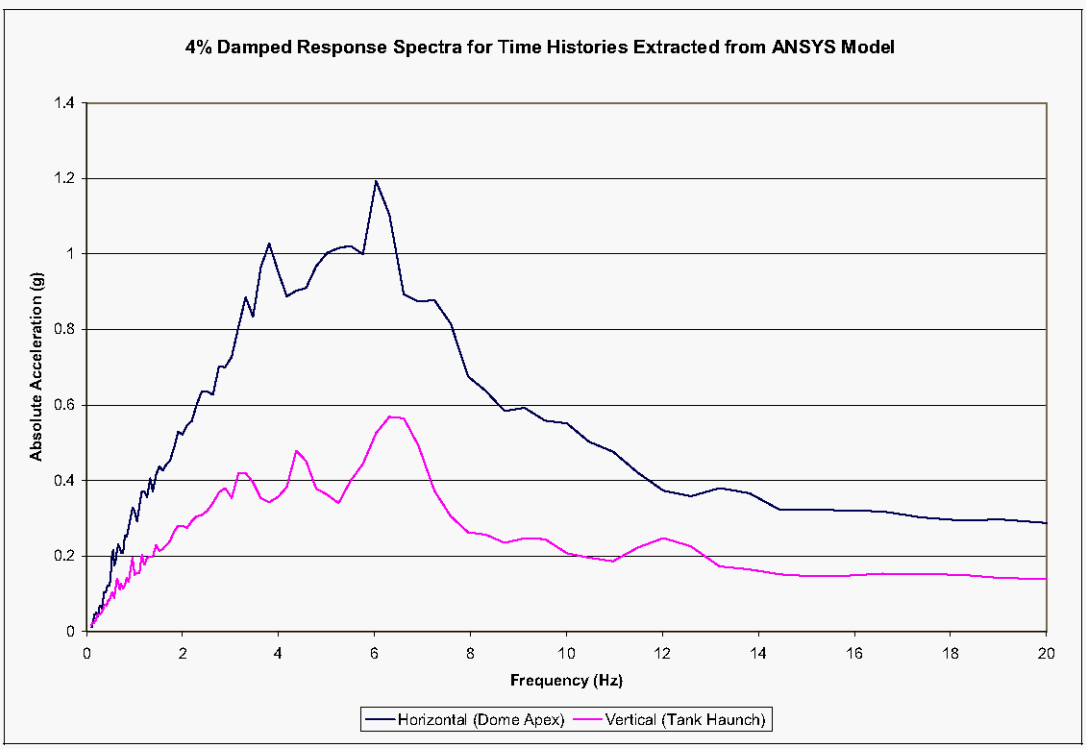

Figure 2-20. Comparison of Horizontal Dome Apex Response Spectra at Different Damping Values.

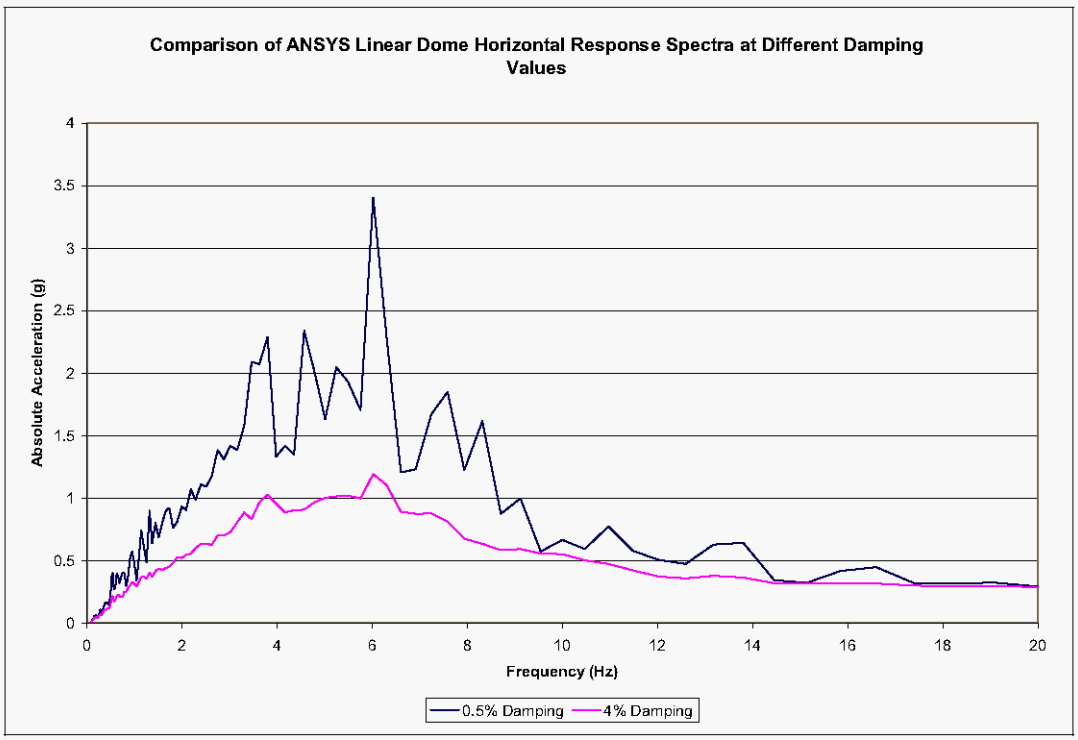

Figure 2-21. Comparison of Horizontal Dome Apex Response Spectra at Different Damping Values for Low Frequencies.

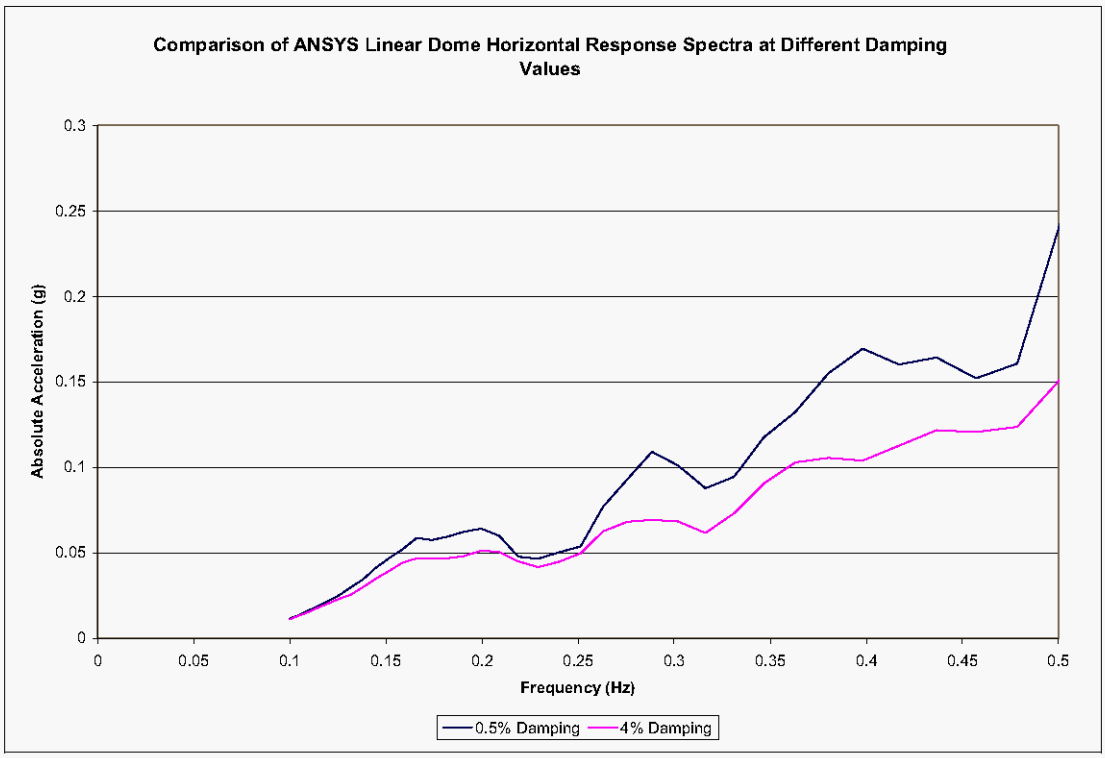

3.0 RIGID DYTRAN MODEL AT 422 INCH WASTE LEVEL

The expected hydrostatic pressure at the centroid of the waste elements is easily calculated knowing the vertical location of the waste elements and the initial pressure using the equation $p = p_0 + \rho g \Delta h$, where p_0 is the ambient pressure at the free surface. The expected hydrostatic pressures for the element sets "plusx_els", "press_45", and "plusz_els" are shown in Table 3-1.

Table 3-1. Expected Hydrostatic Pressure of Waste Elements

"Plusx_els" Element No.	"Press_45" Element No.	"Plusz_els" Element No.	Hydrostatic Pressure (psi absolute)
10482	10290	10146	14.7
9753	9561	9417	15.8
9024	8832	8688	18.0
8295	8103	7959	20.1
7566	7374	7230	22.3
6837	6645	6501	24.5
6108	5916	5772	26.7
5379	5187	5043	28.8
4650	4458	4314	31.0
3921	3729	3585	33.2
3192	3000	2856	35.4
2463	2271	2127	37.5
1734	1542	1398	39.7

In the case of horizontal excitation, the gravity load was run for 5 s before beginning the seismic input. The 20.48 s seismic record was followed by 20 s of unforced motion with gravity loading. For vertical excitation, the gravity load was run for 2 s before beginning the seismic input. The 20.48 s seismic record was followed by 20 s of unforced motion with gravity loading.

The problem was originally run at gage pressure, but all results reported are from subsequent runs made at absolute pressure.

3.1 HYDRODYNAMIC FORCES

Dytran provides output of the overall reaction forces between the Euler elements (fluid elements) and the coupling surface that is the interface between the fluid elements and the structural elements. The coupling surface reaction forces are compared to the total hydrodynamic forces calculated using the methodology described in BNL 1995 and shown in Appendix B.

3.1.1 Horizontal Excitation

The peak hydrodynamic force induced against the tank wall due to horizontal excitation can be calculated via Equation 4.31 of BNL 1995 with the instantaneous accelerations replaced by the appropriate spectral accelerations. If the contributions of the impulsive mode and first three convective modes are combined in a square-root-sum-of-squares (SRSS) fashion, the theoretical maximum horizontal hydrodynamic force is 2.42×10^6 lbf, based on a zero-period acceleration for the impulsive response, and convective accelerations from the 0.5% damped spectrum. The coupling surface reaction force time histories reported by Dytran for horizontal excitation are shown in Figure 3-1. The peak reaction force is 2.45×10^6 lbf, which is approximately 1% greater than the predicted value. A plot of the horizontal reaction force is shown in Figure 3-2.

Although the total horizontal hydrodynamic force is slightly greater than predicted by theory, the convective contribution is less than predicted by theory. The theoretical peak reaction force due to the first three convective modes only is 4.62×10^5 lbf. The Dytran calculated convective component of the horizontal reaction force during the free vibration phase following the seismic excitation appears as Figure 3-2. The peak reaction force due to the convective response is approximately 3×10^5 lbf or 65% of the theoretical value, if only the long-period first mode response is considered. Also apparent in the free vibration response is the period of the first convective mode. The period shown in Figure 3-1 during the free vibration phase is approximately 5.25 s, which matches the theoretical fundamental convective frequency of 0.19 Hz.

The theoretical solution for the rigid tank is for an open tank with vertical walls. The rigid tank modeled in Dytran nearly reflects that configuration, but not exactly. It can be seen from Figure 2-3 that the initial waste level corresponds to the top of the vertical wall. The next structural element up the tank begins to reflect the dome curvature to a mild degree, and the expected slosh height is less than height of this next row of elements. However, this is a slightly different configuration than represented by the theoretical solution. It may be that the beginning of the dome curvature has the effect of inhibiting the convective response and increasing the impulsive response, and may account for the difference in the two solutions. This behavior will be seen clearly when results from the simulations at the 460 in. waste level are presented.

Figure 3-1. Coupling Surface Reaction Forces for the Rigid Tank at 422 in. Waste Level Under Horizontal Seismic Input.

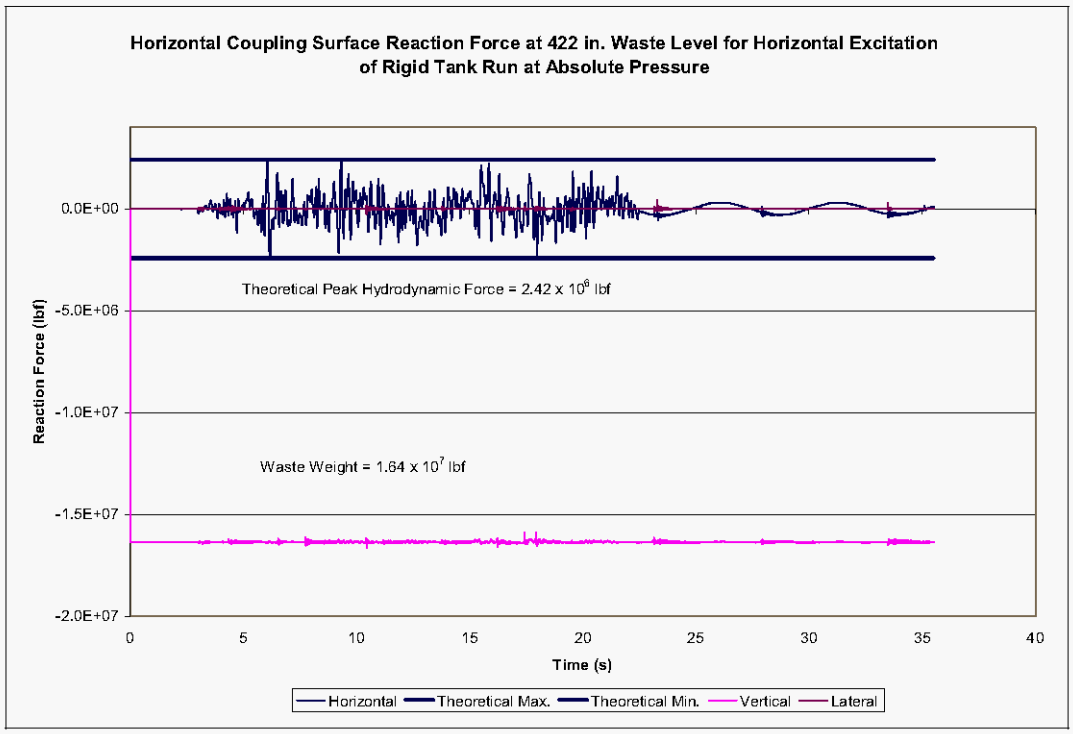

Figure 3-2. Horizontal Coupling Surface Reaction Force for the Rigid Tank at 422 in. Waste Level Under Horizontal Seismic Input.

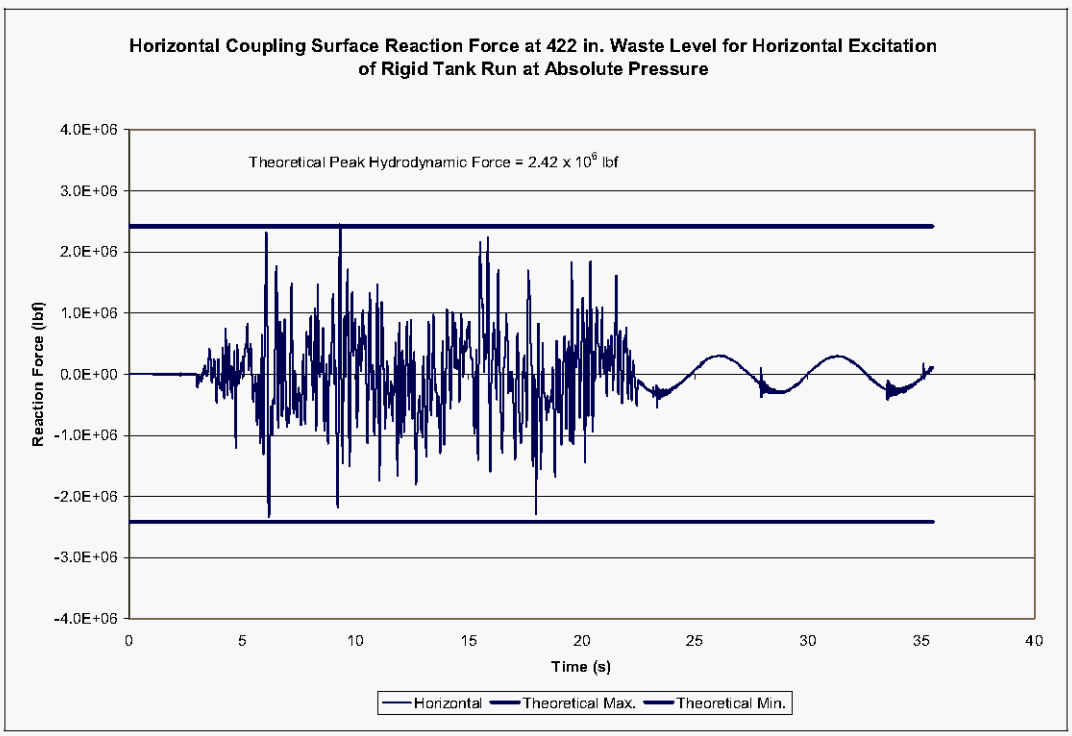

Figure 3-3. Horizontal Coupling Surface Reaction Force for Rigid Tank at 422 in. Waste Level Under Horizontal Seismic Excitation – Convective Response.

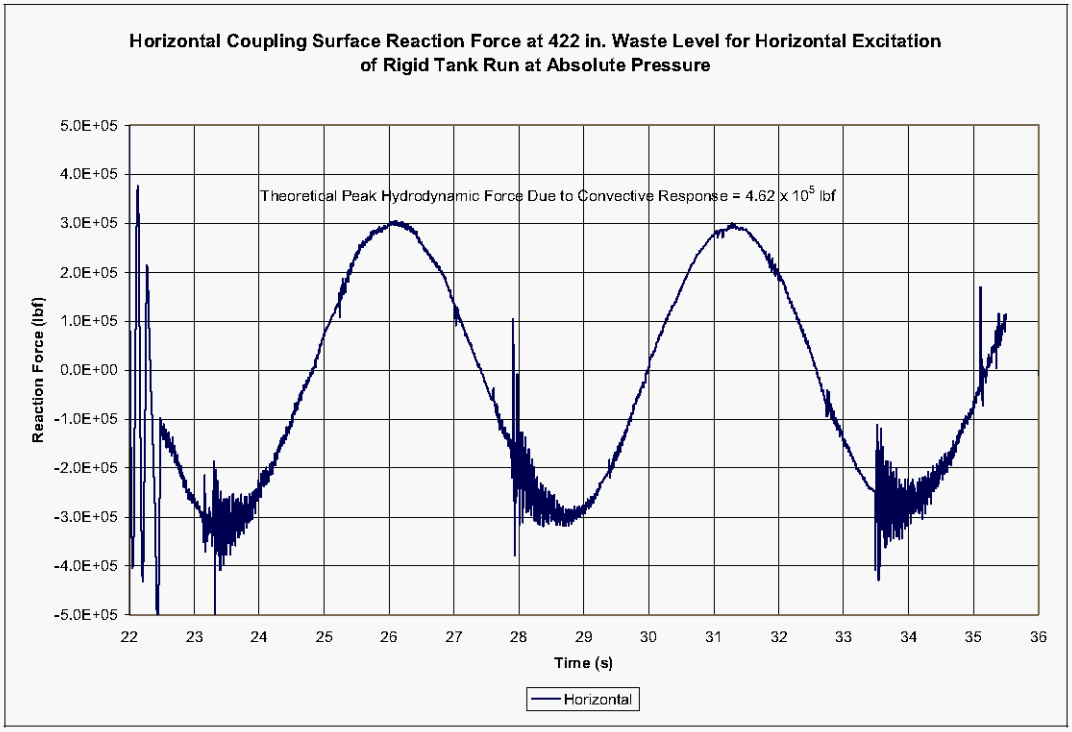

3.1.2 Vertical Excitation

Under vertical seismic excitation, the peak vertical hydrodynamic force for a rigid tank is simply the product of the waste mass and the peak acceleration. Given the waste mass of 4.23×10^4 lbf-s^2/in, and the vertical zero period acceleration of 0.12g (shown in the vertical acceleration time history in Figure 2-15), the peak vertical hydrodynamic base force is 1.96×10^6 lbf. The coupling surface reaction force shown in Figure 3-4 is slightly greater than predicted by theory with the peak hydrodynamic force of 2.15×10^6 lbf. The spike in the vertical reaction force at 22.5 s is due to the final point in the vertical velocity time history being zero, bringing the tank to a sudden stop.

Figure 3-4. Coupling Surface Reaction Forces for Rigid Tank at 422 in. Waste Level Under Vertical Seismic Input.

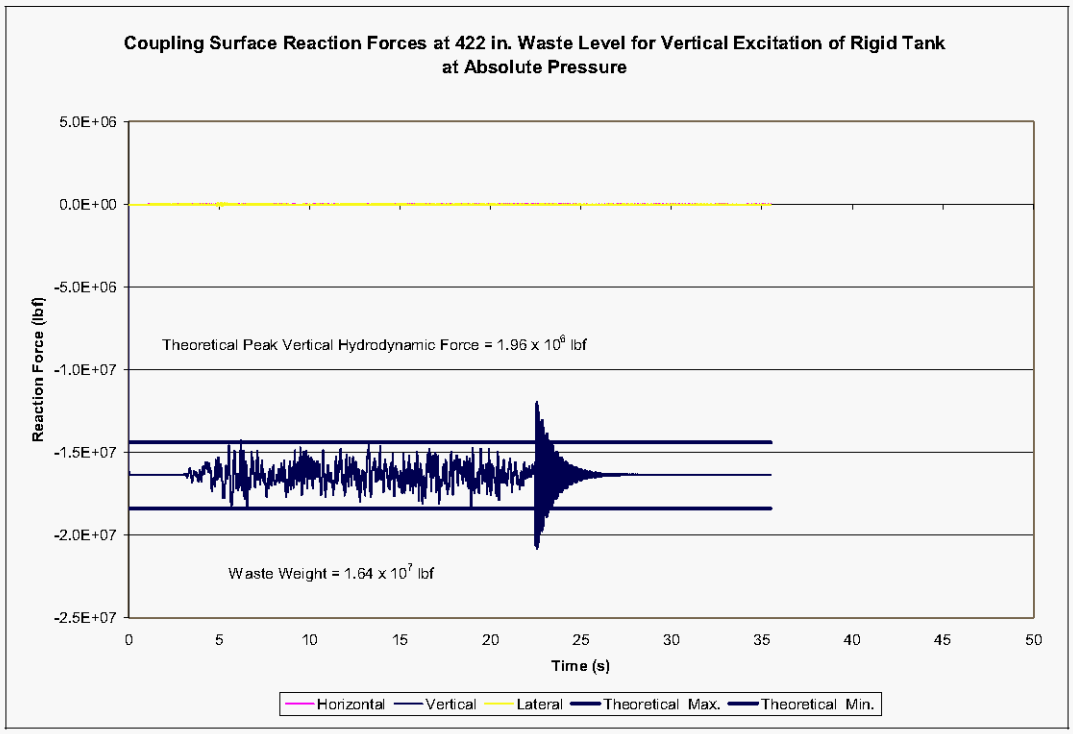

Figure 3-5. Vertical Coupling Surface Reaction Force for Rigid Tank at 422 in. Waste Level Under Vertical Seismic Input.

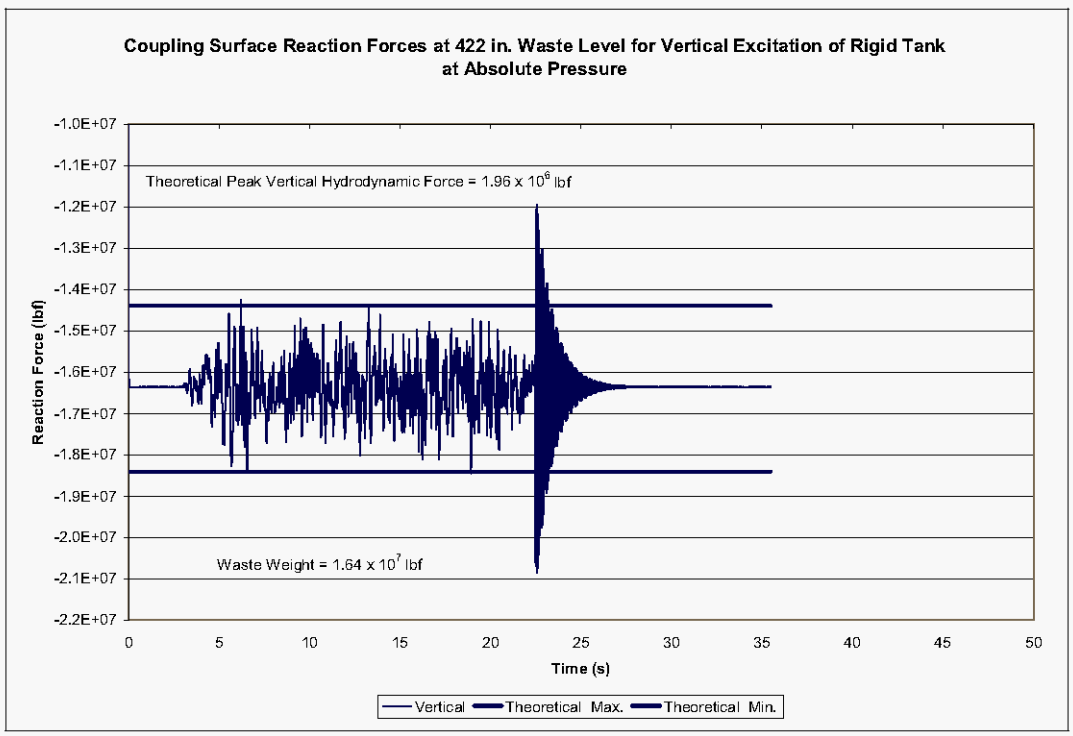

3.2 WASTE PRESSURES

3.2.1 Horizontal Excitation Run at Absolute Pressure

The hydrodynamic pressures in the tank are caused by impulsive and convective components and depend on the location of the fluid element within the tank. In the case of horizontal excitation, both the impulsive and convective components vary in the circumferential direction as $\cos\theta$, with the maximum theoretical values occurring along the plane of excitation, and decreasing to zero hydrodynamic pressure at $\theta=90°$ to the plane of excitation. The impulsive hydrodynamic pressure increases with depth, while the convective dynamic pressure is a maximum at the top of the waste. The theoretical peak hydrodynamic pressures are given by Equation 4.24 of BNL 1995, and the total pressures are the sum of the hydrostatic pressures and the hydrodynamic pressures. The hydrostatic, peak hydrodynamic and peak total pressures for the elements in the sets "plusx_els", "press_45", are shown in Table 3-2 and Table 3-3. The maximum theoretical pressures for the elements set "plusz_els" is simply the hydrostatic pressures shown in Table 3-1 because the theoretical hydrodynamic pressures are zero at $\theta=90°$. The pressure time histories for the waste element sets at $\theta=0$, 45, and 90°, are shown in Figure 3-6, Figure 3-8, and Figure 3-9.

Table 3-2. Theoretical Maximum Waste Pressures for Horizontal Excitation in the Rigid Tank at 422 in. Waste Level for Elements at θ=0 Run at Absolute Pressure.

"Plusx_els" Element No.	Hydrostatic Pressure (psi absolute)	Peak Hydrodynamic Pressure (psi absolute)	Peak Total Pressure (psi absolute)
10482	14.7	0	14.7
9753	15.8	1.7	17.5
9024	18.0	2.4	20.3
8295	20.1	3.0	23.1
7566	22.3	3.6	25.9
6837	24.5	4.0	28.5
6108	26.7	4.4	31.1
5379	28.8	4.7	33.6
4650	31.0	5.0	36.0
3921	33.2	5.2	38.3
3192	35.4	5.3	40.7
2463	37.5	5.4	42.9
1734	39.7	5.4	45.1

Table 3-3. Theoretical Maximum Waste Pressures for Horizontal Excitation in the Rigid Tank at 422 in. Waste Level for Elements at θ=45° Run at Absolute Pressure.

"Press_45" Element No.	Hydrostatic Pressure (psi absolute)	Peak Hydrodynamic Pressure (psi absolute)	Peak Total Pressure (psi absolute)
10290	14.7	0	14.7
9561	15.8	1.2	17.0
8832	18.0	1.7	19.6
8103	20.1	2.1	22.2
7374	22.3	2.5	24.8
6645	24.5	2.8	27.3
5916	26.7	3.1	29.8
5187	28.8	3.3	32.2
4458	31.0	3.5	34.5
3729	33.2	3.7	36.8
3000	35.4	3.8	39.1
2271	37.5	3.8	41.3
1542	39.7	3.9	43.5

Figure 3-6. Waste Pressure Time Histories for the Rigid Tank With 422 in. of Waste Under Horizontal Excitation at θ=0 Run at Absolute Pressure.

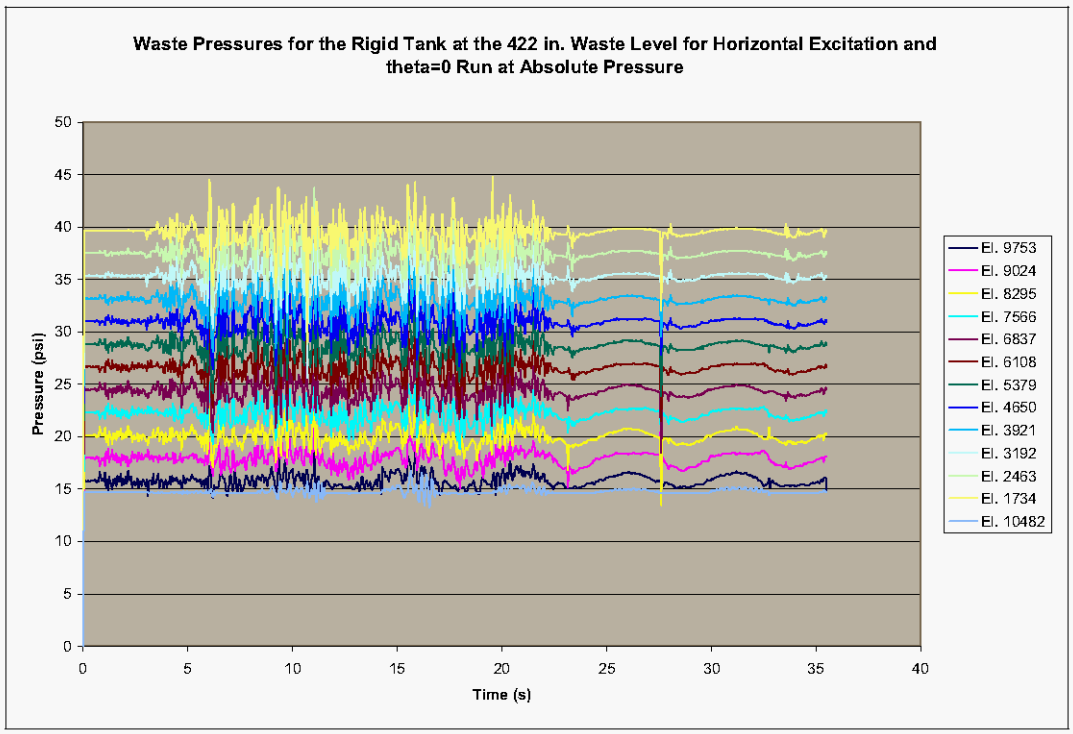

Figure 3-7. Selected Waste Pressure Time Histories for the Rigid Tank With 422 in. of Waste Under Horizontal Excitation at θ=0 Run at Absolute Pressure.

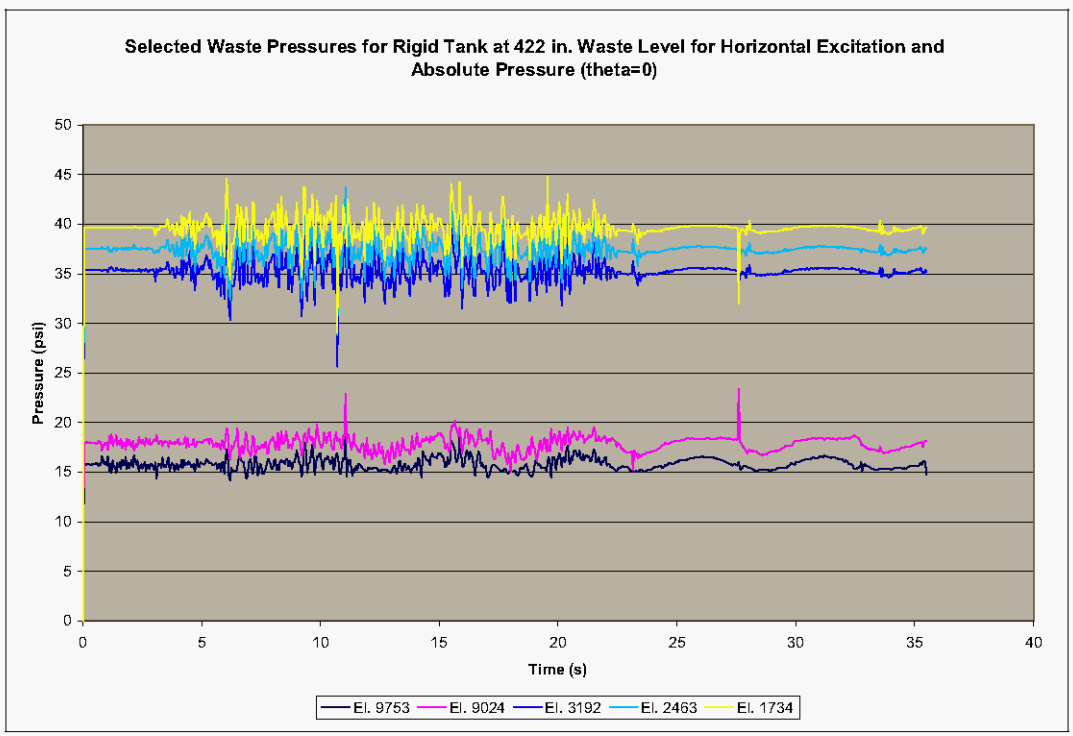

Figure 3-8. Waste Pressure Time Histories for the Rigid Tank With 422 in. of Waste Under Horizontal Excitation at θ=45° Run at Absolute Pressure.

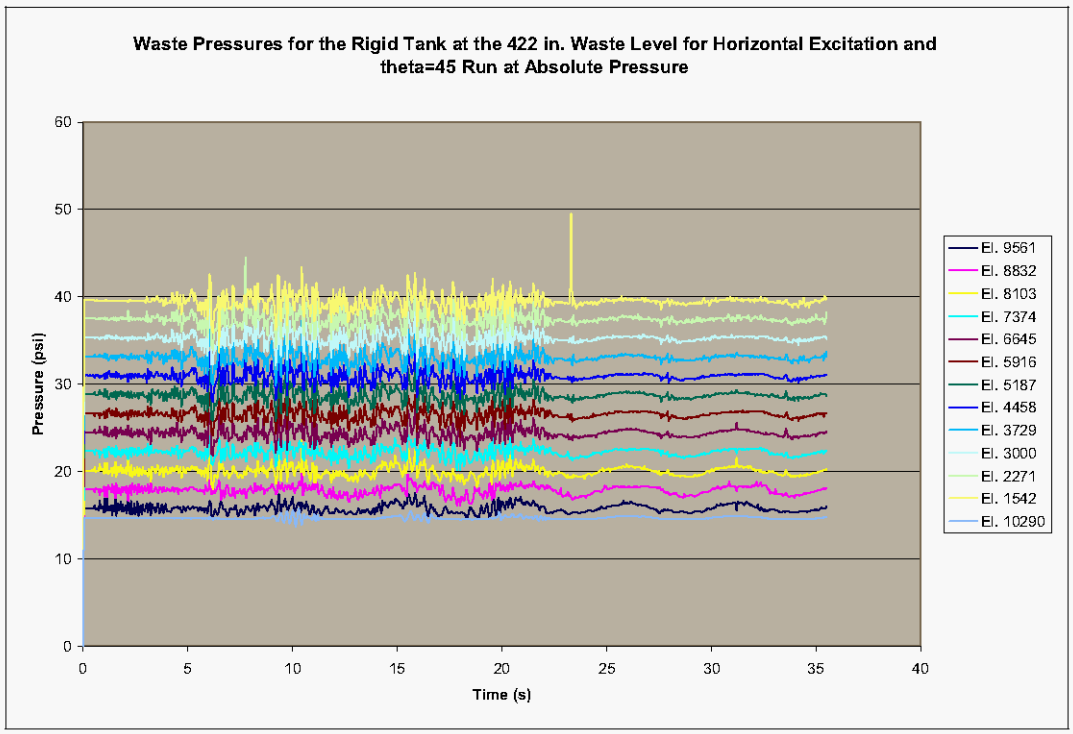

Figure 3-9. Waste Pressure Time Histories for the Rigid Tank With 422 in. of Waste Under Horizontal Excitation at θ=90° Run at Absolute Pressure.

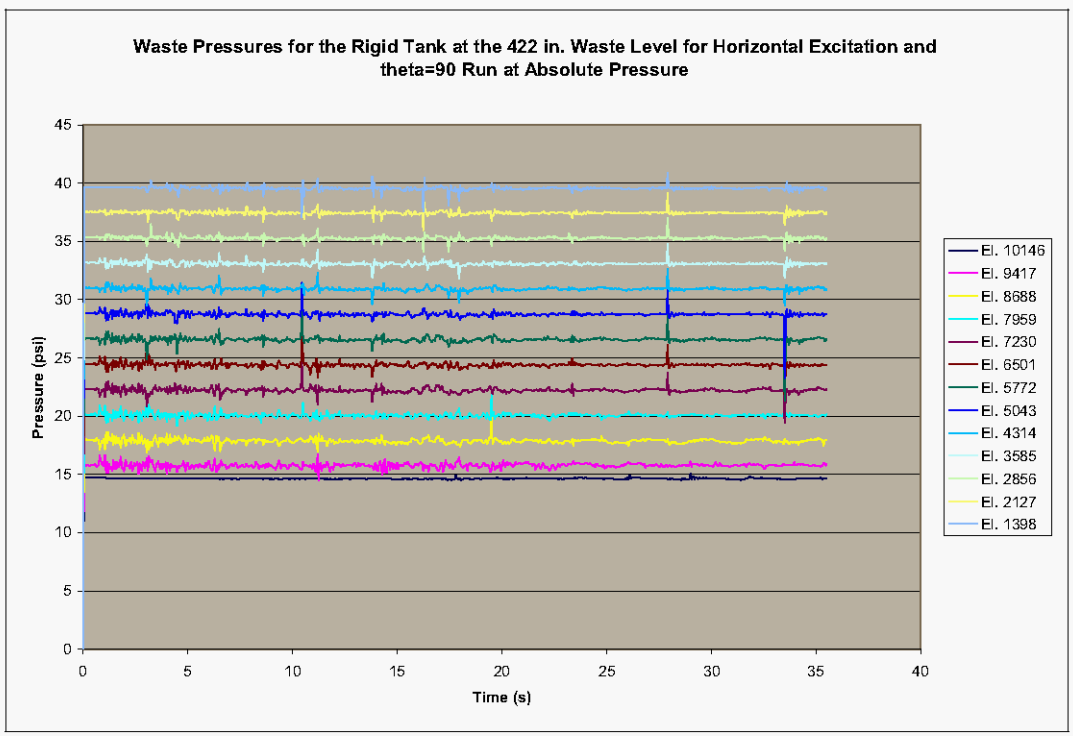

Another way of presenting some of the information in the previous plots is to look at maximum and minimum pressures as a function of angular position and waste depth. Plots of the actual (as calculated by Dytran – hereafter referred to as "actual") and theoretical maximum and minimum waste pressures at θ=0, 45, and 90° are shown in Figure 3-10, Figure 3-11, and Figure 3-12. The lower than predicted minimum pressures for the waste elements near the bottom of the tank as shown in Figure 3-10 are due to the isolated low peak pressures in waste elements 1734, 2463, and 3192 as seen in Figure 3-7. This behavior of isolated maxima and minima that stray from theoretical predictions will be observed in other simulations presented in this report.

Figure 3-10. Maximum and Minimum Waste Pressures vs. Normalized Height from Tank Bottom for Horizontal Excitation at θ=0 Run at Absolute Pressure.

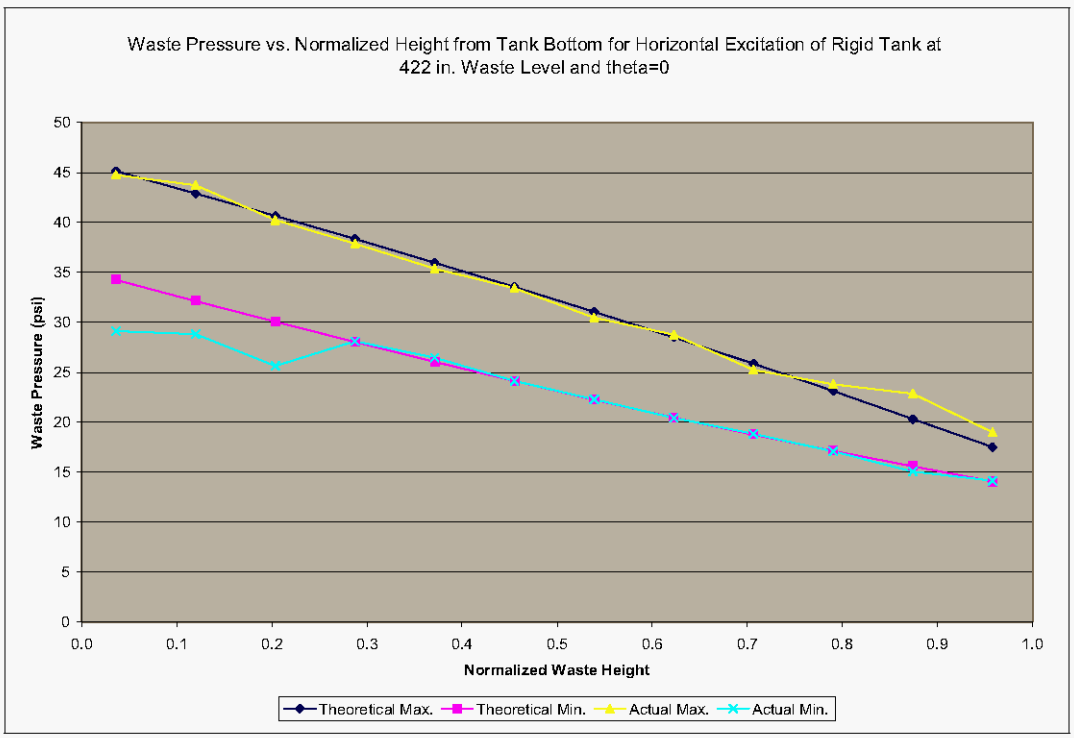

Figure 3-11. Maximum and Minimum Waste Pressures vs. Normalized Height from Tank Bottom for Horizontal Excitation at θ=45° Run at Absolute Pressure.

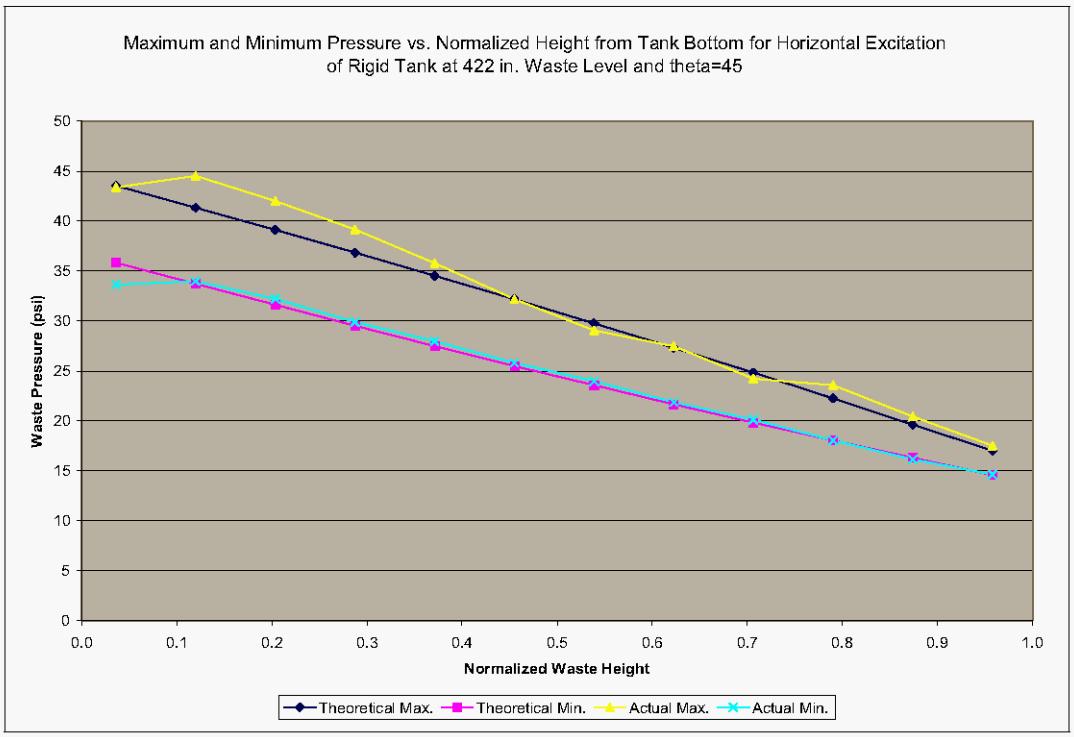

Figure 3-12. Maximum and Minimum Waste Pressures vs. Normalized Height from Tank Bottom for Horizontal Excitation at θ=90° Run at Absolute Pressure.

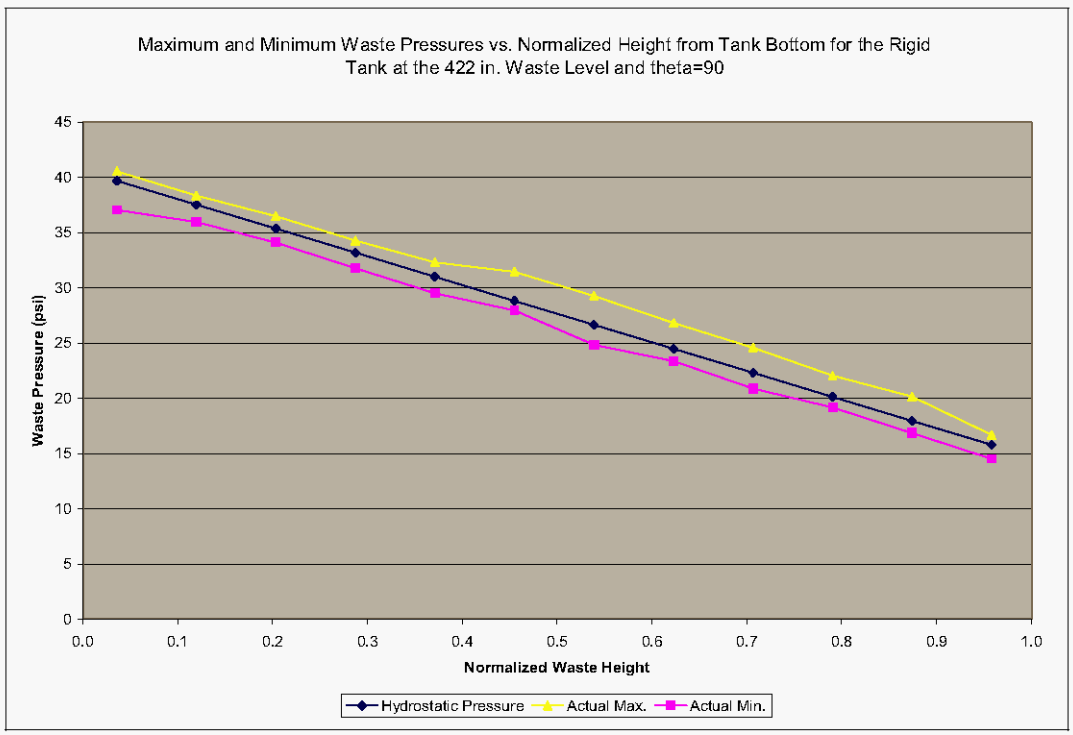

3.2.2 Vertical Excitation

The maximum hydrodynamic pressures induced by the waste on the tank wall due to vertical excitation depend on the vertical location in the waste and are given by Equation 4.55 of BNL 1995. The maximum hydrodynamic and total pressures for the elements in sets "plusx_els", "press_45", and "plusz_els" are shown in Table 3-4.

Table 3-4. Theoretical Maximum Wall Pressures for Vertical Excitation in the Rigid Tank at 422 in. Waste Level.

"Plusx_els" Element No.	"Press_45" Element No.	"Plusz_els" Element No.	Hydrostatic Pressure (psi absolute)	Peak Hydrodynamic Wall Pressure (psi absolute)	Peak Total Pressure (psi absolute)
10482	10290	10146	14.7	0	14.7
9753	9561	9417	15.8	0.2	16.0
9024	8832	8688	18.0	0.5	18.5
8295	8103	7959	20.1	0.8	20.9
7566	7374	7230	22.3	1.1	23.4
6837	6645	6501	24.5	1.4	25.9
6108	5916	5772	26.7	1.7	28.4
5379	5187	5043	28.8	1.9	30.7
4650	4458	4314	31.0	2.1	33.1
3921	3729	3585	33.2	2.2	35.4
3192	3000	2856	35.4	2.4	37.8
2463	2271	2127	37.5	2.5	40.0
1734	1542	1398	39.7	2.5	42.2

Waste pressure time histories for the waste elements at θ=0, 45 and 90° are shown in Figure 3-13, Figure 3-14, and Figure 3-15.

Figure 3-13. Waste Pressure Time Histories for the Rigid Tank With 422 in. of Waste Under Vertical Excitation at θ=0 Run at Absolute Pressure.

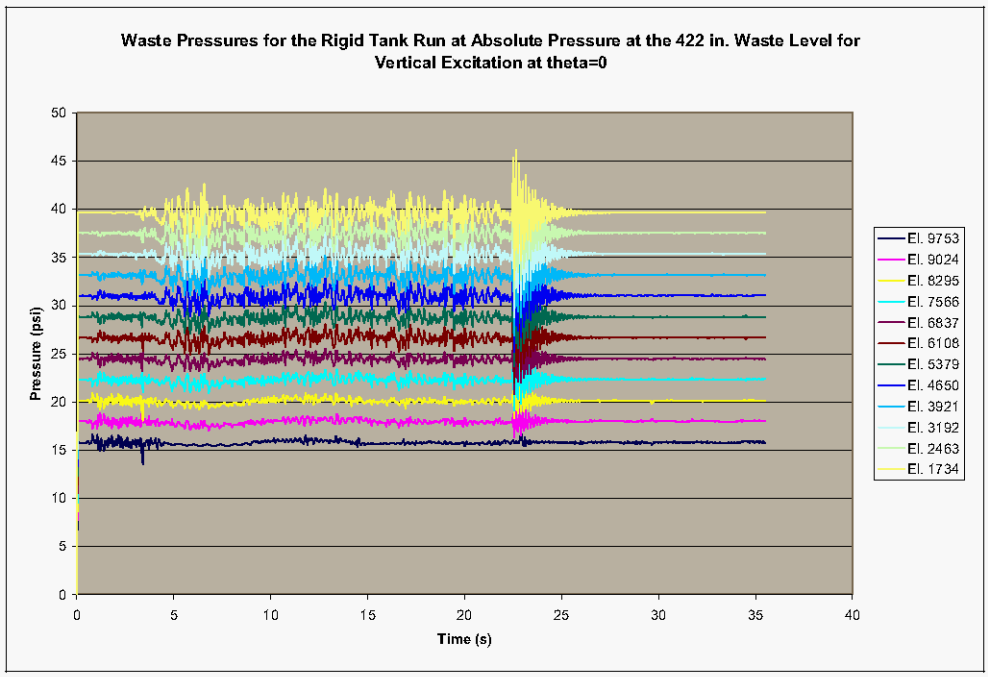

Figure 3-14. Waste Pressure Time Histories for the Rigid Tank With 422 in. of Waste Under Vertical Excitation at θ=45° Run at Absolute Pressure.

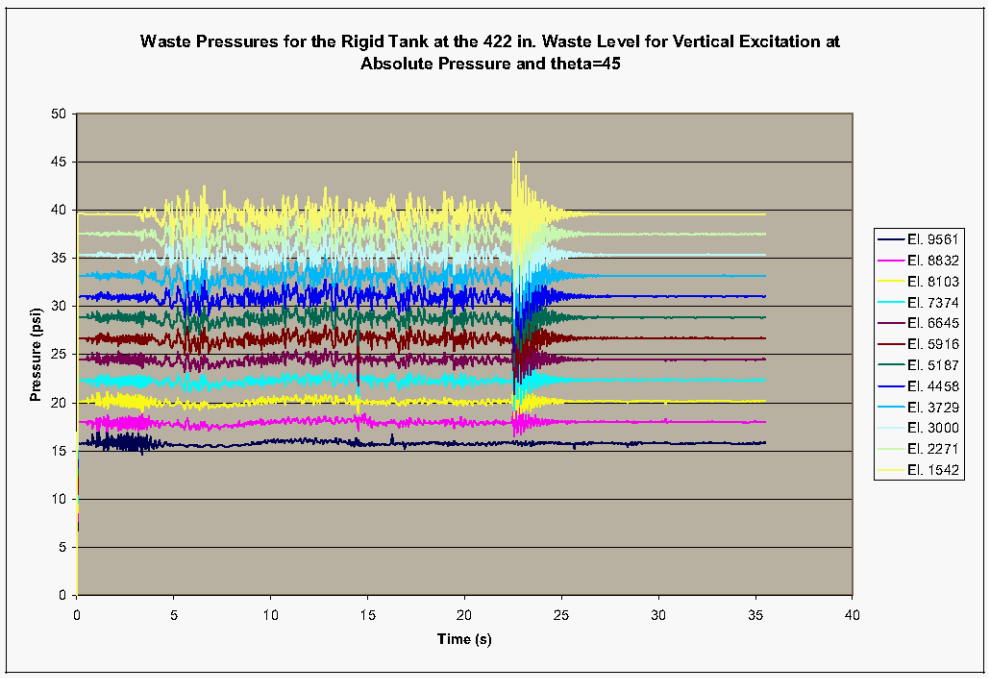

Figure 3-15. Waste Pressure Time Histories for the Rigid Tank With 422 in. of Waste Under Vertical Excitation at θ=90° Run at Absolute Pressure.

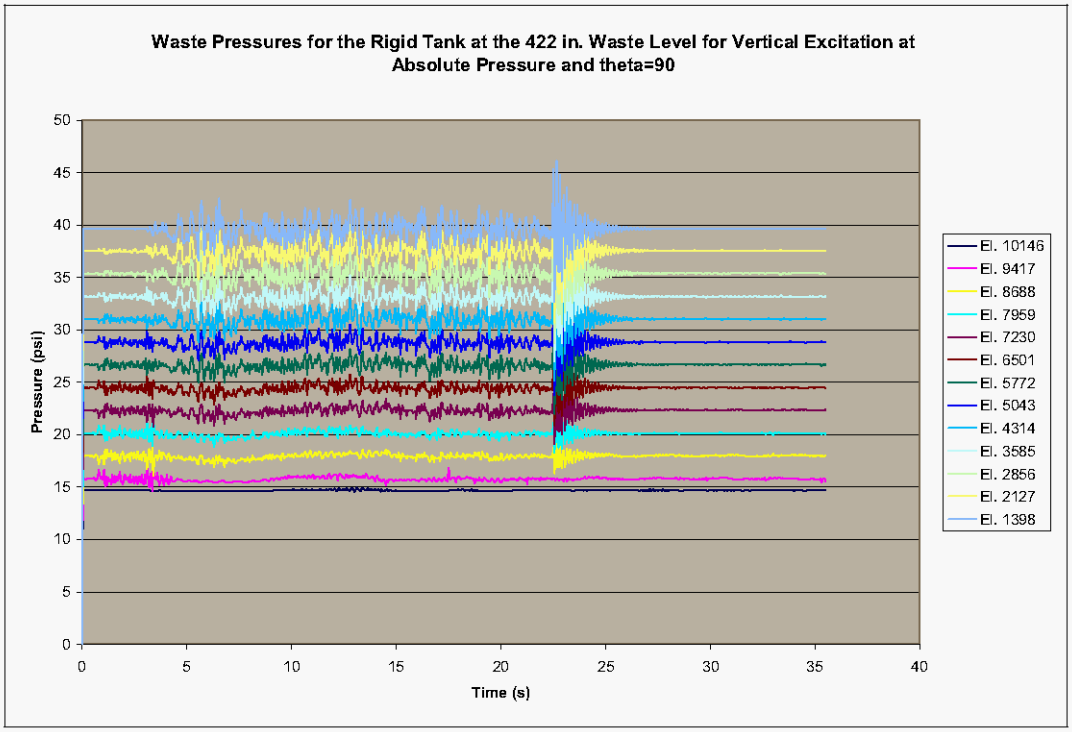

The pressure time history of waste element 1722 located at the center of the tank near the bottom is shown as Figure 3-16. The maximum total pressure is 7% greater than predicted by theory, and the peak dynamic pressure is approximately twice that predicted by theory, although this appears to occur at a single isolated point at approximately 15 s. The minimum pressure is as predicted by theory.

Figure 3-16. Pressure Time History for Bottom Center Waste Element for the Rigid Tank at the 422 in. Waste Level and Vertical Excitation Run at Absolute Pressure.

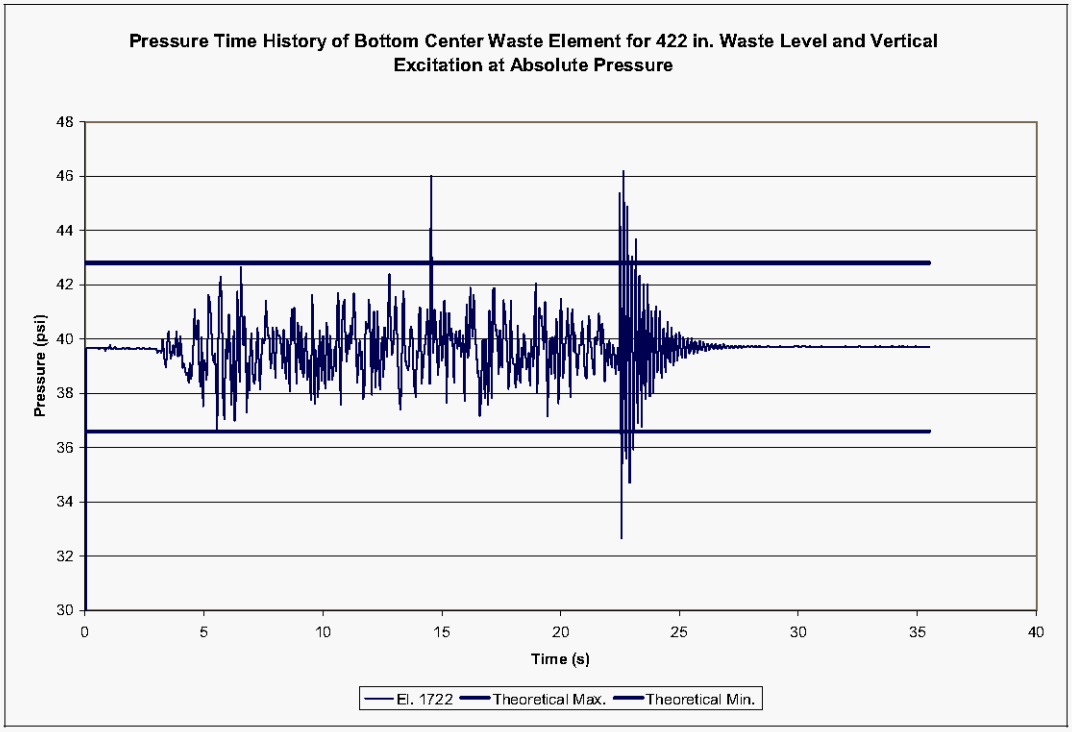

The actual (that is, as predicted by Dytran) maximum and minimum pressure for the elements at θ=0, 45, and 90° is shown in Figure 3-17, Figure 3-18, and Figure 3-19, along with the theoretical maximum and minimum pressures for the elements. The results show very good agreement with theoretical predictions.

Figure 3-17. Maximum and Minimum Waste Pressures vs. Normalized Height from Tank Bottom for Vertical Excitation of Rigid Tank at 422 in. Waste Level and θ=0 Run at Absolute Pressure.

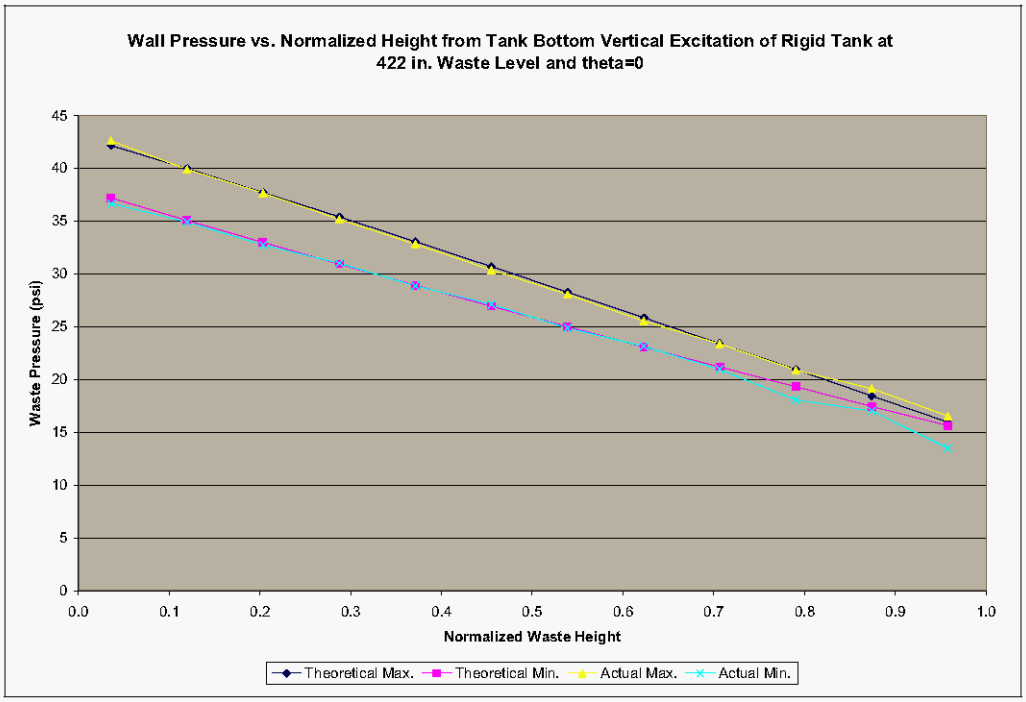

Figure 3-18. Maximum and Minimum Waste Pressures vs. Normalized Height from Tank Bottom for Vertical Excitation of Rigid Tank at 422 in. Waste Level and θ=45° Run at Absolute Pressure.

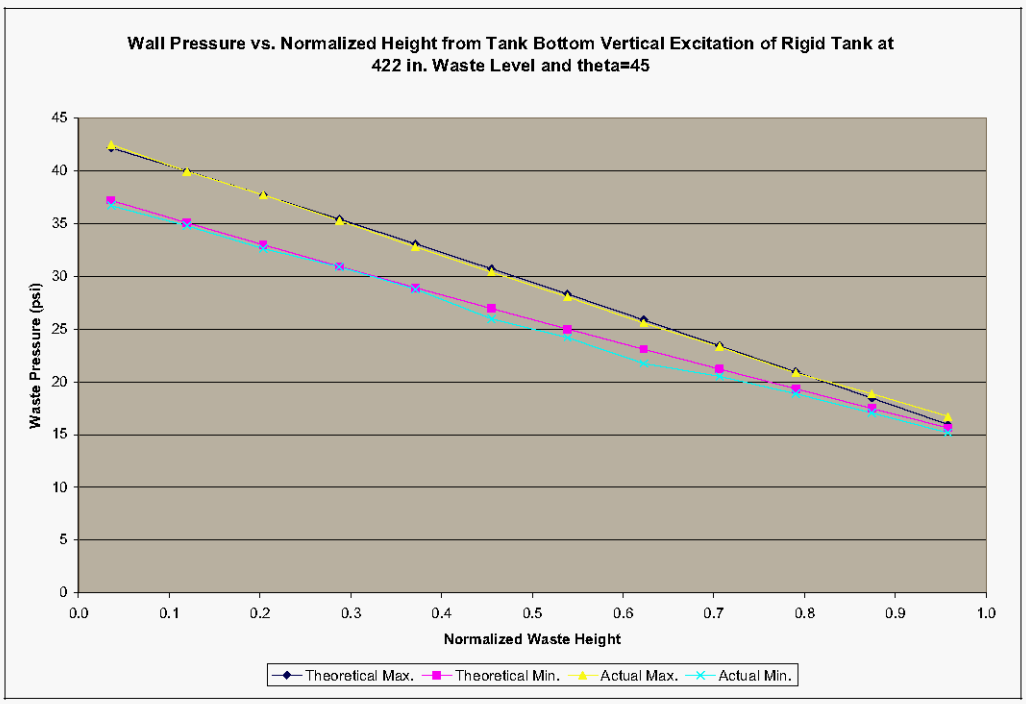

Figure 3-19. Maximum and Minimum Waste Pressures vs. Normalized Height from Tank Bottom for Vertical Excitation of Rigid Tank at 422 in. Waste Level and θ=90° Run at Absolute Pressure.

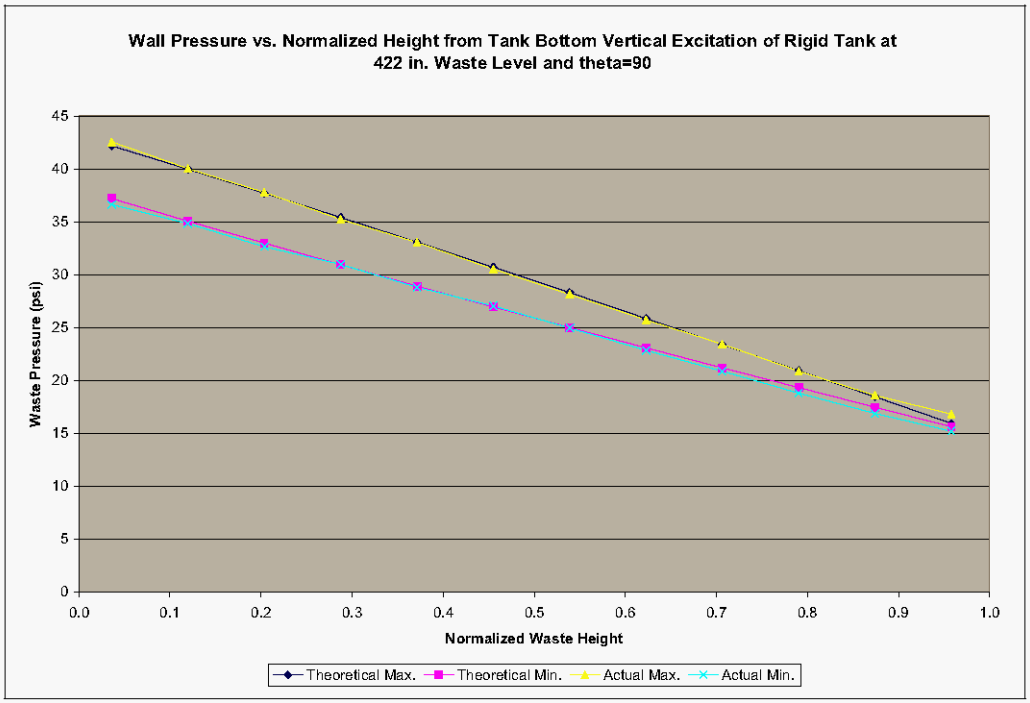

3.3 SLOSH HEIGHT RESULTS

According to Equation 4.60 of BNL 1995, the maximum predicted slosh height due to horizontal excitation is 23.7 in. The time history of the maximum slosh height across all elements is shown in Figure 3-20, where the maximum height of the free surface is shown as 25.4 in. above the initial level.

The slosh height subroutine works by representing the waste free surface as discrete triangular facets in space. At each output time step, the position of each corner node of each facet is known. At each time, the maximum slosh height is reported as the maximum height over all corner nodes representing the free surface position. A physical interpretation of slosh height time history is to think of a massless rigid plate that remains horizontal at all times and floats on top of the waste free surface. The vertical position of the plate corresponds to the peak height of any point on the free surface. The slosh height time history may then be thought of as the vertical displacement time history of the floating plate, starting from the initial position.

Figure 3-20. Maximum Slosh Height Time History Over All Waste Elements for Horizontal Excitation.

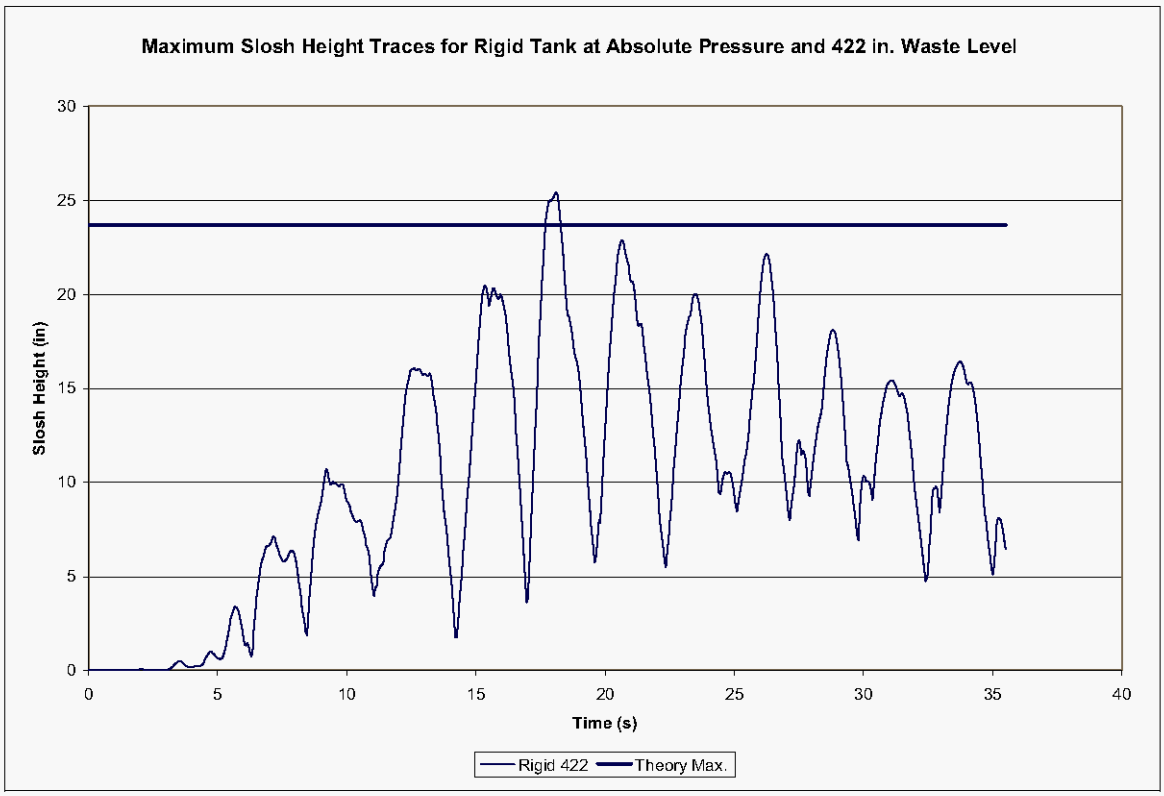

4.0 RIGID TANK MODEL AT 460 INCH WASTE LEVEL

The response of the tank and contained liquid to seismic excitation with the liquid initially at the 460 in. level *does not have a closed form analytical solution* because of the interaction of the liquid free surface with the curved surface of the tank dome. However, the *solutions obtained with Dytran will be compared to the theoretical solution for the rigid open tank with the hinged top condition and 460 in. waste level* as well as with the Dytran solution for the rigid tank at the 422 in. level.

The problem was originally run at gage pressure, but all results reported are from subsequent runs made at absolute pressure.

4.1 HYDRODYNAMIC FORCES

4.1.1 Horizontal Excitation at Absolute Pressure

If the contributions of the impulsive mode and first three convective modes are combined in a square-root-sum-of-squares (SRSS) fashion, the theoretical maximum horizontal hydrodynamic force is 3.0×10^6 lbf, based on a zero-period acceleration for the impulsive response, and convective accelerations from the 0.5% damped spectrum. The coupling surface reaction force time histories reported by Dytran for horizontal excitation are shown in Figure 4-1. The horizontal coupling surface reaction force appears as Figure 4-2. The peak reaction force is 3.02×10^6 lbf, which is essentially the same as the theoretical maximum.

The theoretical peak reaction force due to the first three convective modes only is 5.21×10^5 lbf. The convective component of the horizontal reaction force during the free vibration phase following the seismic excitation appears as Figure 4-3. The peak reaction force due to the convective response is approximately 2×10^5 lbf – much less than the predicted value. Also apparent in the free vibration response is the period of the first convective mode. The period shown in Figure 4-3 during the free vibration phase is approximately 5 s, which matches the theoretical fundamental convective frequency of 0.2 Hz, and is slightly lower than the 5.25 s period for the rigid tank at the 422 in. level.

As noted in Section 3.1.1, it appears that the presence of the tank dome acts to inhibit the convective waste response.

Figure 4-1. Coupling Surface Reaction Forces at the 460 in. Waste Level for the Rigid Tank Under Horizontal Seismic Excitation.

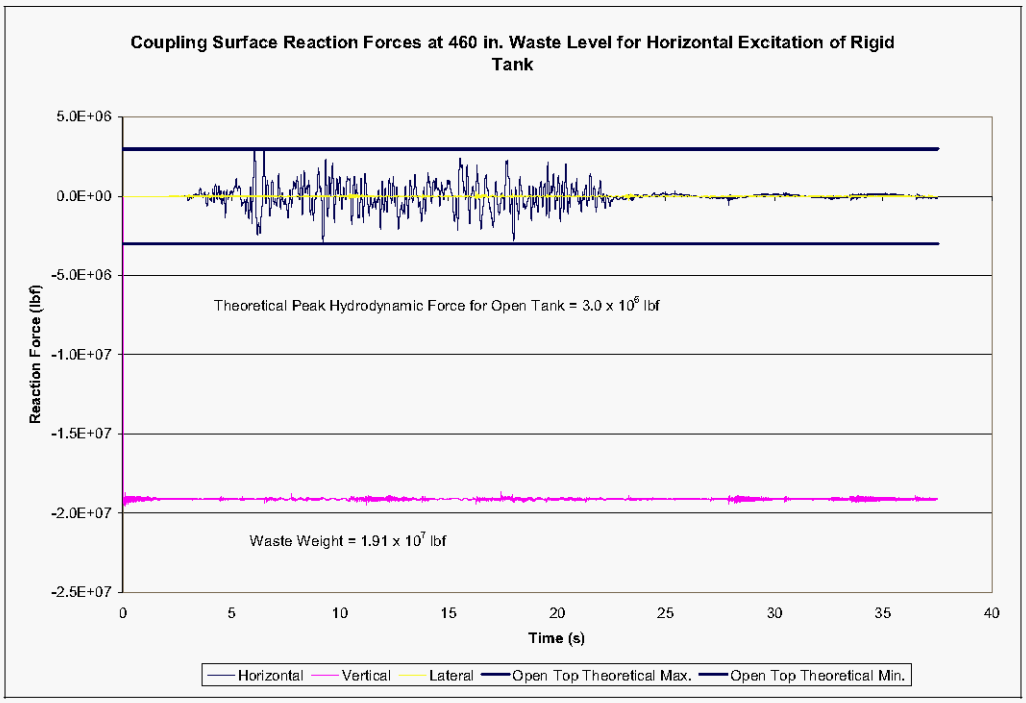

Figure 4-2. Horizontal Coupling Surface Reaction Force for Rigid Tank at 460 in. Waste Level Under Horizontal Seismic Excitation.

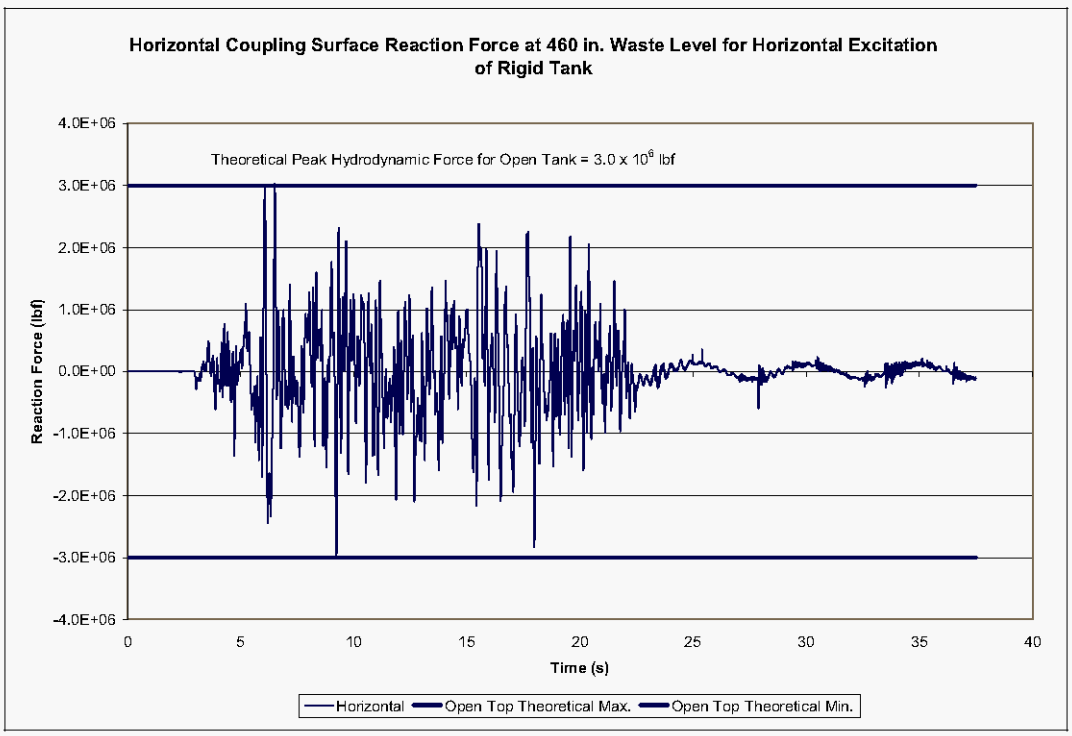

Figure 4-3. Horizontal Coupling Surface Reaction Force for Rigid Tank at 460 in. Waste Level Under Horizontal Seismic Excitation – Convective Response.

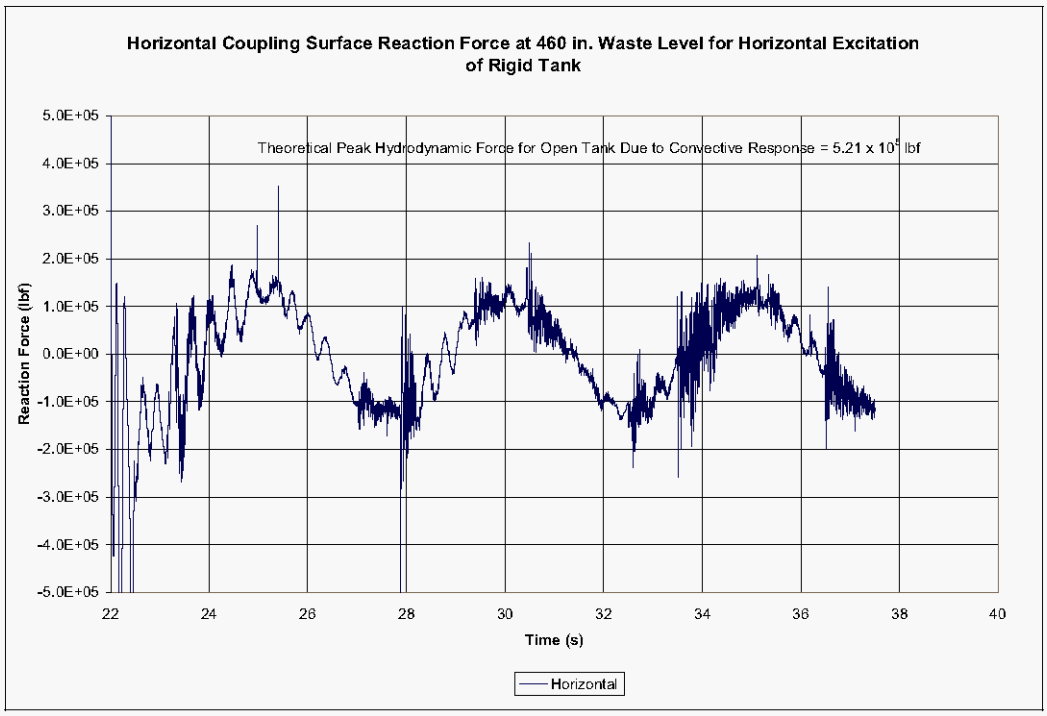

4.1.2 Vertical Excitation at Absolute Pressure

Given the waste mass of 4.95 x 10^4 lbf-s^2/in, and the vertical zero period acceleration of 0.12*g* (shown in the vertical acceleration time history in Figure 2-15), the peak theoretical vertical hydrodynamic base force is 2.30 x 10^6 lbf. The coupling surface reaction force shown in Figure 4-4 is greater than predicted by theory with the peak hydrodynamic force of 3.1 x 10^6 lbf. The spike in the vertical reaction force at 22.5 s is due to the final point in the vertical velocity time history being zero, bringing the tank to a sudden stop.

Figure 4-4. Vertical Coupling Surface Reaction Force for Rigid Tank at 460 in. Waste Level Under Vertical Seismic Excitation.

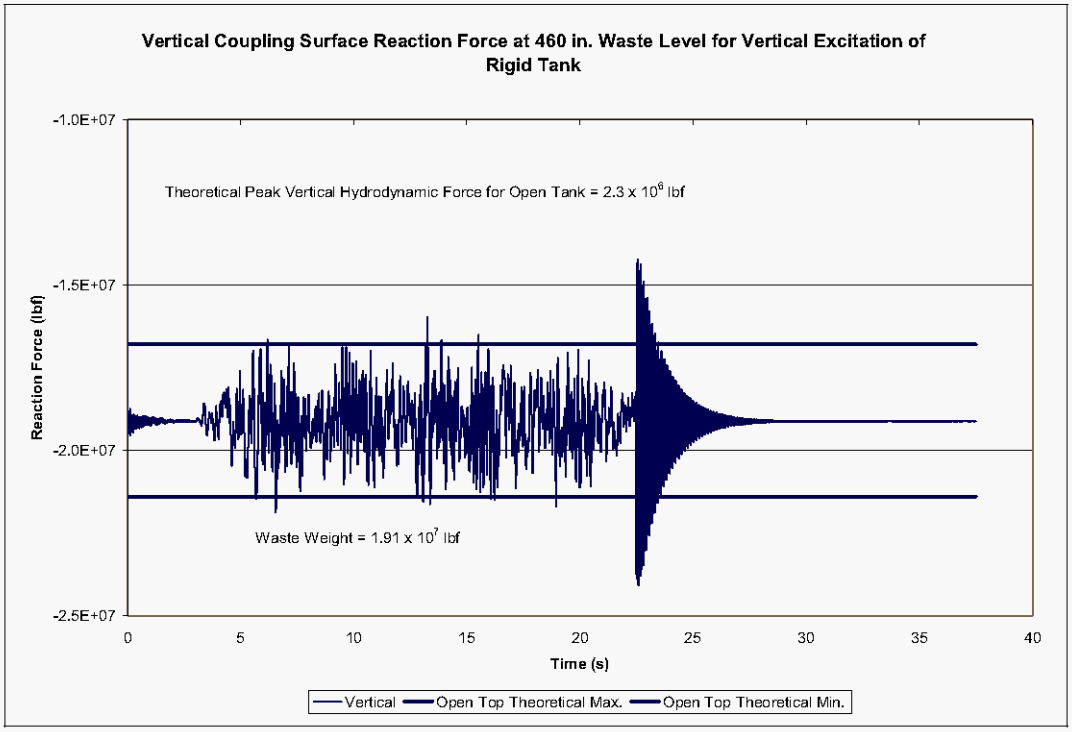

4.2 WASTE PRESSURES

4.2.1 Horizontal Excitation Run at Absolute Pressure

Although no closed form solution exists for the 460 in. waste level, theoretical dynamic pressures were calculated Equation 4.24 of BNL 1995 *based on an open tank with 460 in. of waste and a hinged top condition*. This solution is presented along with the actual results for comparison purposes.

The hydrostatic, peak hydrodynamic and peak total pressures for the elements in the sets "plusx_els", "press_45", are shown in Table 4-1and Table 4-2. The maximum theoretical pressures for the elements set "plusz_els" are simply the hydrostatic pressures shown in the two tables because the theoretical hydrodynamic pressures are zero at θ=90°. The pressure time histories for waste element sets at θ=0, 45, and 90°, are shown in Figure 4-5 through Figure 4-9.

Table 4-1. Theoretical Maximum Absolute Waste Pressures for Horizontal Excitation in the Rigid Open Top Tank at 460 in. Waste Level for Elements at θ=0.

"Plusx_els" Element No.	Hydrostatic Pressure (psi)	Peak Hydrodynamic Pressure (psi)	Peak Total Pressure (psi)
11211	14.7	0	14.7
10482	16.0	1.9	17.9
9753	18.4	2.6	21.0
9024	20.7	3.3	24.0
8295	23.1	3.9	27.0
7566	25.4	4.4	29.8
6837	27.7	4.9	32.6
6108	30.1	5.2	35.3
5379	32.4	5.5	37.9
4650	34.7	5.7	40.4
3921	37.1	5.9	43.0
3192	39.4	6.1	45.5
2463	41.8	6.1	47.9
1734	44.1	6.2	50.3

Table 4-2. Theoretical Maximum Absolute Waste Pressures for Horizontal Excitation in the Rigid Open Top Tank at 460 in. Waste Level for Elements at θ=45°.

"Press_45" Element No.	Hydrostatic Pressure (psi)	Peak Hydrodynamic Pressure (psi)	Peak Total Pressure (psi)
11019	14.7	0	14.7
10290	16.0	1.4	17.4
9561	18.4	1.9	20.3
8832	20.7	2.3	23.0
8103	23.1	2.8	25.9
7374	25.4	3.1	28.5
6645	27.7	3.4	31.1
5916	30.1	3.7	33.8
5187	32.4	3.9	36.3
4458	34.7	4.1	38.8
3729	37.1	4.2	41.3
3000	39.4	4.3	43.7
2271	41.8	4.3	46.1
1542	44.1	4.4	48.5

Figure 4-5. Waste Pressure Time Histories for the Rigid Tank With 460 in. of Waste Under Horizontal Excitation at θ=0 Run at Absolute Pressure.

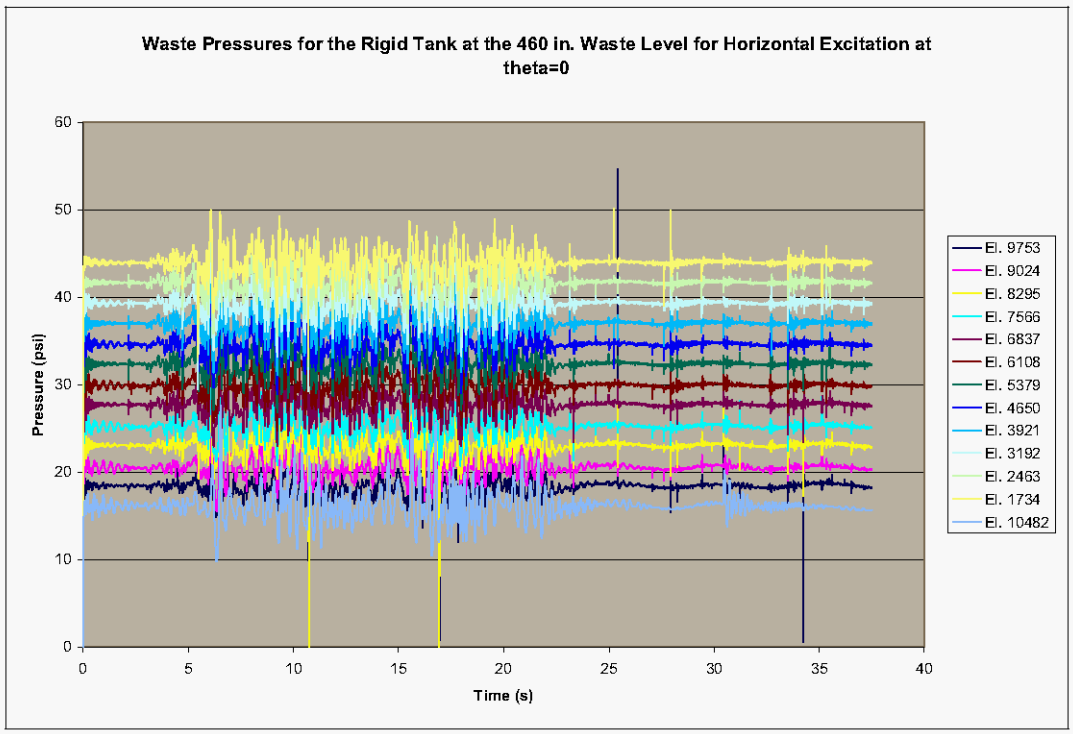

Figure 4-6. Selected Waste Pressure Time Histories for the Rigid Tank With 460 in. of Waste Under Horizontal Excitation at θ=0 Run at Absolute Pressure.

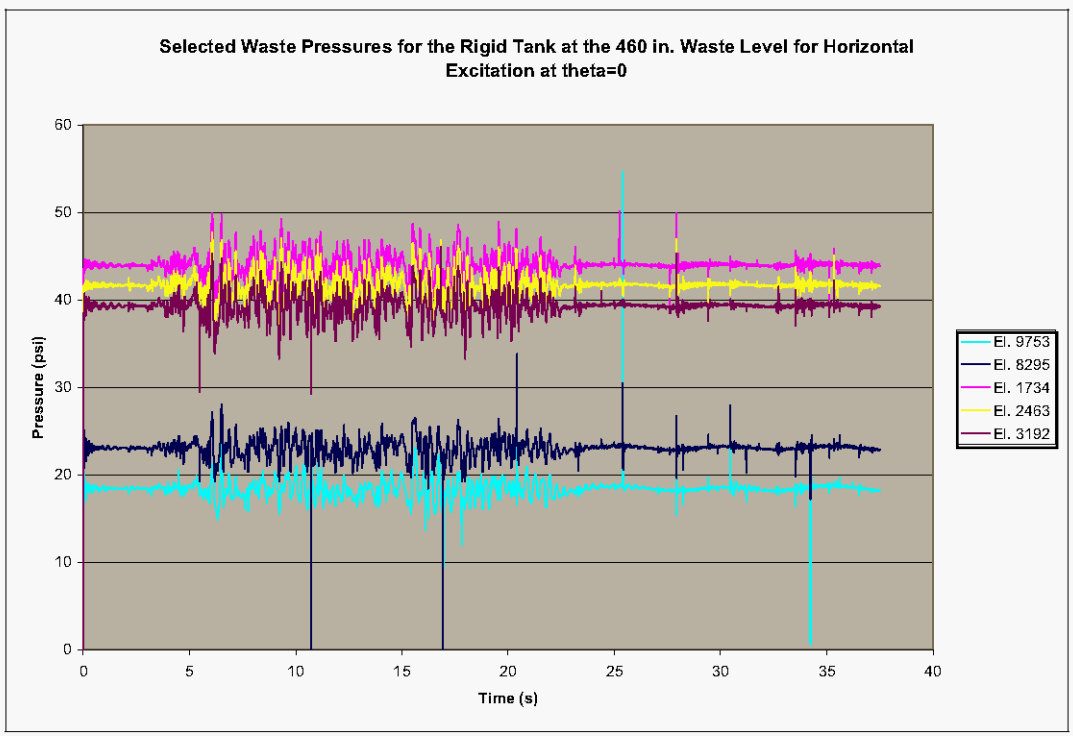

Figure 4-7. Waste Pressure Time Histories for the Rigid Tank With 460 in. of Waste Under Horizontal Excitation at θ=45° Run at Absolute Pressure.

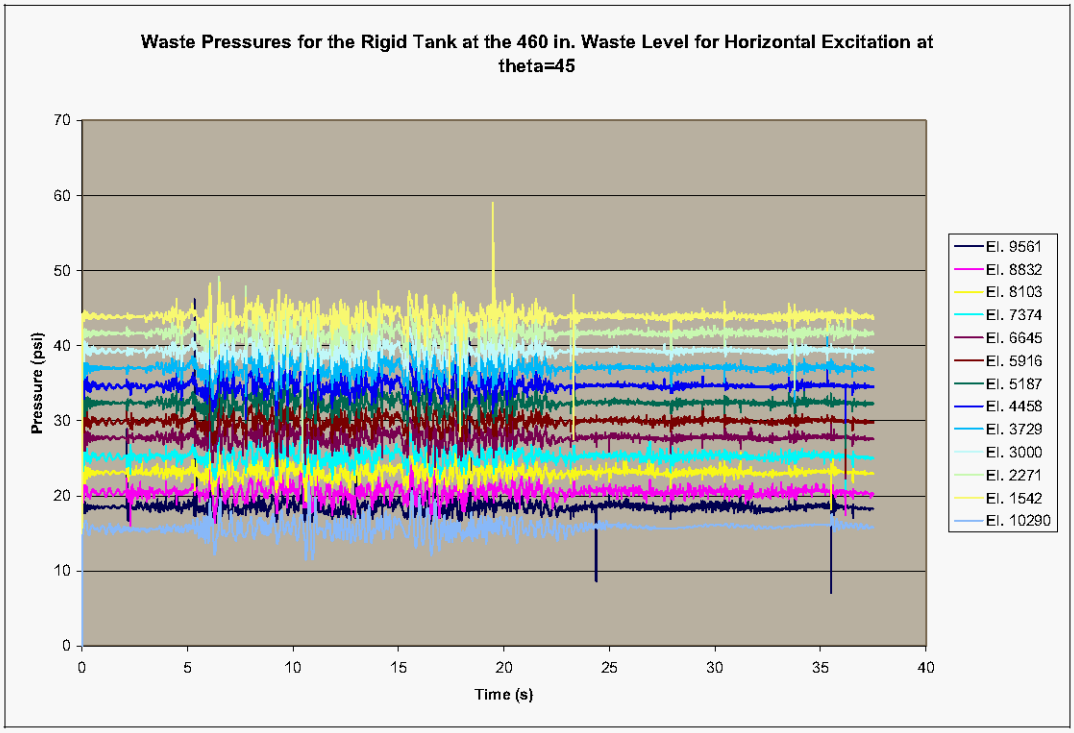

Figure 4-8. Selected Waste Pressure Time Histories for the Rigid Tank With 460 in. of Waste Under Horizontal Excitation at θ=45° Run at Absolute Pressure.

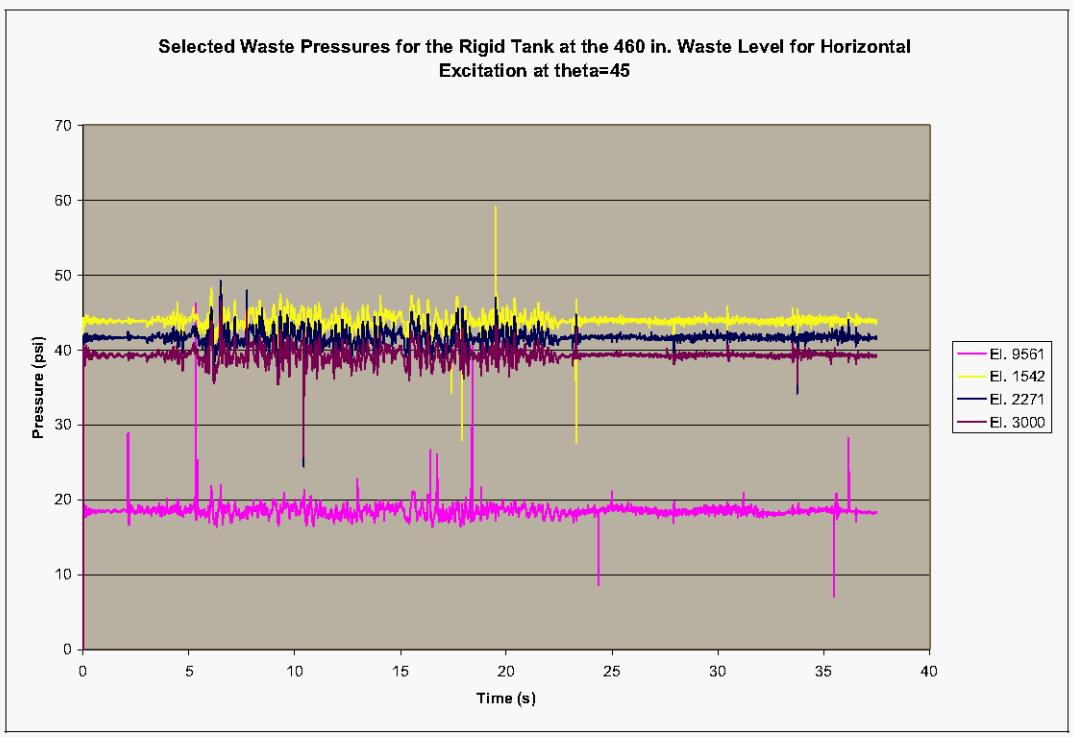

Figure 4-9. Waste Pressure Time Histories for the Rigid Tank With 460 in. of Waste Under Horizontal Excitation at θ=90° Run at Absolute Pressure.

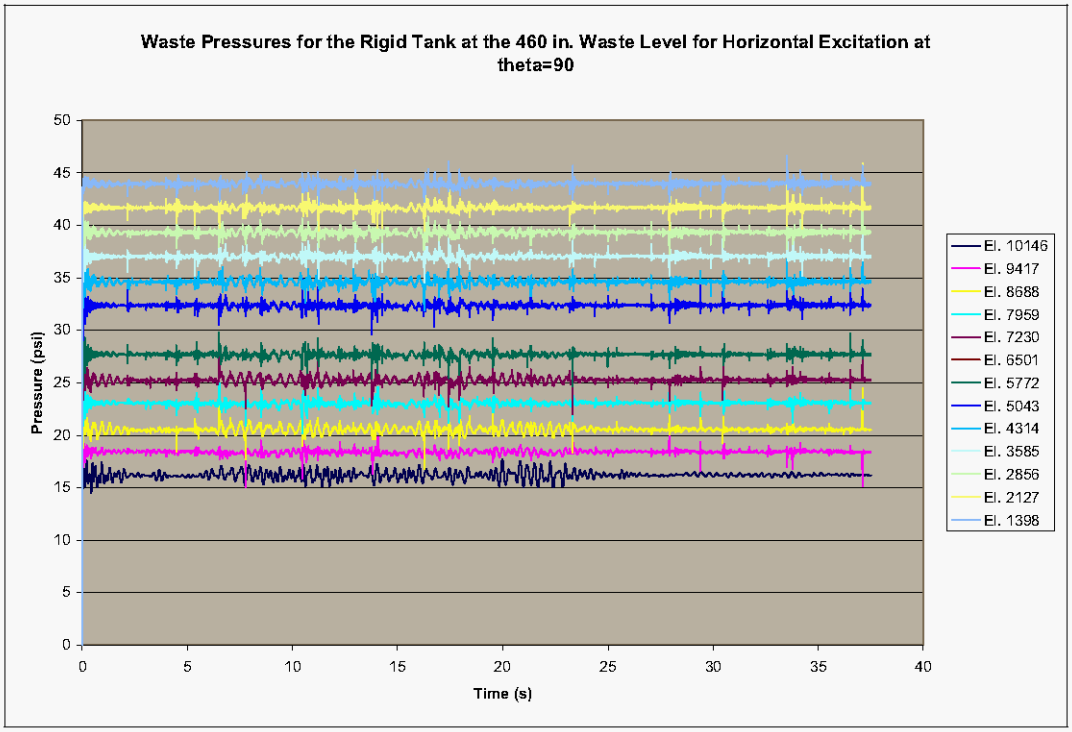

Comparisons of the maximum and minimum pressures expected for an open top tank to the maximum and minimum pressures obtained from the computer simulations (labeled as "actual max." and "actual min.") are shown in Figure 4-10, Figure 4-11, and Figure 4-12. Excursions from the open top solution are evident in Figure 4-10 and Figure 4-11. In Figure 4-10 the biggest differences occur in waste elements 8295 and 9753 near the free surface. The pressure time histories for these elements is shown in Figure 4-6 where it can be seen that the large differences from the theoretical solution for the open top tank come at isolated points. Similar remarks apply to Figure 4-11 and the time history plots shown in Figure 4-8.

The time history data was saved every 0.01 s, which is the same resolution as the seismic input. It is difficult to know which peaks in a time history record are physically meaningful and which peaks are due to numerical noise. However, two observations are readily apparent. First, if the high isolated peaks are neglected, the time history records show good agreement with the theory. Second, some of the high isolated peaks occur after 22.48 s which is the end of the seismic input and after which the tank experiences unforced motion. These two observations suggest that peaks of this nature are caused by numerical noise in the solution, and may not be physically meaningful.

Figure 4-10. Maximum and Minimum Waste Pressures vs. Normalized Height from Tank Bottom for Horizontal Excitation of Rigid Tank at 460 in. Waste Level and θ=0 Run at Absolute Pressure.

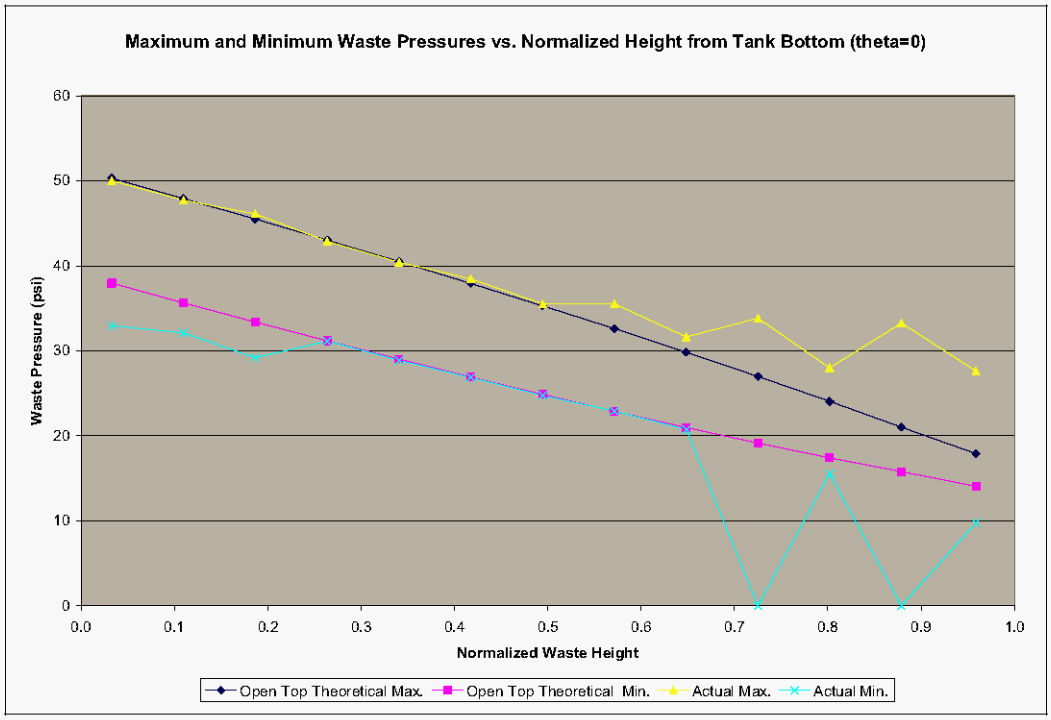

Figure 4-11. Maximum and Minimum Waste Pressures vs. Normalized Height from Tank Bottom for Horizontal Excitation of Rigid Tank at 460 in. Waste Level and θ=45° Run at Absolute Pressure.

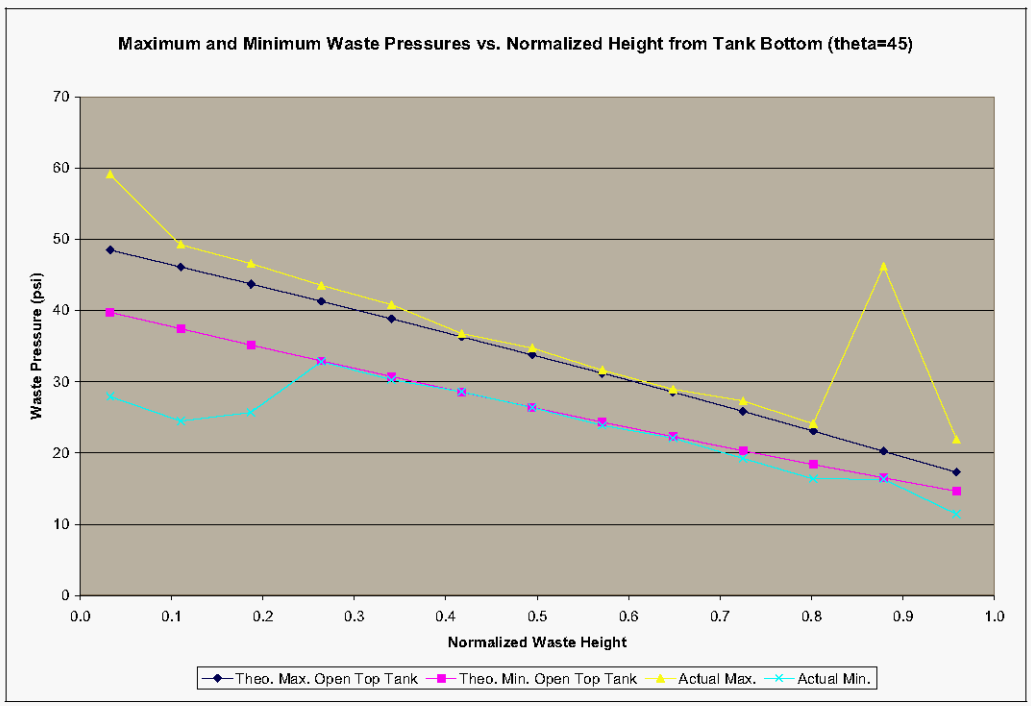

Figure 4-12. Maximum and Minimum Waste Pressures vs. Normalized Height from Tank Bottom for Horizontal Excitation of Rigid Tank at 460 in. Waste Level and θ=90° Run at Absolute Pressure.

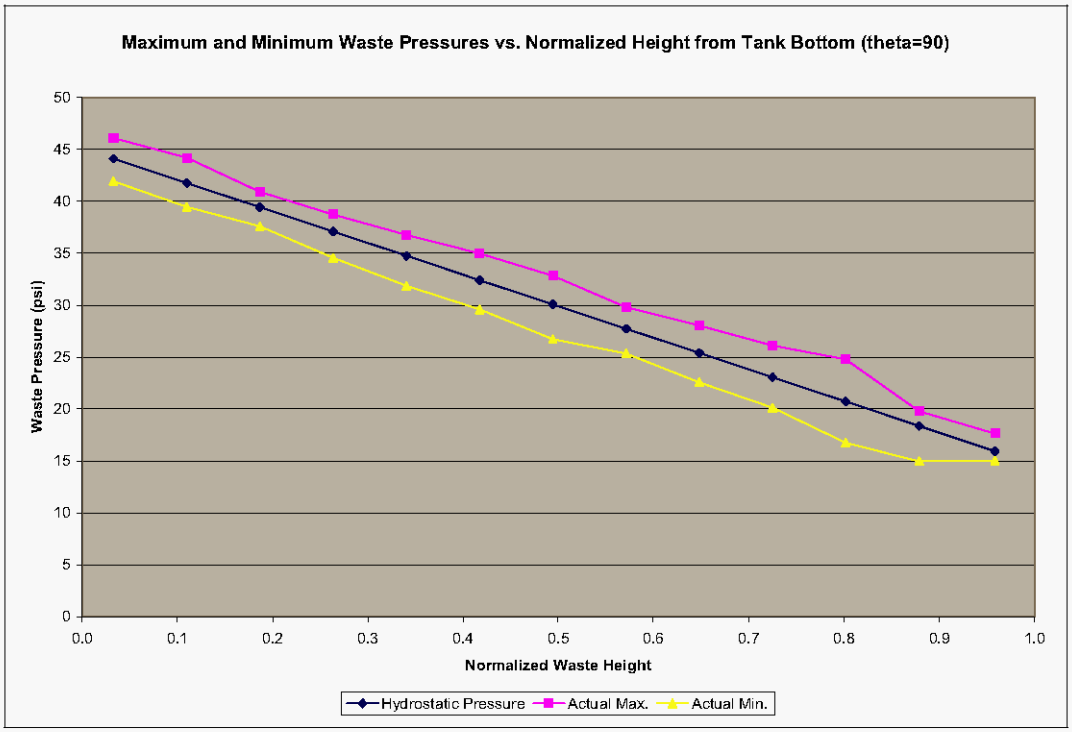

4.2.2 Vertical Excitation Run at Absolute Pressure

Waste element time histories for vertical excitation are shown in Figure 4-13 through Figure 4-19. Comparisons of maximum and minimum pressures from the simulation (labeled as "actual max." and "actual min") and the open top solution are presented as Figure 4-20, Figure 4-21, and Figure 4-22. The agreement between the simulation and the open top theory is good, but shows some deviations at elements near the free surface. The details for the θ=0, 45, and 90° locations are shown in Figure 4-14, Figure 4-15, and Figure 4-16. Once again, at least some of the differences appear to be due to isolated peaks in the time history records.

According to the theory for an open top tank, the maximum and minimum waste pressures for the bottom center waste element are 47.7, and 40.4 lbf/in^2, respectively. The actual maximum and minimum pressures (that is, as calculated by Dytran) shown in Figure 4-19 are 48.4, and 38.3 lbf/in^2, respectively.

Figure 4-13. Waste Pressure Time Histories for the Rigid Tank With 460 in. of Waste Under Vertical Excitation at θ=0 Run at Absolute Pressure.

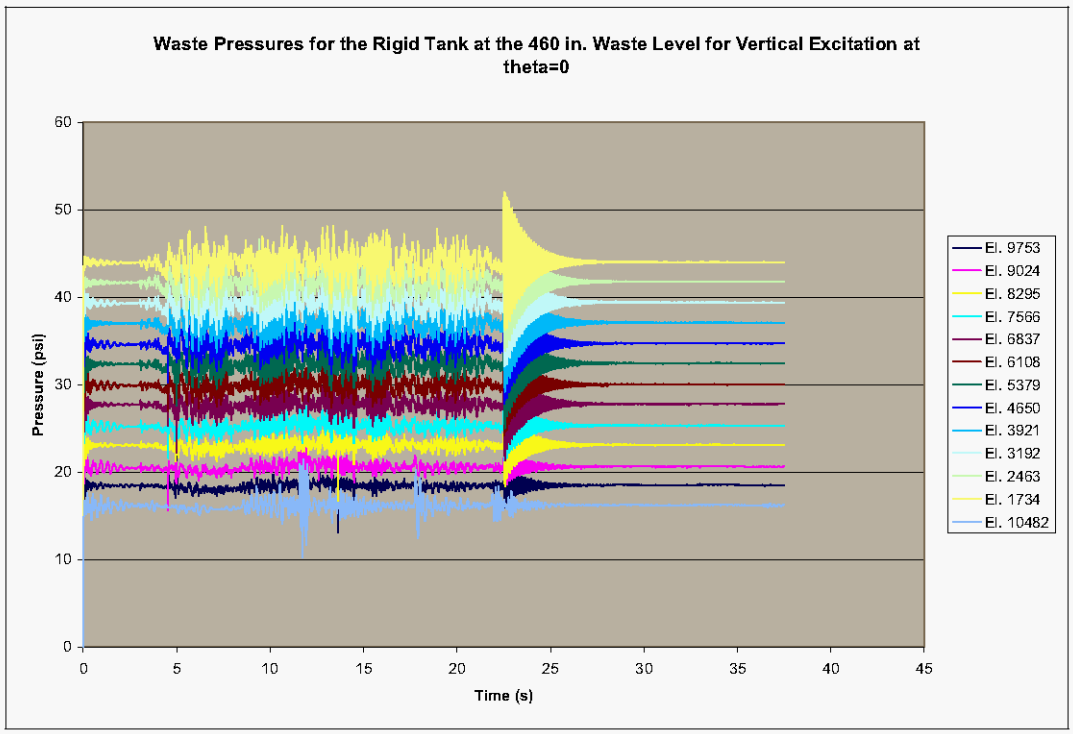

Figure 4-14. Selected Waste Pressure Time Histories for the Rigid Tank With 460 in. of Waste Under Vertical Excitation at θ=0 Run at Absolute Pressure.

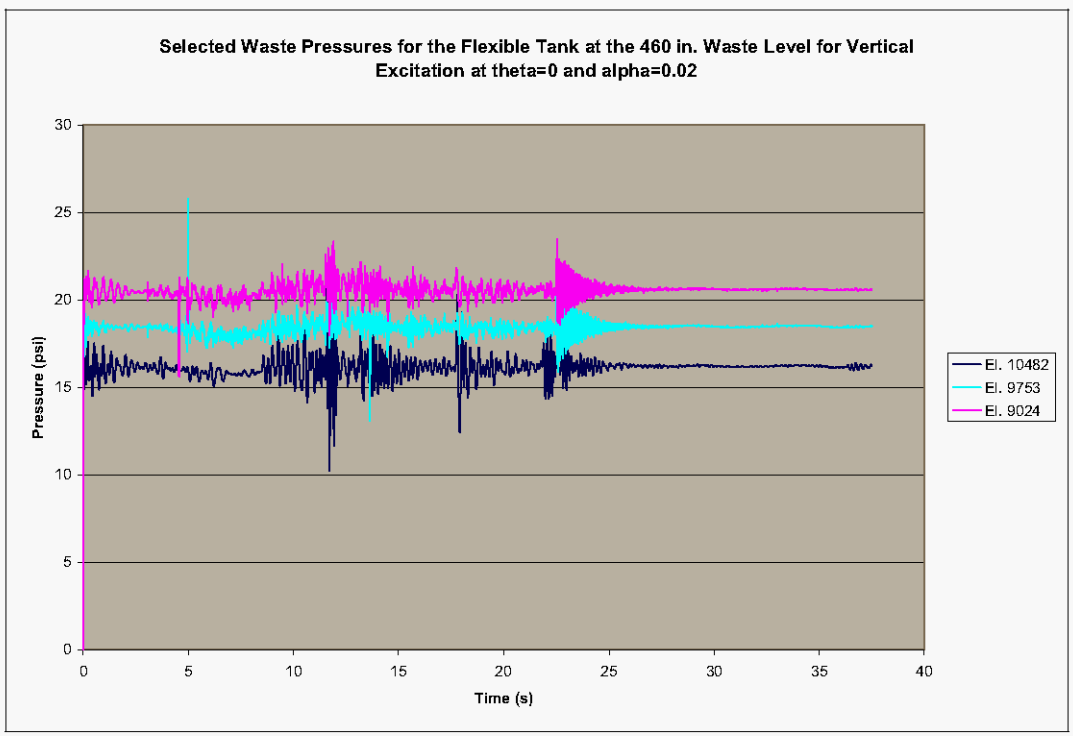

Figure 4-15. Waste Pressure Time Histories for the Rigid Tank With 460 in. of Waste Under Vertical Excitation at θ=45° Run at Absolute Pressure.

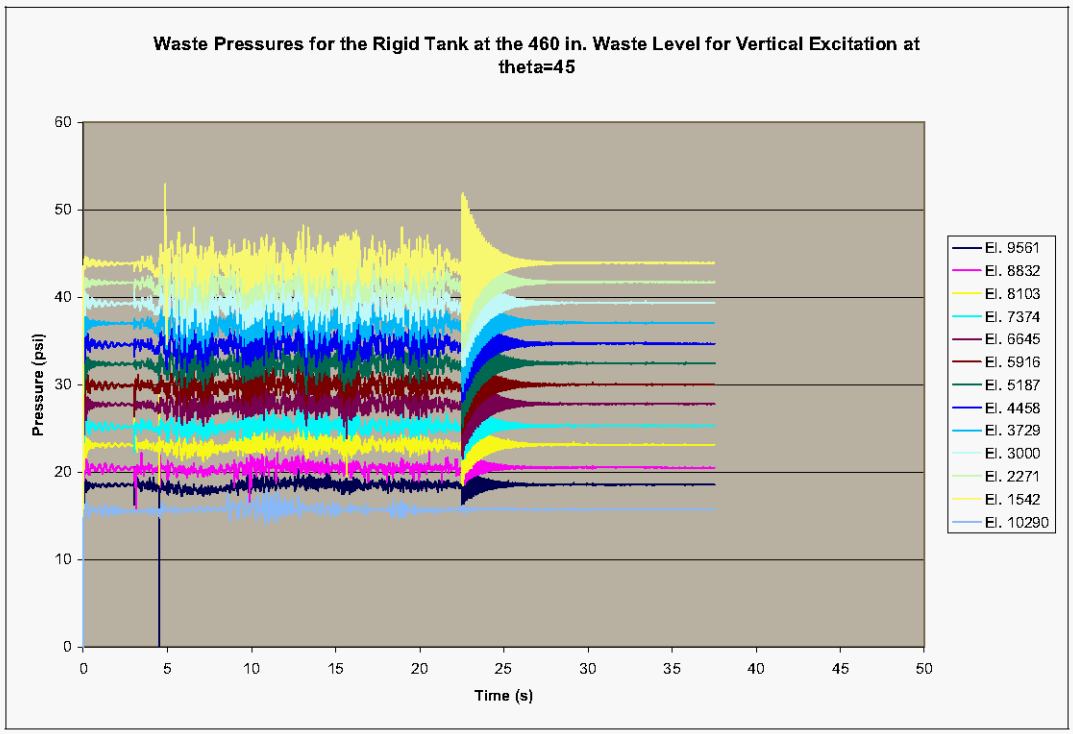

Figure 4-16. Selected Waste Pressure Time Histories for the Rigid Tank With 460 in. of Waste Under Vertical Excitation at θ=45° Run at Absolute Pressure.

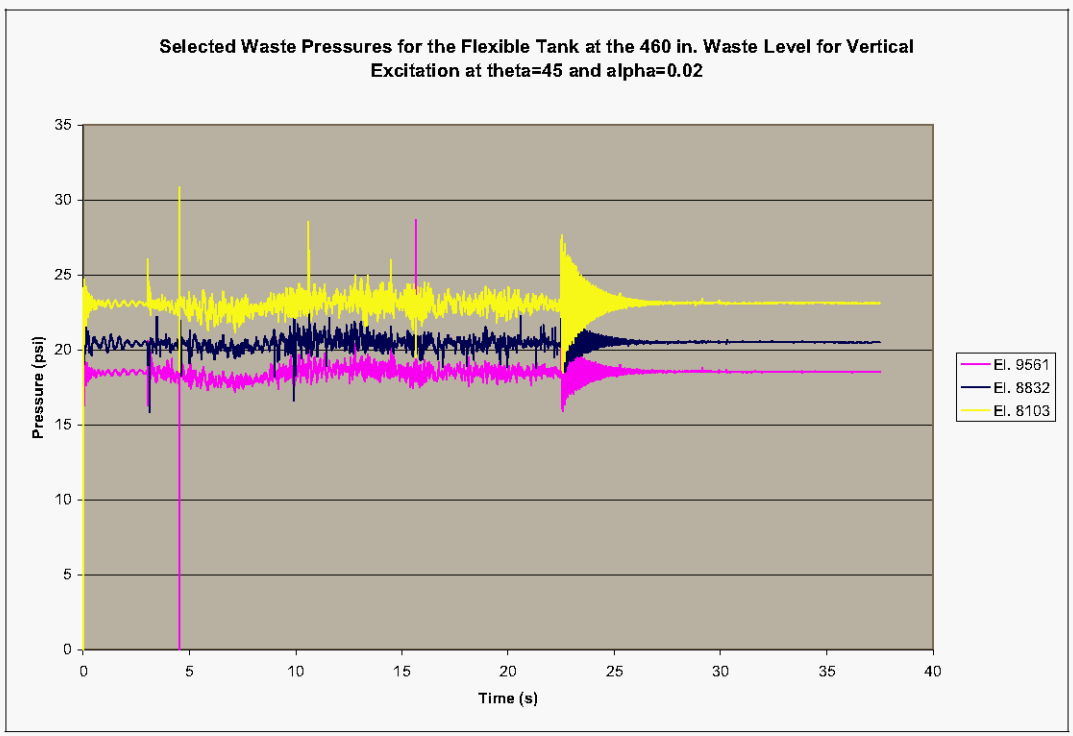

Figure 4-17. Waste Pressure Time Histories for the Rigid Tank With 460 in. of Waste Under Vertical Excitation at θ=90° Run at Absolute Pressure.

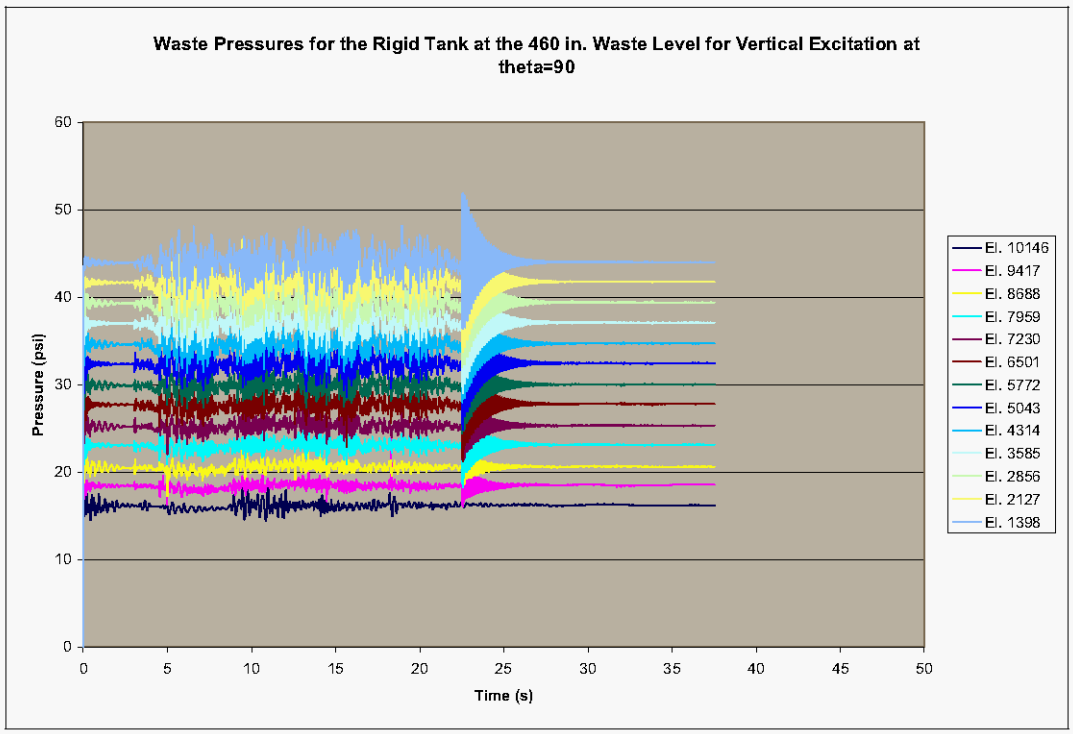

Figure 4-18. Selected Waste Pressure Time Histories for the Rigid Tank With 460 in. of Waste Under Vertical Excitation at θ=90° Run at Absolute Pressure.

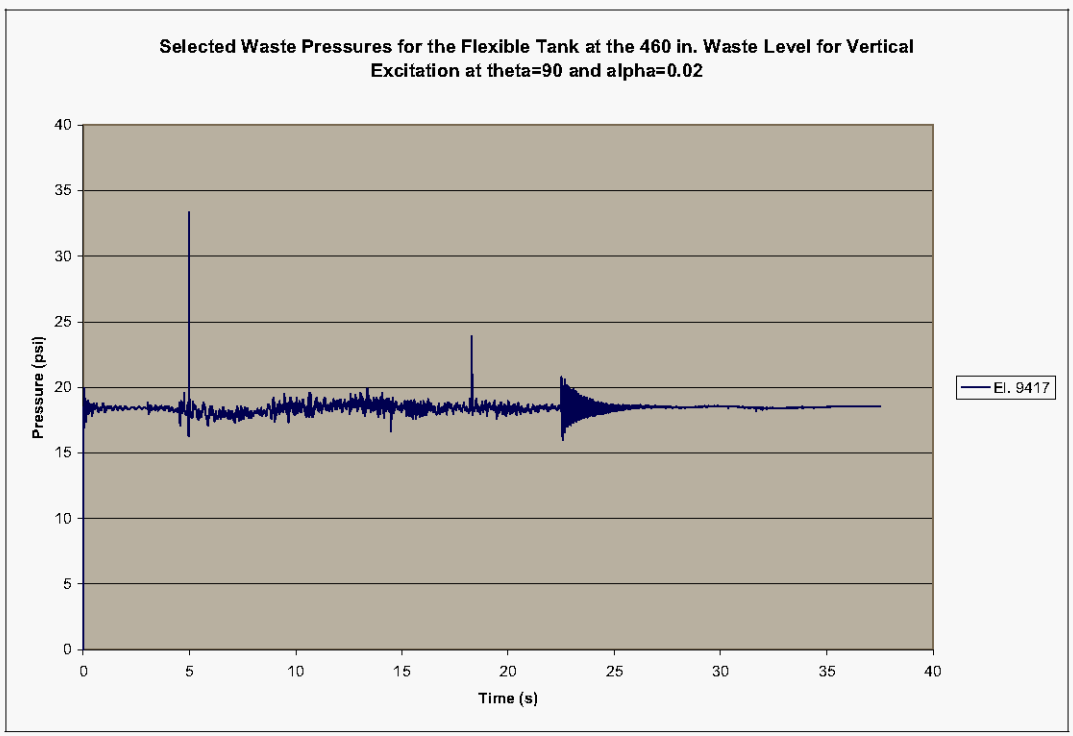

Figure 4-19. Pressure Time History for Bottom Center Waste Element for the Rigid Tank at the 460 in. Waste Level and Vertical Excitation Run at Absolute Pressure.

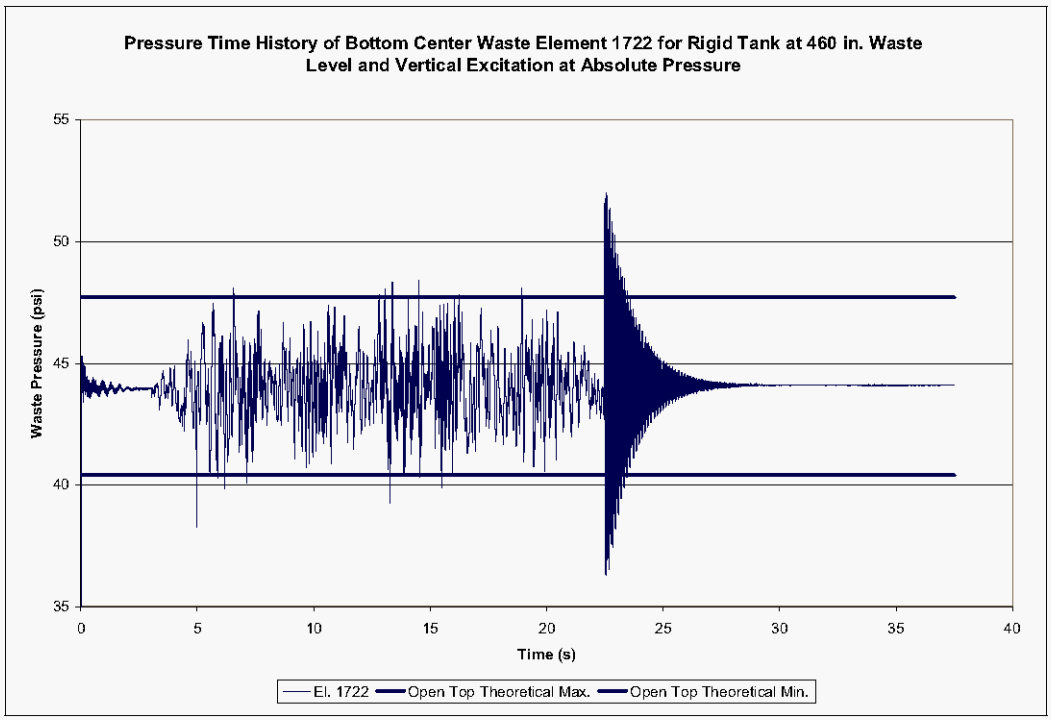

Figure 4-20. Maximum and Minimum Waste Pressures vs. Normalized Height from Tank Bottom for Vertical Excitation of Rigid Tank at 460 in. Waste Level and θ=0 Run at Absolute Pressure.

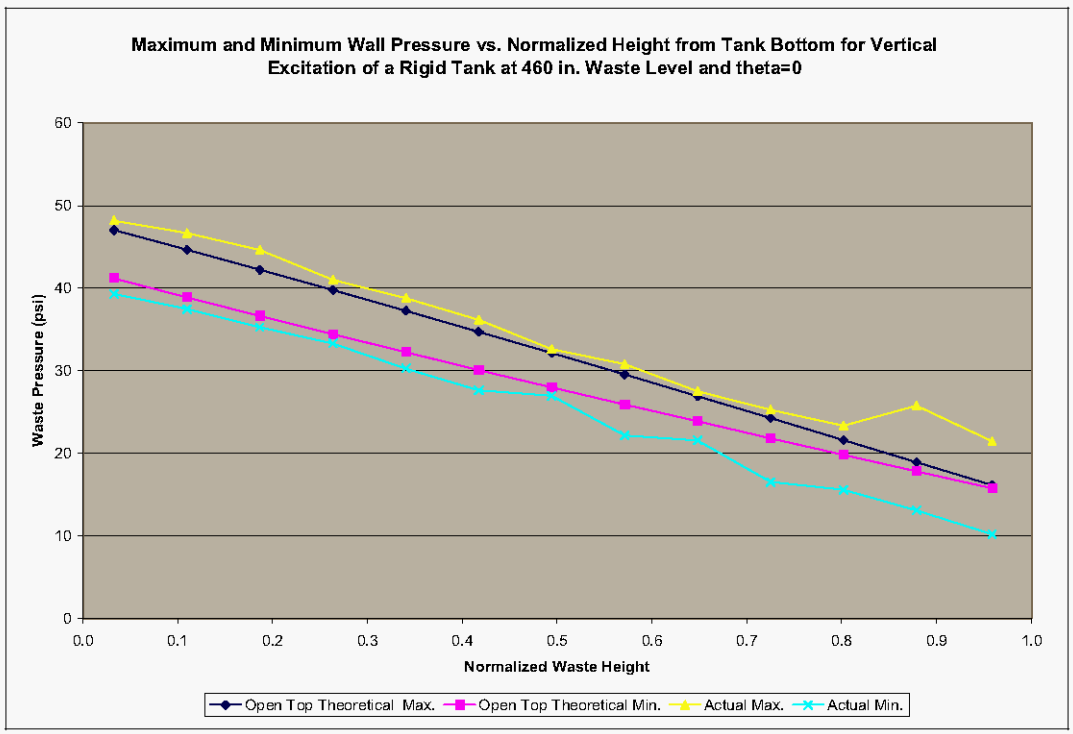

Figure 4-21. Maximum and Minimum Waste Pressures vs. Normalized Height from Tank Bottom for Vertical Excitation of Rigid Tank at 460 in. Waste Level and θ=45° Run at Absolute Pressure.

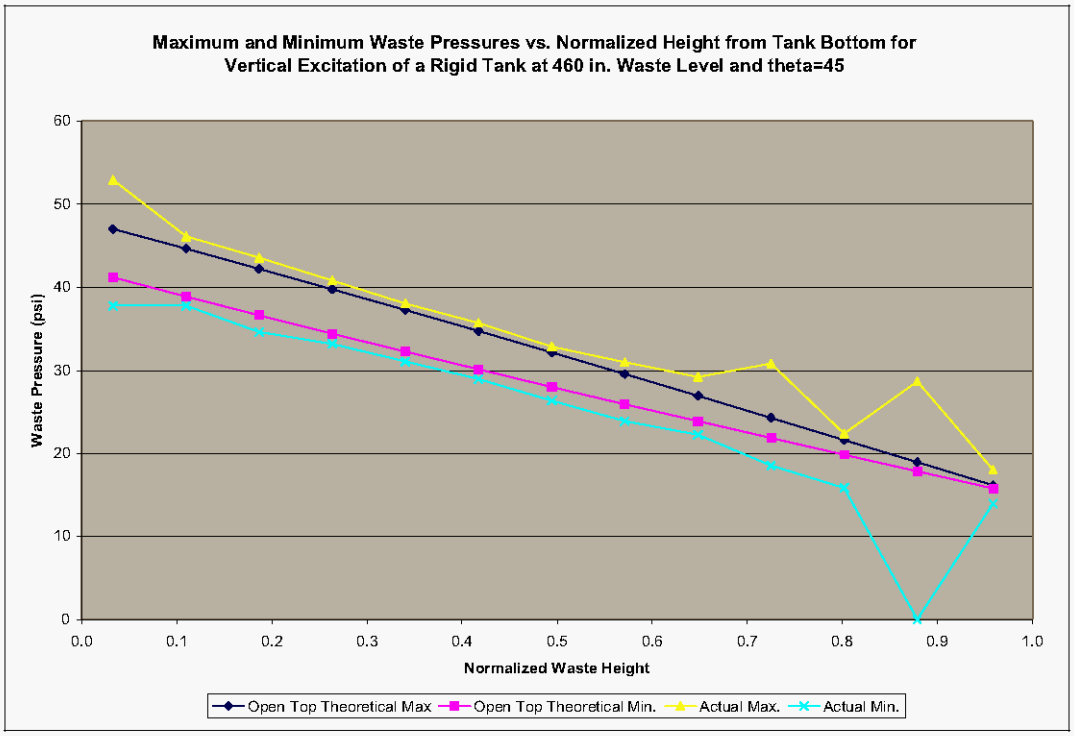

Figure 4-22. Maximum and Minimum Waste Pressures vs. Normalized Height from Tank Bottom for Vertical Excitation of Rigid Tank at 460 in. Waste Level and θ=90° Run at Absolute Pressure.

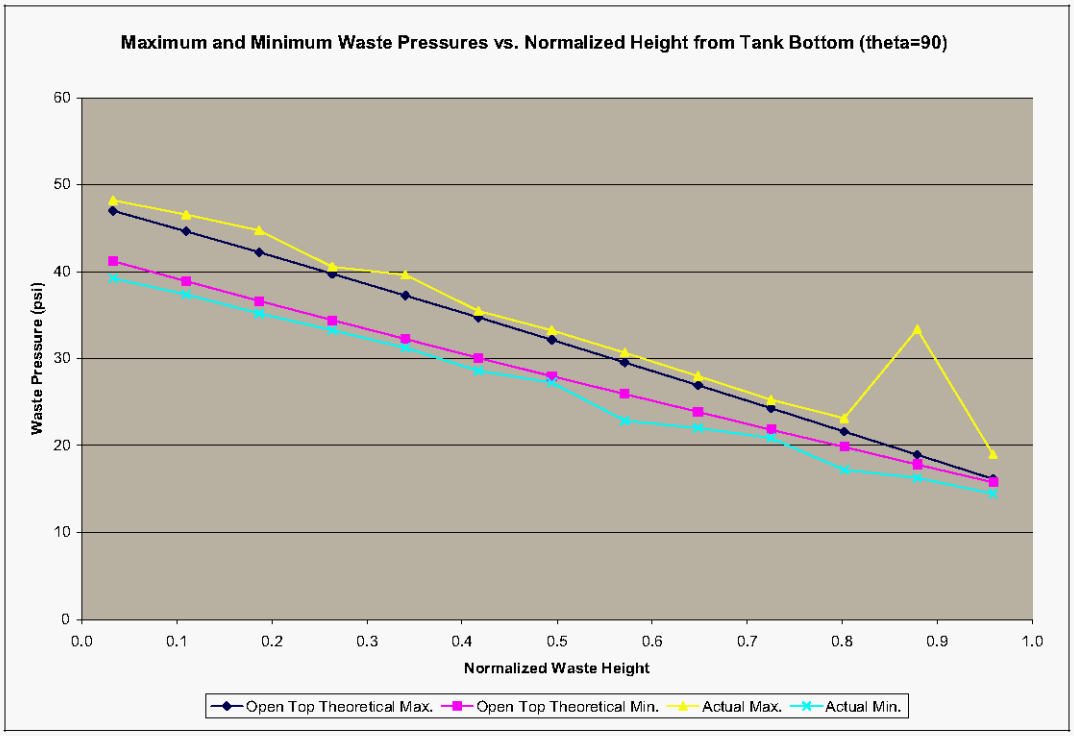

4.3 SLOSH HEIGHT RESULTS

The time history of the maximum slosh height over all waste elements is shown as Figure 4-23. The maximum slosh height according to the theory for the open top tank is 24.5 in. while the maximum slosh height from the simulation is 21.1 in. or 86% of the open top theoretical value. Again, it appears that the presence of the dome act to inhibit the convective response. Recall also that the only damping present for the rigid tank simulations are the artificial bulk viscosities that are not expected to affect the convective response or maximum slosh height. In other words, the lower maximum slosh height does appear to be due to the presence of the dome rather than by over-damping of the convective response.

The unusual behavior noted in Figure 4-23 is that the maximum height of the free surface is greater than 10 in. during the first 5 s under gravity load alone. This was not seen in the maximum slosh height time histories shown in Figure 3-20 for the 422 in. waste level, and it appears to be either a limitation in the post processing routine used to calculate the free surface height at the higher waste level or else a result of the mesh density. It may very well be that this effect could be minimized by including more resolution in the waste element mesh where the waste elements contact the dome, but this was not tested.

Investigation of the waste free surface shape under gravity loading showed that the initial "slosh height" under gravity loading was actually the result of increased waste height near the tank boundary that appears similar to a meniscus as shown in Figure 4-24.

Figure 4-23. Maximum Slosh Height Time History Over All Waste Elements for Horizontal Excitation of the Rigid Tank at the 460 in. Waste Level.

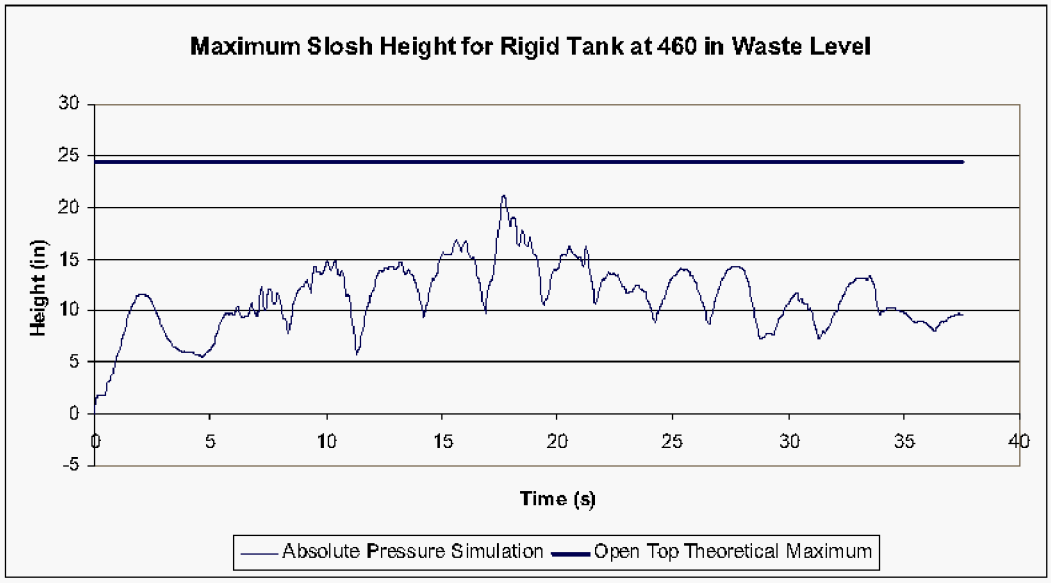

Figure 4-24. Plot of Waste Free Surface Under Gravity Loading Only for the Rigid Tank at the 460 in. Waste Level.

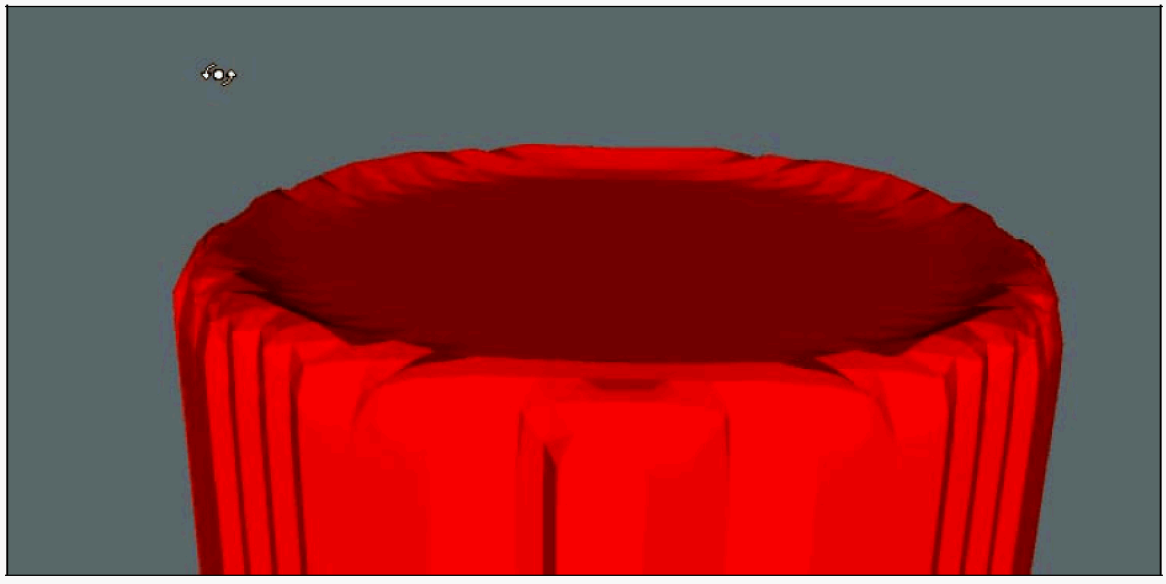

5.0 FLEXIBLE TANK DYTRAN MODEL AT 422 INCH WASTE LEVEL

5.1 DAMPING IMPLEMENTATION AND CALIBRATION

The section presents the results of several runs that were performed to determine the best way to implement damping and the best value of the dynamic relaxation factor to be used in Dytran in order to achieve the desired effective damping. The target effective damping was based on the guidelines given in DOE-STD-1020-2002. Target damping for the fluid convective response is 0.5% critical damping, and the target effective damping for the fluid impulsive response is in the range of 2-4% critical damping.

The initial screening as to the appropriate value of the dynamic relaxation factor was made based on the decay behavior and peak values of the horizontal hydrodynamic force time history. However, very similar behavior occurs in other response parameters such as pressure time histories, and nodal displacement time histories.

The initial calibration study was performed by running the simulations at gage rather than absolute pressure because initially it was more difficult to get stable solutions running at absolute pressure. Once stable solutions were achieved using absolute pressure, and the best damping implementation had been identified tentatively, this configuration was rerun at absolute pressure to ensure that the gage and absolute pressure simulations behaved similarly. Not all cases described below were rerun at absolute pressure – in fact, a stable solution was not achieved running Case 3 (described below) at absolute pressure.

The damping implemented in the Dytran tank models consists of a single damping or dynamic relaxation parameter that is introduced in the central difference integration scheme of the equations of motion using the VISCDMP command. The damping takes the form

$$v^{n+\frac{1}{2}} = v^{n\ \frac{1}{2}}(1-\alpha) + a^n \cdot \Delta t\,,$$

where v denotes the grid point velocity, a is the acceleration, Δt is the time step, and α is the dynamic relaxation parameter or damping coefficient (not the same as the mass proportional damping parameter α in ANSYS). The dynamic relaxation parameter can be defined individually for each available structural element type. In the tank models, the damping was applied to the grid points of the tank shell elements, including the shell elements that form the rigid portion of the tank model.

The choice of the dynamic relaxation parameter depends on the frequency, and the critical damping value at a given frequency, and according to the guideline given in MSC 2005a, should be taken to be approximately 5/3 times the product of the frequency and the time step,. That is,

$$\alpha_{crit} = \frac{5}{3}\omega \cdot \Delta t .$$

It is clear from the Dytran damping formulation that frequencies below the selected frequency will be over-damped and frequencies above the selected frequency will be under-damped.

The impulsive frequency for the tank calculated via Equation 4.16 of BNL 1995 is approximately 7 Hz. The nominal damping value to enforce 4% critical damping at the impulsive frequency of 7 Hz is 3.4 x 10^{-4}.

$$\alpha_{impulsive} = (0.04)(\frac{5}{3})(2\pi f_i)\Delta t = (0.04)(\frac{5}{3})(2\pi \cdot 7Hz)(1.158x10^{-4}s) = 3.4x10^{-4}$$

Several different combinations of damping were run to determine the effect of damping on the solution. The cases presented are as follows:

Case 1: The damping parameter (α) was fixed throughout the simulation at the nominal value of 3.4 x 10^{-4} per MSC 2005a with the intent of enforcing 4% critical damping at the impulsive frequency.

Case 2 (a, b, c, and d): The damping parameter was fixed throughout the simulation at much higher values of 0.08, 0.04, 0.02, and 0.01. These values were selected by trial and error by attempting to achieve a balance between an appropriate effective damping during the initial free vibration period and the response during the seismic transient. These damping values were intended to provide approximately 4% critical damping during the initial free vibration phase of the breathing mode under the gravity load. According to Equation 4.53 of BNL 1995, the breathing mode frequency of the tank is 6.1 Hz, for the 422 in. waste level.

Case 3: The damping parameter was set to 0.08 during the initial application of the gravity load, then was set to zero at the beginning of the seismic loading and left at zero for the remainder of the simulation.

The damping in Cases 2 a, b, c, and d was increased significantly above the damping in Case 1 because it was apparent from the results in Case 1 that the initial free vibration period was highly under-damped, in spite of the guideline given in MSC 2005a.

The effects of damping in each of the cases will be determined from the results of the initial free vibration period and horizontally applied seismic load. The results reviewed consist of the peak horizontal hydrodynamic force, waste pressures, stresses, and displacement time history of a node near the middle of the tank wall.

Due to the extensive amount of data, the results presented during the initial evaluation of damping will focus mostly on the coupling surface reaction forces for the different cases.

However, the same conclusions would be reached by studying the behavior of the other system responses such as the waste pressures, tank stresses, or nodal displacements.

The effective damping during the initial free vibration phase was quantified by determining the rate of decay of the various responses. The effective damping during the seismic excitation was qualitatively determined by comparing the actual peak responses to the theoretical peak responses.

Application of the logarithmic decrement δ to the decay of a selected response implies that for a constant critical damping ratio ξ, the ratio of successive peak responses is constant. For small critical damping ratios, the logarithmic decrement can be approximated as

$$\delta \equiv \ln(\frac{x_1}{x_2}) \approx 2\pi\xi .$$

More generally, the number of cycles n required to achieve a R% reduction in amplitude for a given critical damping ratio ξ is

$$n \approx \frac{1}{2\pi\xi} \ln(\frac{100}{100 - R}) .$$

The investigation showed that the effective damping appeared to be slightly higher during the seismic excitation than during the initial free vibration phase. Because damping is applied to grid point motion in Dytran, this is likely due to the fact that many more grid points are moving during the seismic excitation (the dome and primary tank bottom), and much more mass is in motion.

The simulation time of the initial free vibration phase varied depending on the case. The goals of the initial phase were to achieve a steady-state solution to the gravity loading before introducing the seismic load, to quantify the effective system damping by response decay, and to isolate the breathing mode frequency of the tank. The simulation time needed to achieve a steady-state solution to the gravity load depends on the damping. A lower value of the damping parameter requires a longer initial period, whereas a shorter initial phase will suffice with a higher value of the damping parameter. All cases could have been run with a long initial phase, but this would have resulted in significant run time penalties.

5.2 HYDRODYNAMIC FORCES

5.2.1 Horizontal Excitation

The peak horizontal hydrodynamic forces for the flexible tank are again calculated via Equation 4.31 of BNL 1995 with the instantaneous accelerations replaced by the

appropriate spectral accelerations. If the contributions of the impulsive mode and first three convective modes are combined in a square-root-sum-of-squares (SRSS) fashion, the theoretical maximum horizontal hydrodynamic force is 7.56×10^6 lbf. The above value is based on spectral accelerations from the 4% damped spectrum.

For horizontal excitation in Case 1, gravity was run for 15 s before the application of the seismic input. At the end of the seismic input, the simulation was run for approximately 16 s of unforced motion.

The peak horizontal reaction force shown in Figure 5-1 for Case 1 is 7.52×10^6 lbf, or 99% of the theoretical value. The sloshing period of approximately 5 s is reflected at the end of the horizontal force time history. The effective damping can be evaluated by reviewing the decay of the vertical coupling surface reaction force shown in Figure 5-1. The vertical reaction force trace reflects the breathing mode frequency of approximately 6 Hz as shown in Figure 5-2.

It is evident in Figure 5-1 and Figure 5-2 that with the relatively low damping parameter in Case 1, the effective damping decreases during the initial free vibration phase. The logarithmic decrement equation also shows that for 4% critical damping, the ratio of successive peaks should be 1.29. That is, each subsequent peak should be approximately 78% of the preceding peak. With this rate of decay, the vertical reaction force should be within 10% of the steady state value within nine cycles (~1.5 s) and within 1% of the steady state value within 18 cycles (~3 s). Clearly, the decay rate shown in Figure 5-1 and Figure 5-2 is much slower, showing that the solution is under-damped during the initial free vibration phase. Similarly, the solution is under-damped during the final free vibration phase following the seismic excitation. On the other hand, because the peak horizontal reaction force achieves 99% of the theoretical value during the seismic transient, the solution is apparently not under-damped during the seismic excitation.

Similar behavior is displayed in the decay of waste pressures and tank stresses. As an example, the hoop stress time history for element 433 near the mid-height of the tank wall at $\theta=0$ is shown in Figure 5-3.

Figure 5-1. Coupling Surface Reaction Forces for the Flexible Tank Under Horizontal Seismic Input at Gage Pressure– Case 1.

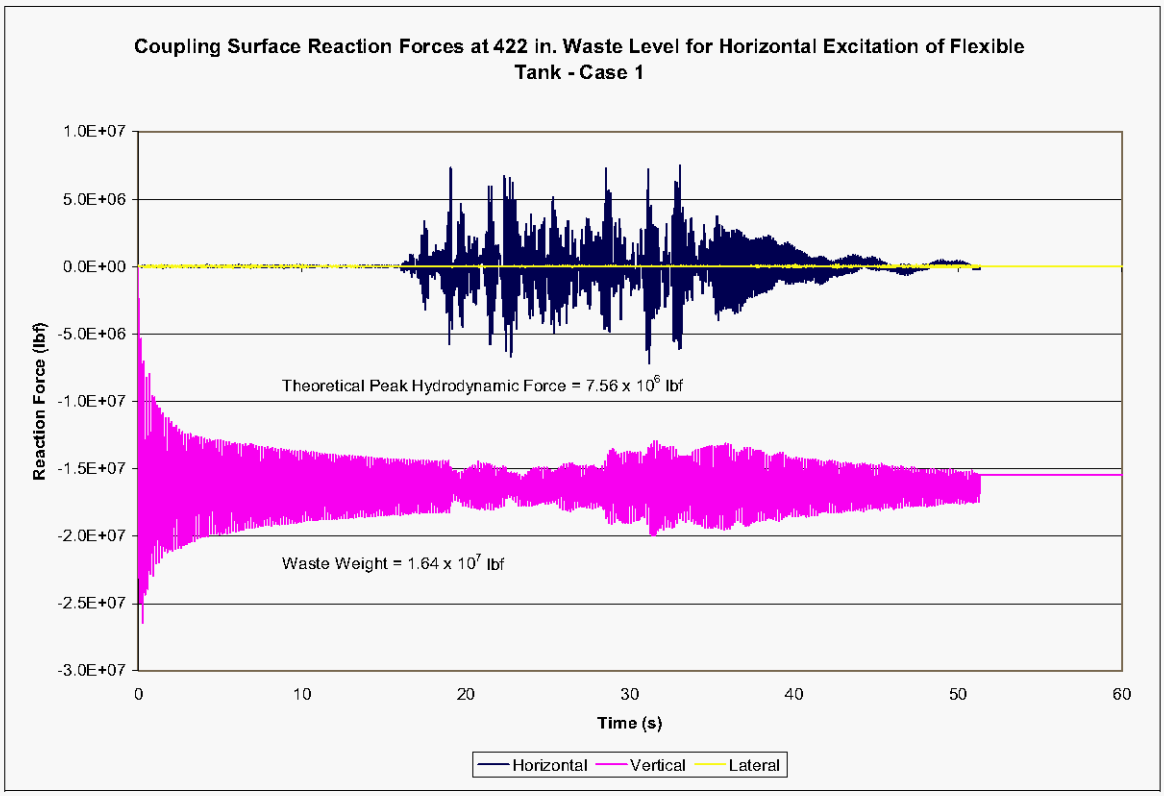

Figure 5-2. Coupling Surface Reaction Forces for the Flexible Tank Under Horizontal Seismic Input at Gage Pressure During the Initial Free Vibration Phase – Case 1.

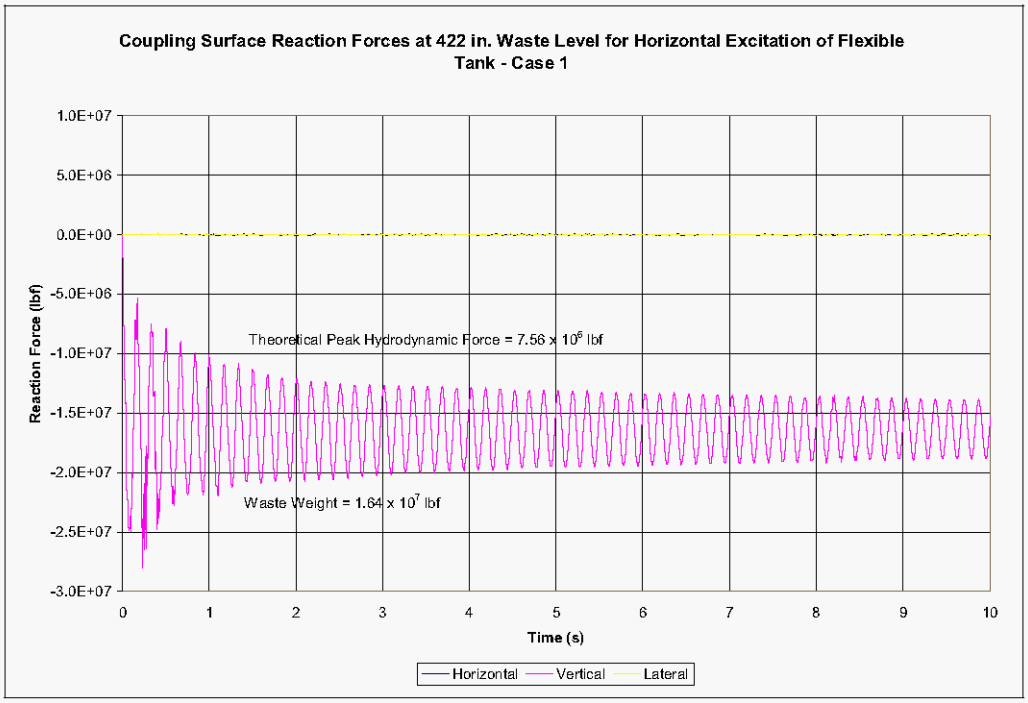

Figure 5-3. Mid-Wall Hoop Stress for Flexible Tank at Gage Pressure and θ=0 – Case 1.

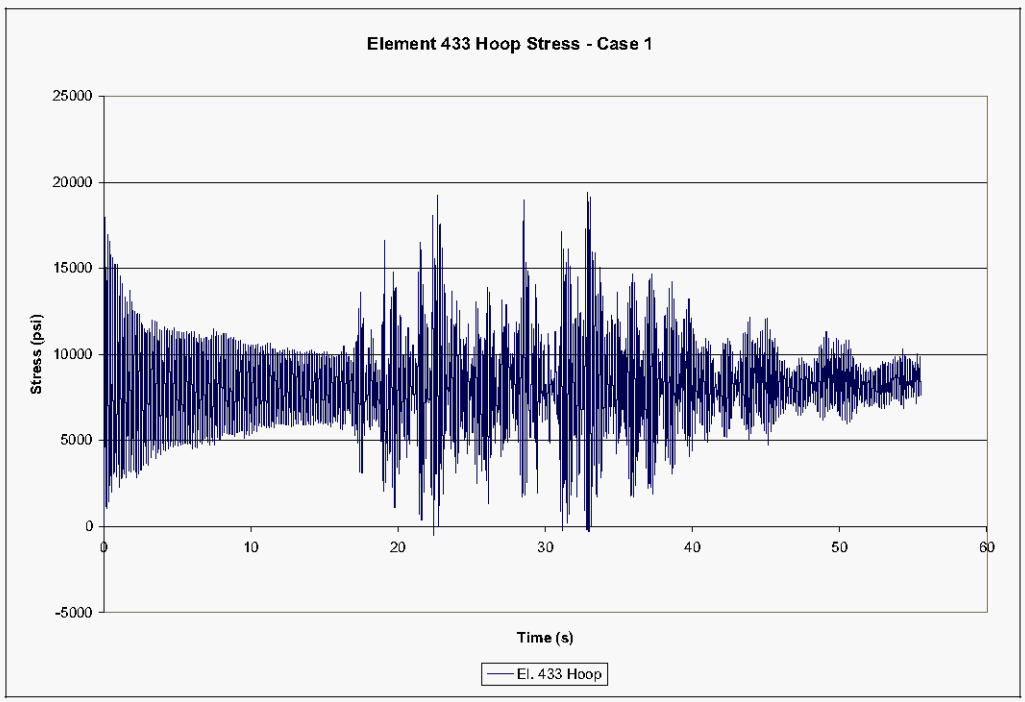

Since the initial free vibration phase was under-damped in Case 1, the damping parameter was increased in Cases 2a, 2b, 2c, and 2d in an attempt to achieve approximately 4% damping during the initial free vibration phase. The values of 0.08, 0.04, 0.02, and 0.01 were selected based on trial and error and gave initial damping in the range of a few percent based on the decay during the initial gravity phase.

For horizontal excitation in Case 2a, gravity was run for 2 s before the application of the seismic input. At the end of the seismic input, the simulation was run for an additional 20 s of unforced motion. The coupling surface reaction forces for Case 2a are shown in Figure 5-4 and Figure 5-5. The results show that the vertical reaction force has essentially reached the steady state value in 1.5 s (9 cycles) giving an effective damping during the initial phase of approximately 7-8% critical damping.

The peak horizontal hydrodynamic reaction force shown in Figure 5-5 is approximately 5 x 10^6 lbf, or 63% of the theoretical value, showing that the solution is still over-damped during the seismic excitation.

Essentially the same conclusions regarding effective damping during free vibration can be drawn from other response parameters such as pressure time-history plots or from time-history plots of nodal displacements along the tank wall.

Figure 5-4. Coupling Surface Reaction Forces at the 422 in. Waste Level for the Flexible Tank at Gage Pressure Under Horizontal Seismic Input During the Initial Free Vibration Phase – Case 2a (alpha=0.08).

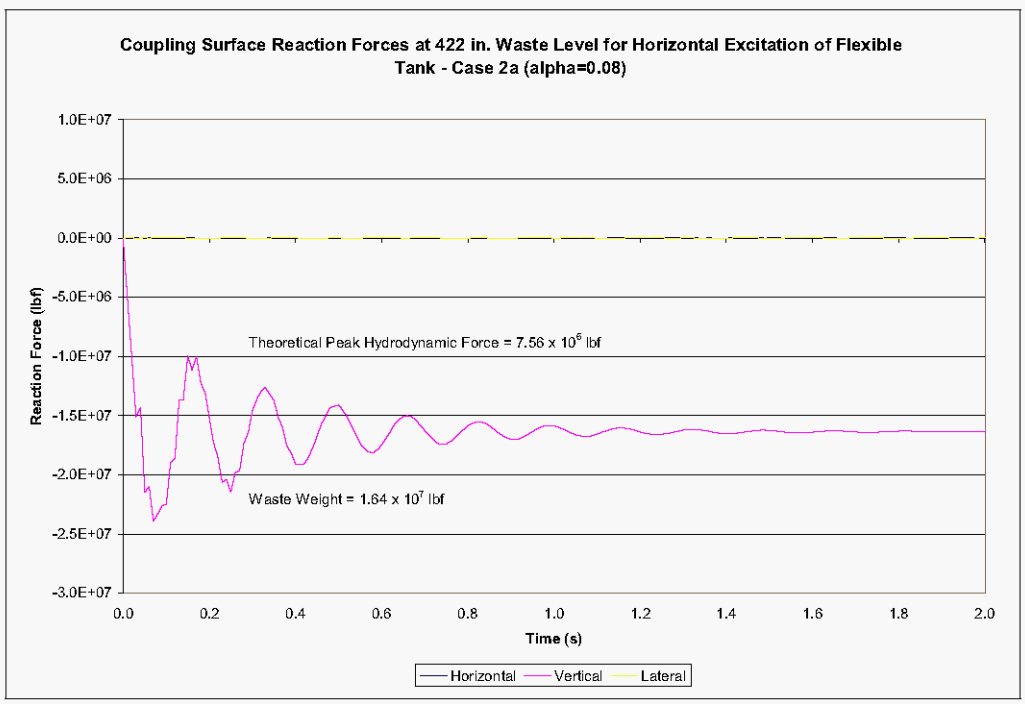

Figure 5-5. Coupling Surface Reaction Forces at the 422 in. Waste Level for the Flexible Tank at Gage Pressure Under Horizontal Seismic Input – Case 2a (alpha=0.08).

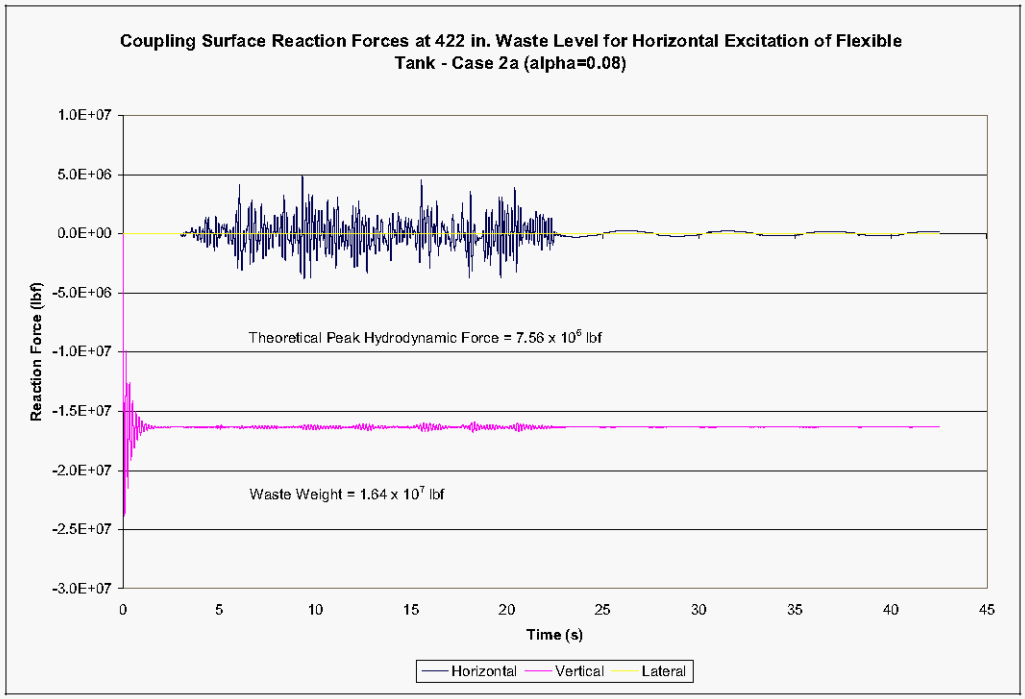

For horizontal excitation in Case 2b, gravity was run for 3 s before the application of the seismic input. At the end of the seismic input, the simulation was run for an additional 19 s of unforced motion. The coupling surface reaction forces for Case 2b are shown in Figure 5-6 and Figure 5-7. The results show that the vertical reaction force has essentially reached the steady state value in 3.0 s (18 cycles) giving an effective damping during the initial phase of approximately 4% critical damping.

The peak horizontal hydrodynamic reaction force shown in Figure 5-7 is approximately 6.4 x 10^6 lbf, or 85% of the theoretical value, showing that the solution is still over-damped during the seismic excitation.

Figure 5-6, Coupling Surface Reaction Forces at the 422 in. Waste Level for the Flexible Tank at Gage Pressure Under Horizontal Seismic Input During the Initial Free Vibration Phase – Case 2b (alpha=0.04).

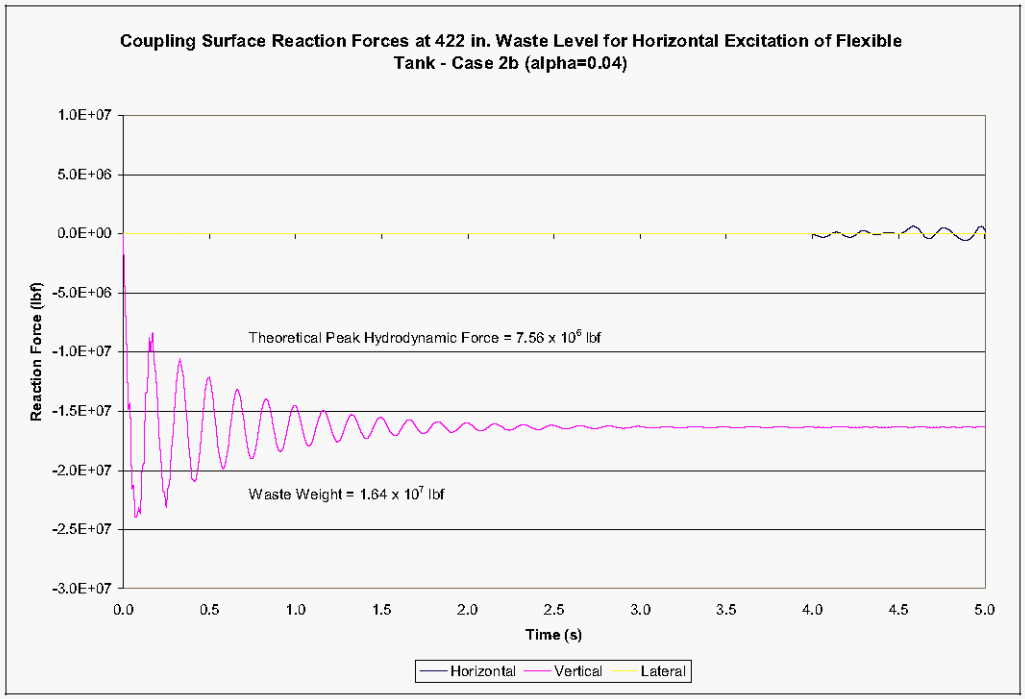

Figure 5-7. Coupling Surface Reaction Forces at the 422 in. Waste Level for the Flexible Tank at Gage Pressure Under Horizontal Seismic Input – Case 2b (alpha=0.04).

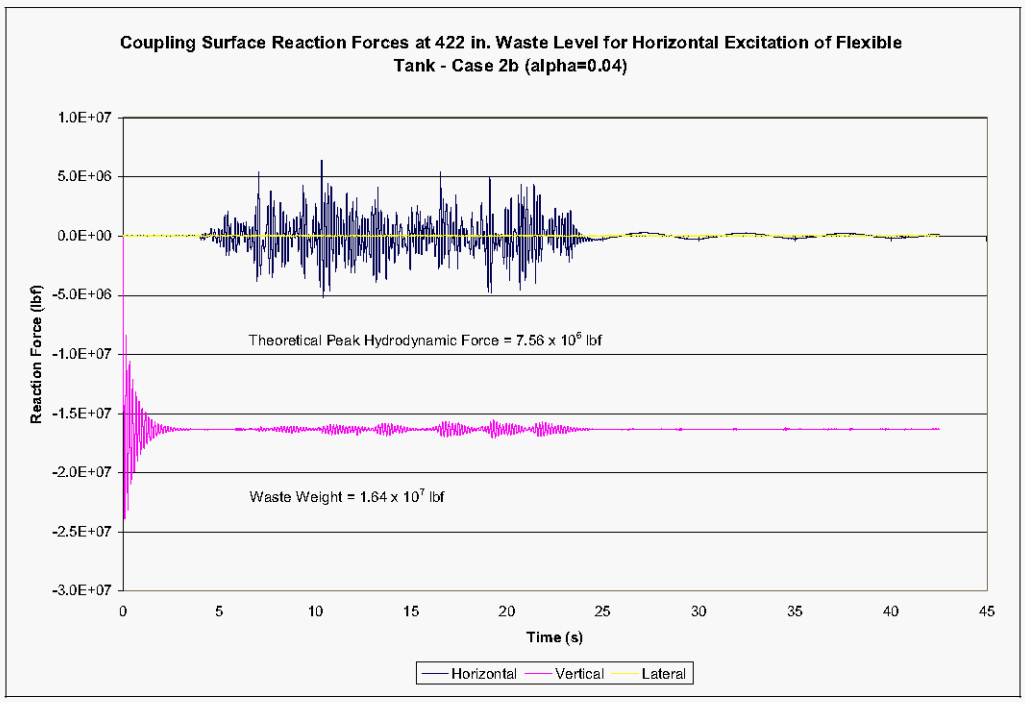

In Case 2c, gravity was run for 5 s before the application of the seismic input, and the simulation was run for an additional 20 s of unforced motion after the end of the seismic excitation. The coupling surface reaction forces for Case 2c are shown in Figure 5-8 and Figure 5-9. The vertical reaction force has essentially reached the steady state value in 5-6 s (30-36 cycles) giving an effective damping during the initial phase of approximately 2% critical damping. The breathing mode frequency of approximately 6 Hz is apparent in the vertical reaction force.

The peak horizontal hydrodynamic reaction force shown in Figure 5-9 is 7.09 x 10^6 lbf, or 94% of the theoretical value, when the problem is run at gage pressure. The first convective period of slightly greater than 5 s is displayed in the horizontal reaction force during the period of unforced motion during the last 20 s of the simulation. The coupling surface reaction force during the first three seconds of the second period of unforced motion is shown as Figure 5-10. Evident in that plot are the impulsive frequency of slightly less than 7 Hz in the horizontal reaction force, and the breathing mode frequency of approximately 6 Hz in the vertical reaction force.

When this case was rerun at absolute pressure as discussed in Section 5.3, the peak horizontal reaction force increased slightly to 7.25 x 10^6 lbf, or 96% of the theoretical value as shown in Figure 5-12. The frequency behavior remained the same as shown in Figure 5-11 and Figure 5-13. The peak reaction force during the final free vibration phase shown in Figure 5-12 decays approximately 20% over three cycles from the peak at 29 s to the peak at 45 s. This results in slightly greater than 1% damping for the convective response during free oscillation.

Figure 5-8. Coupling Surface Reaction Forces at the 422 in. Waste Level for the Flexible Tank at Gage Pressure Under Horizontal Seismic Input During the Initial Free Vibration Phase – Case 2c (alpha=0.02).

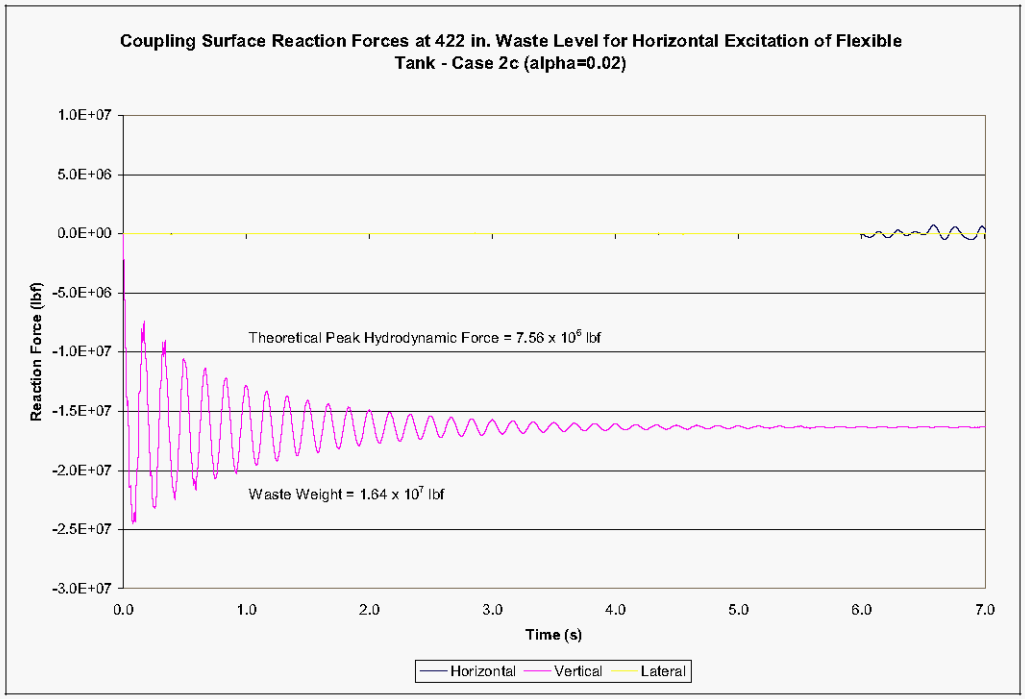

Figure 5-9. Coupling Surface Reaction Forces at the 422 in. Waste Level for the Flexible Tank at Gage Pressure Under Horizontal Seismic Input – Case 2c (alpha=0.02).

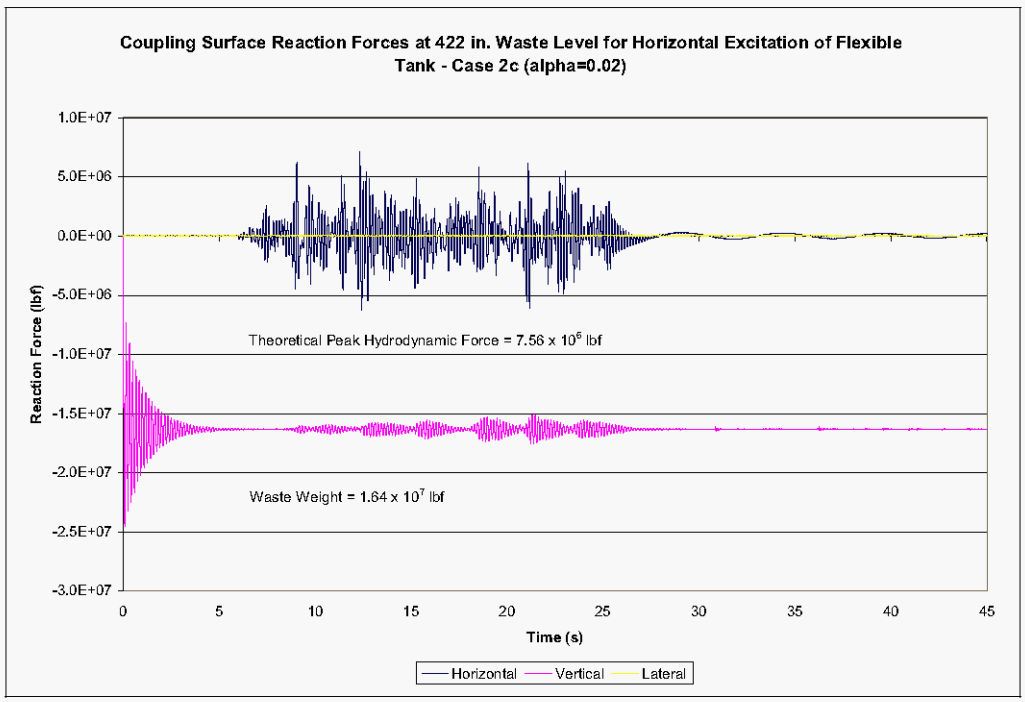

Figure 5-10. Coupling Surface Reaction Forces at the 422 in. Waste Level for the Flexible Tank at Gage Pressure Under Horizontal Seismic Input During the Final Free Vibration Phase – Case 2c (alpha=0.02).

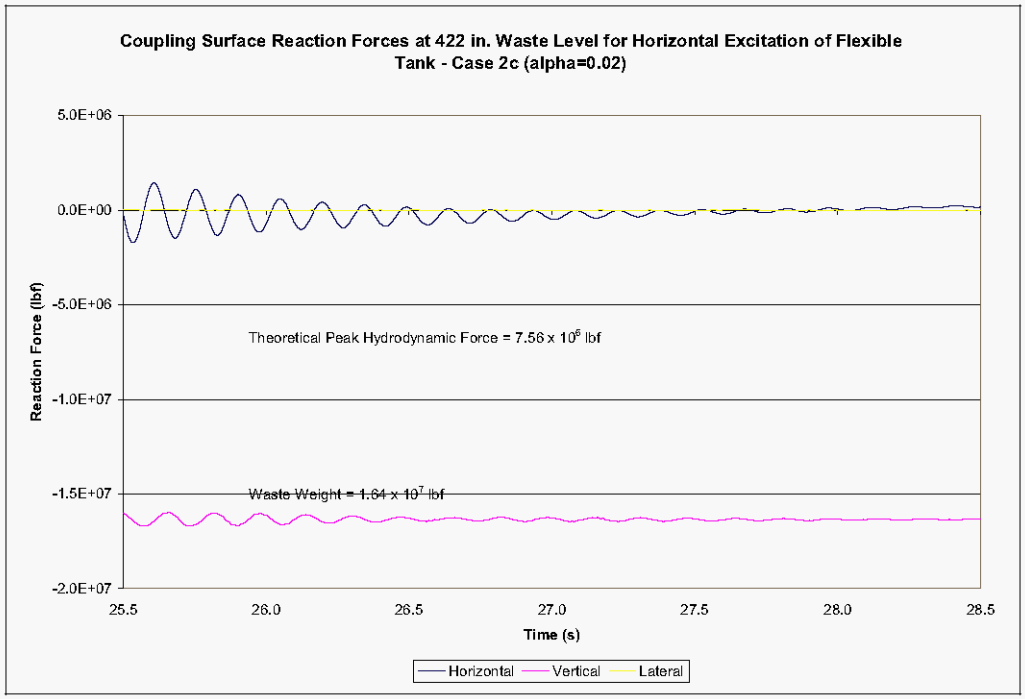

Figure 5-11. Coupling Surface Reaction Forces at the 422 in. Waste Level for the Flexible Tank at Absolute Pressure Under Horizontal Seismic Input During the Initial Free Vibration Phase – Case 2c (alpha=0.02).

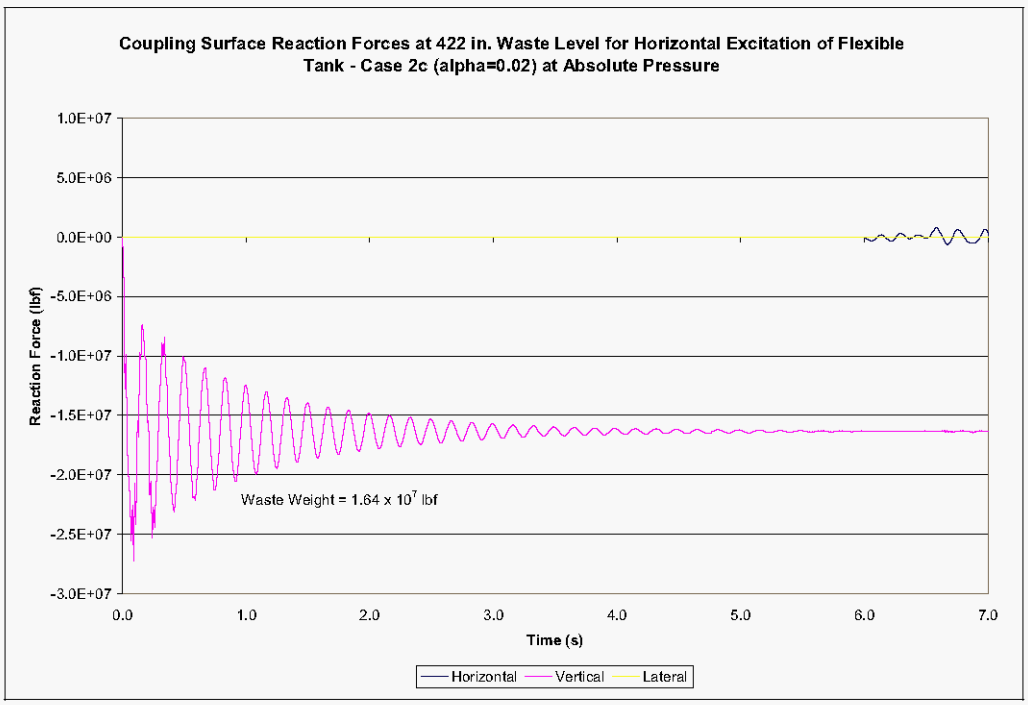

Figure 5-12. Horizontal Coupling Surface Reaction Force at the 422 in. Waste Level for the Flexible Tank at Absolute Pressure Under Horizontal Seismic Input – Case 2c (alpha=0.02).

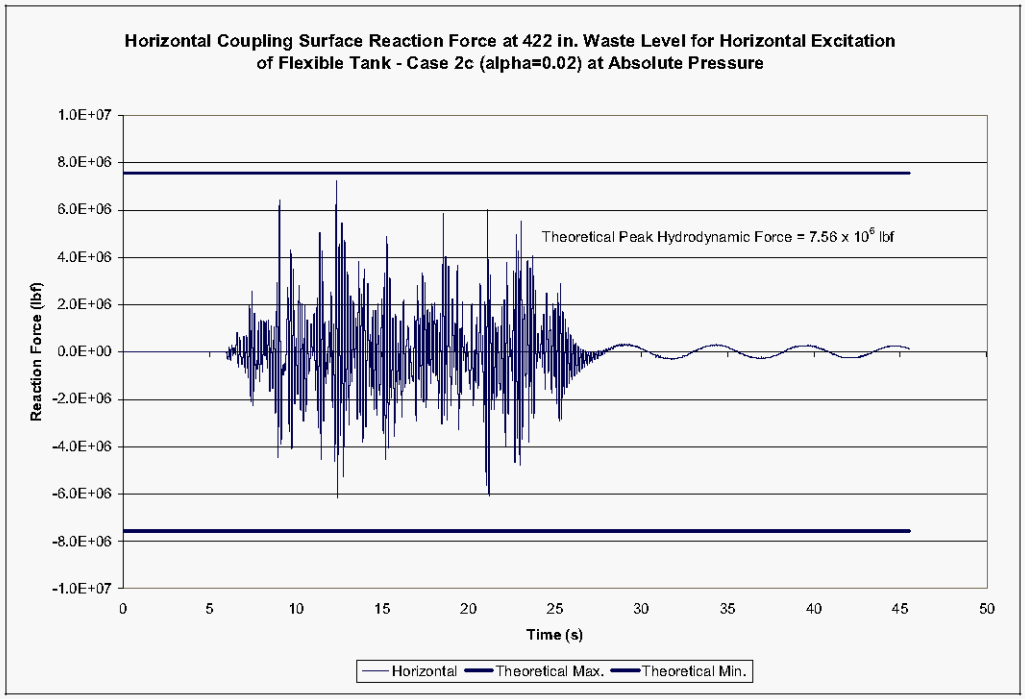

Figure 5-13. Coupling Surface Reaction Forces at the 422 in. Waste Level for the Flexible Tank at Absolute Pressure Under Horizontal Seismic Input During the Final Free Vibration Phase – Case 2c (alpha=0.02).

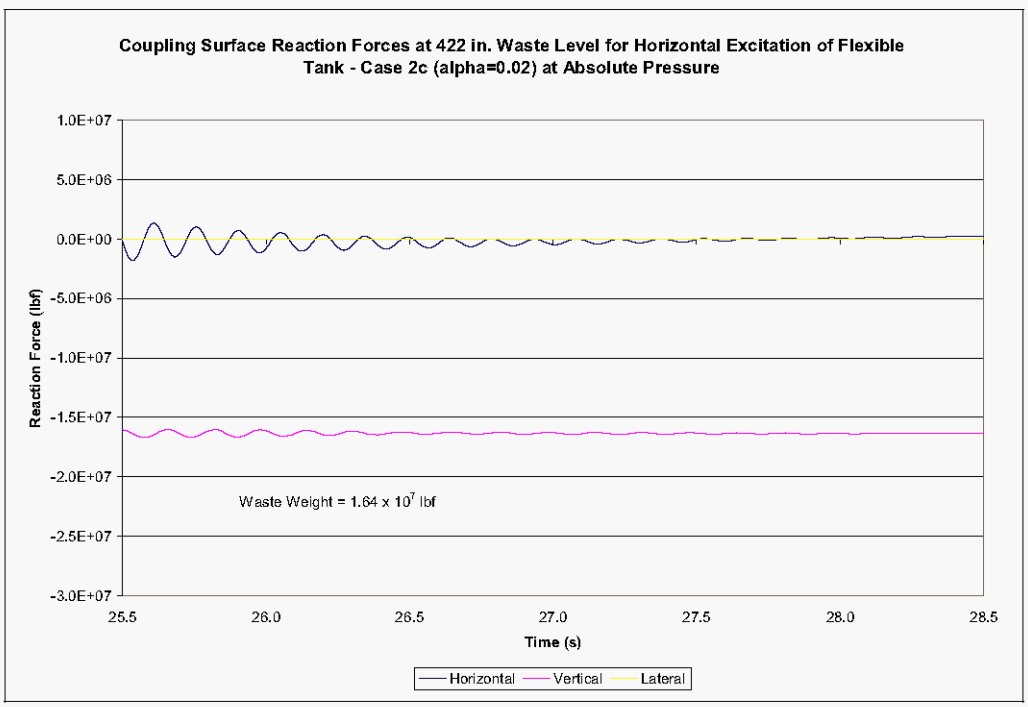

In Case 2d, gravity was run for 8 s before the application of the seismic input, and the simulation was run for an additional 20 s of unforced motion after the end of the seismic excitation. The coupling surface reaction forces for Case 2d are shown in Figure 5-14, Figure 5-15, and Figure 5-16. The vertical reaction force has essentially reached the steady state value in 10 s (60 cycles) giving an effective damping during the initial phase of approximately 1% critical damping. The breathing mode frequency of approximately 6 Hz is apparent in the vertical reaction force.

The peak horizontal hydrodynamic reaction force shown in Figure 5-15 is approximately 7.08 x 10^6 lbf, also 94% of the theoretical value. The first convective period of slightly greater than 5 s is displayed in the horizontal reaction force during the period of unforced motion during the last 20 s of the simulation. The coupling surface reaction force during the first three seconds of the second period of unforced motion is shown as Figure 5-16. As before, the impulsive frequency of approximately 7 Hz is reflected in the horizontal reaction force, and the breathing mode frequency of approximately 6 Hz is reflected in the vertical reaction force.

Figure 5-14. Coupling Surface Reaction Forces at the 422 in. Waste Level for the Flexible Tank at Gage Pressure Under Horizontal Seismic Input During the Initial Free Vibration Phase – Case 2d (alpha=0.01).

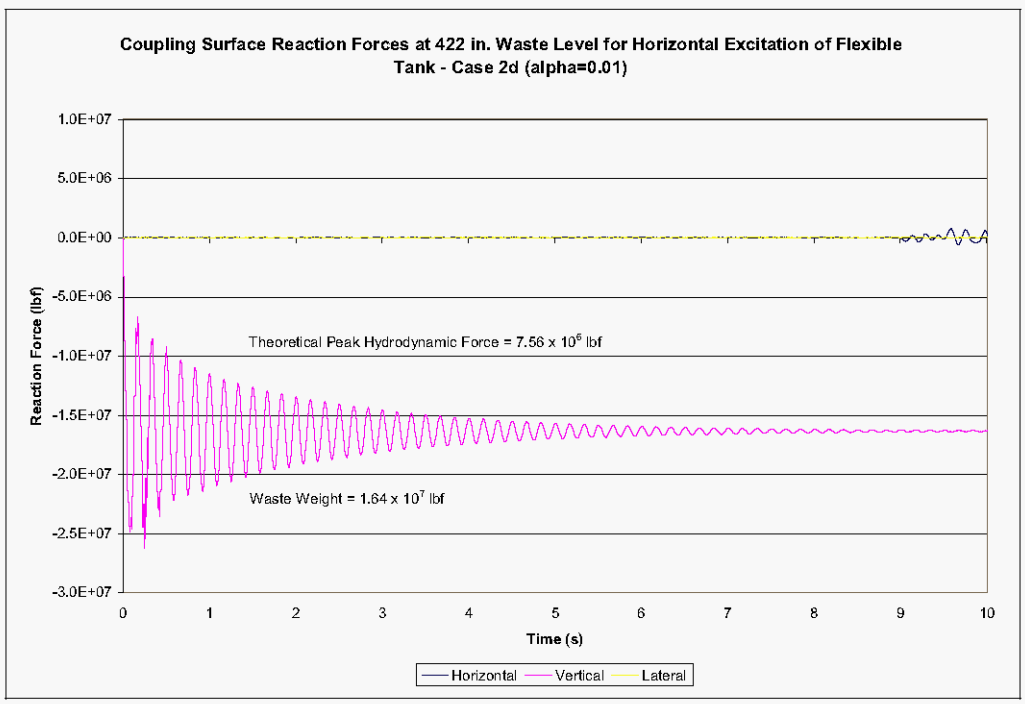

Figure 5-15. Coupling Surface Reaction Forces at the 422 in. Waste Level for the Flexible Tank at Gage Pressure Under Horizontal Seismic Input – Case 2d (alpha=0.01).

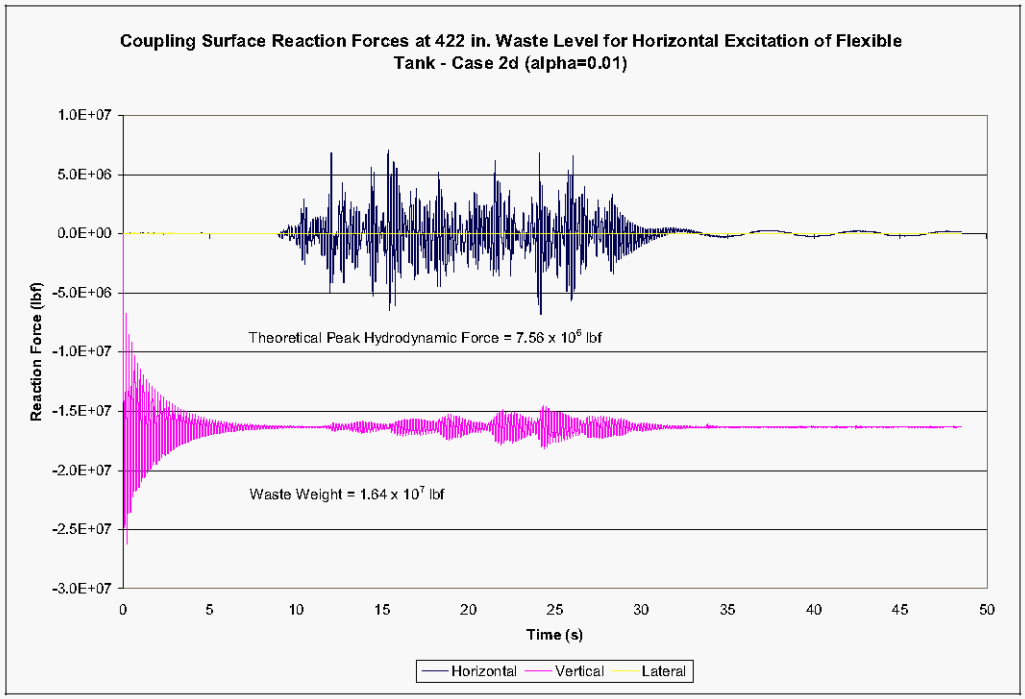

Figure 5-16. Coupling Surface Reaction Forces at the 422 in. Waste Level for the Flexible Tank at Gage Pressure Under Horizontal Seismic Input During the Final Free Vibration Phase – Case 2d (alpha=0.01).

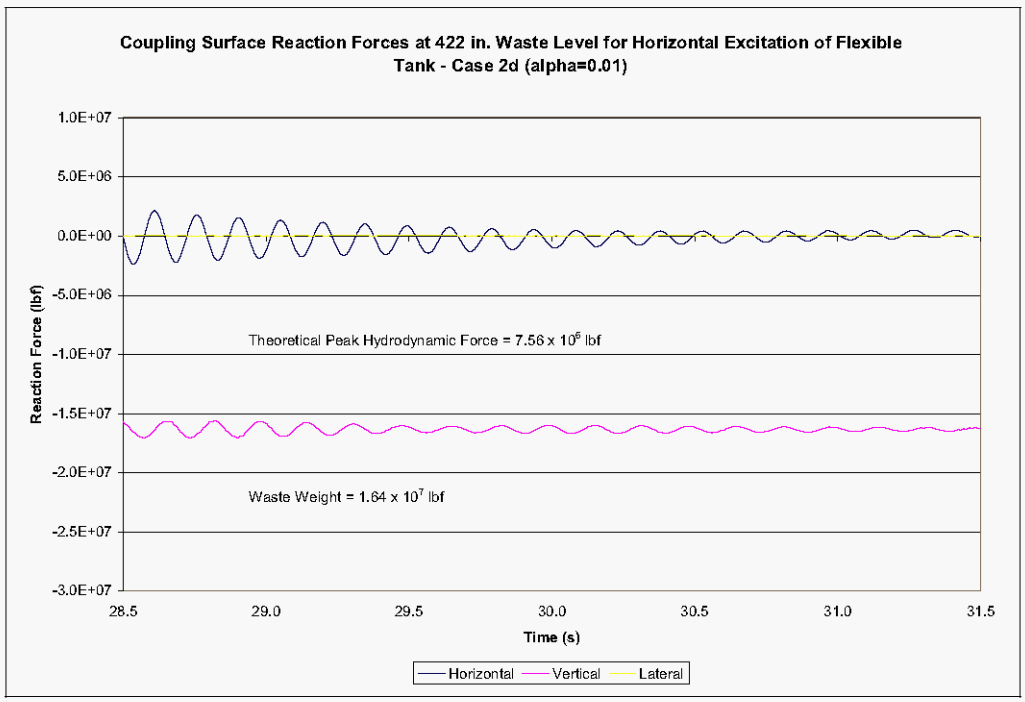

In Case 3, gravity was run for 2 s before the application of seismic input, and the simulation was run for an additional 20 s of unforced motion after the end of the seismic excitation. The peak horizontal reaction force shown in Figure 5-17 for Case 3 is 7.57 x 10^6 lbf, or 101% of the theoretical value. The sloshing period of approximately 5 s is reflected at the end of the horizontal force time history. Figure 5-18 shows the coupling surface reaction forces for Case 3 during the period of unforced motion from 23.0 to 25.0 s. The impulsive frequency of 7 Hz is evident in the horizontal reaction force, while the breathing mode frequency of approximately 6 Hz is displayed in the vertical reaction force.

Figure 5-17. Coupling Surface Reaction Forces for the Flexible Tank at Gage Pressure Under Horizontal Seismic Input – Case 3.

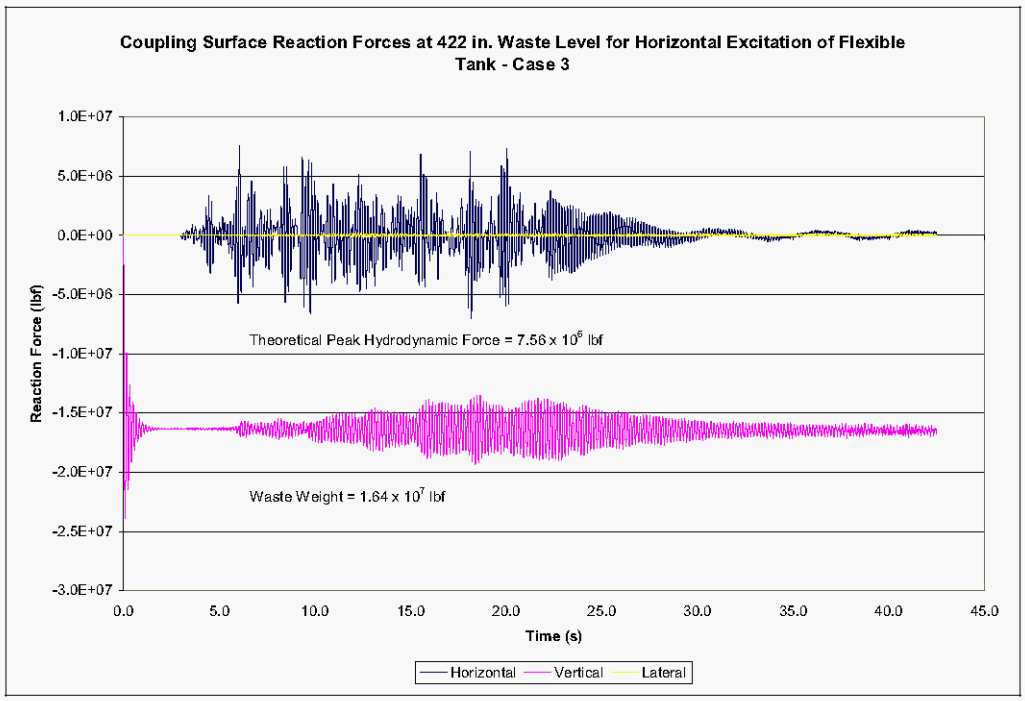

Figure 5-18. Coupling Surface Reaction Forces for the Flexible Tank at Gage Pressure Under Horizontal Seismic Input from 23.0 to 25.0 s – Case 3

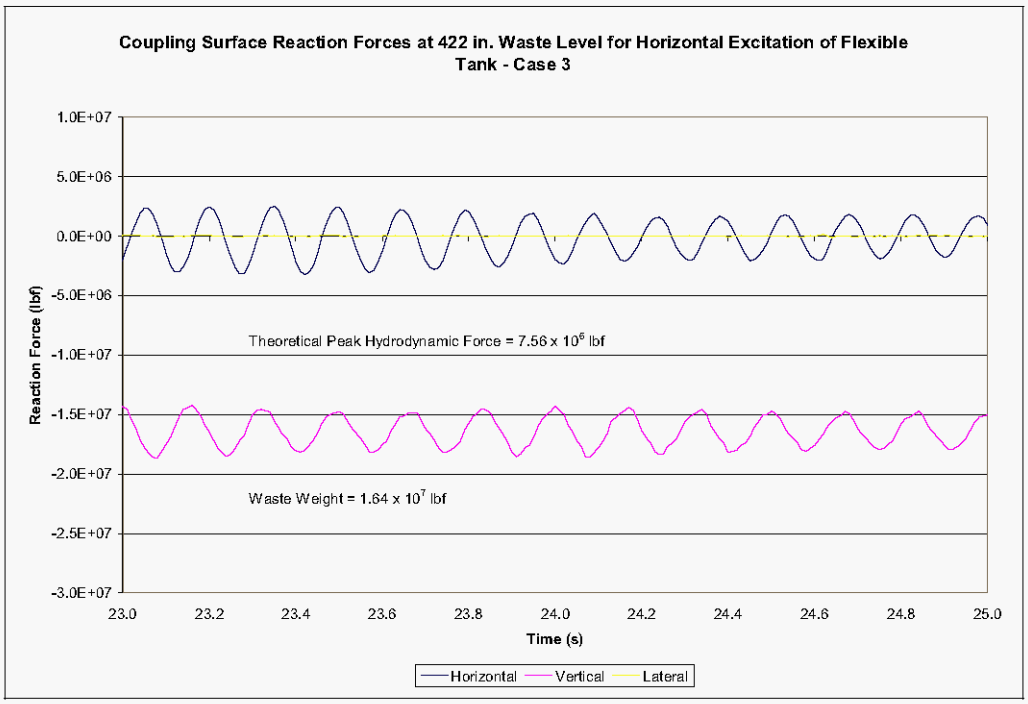

The coupling surface reaction forces show that Case 1 is significantly under-damped, and Cases 2a and 2b are somewhat over-damped. Cases 2c and 2d are nearly the same, very slightly over-damped, and both agree well with theory. Case 3 also shows good agreement with theory, but as noted above, a stable solution was not achieved for Case 3 when run at absolute pressure – a decided disadvantage for this damping implementation. Thus, on the basis of the results of horizontal excitation, only the results for Cases 2c and 3 will be presented for vertical excitation.

It will be shown in Section 5.2.2 that the response to Case 2c under vertical excitation is slightly under-damped and the response to vertical excitation for Case 3 is significantly under-damped. This behavior coupled with the noted deficiencies of the damping implementation in Case 3 will lead to Case 2c being the best overall choice for the implementation of damping.

5.2.2 Vertical Excitation

The peak vertical hydrodynamic forces for the flexible tank calculated via Equation 4.57 of BNL 1995 with the instantaneous accelerations replaced by the appropriate spectral accelerations and the impulsive and convective components combined via the SRSS rule. The theoretical maximum vertical hydrodynamic force based on spectral accelerations from the 4% damped spectrum is 5.24 x 10^6 lbf. Accordingly, the vertical coupling surface reaction force should vary between

$$(-1.64 \times 10^7 - 5.24 \times 10^6)\text{lbf} = -2.16 \times 10^7 \text{ lbf}$$

and

$$(-1.64 \times 10^7 + 5.24 \times 10^6)\text{lbf} = -1.12 \times 10^7 \text{ lbf}.$$

The results in Section 5.2 show that damping implemented in Case 2c and Case 3 provided the best match to theoretical results. Accordingly, additional results from the other cases will not be presented in the body of the report.

The coupling surface reaction force due to vertical excitation for Case 2c at gage pressure is shown as Figure 5-19. The maximum and minimum values for the vertical force are -1.07×10^7 and -2.27×10^7 lbf, respectively. That is, the peak vertical hydrodynamic force is 109% of the theoretical value in the positive direction

$$((1.64 \times 10^7 - 1.07 \times 10^7)/(5.24 \times 10^6)) \times 100 = 109,$$

and 120% of the theoretical value in the negative direction

$$((2.27 \times 10^7 - 1.64 \times 10^7)/(5.24 \times 10^6)) \times 100 = 120.$$

Figure 5-19. Coupling Surface Reaction Forces for the Flexible Tank at Gage Pressure Under Vertical Seismic Input – Case 2c.

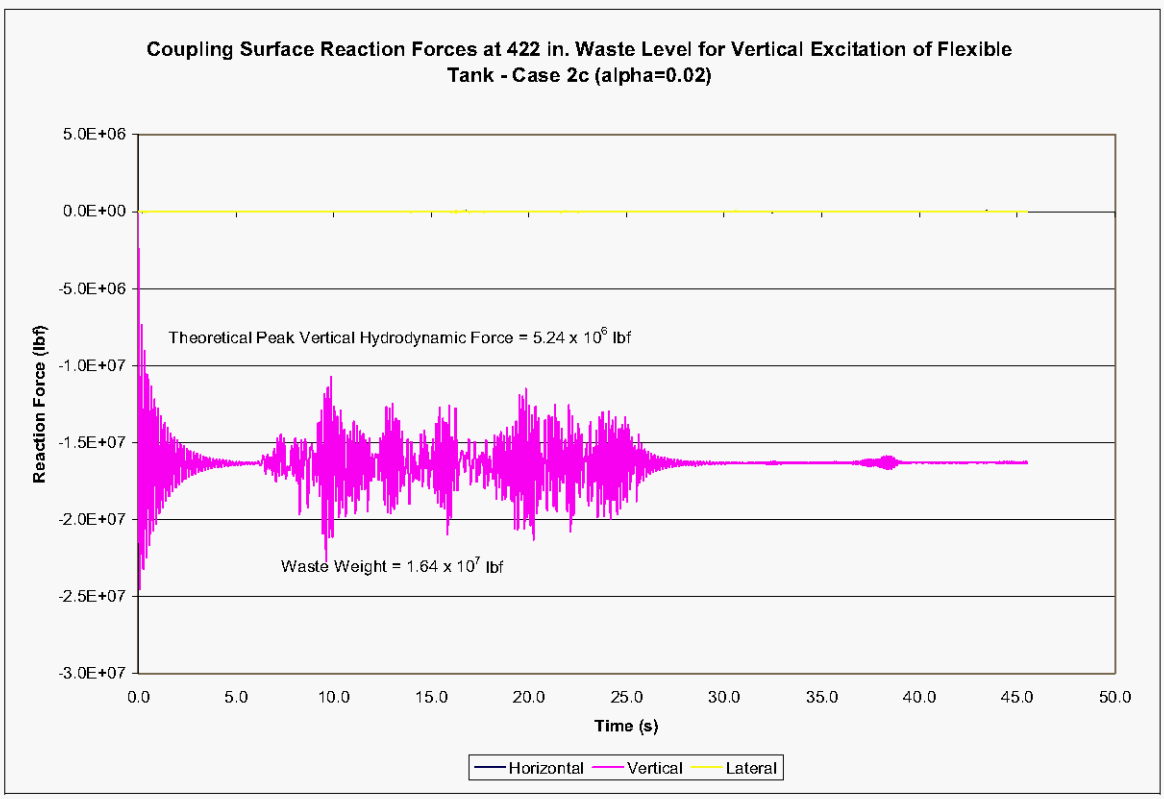

The coupling surface reaction force due to vertical excitation for Case 3 is shown as Figure 5-20. The maximum and minimum values for the vertical force are -97.7×10^7

and -2.35 x 10^7 lbf, respectively. That is, the peak vertical hydrodynamic force is 127% of the theoretical value in the positive direction

$$((1.64 \times 10^7 - 97.7 \times 10^7)/(5.24 \times 10^6)) \times 100=127,$$

and 135% of the theoretical value in the negative direction

$$((2.35 \times 10^7 - 1.64 \times 10^7)/(5.24 \times 10^6)) \times 100=135.$$

Figure 5-20. Coupling Surface Reaction Forces for the Flexible Tank at Gage Pressure Under Vertical Seismic Input – Case 3.

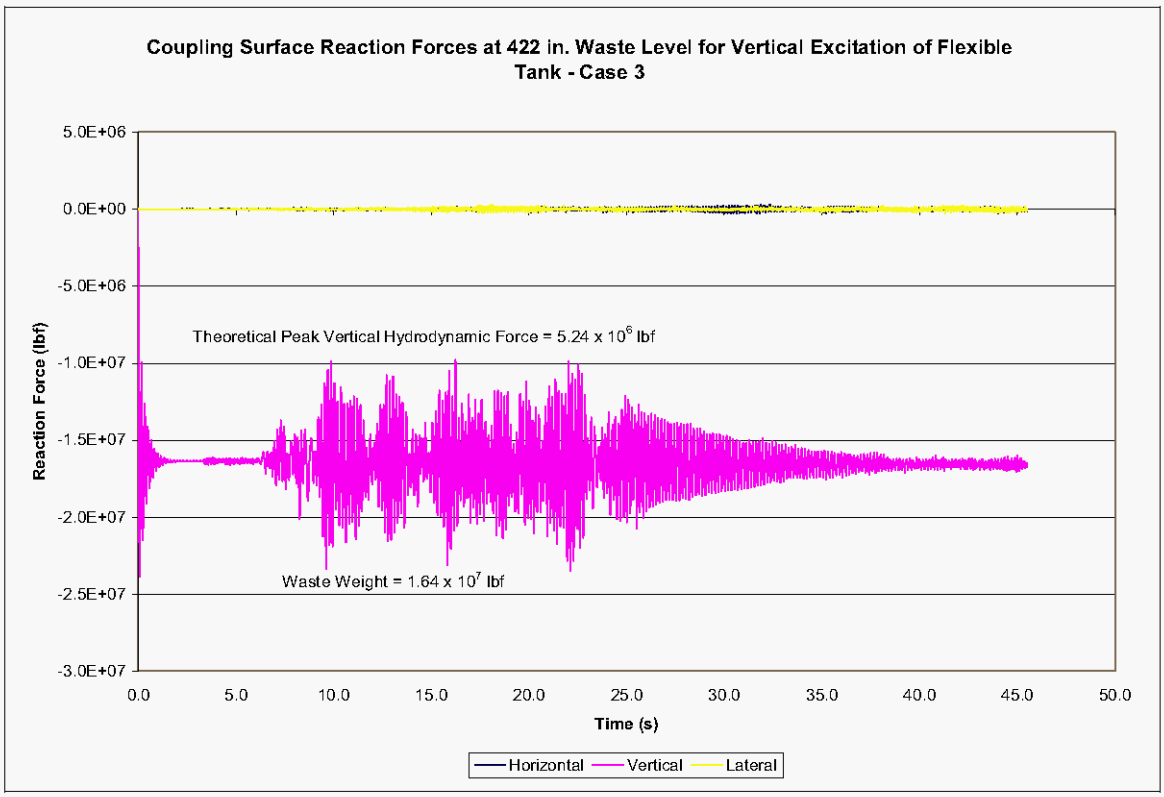

Based on the peak hydrodynamic forces caused by vertical excitation, Case 3 is significantly under-damped, and Case 2c is slightly under-damped. Since Case 3 is somewhat under-damped for horizontal excitation (evidenced by pressure and hydrodynamic force results), and Case 2c is slightly over-damped for horizontal excitation, the damping value used in Case 2c is judged to provide the best overall match to the theoretical predictions.

Consequently, the focus of the remainder of the analysis will be on results from Case 2c. Results from other cases are included in the appendices.

For reference, the coupling surface reaction forces for vertical excitation at absolute pressure are shown in Figure 5-21. The maximum and minimum vertical reaction forces

are -1.07 x 10^7 lbf and -2.27 x 10^7 lbf, exactly the same as in the gage pressure simulation.

Figure 5-21. Coupling Surface Reaction Forces for the Flexible Tank at Absolute Pressure Under Vertical Seismic Input – Case 2c.

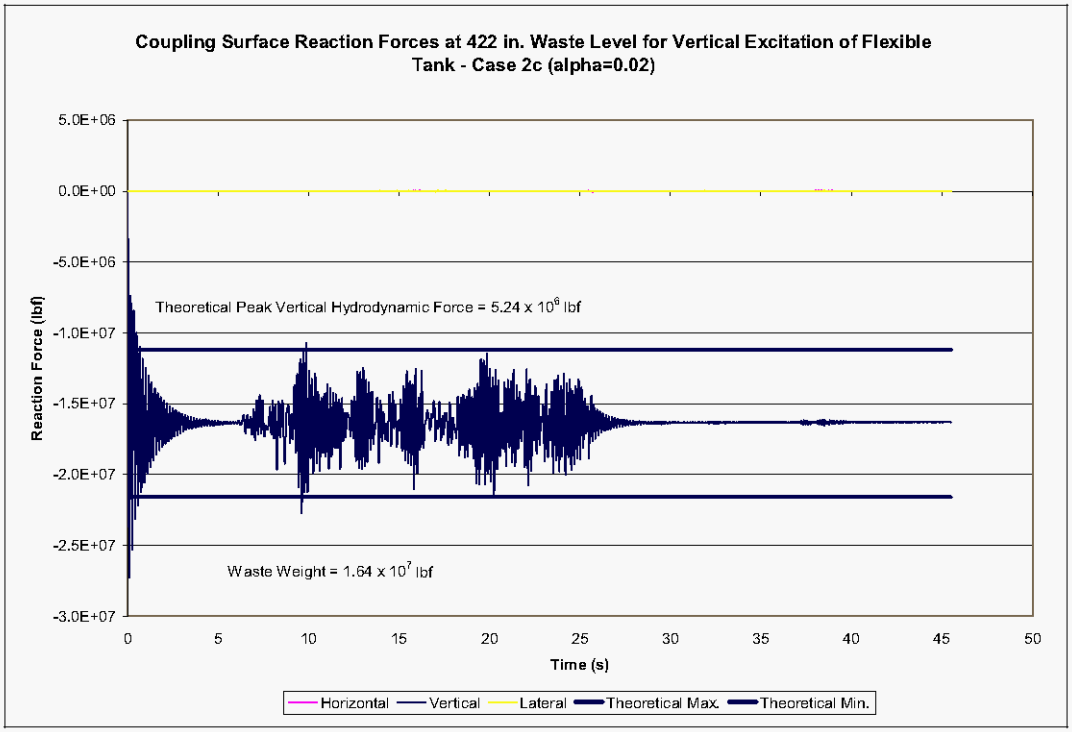

5.3 WASTE PRESSURES

5.3.1 Horizontal Excitation Run at Absolute Pressure

The theoretical peak hydrodynamic pressures due to horizontal excitation are given by Equation 4.24 of BNL 1995. The total pressures are the sum of the hydrostatic pressures and the hydrodynamic pressures. The hydrostatic, peak hydrodynamic and peak total pressures for the elements in the sets "plusx_els", "press_45", are shown in Table 5-1 and Table 5-2. The maximum theoretical pressures for the elements set "plusz_els" is simply the hydrostatic pressures shown in Table 3-1 because the theoretical hydrodynamic pressures are zero at θ=90°.

Table 5-1. Theoretical Maximum Absolute Waste Pressures for Horizontal Excitation in the Flexible Tank at 422 in. Waste Level for Elements at θ=0.

"Plusx_els" Element No.	Hydrostatic Pressure (psi)	Peak Hydrodynamic Pressure (psi)	Peak Total Pressure (psi)
10482	14.7	0	14.7
9753	15.8	3.6	19.4
9024	18.0	6.6	24.6
8295	20.1	9.0	29.1
7566	22.3	10.9	33.2
6837	24.5	12.5	37.0
6108	26.7	13.8	40.5
5379	28.8	14.8	43.6
4650	31.0	15.7	46.7
3921	33.2	16.3	49.5
3192	35.4	16.8	52.2
2463	37.5	17.1	54.6
1734	39.7	17.2	56.9

Table 5-2. Theoretical Maximum Absolute Waste Pressures for Horizontal Excitation in the Flexible Tank at 422 in. Waste Level for Elements at θ=45°.

"Press_45" Element No.	Hydrostatic Pressure (psi)	Peak Hydrodynamic Pressure (psi)	Peak Total Pressure (psi)
10290	14.7	0	14.7
9561	15.8	2.6	18.4
8832	18.0	4.6	22.6
8103	20.1	6.3	26.4
7374	22.3	7.7	30.0
6645	24.5	8.8	33.3
5916	26.7	9.8	36.5
5187	28.8	10.5	39.3
4458	31.0	11.1	42.1
3729	33.2	11.5	44.7
3000	35.4	11.9	47.3
2271	37.5	12.1	49.6
1542	39.7	12.2	51.9

The pressure time histories for the waste elements along the tank wall at θ=0 are shown in Figure 5-22. The pressure time histories for elements 1734, 6108, and 9753 are shown again in Figure 5-23. These three elements were selected since they are near the bottom, mid-height, and top of the waste, respectively. Figure 5-24, Figure 5-25, Figure 5-26, and Figure 5-27, show similar plots for the waste elements located at θ=45 and 90°.

The data in Figure 5-22 through Figure 5-27 indicate that the hydrostatic pressures match the theoretical values, and that the decay in waste pressures is very similar to the decay in the hydrodynamic forces. The typical peak pressures are approximately 95% of the

theoretical peak values, but at waste elements higher in the tank, pressures exceed theoretical values at a few isolated peaks.

Figure 5-22. Waste Pressures Time Histories for the Flexible Tank at the 422 in. Waste Level for Horizontal Excitation at θ=0, Case 2c (alpha=0.02) Run at Absolute Pressure.

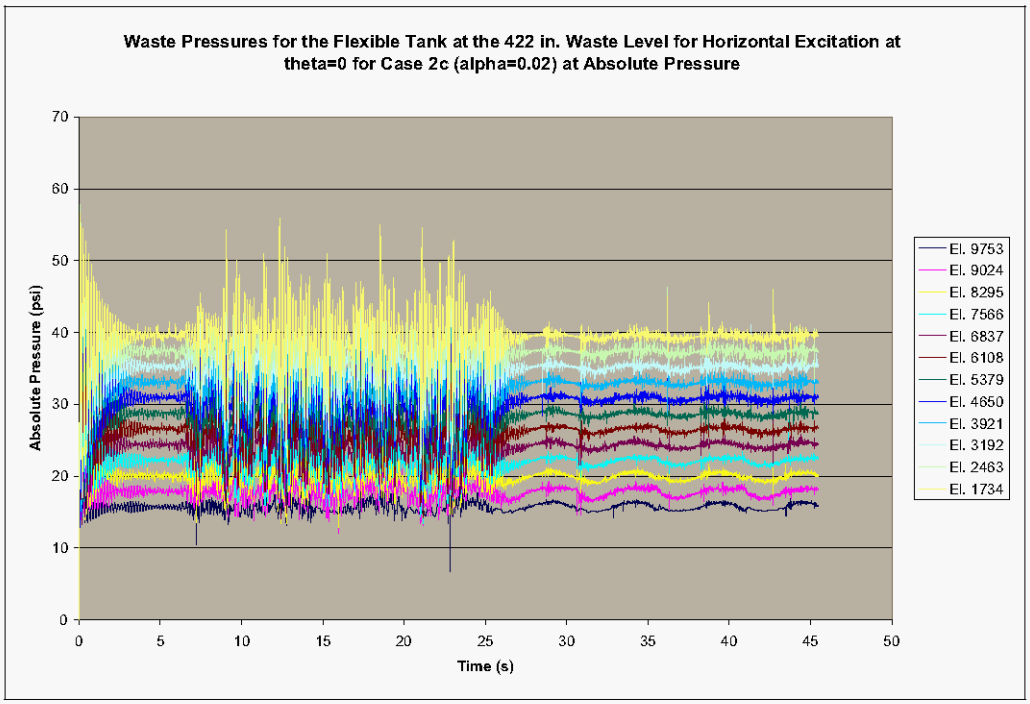

Figure 5-23. Selected Element Pressure Time Histories for the Flexible Tank at the 422 in. Waste Level for Horizontal Excitation at θ=0, Case 2c (alpha=0.02) Run at Absolute Pressure.

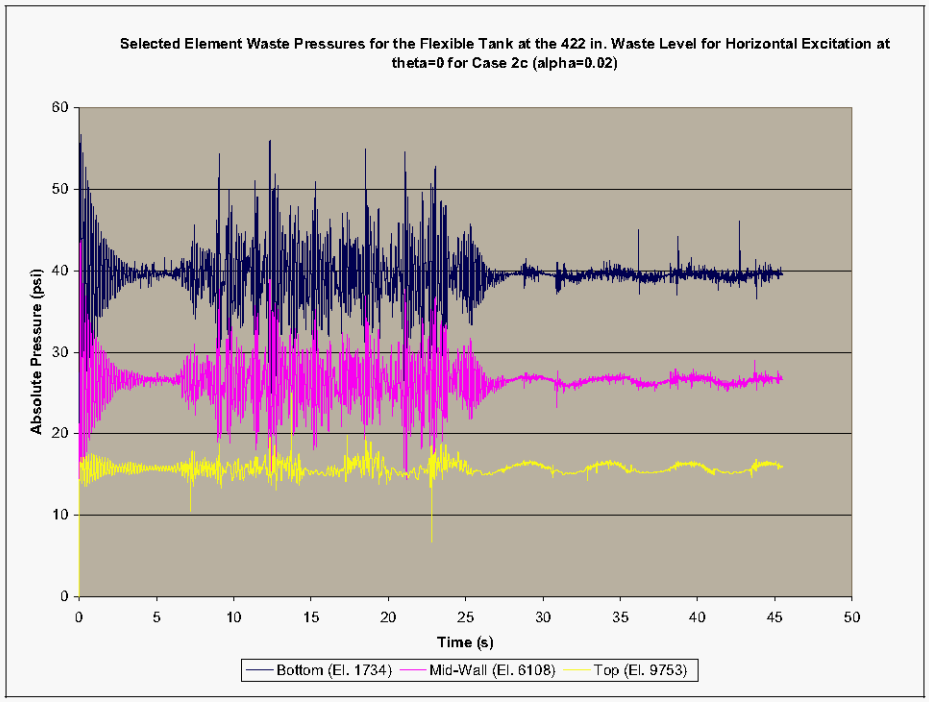

Figure 5-24. Waste Pressures Time Histories for the Flexible Tank at the 422 in. Waste Level for Horizontal Excitation at θ=45, Case 2c (alpha=0.02) Run at Absolute Pressure.

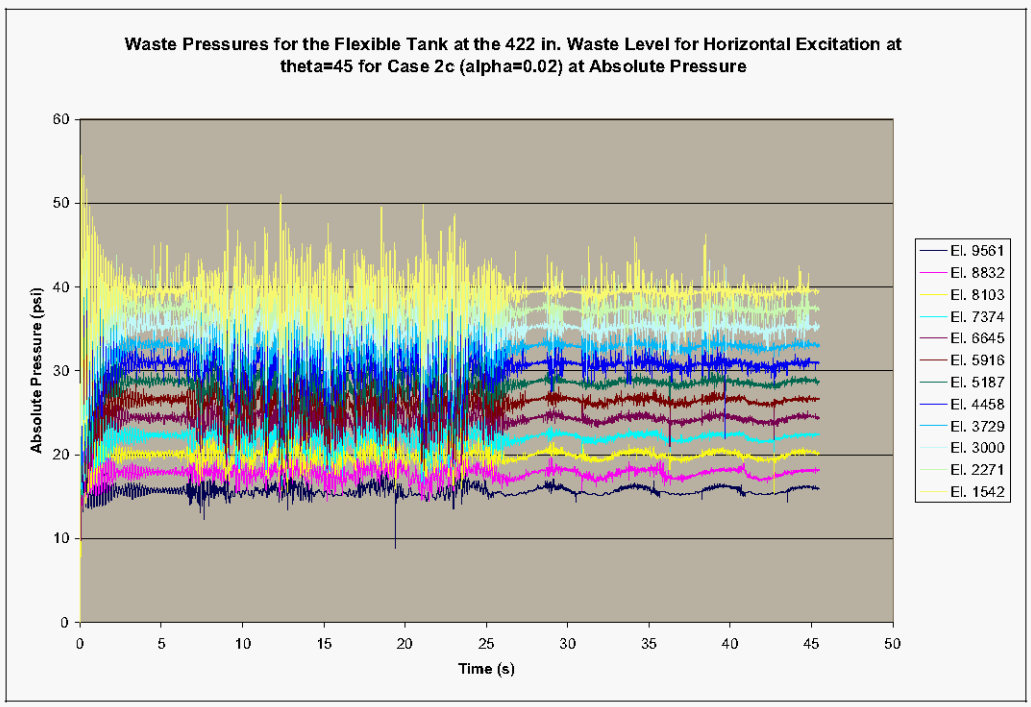

Figure 5-25. Selected Element Pressure Time Histories for the Flexible Tank at the 422 in. Waste Level for Horizontal Excitation at θ=45, Case 2c (alpha=0.02) Run at Absolute Pressure.

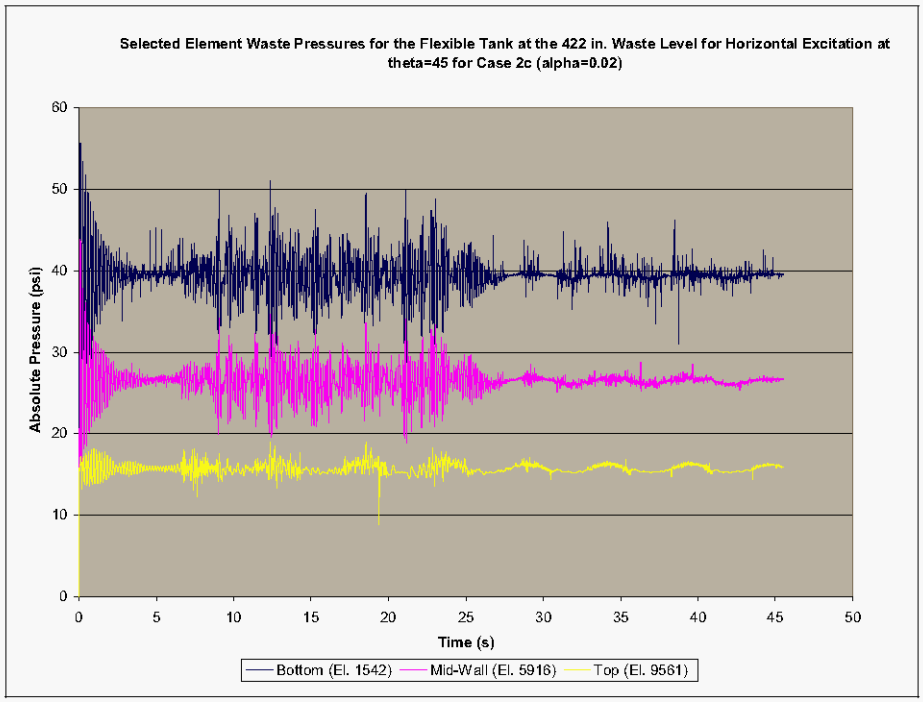

Figure 5-26. Waste Pressures Time Histories for the Flexible Tank at the 422 in. Waste Level for Horizontal Excitation at θ=90, Case 2c (alpha=0.02) Run at Absolute Pressure.

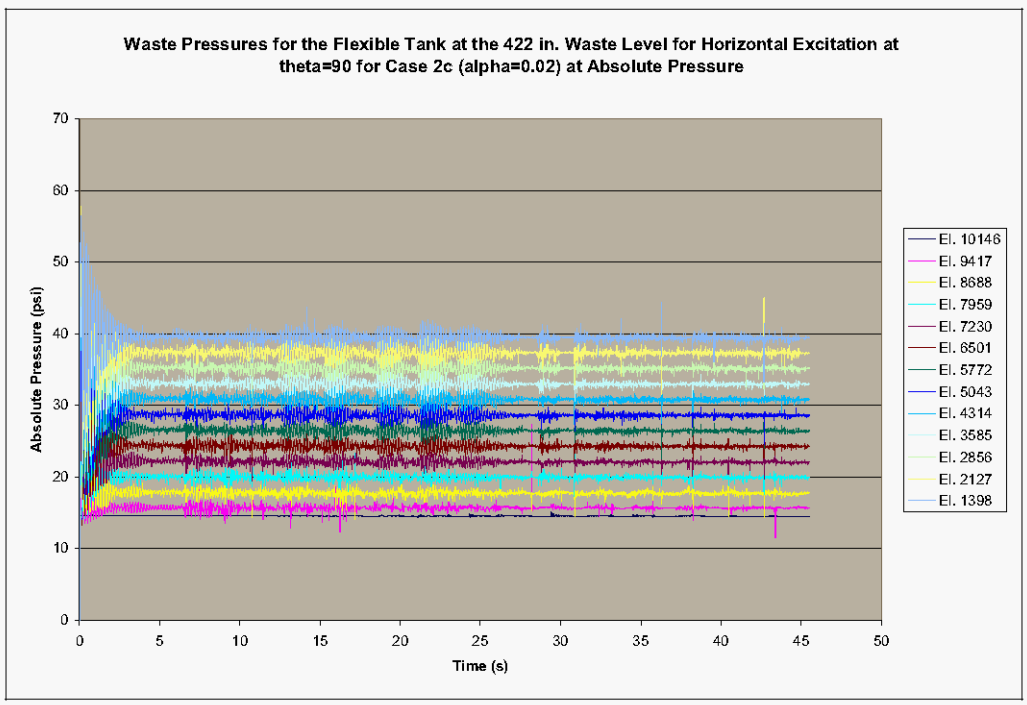

Figure 5-27. Selected Element Pressure Time Histories for the Flexible Tank at the 422 in. Waste Level for Horizontal Excitation at θ=90, Case 2c (alpha=0.02) Run at Absolute Pressure.

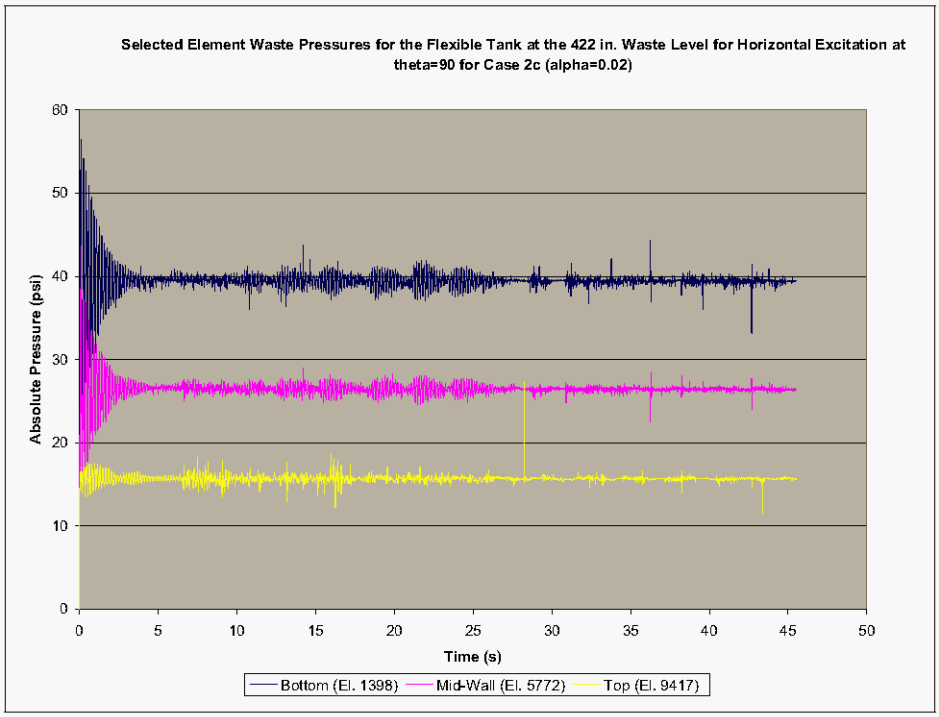

Figure 5-28, Figure 5-29, and Figure 5-30 show comparisons between the solutions at absolute and gage pressure for selected waste elements at θ=0, 45, and 90°. Comparison of the two solutions shows several trends. When the problem is run at absolute pressure, the pressure time histories in the upper portion of the waste are much more regular since the pressures are not near zero. This also has the effect of eliminating some of the high isolated spikes, or spurious peaks that occurred in the uppermost waste elements when the problem was run at gage pressure. This can be seen most easily in Figure 5-29 Figure 5-30. It is also apparent from the plots that during the final free vibration phase the gage pressure solution shows some slight upward drift in the pressures that is not present in the absolute pressure solution.

Figure 5-28. Comparison of Waste Pressures in the Flexible Tank at the 422 in. Waste Level at Absolute and Gage Pressure for Selected Elements at θ=0.

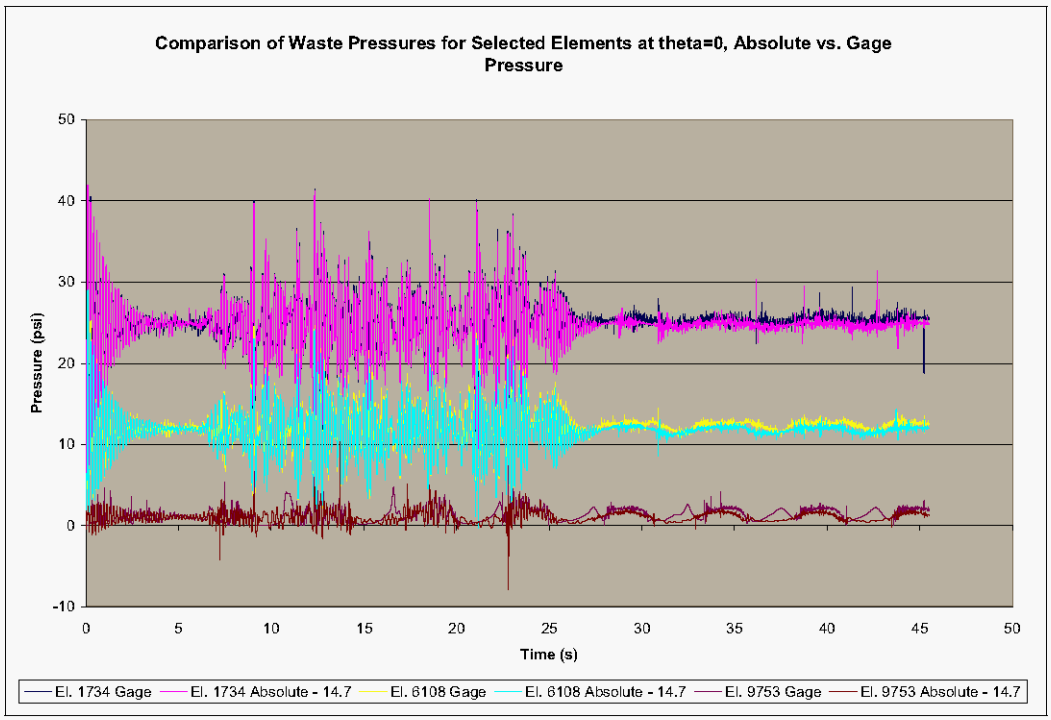

Figure 5-29. Comparison of Waste Pressures in the Flexible Tank at the 422 in. Waste Level at Absolute and Gage Pressure for Selected Elements at θ=45°.

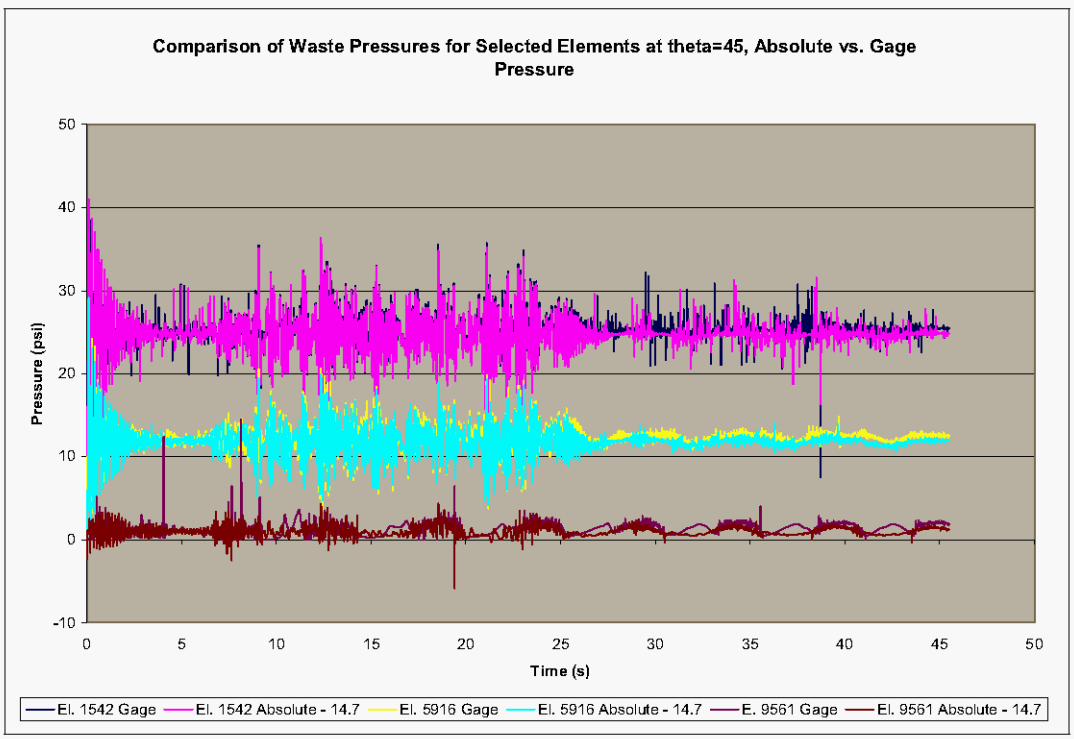

Figure 5-30. Comparison of Waste Pressures in the Flexible Tank at the 422 in. Waste Level at Absolute and Gage Pressure for Selected Elements at θ=90°.

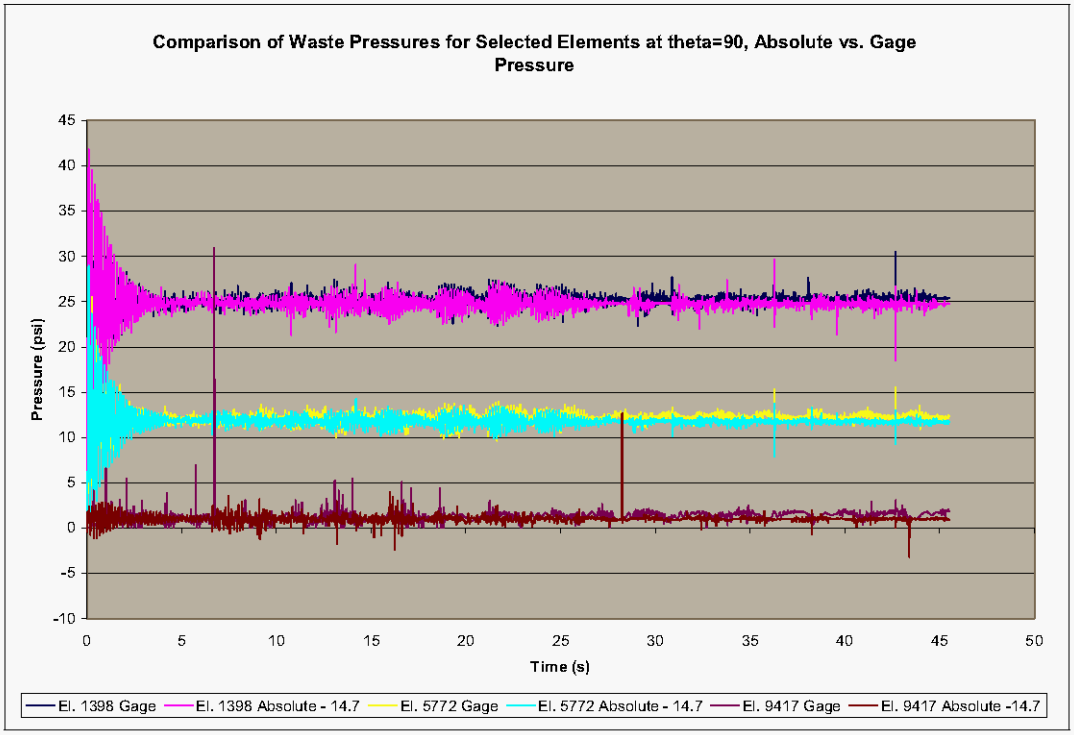

Plots of the actual (that is, as calculated by Dytran) and theoretical maximum and minimum waste pressures at θ=0, 45, and 90° are shown in Figure 5-31 through Figure 5-33.

Figure 5-31. Maximum and Minimum Waste Pressures vs. Normalized Height from Tank Bottom for the Flexible Tank at the 422 in. Waste Level Under Horizontal Excitation for α=0.02 and θ=0.

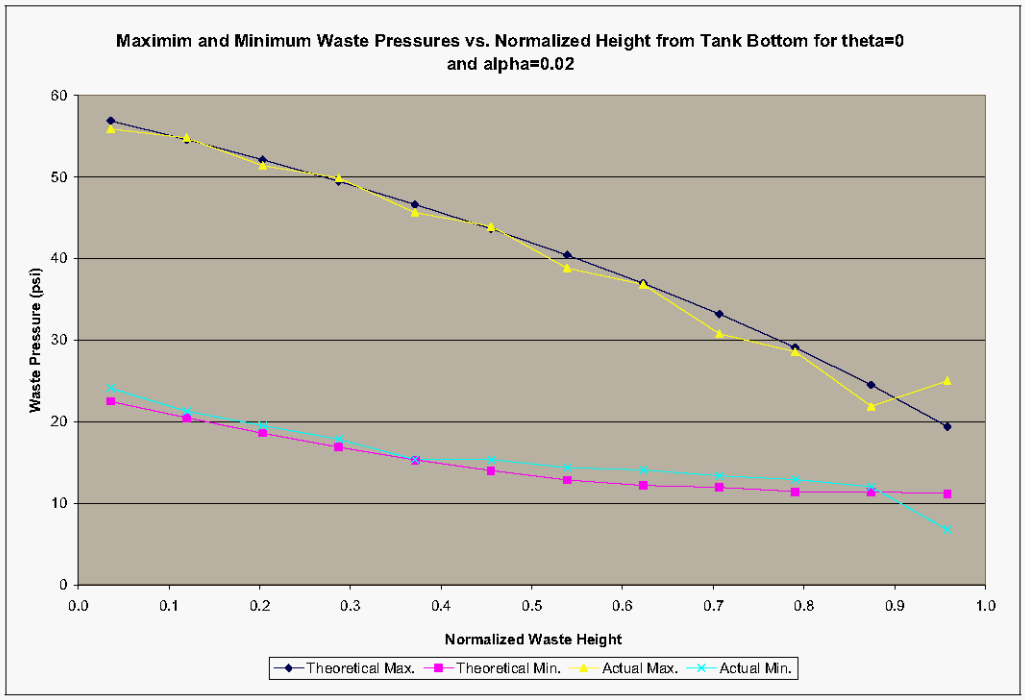

Figure 5-32. Maximum and Minimum Waste Pressures vs. Normalized Height from Tank Bottom for the Flexible Tank at the 422 in. Waste Level Under Horizontal Excitation for α=0.02 and θ=45°.

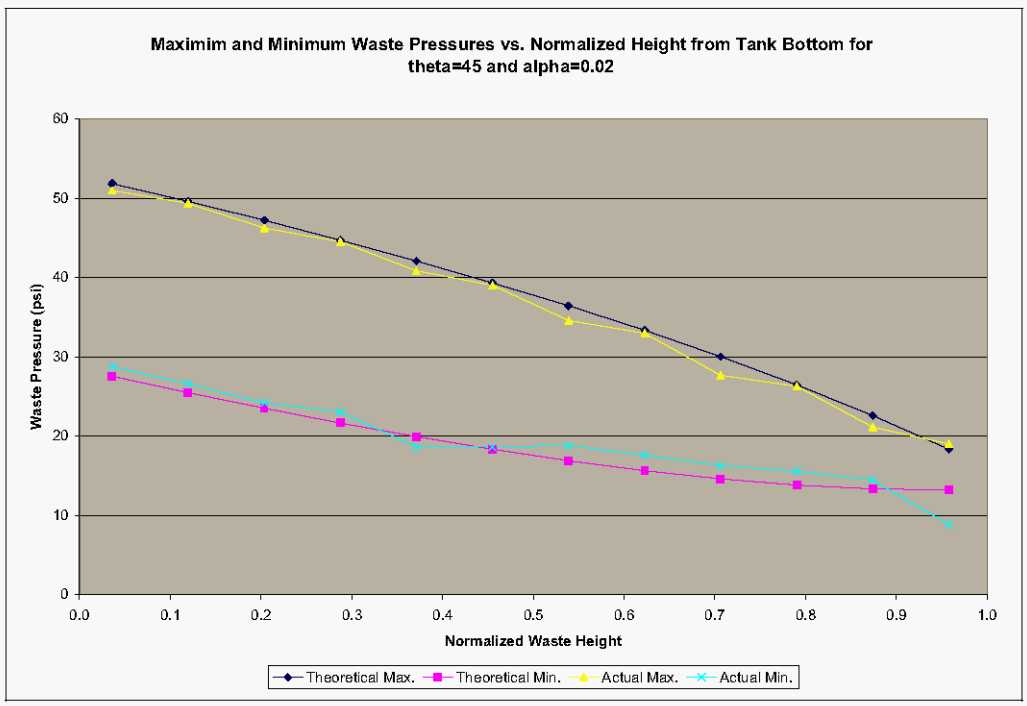

Figure 5-33. Maximum and Minimum Waste Pressures vs. Normalized Height from Tank Bottom for the Flexible Tank at the 422 in. Waste Level Under Horizontal Excitation for α=0.02 and θ=90°.

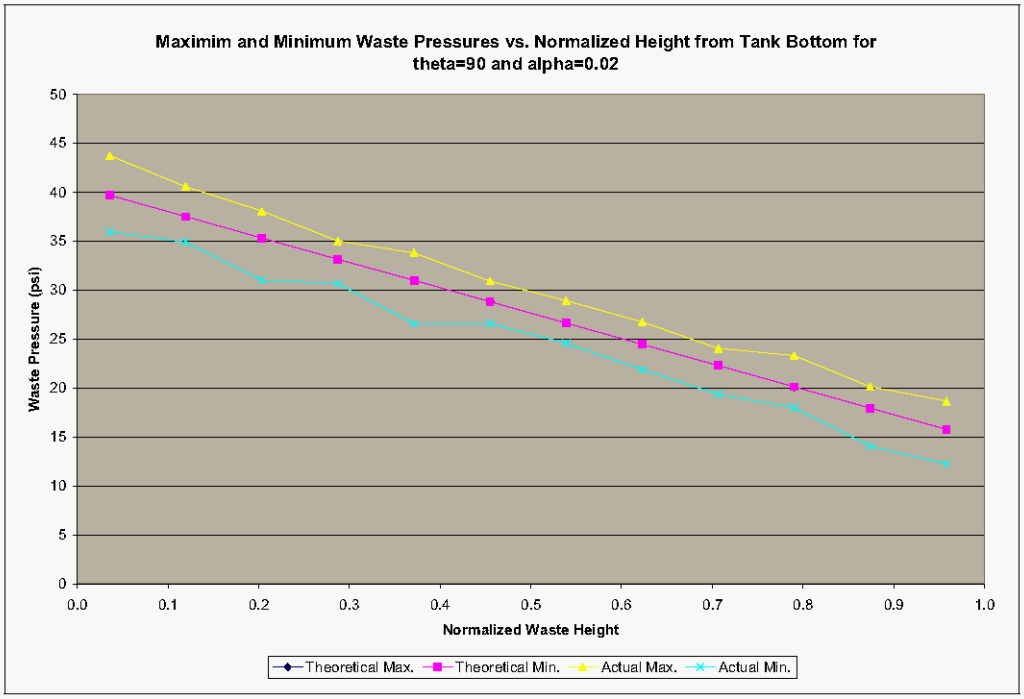

5.3.2 Wall and Base Pressures Due to Vertical Excitation Run at Absolute Pressure

The maximum hydrodynamic pressures induced by the waste on the tank wall and base due to vertical excitation depend on the vertical and radial location in the waste, respectively. The peak wall pressures are given by Equation 4.52 of BNL 1995, and the peak base pressures are given by Equation 4.55 of BNL 1995. The theoretical wall pressures are shown in Table 5-3.

Table 5-3. Theoretical Maximum Absolute Wall Pressures for Vertical Excitation in at the 422 in. Waste Level.

"Plusx_els" Element No.	"Press_45" Element No.	"Plusz_els" Element No.	Hydrostatic Pressure (psi)	Peak Hydrodynamic Wall Pressure (psi)	Peak Total Pressure (psi)
10482	10290	10146	14.7	0	14.7
9753	9561	9417	15.8	0.7	16.5
9024	8832	8688	18.0	2.2	20.2
8295	8103	7959	20.1	3.6	23.7
7566	7374	7230	22.3	4.9	27.2
6837	6645	6501	24.5	6.1	30.6
6108	5916	5772	26.7	7.3	34.0
5379	5187	5043	28.8	8.3	37.1
4650	4458	4314	31.0	9.2	40.2
3921	3729	3585	33.2	9.9	43.1
3192	3000	2856	35.4	10.4	45.8
2463	2271	2127	37.5	10.8	48.3
1734	1542	1398	39.7	11.0	50.7

The pressure time histories for the waste elements adjacent to the tank wall at θ=0 are shown in Figure 5-34, and pressure time-histories for three selected elements near the top, middle, and bottom of the waste are shown in Figure 5-35. A plot of the pressure decay for the same three elements during the initial gravity loading is shown in Figure 5-36. Evident in the plot is the breathing mode frequency of 6 Hz.

A plot of the maximum and minimum waste pressures as a function of waste depth is shown in Figure 5-37, where the results labeled as "actual" refer to the values predicted by Dytran. The results of the computer simulation are conservative relative to the theoretical results, and are generally in quite good agreement. The maximum pressure of 58 lbf/in^2 near the bottom of the tank wall in element 2463 is significantly higher than the 48 lbf/in^2 value predicted by theory. However, that maximum value occurs at a single isolated point as seen in Figure 5-34 and Figure 5-35.

A comparison of the pressure in element 2463 and the hoop stress in the adjacent tank wall element 447 is shown in Figure 5-38. It can be seen from this plot that the isolated spike in the pressure time history does not appear in the stress time history. The absence of high isolated peaks in the hoop stresses is typical. Apparently brief pressure spikes at single waste elements are transparent to the tank wall stresses, at least in some cases.

The pressure spikes generally occur at a single isolated point and the frequency of output is 0.01 s. This results in a triangular pulse with duration of 0.02 s. Given that the fundamental breathing mode frequency of the tank is 6 Hz, this nominally leads to a ratio of 0.12 for pulse duration to the natural period of the structure. Depending on the assumed actual pulse shape, the resulting dynamic magnification factor is in the range of 0.4 to 0.8 (Clough and Penzien [1975]). However, the pulse duration should be viewed as an upper bound, since it depends on the output frequency. In fact, the true pulse

duration and hence the dynamic magnification factor may be less. This could be investigated by re-running the problem with a higher output frequency, although this was not done.

It is also obvious from Figure 5-38 and evident in Figure 5-34 and Figure 5-35 that there is a slight downward drift in the pressure time histories that did not occur during the horizontal excitation.

Comparisons of the actual (that is, as predicted by Dytran) maximum and minimum waste pressures to the theoretical maximum pressures at the 45 and 90° locations are shown in Figure 5-39 and Figure 5-40.

The pressure time history for the bottom center waste element (element 1722) is shown as Figure 5-41. The theoretical hydrostatic pressure at the centroid of element 1722 is 39.7 lbf/in^2, and the theoretical peak hydrodynamic pressure is 8.0 lbf/in^2. That is, the predicted maximum and minimum pressures at this location are 47.7 and 31.7 lbf/in^2, respectively. The maximum and minimum values shown in Figure 5-41 are 47.2 and 32.6 lbf/in^2, respectively.

Figure 5-34. Waste Pressure Time Histories for the Flexible Tank at the 422 in. Waste Level for Vertical Excitation Run at Absolute Pressure for θ=0 and alpha=0.02.

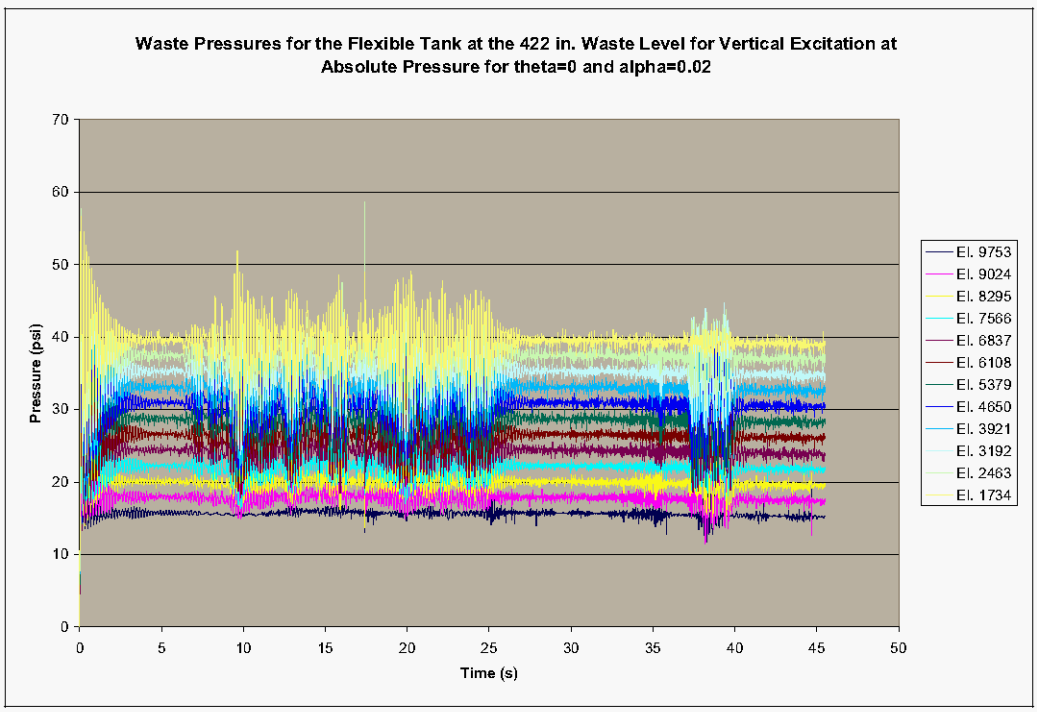

Figure 5-35. Selected Waste Pressure Time Histories for the Flexible Tank at the 422 in. Waste Level for Vertical Excitation Case 2c (alpha=0.02) Run at Absolute Pressure.

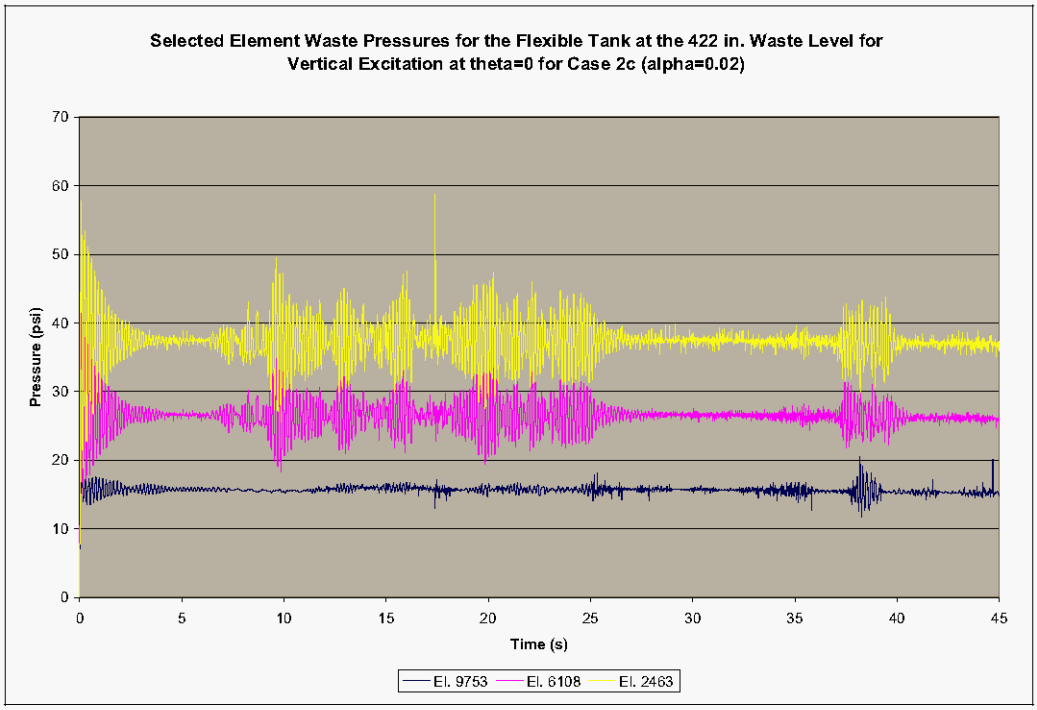

Figure 5-36. Selected Waste Pressure Time Histories for the Flexible Tank at the 422 in. Waste Level for Vertical Excitation Case 2c (alpha=0.02) Run at Absolute Pressure – Time 0 to 3 s

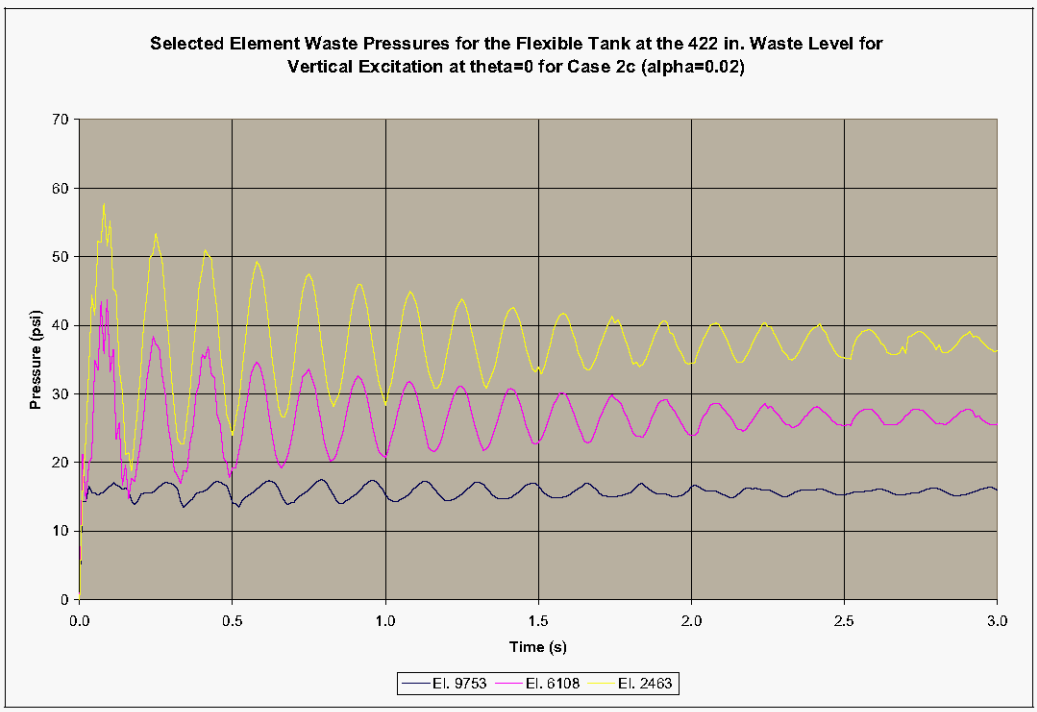

Figure 5-37. Maximum and Minimum Waste Pressures vs. Normalized Height from Tank Bottom for the Flexible Tank at the 422 in. Waste Level Under Vertical Excitation at θ=0 and α=0. 02

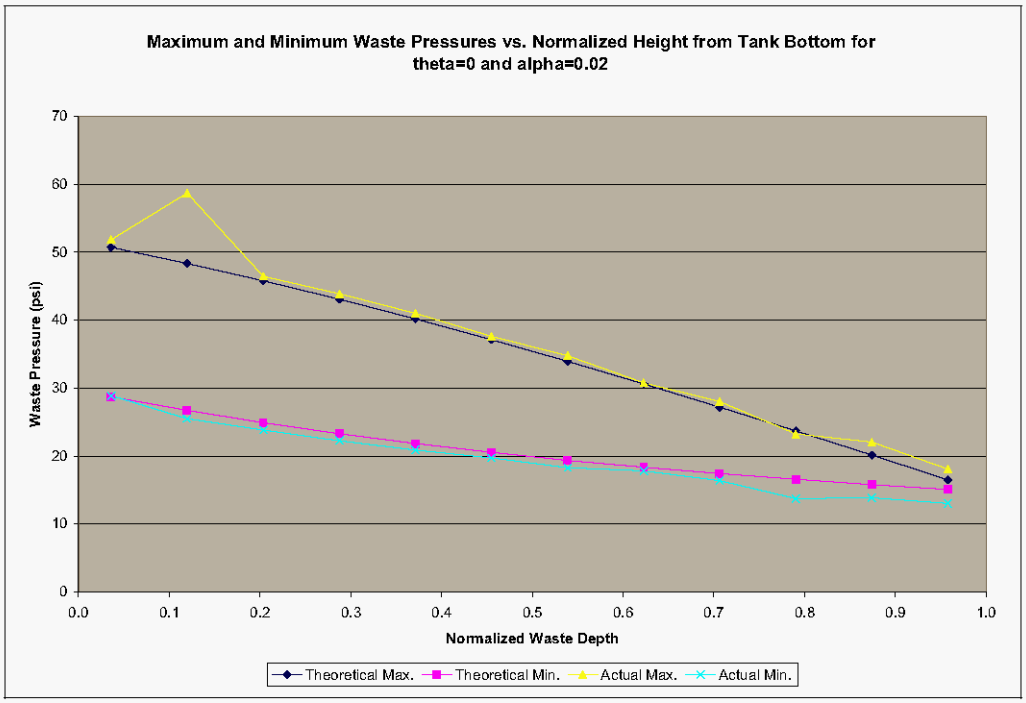

Figure 5-38. Comparison of Waste Pressure to Tank Wall Hoop Stress for the Flexible Tank at the 422 in. Waste Level and Vertical Excitation at Absolute Pressure Near the Tank Bottom at θ=0.

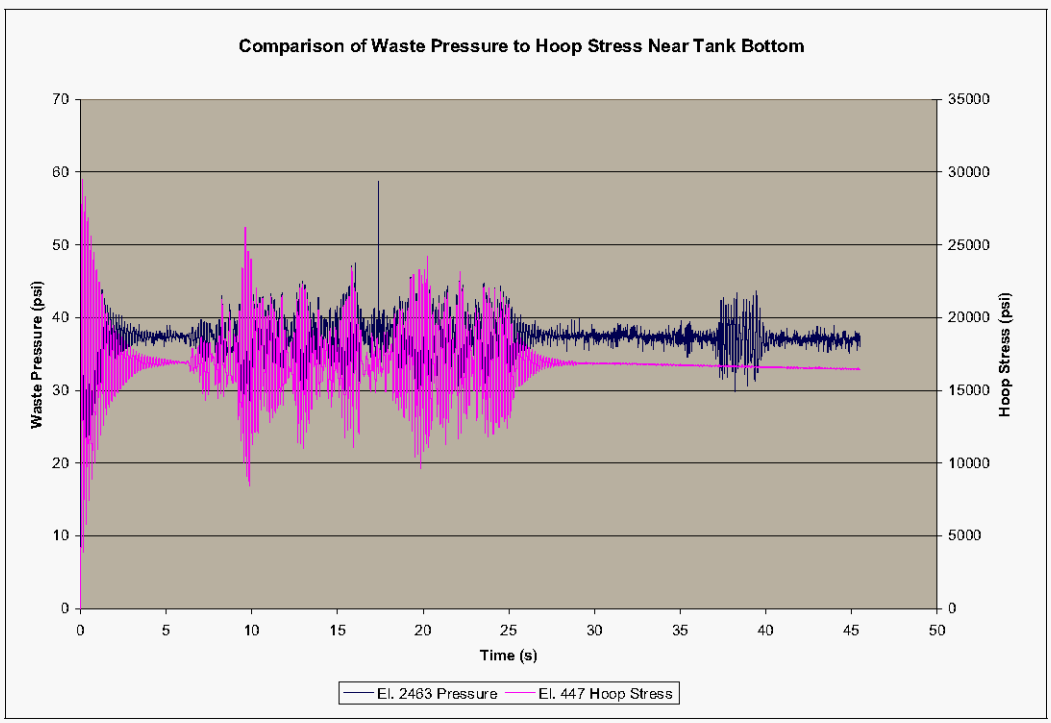

Figure 5-39. Maximum and Minimum Waste Pressures vs. Normalized Height from Tank Bottom for the Flexible Tank at the 422 in. Waste Level Under Vertical Excitation at θ=45° and α=0.02.

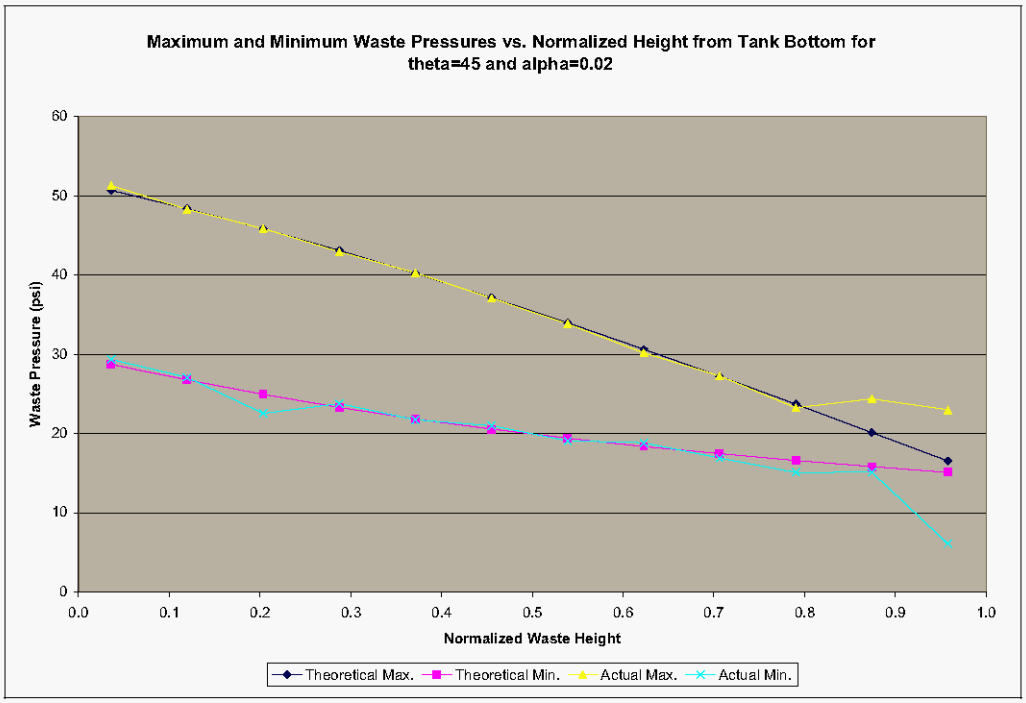

Figure 5-40. Maximum and Minimum Waste Pressures vs. Normalized Height from Tank Bottom for the Flexible Tank at the 422 in. Waste Level at Absolute Pressure with θ=90° and α=0. 02

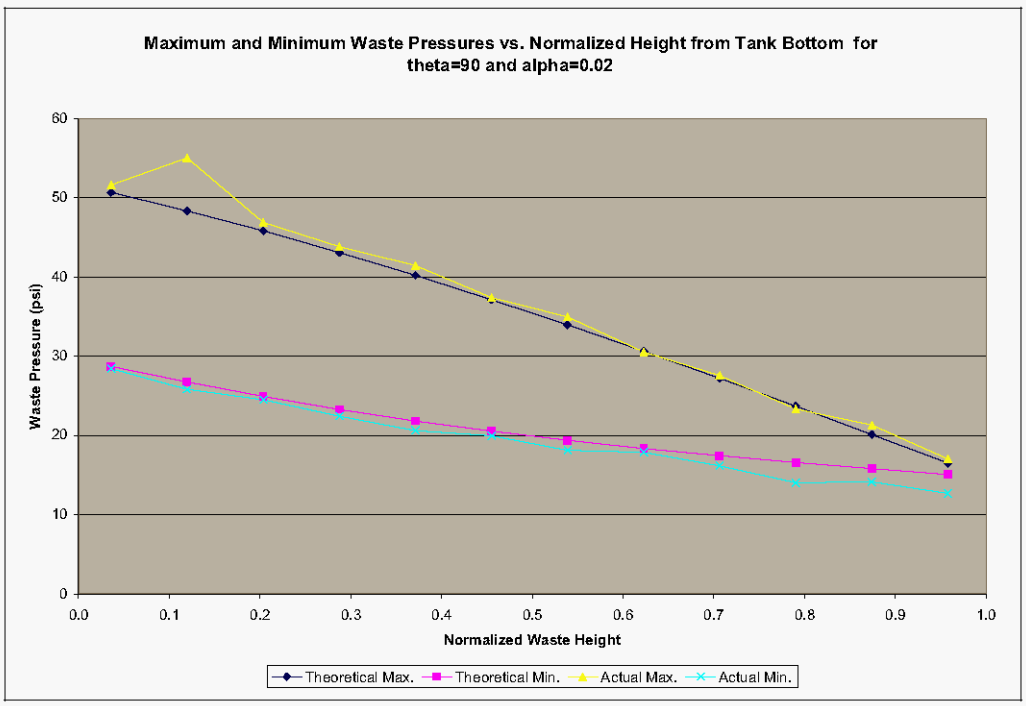

Figure 5-41. Pressure Time History for Bottom Center Waste Element for 422 in. Waste Level and Vertical Excitation at Absolute Pressure and alpha=0.02

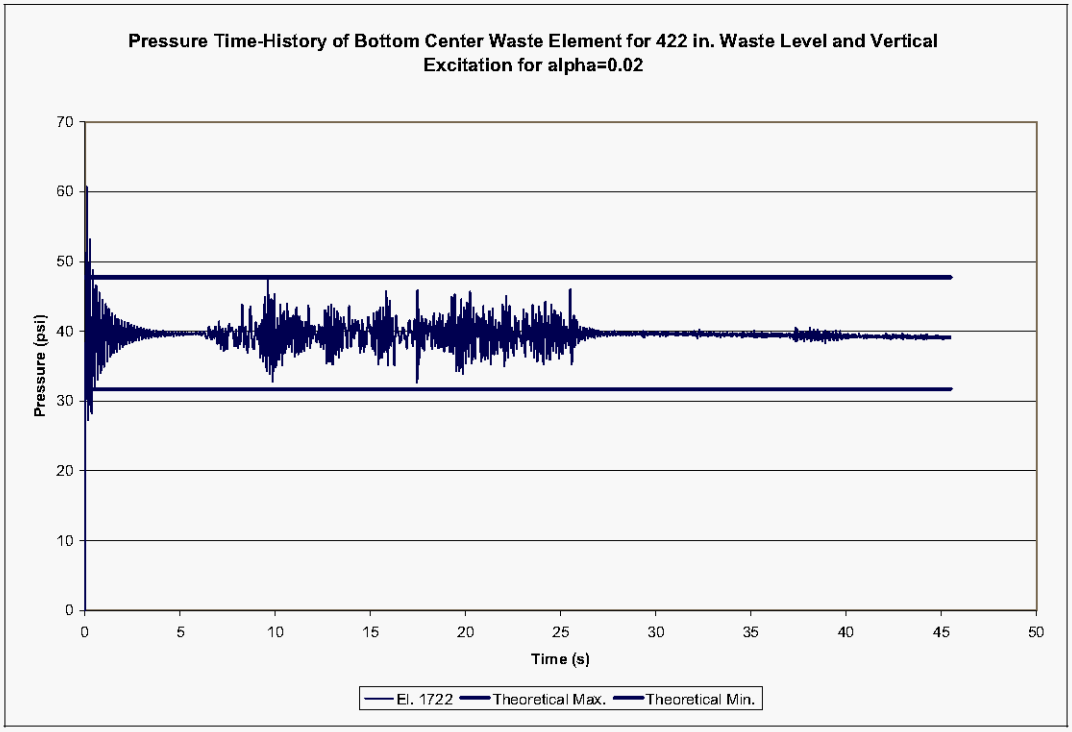

5.4 MAXIMUM SLOSH HEIGHT RESULTS

The maximum slosh height traces for the runs at gage and absolute pressure are shown in Figure 5-42. The results show minor differences, but the peak slosh heights both compare well with the theoretical value of 23.7 in.

Figure 5-43 shows the effect of the damping parameter alpha on the maximum slosh height time histories. The data show that there is very little difference in the maximum slosh height for values of alpha of 0.01 and 0.02, and that both agree well with theory. The maximum slosh height corresponding to alpha=0.04 is approximately 4% less than the maximum slosh height for alpha=0.01, or 0.02.

Figure 5-42. Comparison of Maximum Slosh Height Time-Histories for the Flexible Tank at the 422 in. Waste Level and α=0.02.

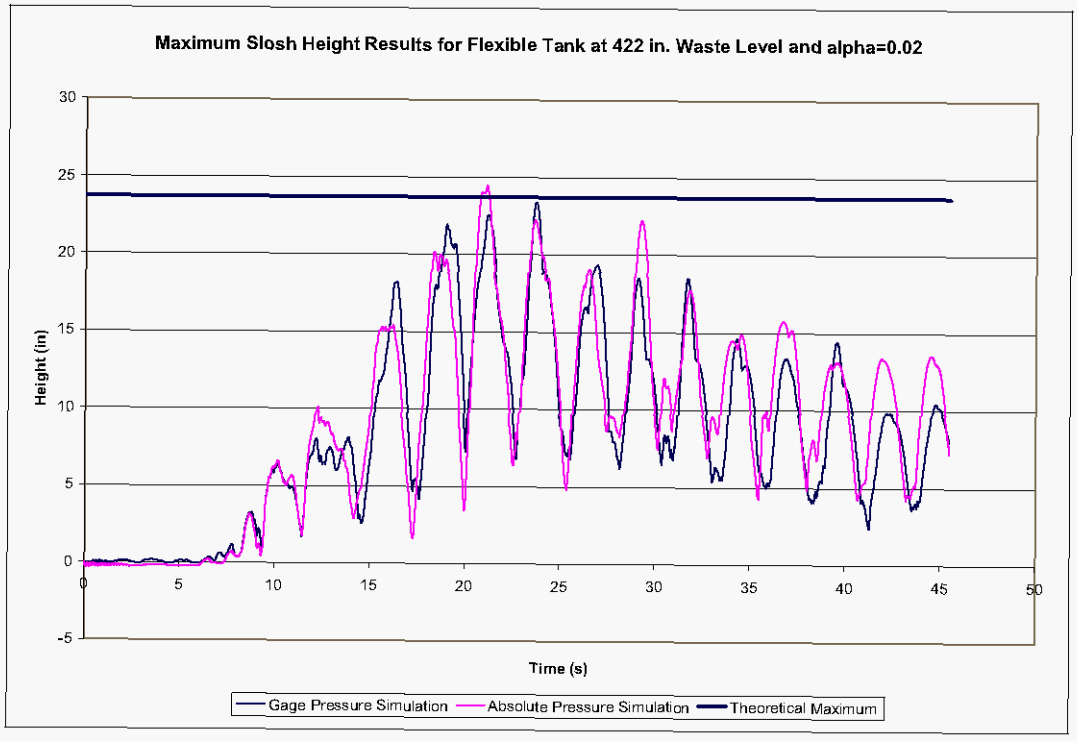

Figure 5-43. Dependence of the Maximum Slosh Height on the Damping Parameter α

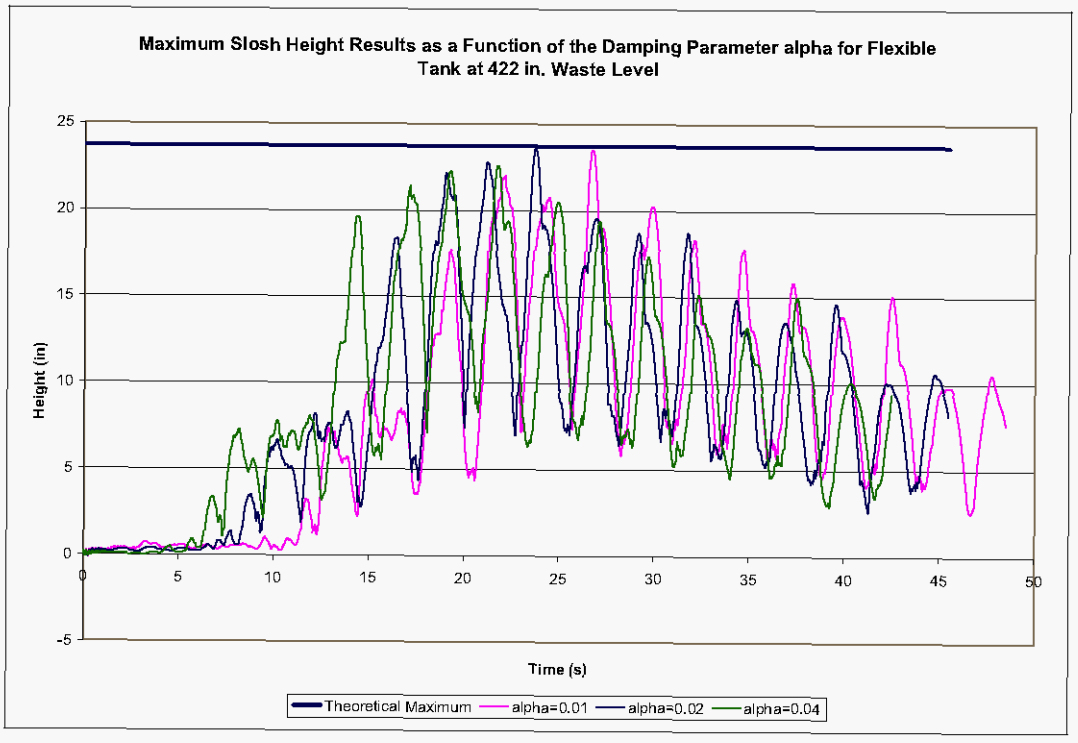

5.5 ELEMENT STRESSES

Selected stress results will be presented for the absolute pressure run. The pressure plots are presented to illustrate trends and as a general check on the behavior of the solution. Although some checks exist for the expected stress values, because of the complexity of the structure, the stress fields will be more complicated that the fluid pressure fields. The primary reason for assuming a uniform wall thickness for the benchmark primary tank model was to simplify the distribution of stress in the tank wall and particular to simplify the hoop stress distribution that can be approximated as

$$\sigma_{hoop} = \frac{pr}{t},$$

where p is the fluid pressure, r is the tank radius, and t is the tank wall thickness. This relationship is, of course, expected to breakdown near the upper and lower portions of the tank wall due to local end effects, but should give a good approximation in the central portion of the tank wall.

Mid-plane or membrane hoop stress is shown in Figure 5-44, Figure 5-45, and Figure 5-46 for tank wall elements at θ=0, 45, and 90°, respectively. A comparison between membrane hoop stress and the expected value of that stress for a tank wall element at mid-height in the wall is shown as Figure 5-47. The hoop stresses are generally as expected and show the proper dependence on the angle θ. A comparison of the hoop stresses at the 90° for the absolute and gage pressure solutions is shown as Figure 5-48. Examination of Figure 5-48 shows that the stresses in the gage pressure solution drift slightly upward over time while the stresses from the absolute pressure solutions are steady. The same behavior was observed in Figure 5-28, Figure 5-29, and Figure 5-30 for the waste pressures.

5.5.1 Horizontal Excitation Run at Absolute Pressure

Figure 5-44. Mid-Plane Hoop Stress for the Flexible Tank at the 422 in. Waste Level at θ=0 and alpha=0.02 Run at Absolute Pressure.

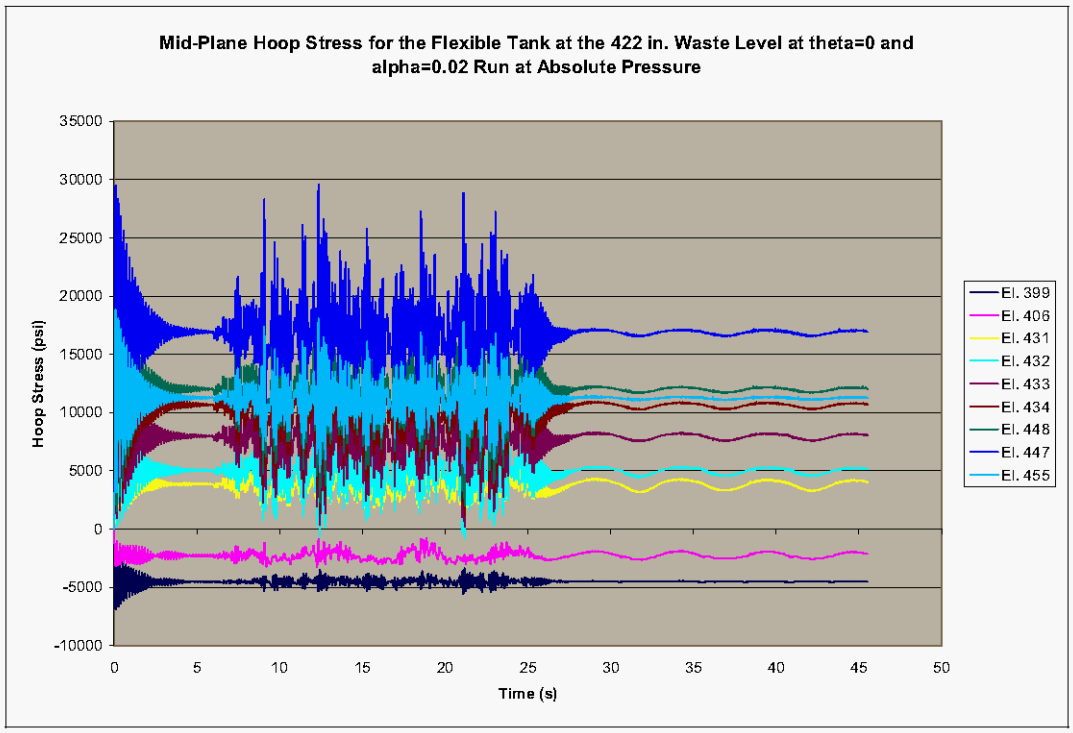

Figure 5-45. Mid-Plane Hoop Stress for the Flexible Tank at the 422 in. Waste Level at θ=45° and alpha=0.02 Run at Absolute Pressure.

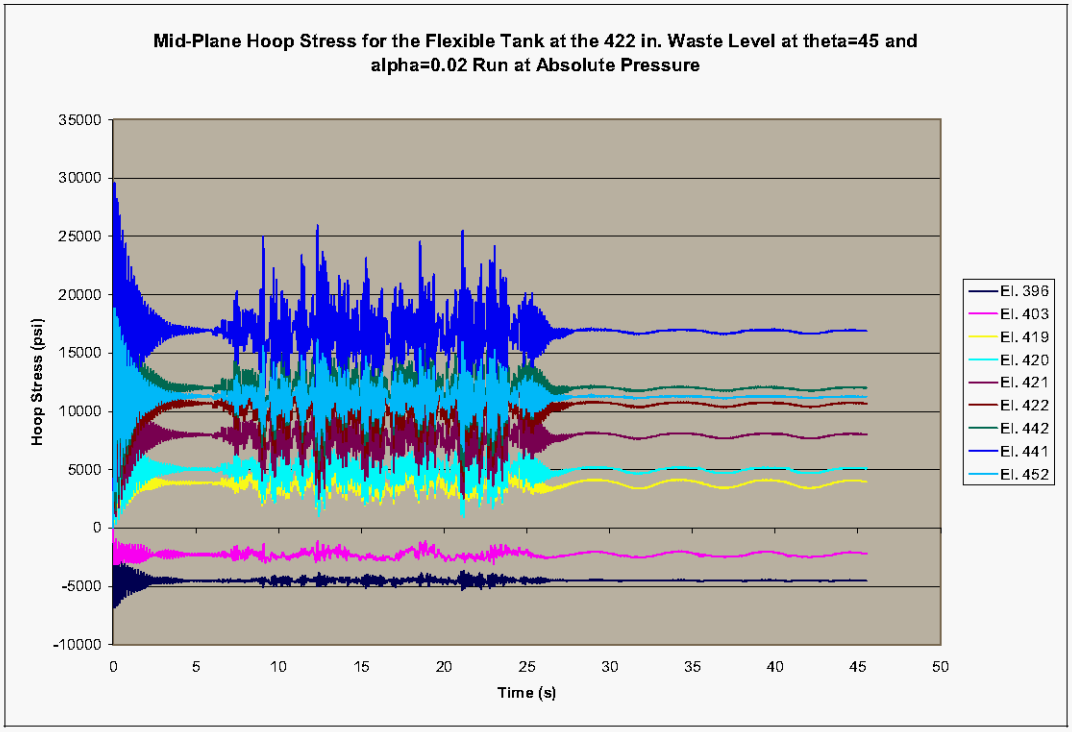

Figure 5-46. Mid-Plane Hoop Stress for the Flexible Tank at the 422 in. Waste Level at θ=90° and alpha=0.02 Run at Absolute Pressure.

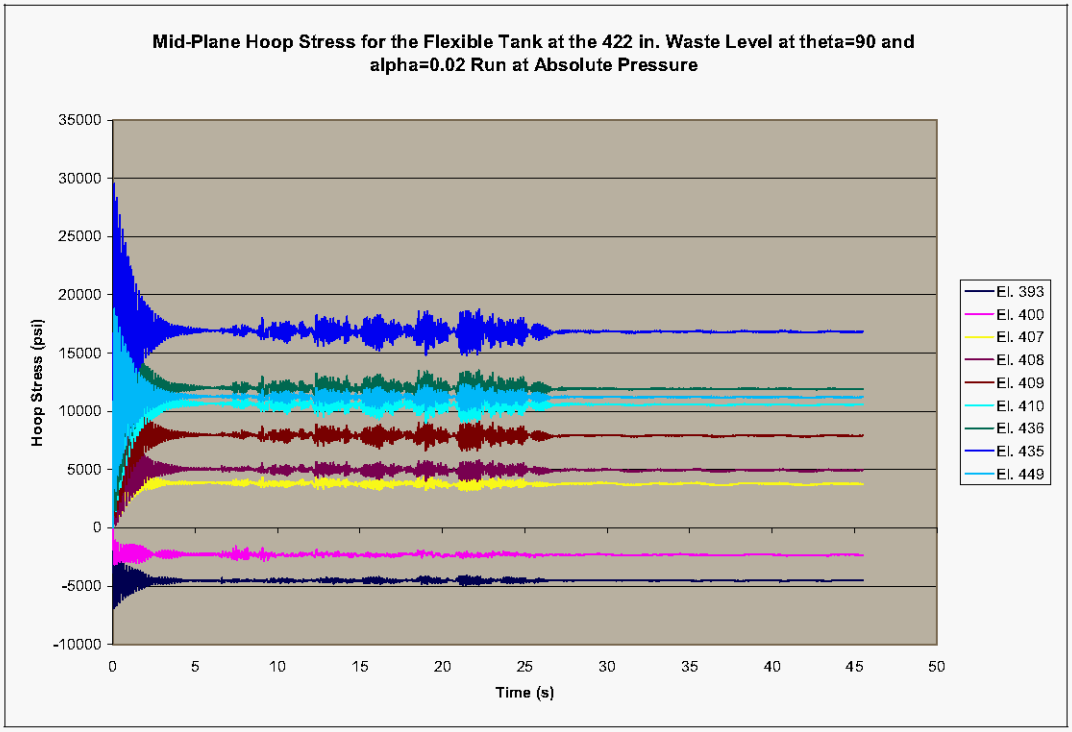

Figure 5-47. Comparison of Mid-Plane Hoop Stress in Tank Wall Element 433 to pr/t for Waste Element 6108 at Wall Mid-Height and θ =0.

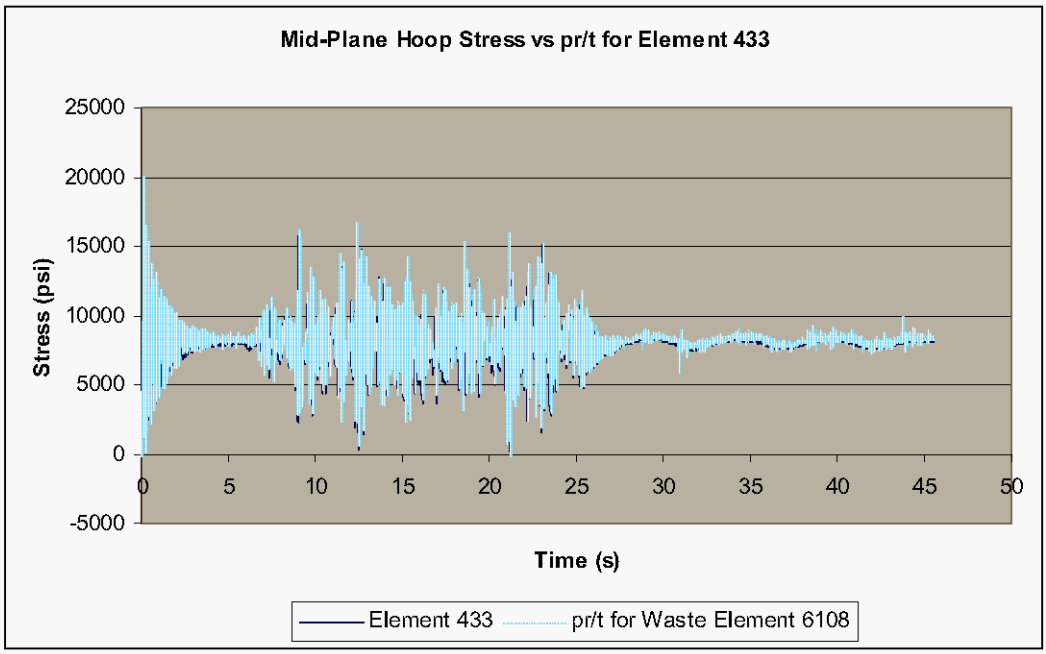

Figure 5-48. Comparison of Mid-Plane Hoop Stress at Absolute and Gage Pressure for Selected Elements at θ =90°.

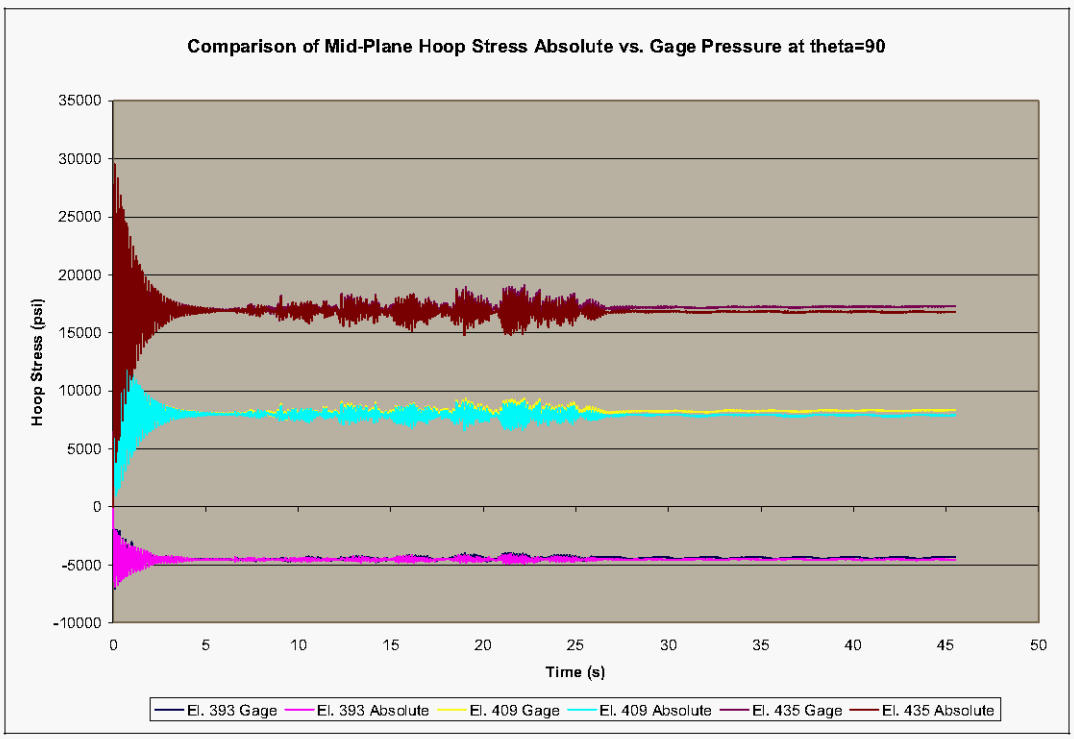

6.0 FLEXIBLE TANK DYTRAN MODEL AT 460 INCH WASTE LEVEL

The response of the tank and contained liquid to seismic excitation with the liquid initially at the 460 in. level does not have a closed form analytical solution because of the interaction of the liquid free surface with the curved surface of the tank dome. However, the solutions obtained with Dytran will be compared to *the theoretical solution for the open tank with the hinged top condition and 460 in.* waste level as well as with the Dytran solution at the 422 in. level.

The problem was run initially at gage pressure. Pressure time histories for the waste elements showed that several waste elements experienced zero pressure indicating that the dynamic pressure exceeded the static pressure. Consequently, the problem was rerun at absolute pressure, and the results presented below are from the absolute pressure case.

6.1 HYDRODYNAMIC FORCES

6.1.1 Horizontal Excitation Run at Absolute Pressure

The vertical reaction force shown in Figure 6-1 during the initial free vibration phase exhibits a breathing mode frequency of 5.5 Hz in agreement with theory, and it has essentially reached steady state in 5-6 s (28-33 cycles), indicating an effective damping of approximately 2.5% during this phase.

The peak hydrodynamic force is 1.02×10^7 lbf as shown in Figure 6-2, or 99% of the value of 1.03×10^7 lbf predicted for the open tank with the hinge top condition at the 460 in. waste level. *That is, according to the Dytran model, the peak horizontal hydrodynamic force is essentially the same as predicted for the open top tank, and any interaction of the fluid with the dome has not significantly changed the peak force from that predicted for the open top tank.*

As shown in Figure 6-3 the horizontal reaction force time history during the second free vibration period beginning at 25.5 s indicates that the impulsive frequency is approximately 6.5 Hz. Thus, both the impulsive and breathing mode frequencies have decreased approximately 0.5 Hz relative to the 422 in. case as predicted by theory. The 36% increase in peak horizontal hydrodynamic force relative to the 422 in. waste level is due not only to the increased waste mass, but also because the lower impulsive frequency associated with the 460 in. waste level has a higher associated spectral acceleration.

Figure 6-4 presents a comparison of the horizontal hydrodynamic force time histories for the 460 and 422 in. waste levels during the second free vibration period beginning at 25.5 s. During this period, the response is dominated by convective effects. The data show that the peak hydrodynamic force during this period is 3.31×10^5 lbf for the 422 in. waste level (72% of theoretical value of 4.62×10^5 lbf), and 2.85×10^5 lbf for the 460 in.

waste level (55% of open top theoretical value of 5.21 x 10^5 lbf). Because of system damping, the values above should not be interpreted as the peak of the convective response, but the relative magnitude shows that the presence of the dome reduces the convective response of the waste. The fundamental convective period is approximately 5 s. Comparison of the two responses shows less effective damping at the 460 in waste level during the convective response in final free oscillation phase than the 1% critical damping at the 422 in level.

Figure 6-1. Coupling Surface Reaction Forces at the 460 in. Waste Level for the Flexible Tank Under Horizontal Seismic Input During the Initial Free Vibration Phase – (alpha=0.02).

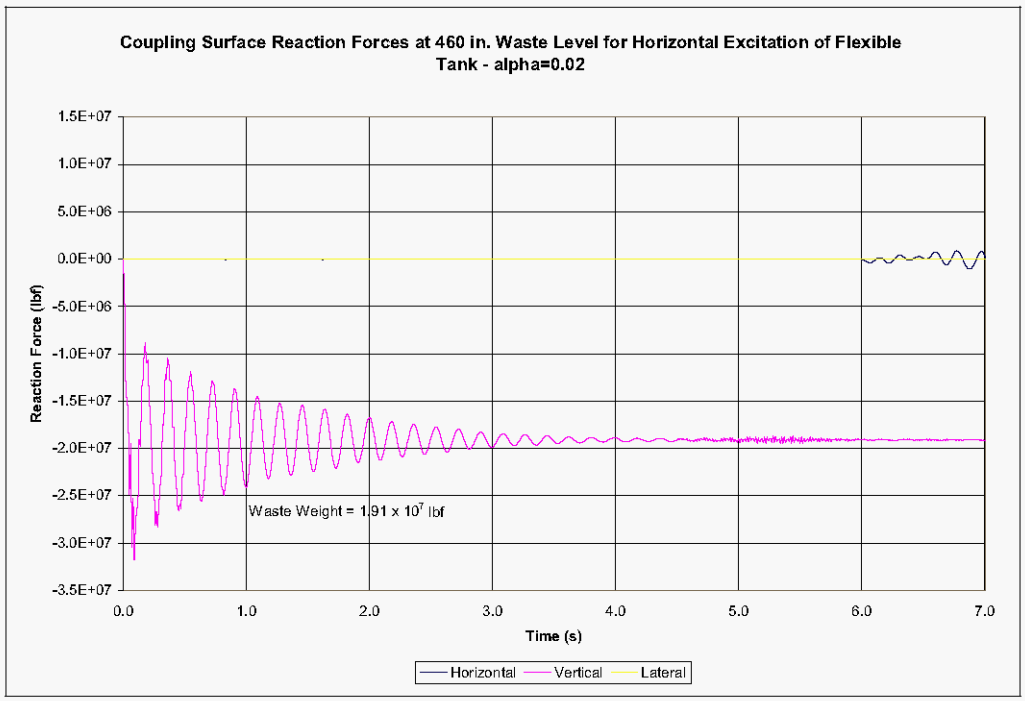

Figure 6-2. Coupling Surface Reaction Forces at the 460 in. Waste Level for the Flexible Tank Under Horizontal Seismic Input – (alpha=0.02).

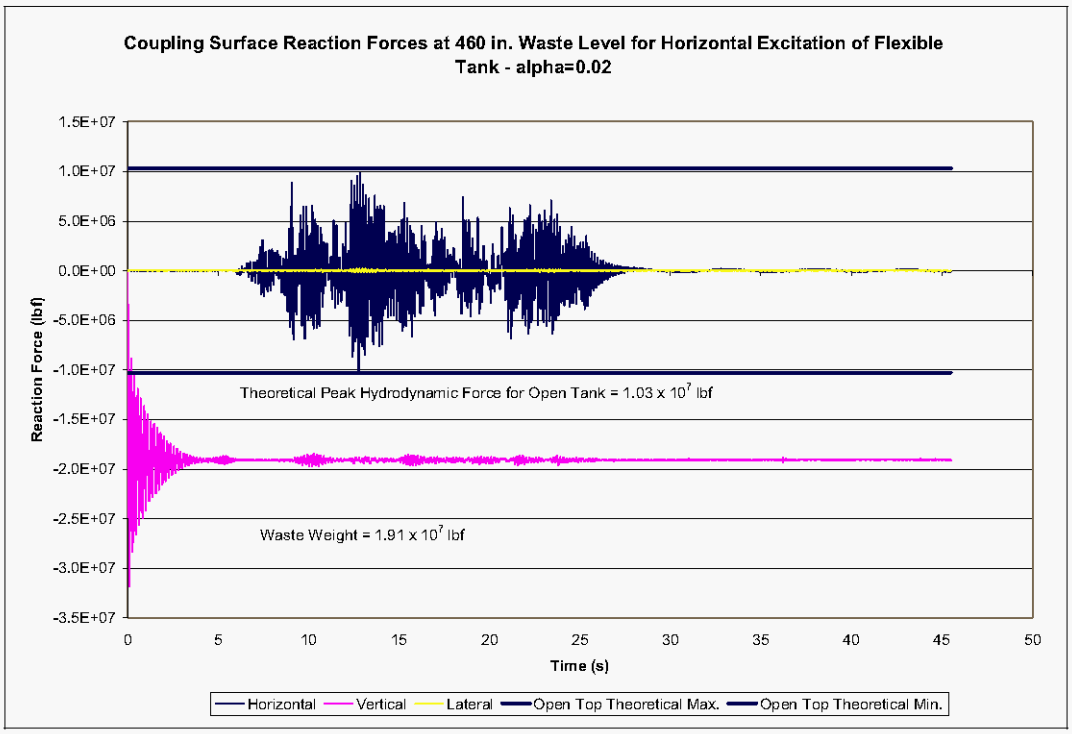

Figure 6-3. Coupling Surface Reaction Forces at the 460 in. Waste Level for the Flexible Tank Under Horizontal Seismic Input During the Final Free Vibration Phase – alpha=0.02.

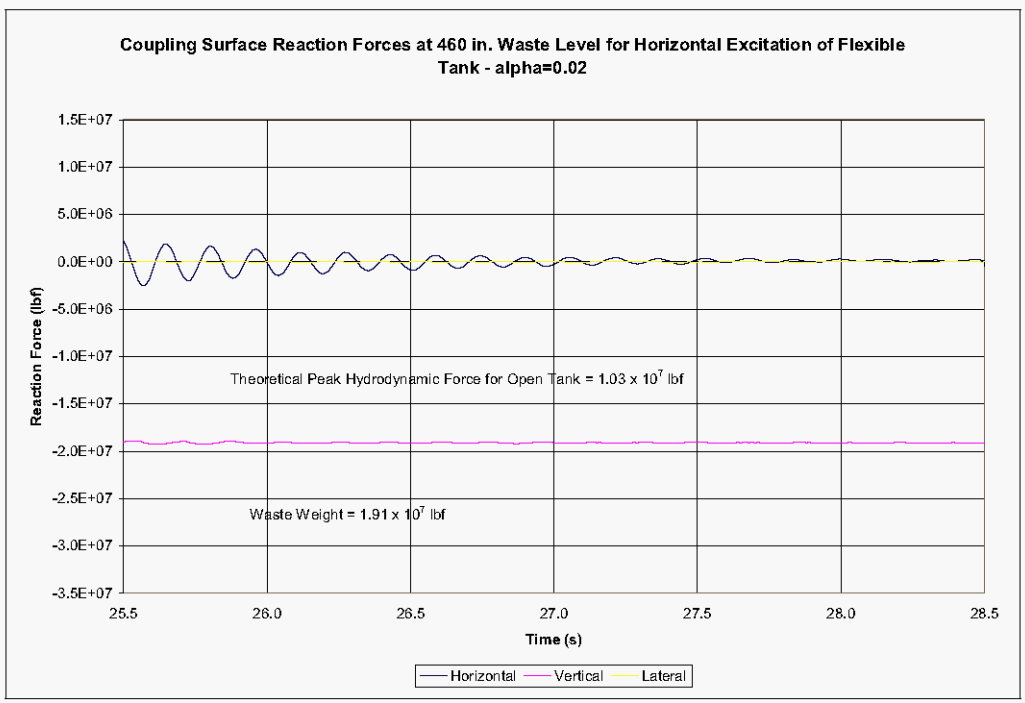

Figure 6-4. Comparison of the Horizontal Coupling Surface Reaction Force for the 460 and 422 in. Waste Levels During the Final Free Vibration Period – alpha=0.02

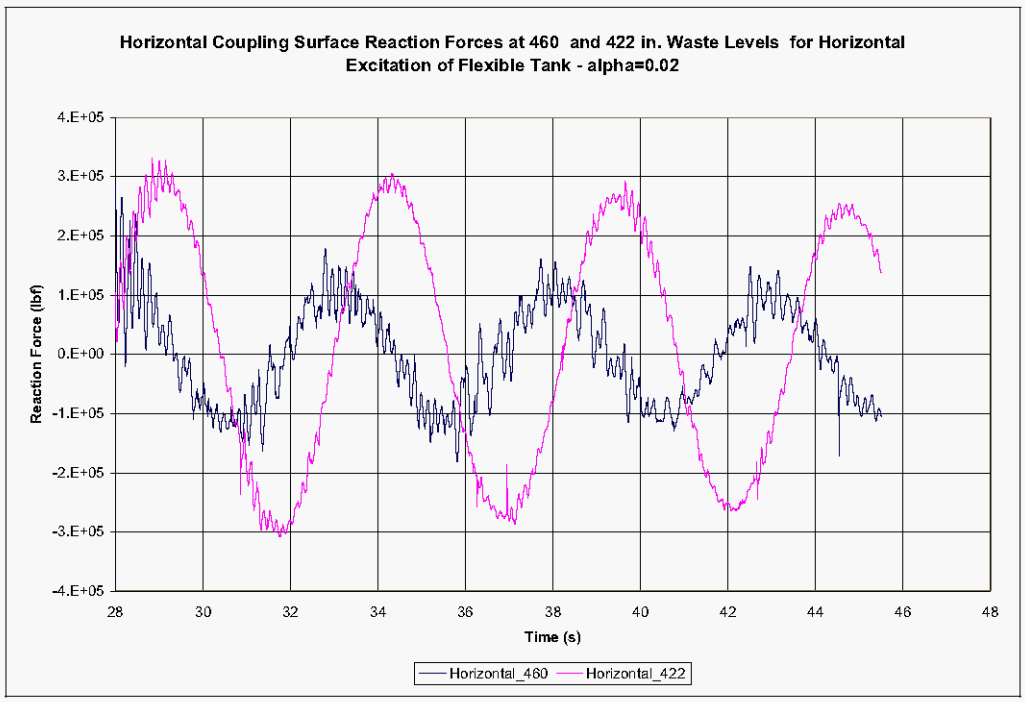

6.1.2 Vertical Excitation Run at Absolute Pressure

The peak vertical hydrodynamic force from the computer simulation was 5.98 x 10^6 lbf, or 32% greater than the value of 4.54 x 10^6 lbf predicted by theory for the open tank at the 460 in. waste level. The majority of the vertical coupling surface reaction force is due to the weight of the waste rather than the hydrodynamic force, so viewed this way, the total peak reaction force of 2.51 x 10^7 lbf is 6% greater than the theoretical value of 2.36 x 10^7 lbf.

Figure 6-5. Vertical Coupling Surface Reaction Force at the 460 in Waste Level for the Flexible Tank Under Vertical Seismic Input.

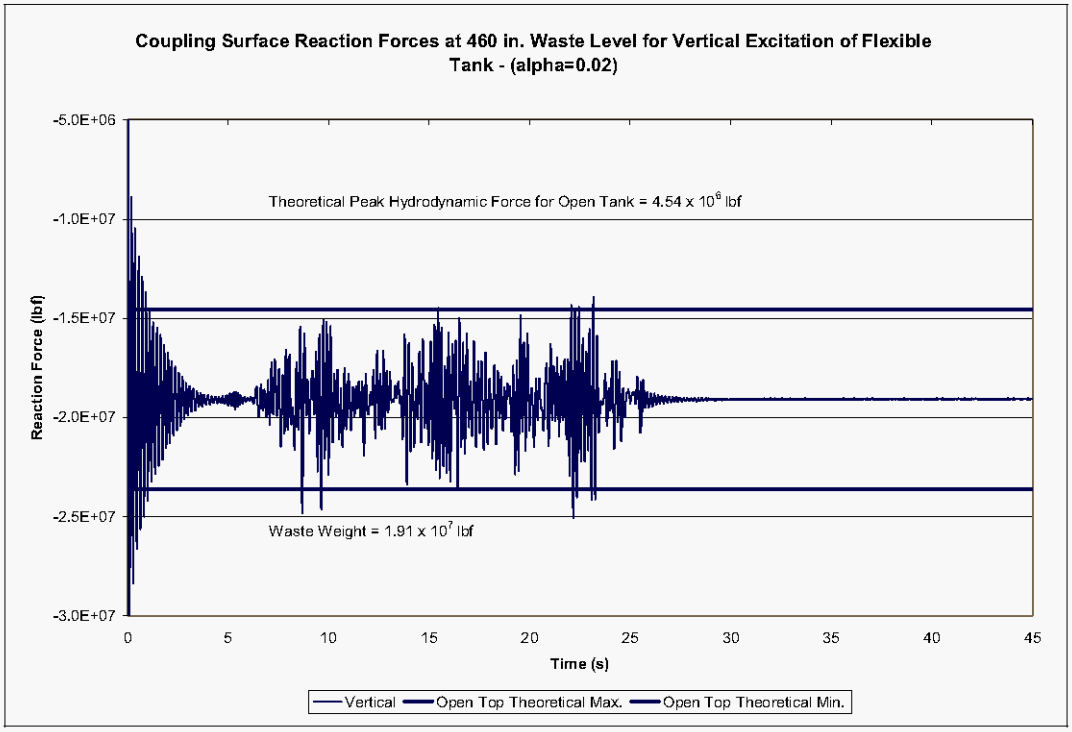

6.2 WASTE PRESSURES

Although no closed form solution exists for the 460 in. waste level, theoretical dynamic pressures were calculated Equation 4.24 of BNL 1995 *based on an open tank with 460 in. of waste and a hinged top condition*. This solution is presented along with the actual results for comparison purposes.

As in Section 5.3, the total pressures are the sum of the hydrostatic pressures and the hydrodynamic pressures. The hydrostatic, peak hydrodynamic and peak total pressures for the elements in the sets "plusx_els", "press_45", are shown in Table 6-1and Table 6-2. The maximum theoretical pressures for the elements set "plusz_els" is simply the hydrostatic pressures shown in Table 6-1 because the theoretical hydrodynamic pressures are zero at $\theta=90°$.

Table 6-1. Theoretical Maximum Absolute Waste Pressures for Horizontal Excitation in the Flexible Open Top Tank at 460 in. Waste Level for Elements at θ=0.

"Plusx_els" Element No.	Hydrostatic Pressure (psi)	Peak Hydrodynamic Pressure (psi)	Peak Total Pressure (psi)
11211	14.7	0	14.7
10482	16.0	4.4	20.4
9753	18.4	8.1	26.5
9024	20.7	11.0	31.7
8295	23.1	13.3	36.4
7566	25.4	15.2	40.6
6837	27.7	16.8	44.5
6108	30.1	18.1	48.2
5379	32.4	19.2	51.6
4650	34.7	20.0	54.7
3921	37.1	20.7	57.8
3192	39.4	21.1	60.5
2463	41.8	21.4	63.2
1734	44.1	21.6	65.7

Table 6-2. Theoretical Maximum Absolute Waste Pressures for Horizontal Excitation in the Flexible Open Top Tank at 460 in. Waste Level for Elements at θ=45.

"Press_45" Element No.	Hydrostatic Pressure (psi)	Peak Hydrodynamic Pressure (psi)	Peak Total Pressure (psi)
11019	14.7	0	14.7
10290	16.0	3.1	19.1
9561	18.4	5.7	24.1
8832	20.7	7.8	28.5
8103	23.1	9.4	32.5
7374	25.4	10.8	36.2
6645	27.7	11.9	39.6
5916	30.1	12.8	42.9
5187	32.4	13.6	46.0
4458	34.7	14.2	48.9
3729	37.1	14.6	51.7
3000	39.4	14.9	54.4
2271	41.8	15.1	56.9
1542	44.1	15.3	59.3

6.2.1 Horizontal Excitation Run at Absolute Pressure

The pressure time histories for the elements adjacent to the tank wall at θ=0 are shown in Figure 6-6. The hydrostatic pressures are evenly spaced between 16 and 44 lbf/in^2 in agreement with the values in Table 6-1. The pressure time histories for elements 9753 and 9024 in the upper portion of the waste are shown separately in Figure 6-7. Evident

are several isolated peaks in the waste pressures. Similar behavior is seen in the upper waste elements 9561 and 8103 at the 45° location in as shown in Figure 6-8 and Figure 6-9. The pressure time histories for the waste elements at θ=90° do not show the isolated peaks present at the other two locations.

Figure 6-6. Waste Pressures Time Histories for the Flexible Tank at the 460 in. Waste Level for Horizontal Excitation at θ=0 and alpha=0.02 Run at Absolute Pressure.

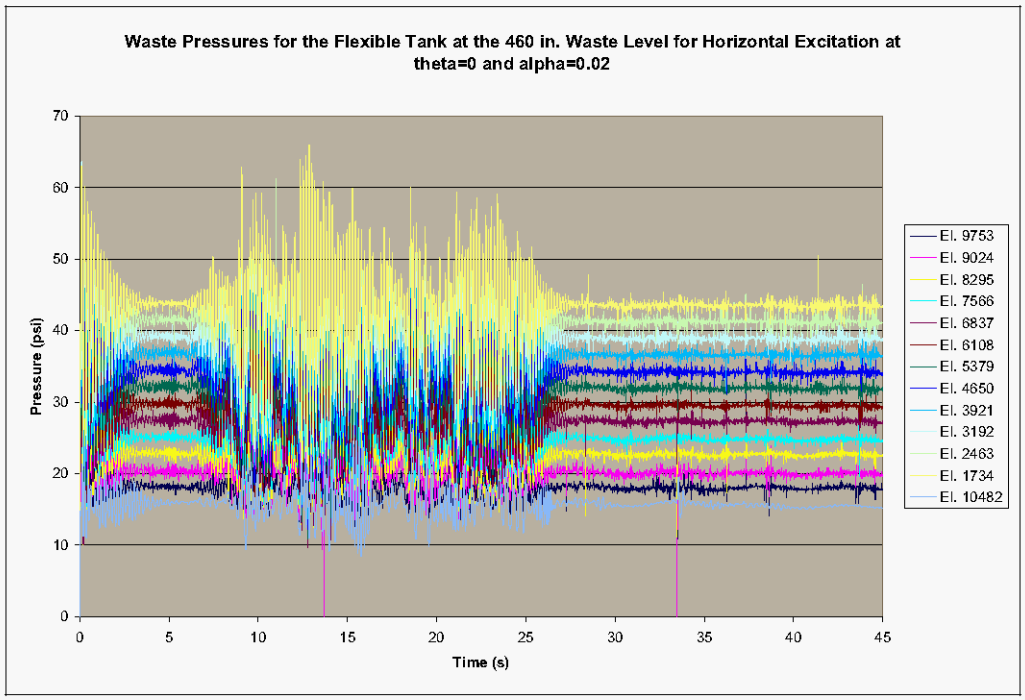

Figure 6-7. Selected Element Pressure Time Histories for the Flexible Tank at the 460 in. Waste Level for Horizontal Excitation at θ=0 and alpha=0.02 Run at Absolute Pressure.

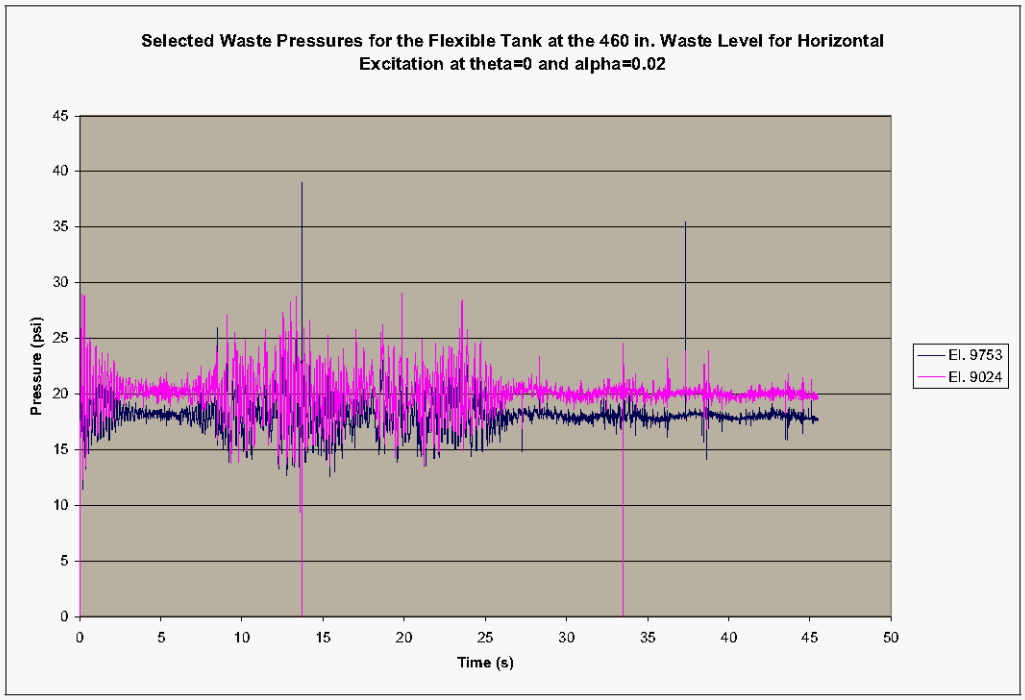

Figure 6-8. Waste Pressures Time Histories for the Flexible Tank at the 460 in. Waste Level for Horizontal Excitation at θ=45 and alpha=0.02 Run at Absolute Pressure.

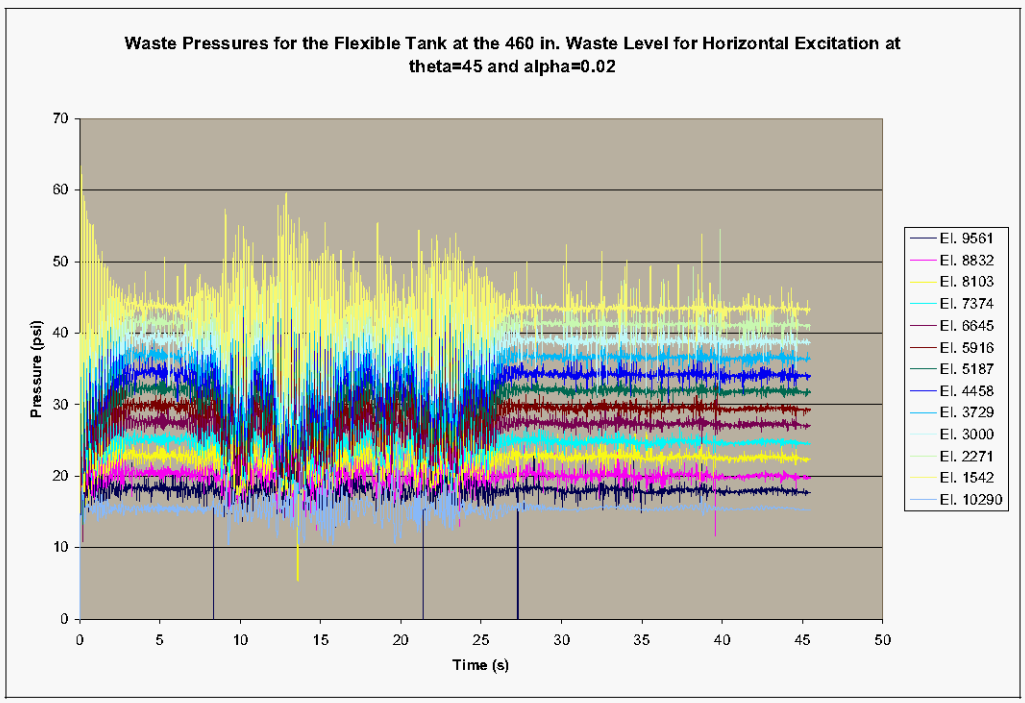

Figure 6-9. Selected Element Pressure Time Histories for the Flexible Tank at the 460 in. Waste Level for Horizontal Excitation at θ=45 and alpha=0.02 Run at Absolute Pressure.

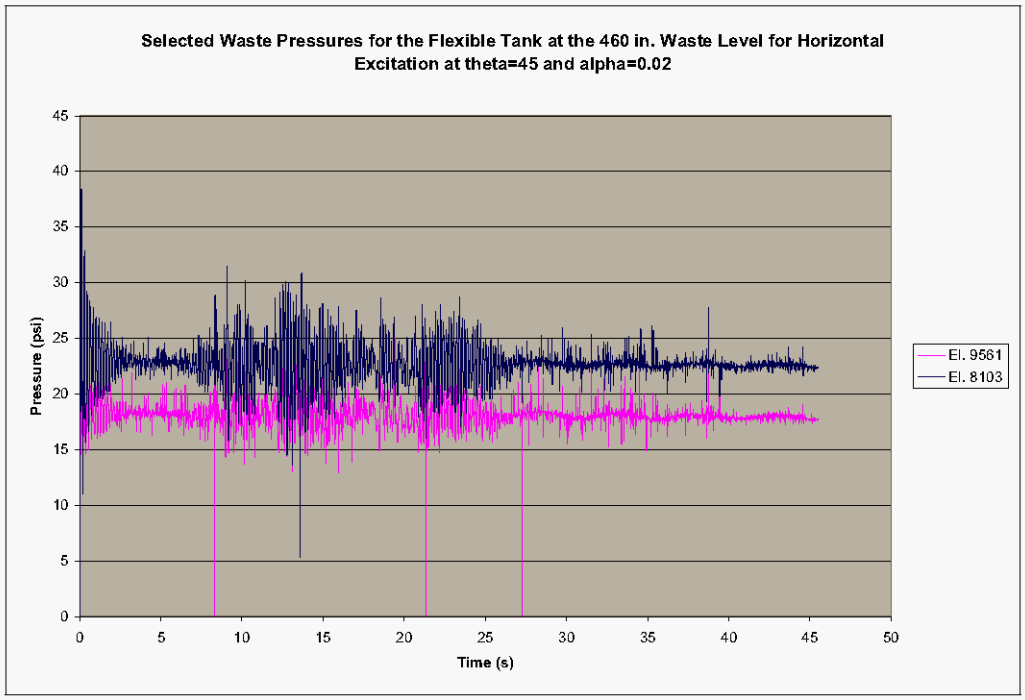

Figure 6-10. Waste Pressures Time Histories for the Flexible Tank at the 460 in. Waste Level for Horizontal Excitation at θ=90 and alpha=0.02 Run at Absolute Pressure.

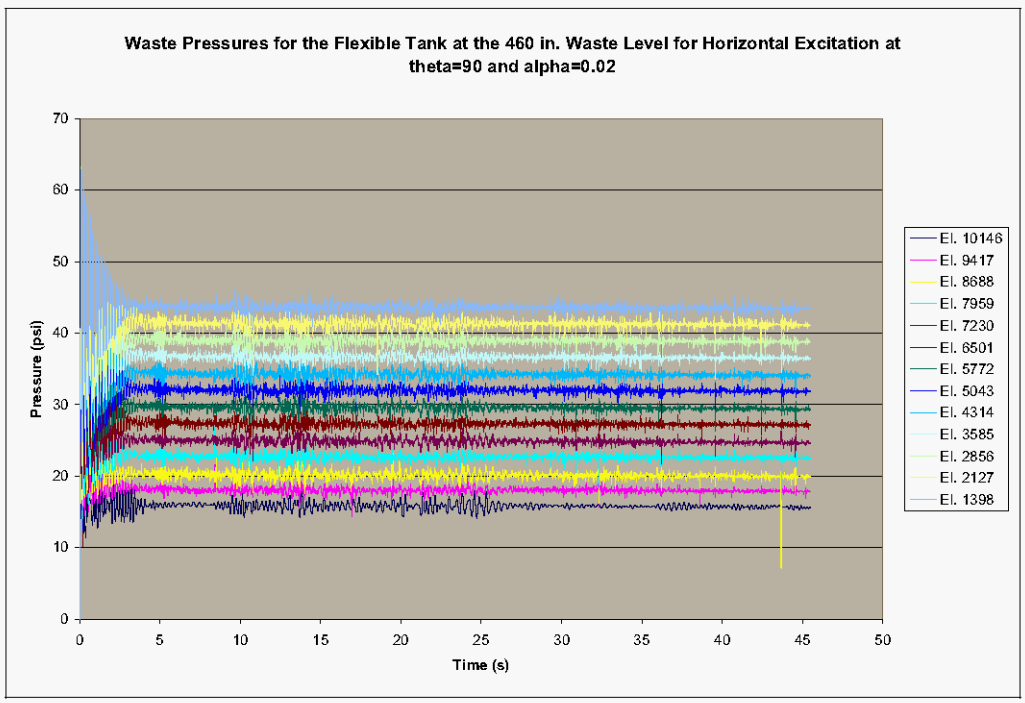

Comparisons of the maximum and minimum waste pressures from the computer simulation (labeled at "actual max." and "actual min.") to the maximum and minimum pressures from the theoretical solution for the open tank at the 460 in. waste level are shown in Figure 6-11, Figure 6-12, and Figure 6-13. In the lower portions of the waste, the results agree well with the theoretical solution for the open tank at the 460 in. waste level. In the upper waste elements, the results for $\theta = 0$ and 45° deviate from the theoretical value. The differences, of course, correspond to the isolated peaks shown in Figure 6-7 and Figure 6-9. If the single point isolated peaks shown in Figure 6-7 are neglected, the remaining maximum and minimum are approximately 29 and 9 lbf/in^2, respectively, and the correlation in Figure 6-11would be much better at the upper waste elements. Likewise, if the isolated high peaks in Figure 6-9 are neglected, the correlation at the upper waste elements in Figure 6-12 would improve. Because no significant isolated peaks exist in the traces shown in Figure 6-10, the correlation of computer results to theoretical results shown in Figure 6-13 is good.

Figure 6-11. Maximum and Minimum Waste Pressures vs. Normalized Height from Tank Bottom for the Flexible Tank Under Horizontal Excitation at the 460 in. Waste Level at θ=0 and α=0.02.

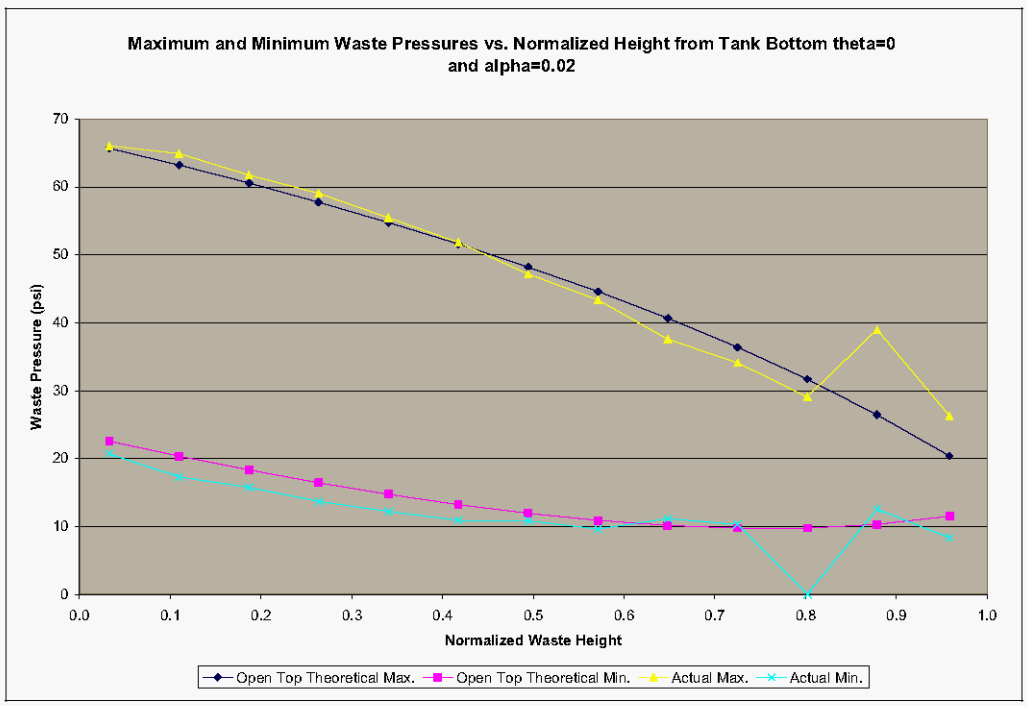

Figure 6-12. Maximum and Minimum Waste Pressures vs. Normalized Height from Tank Bottom for the Flexible Tank Under Horizontal Excitation at the 460 in. Waste Level at θ=45° and α=0.02.

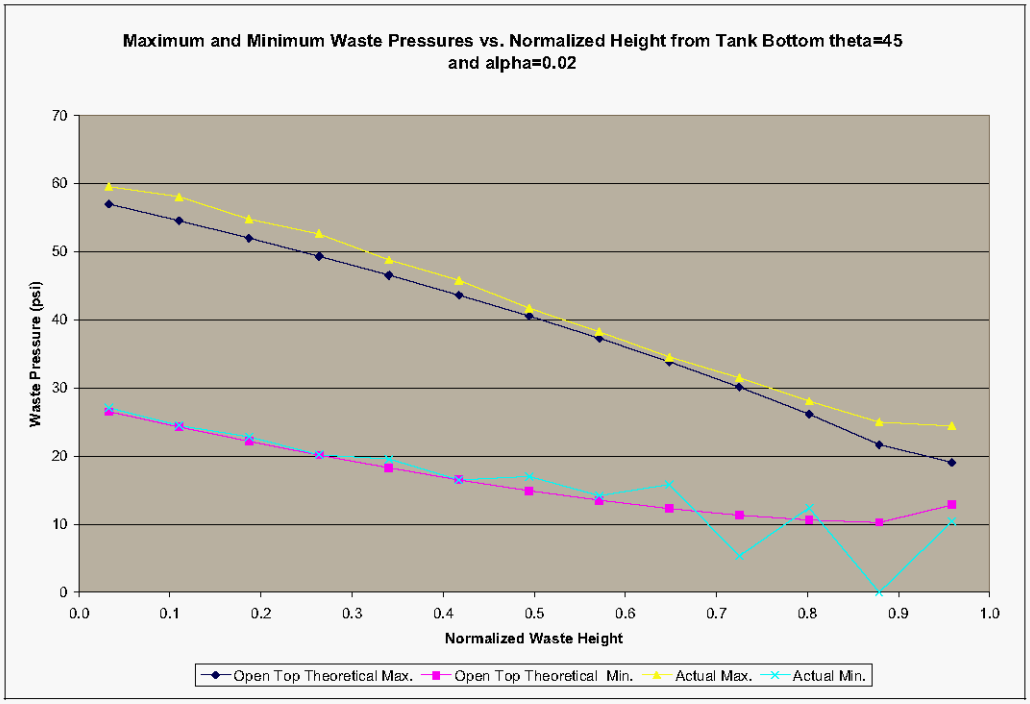

Figure 6-13. Maximum and Minimum Waste Pressures vs. Normalized Height from Tank Bottom for the Flexible Tank Under Horizontal Excitation at the 460 in. Waste Level at θ=90° and α=0.02.

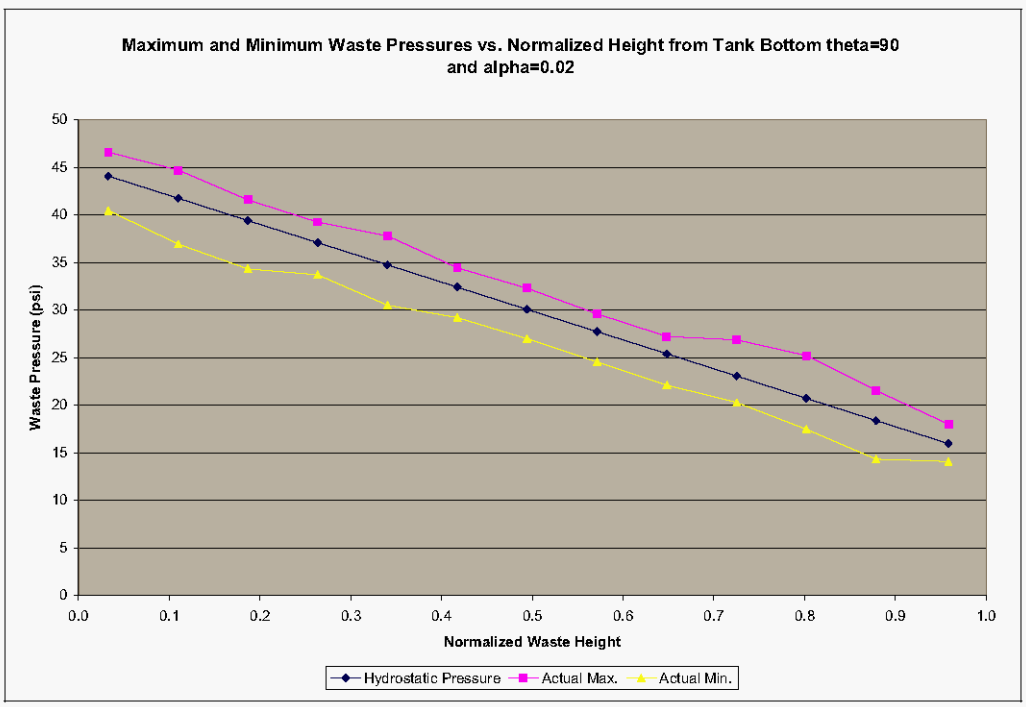

6.2.2 Wall and Base Pressures Due to Vertical Excitation Run at Absolute Pressure

Table 6-3. Theoretical Maximum Absolute Wall Pressures for Vertical Excitation of an Open Top Tank at the 460 in. Waste Level.

"Plusx_els" Element No.	"Press_45" Element No.	"Plusz_els" Element No.	Hydrostatic Pressure (psi absolute)	Peak Hydrodynamic Wall Pressure (psi absolute)	Peak Total Pressure (psi absolute)
10482	10290	10146	16.0	0.9	16.9
9753	9561	9417	18.4	2.7	21.1
9024	8832	8688	20.7	4.4	25.1
8295	8103	7959	23.1	6.0	29.1
7566	7374	7230	25.4	7.5	32.9
6837	6645	6501	27.7	9.0	36.7
6108	5916	5772	30.1	10.2	40.3
5379	5187	5043	32.4	11.4	43.8
4650	4458	4314	34.7	12.3	47.0
3921	3729	3585	37.1	13.1	50.2
3192	3000	2856	39.4	13.7	53.1
2463	2271	2127	41.8	14.1	55.9
1734	1542	1398	44.1	14.3	58.4

The pressure time histories for the waste elements adjacent to the tank wall at θ=0 are shown in Figure 6-14, and pressure time-histories for elements 2463 and 8295 are shown in Figure 6-15. A plot of the pressure decay for the same two elements during the initial gravity loading is shown in Figure 6-16. Evident in the plot is the breathing mode frequency of 5.5 Hz. Similar plots for waste elements at θ=45 and 90° are shown in Figure 6-17 through Figure 6-20.

Plots of the maximum and minimum waste pressures as a function of waste depth are shown in Figure 6-21, Figure 6-22, and Figure 6-23, where the values predicted by Dytran are labeled as "actual max." and "actual min.". The general agreement with open top theory is good, but in each case, isolated peaks in the time histories result in deviations from the theoretical values. The very low value of minimum pressure that occurs at a normalized waste height of 0.11 is in element 2463. This minimum value occurs as in isolated peak at approximately 17 s as shown in Figure 6-15. Similar isolated peaks occur at the 45 and 90° locations and the pressure time histories for the associated waste elements are shown in Figure 6-18 and Figure 6-20.

The pressure time history for the bottom center waste element (element 1722) is shown as Figure 6-24. The theoretical hydrostatic pressure at the centroid of element 1722 is 44.1 lbf/in^2, and the theoretical peak hydrodynamic pressure is 7.3 lbf/in^2. That is, the predicted maximum and minimum pressures at this location are 51.4. and 36.8 lbf/in^2,

respectively. The maximum and minimum values shown in Figure 6-24 are 54.3 and 36.3 lbf/in^2, respectively.

Figure 6-14. Waste Pressure Time Histories for the Flexible Tank at the 460 in. Waste Level for Vertical Excitation at θ=0 and α=0.02.

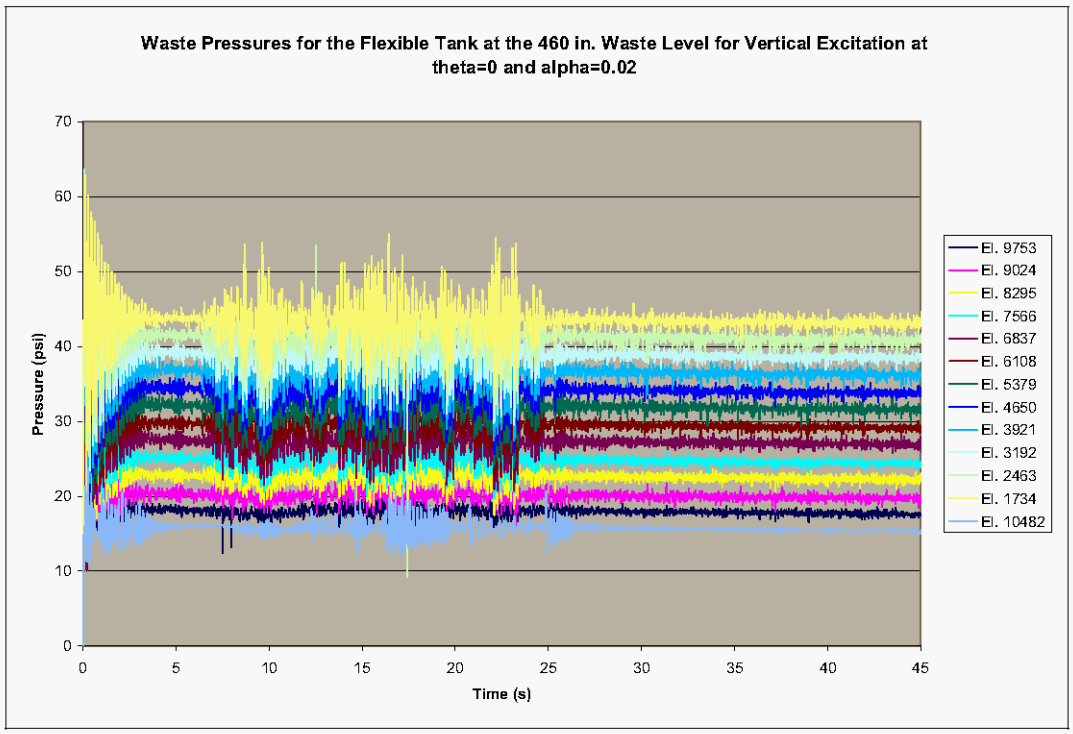

Figure 6-15. Selected Element Waste Pressure for the Flexible Tank at the 460 in. Waste Level for Vertical Excitation at θ=0 and α=0.02.

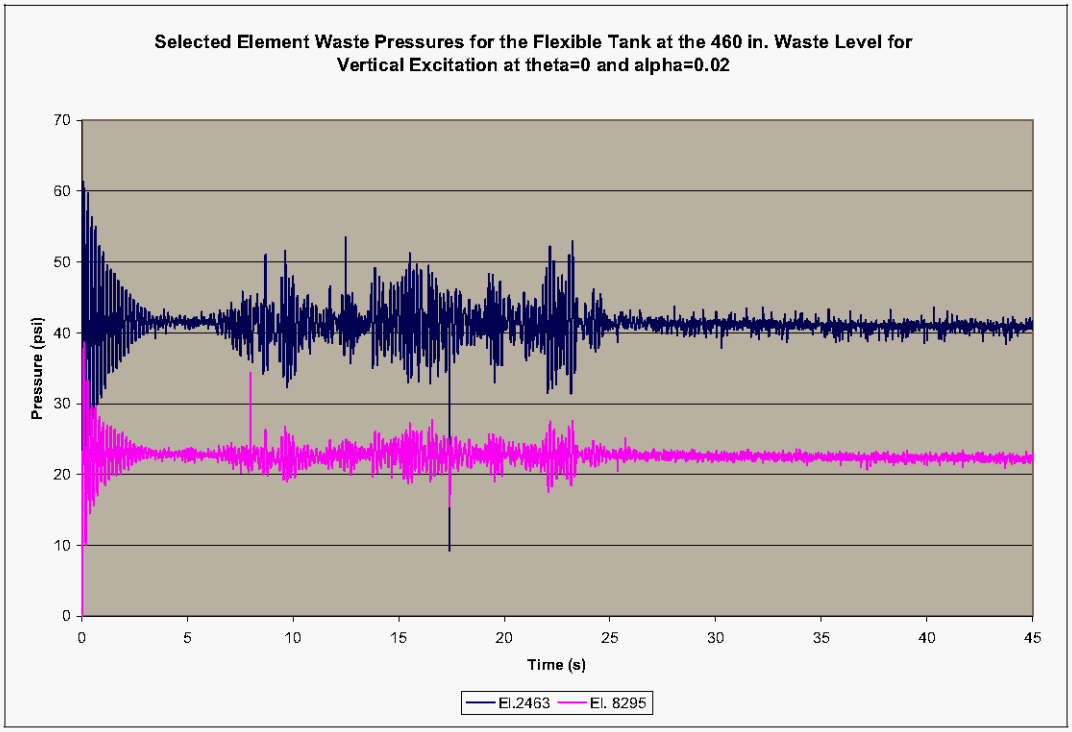

Figure 6-16. Selected Element Waste Pressures for the Flexible Tank at the 460 in. Waste Level for Vertical Excitation at θ=0 and α=0.02 – Time 0 to 3 s.

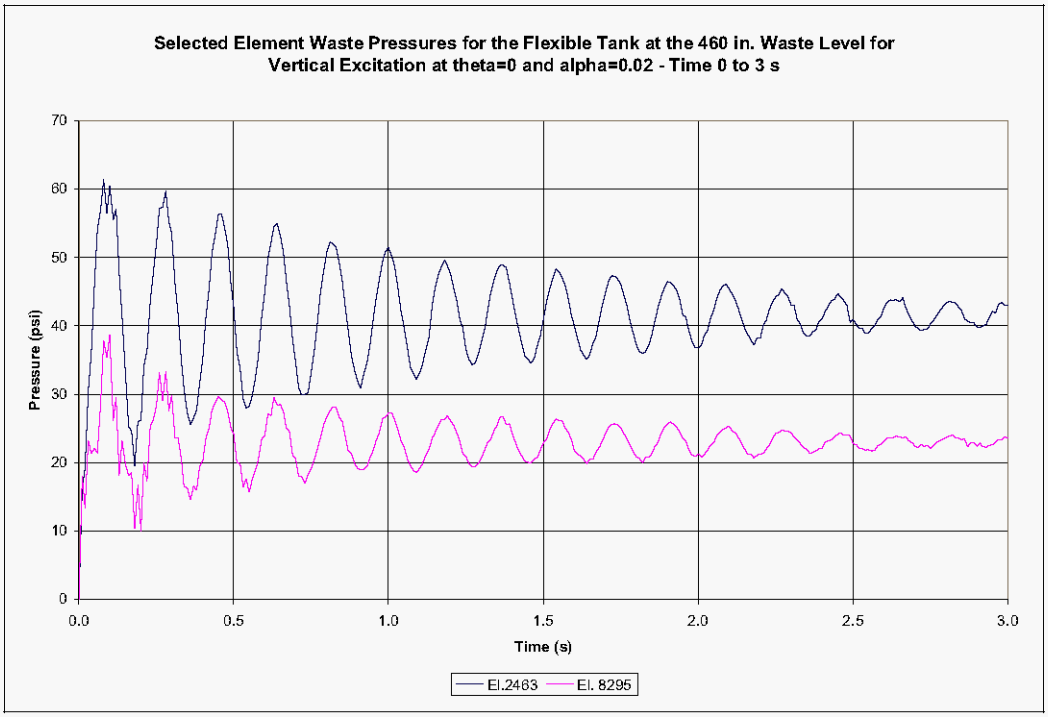

Figure 6-17. Waste Pressure Time Histories for the Flexible Tank at the 460 in. Waste Level for Vertical Excitation at θ=45° and α=0.02.

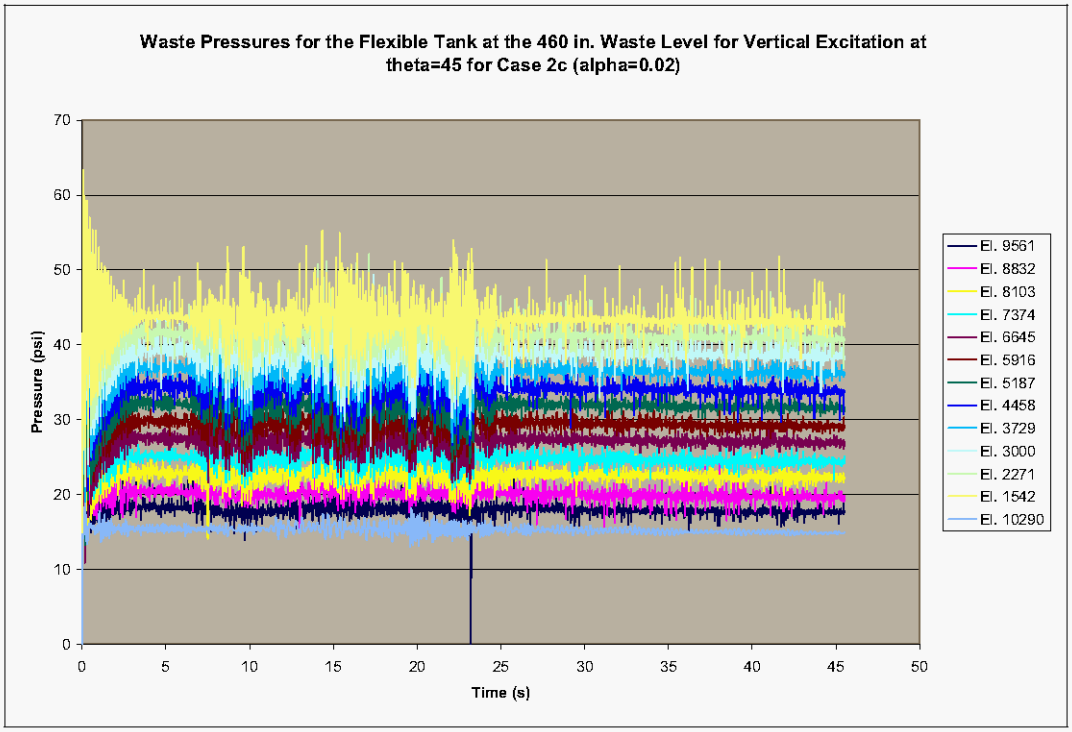

Figure 6-18. Selected Element Waste Pressure for the Flexible Tank at the 460 in. Waste Level for Vertical Excitation at θ=45° and α=0.02.

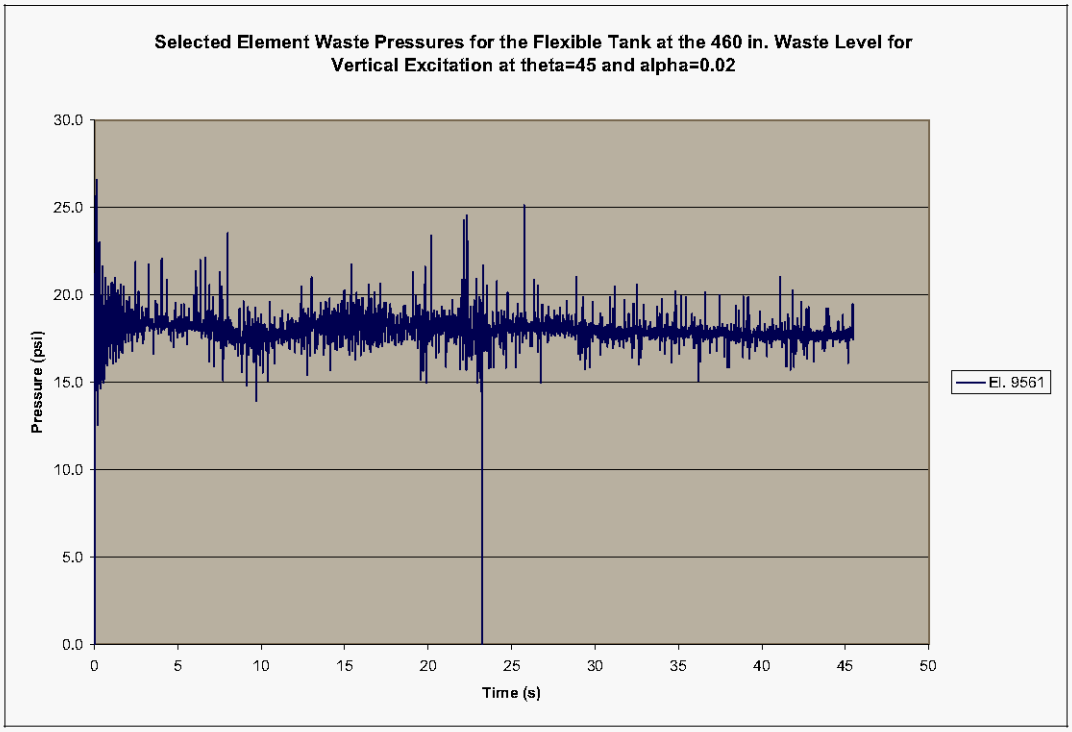

Figure 6-19. Waste Pressure Time Histories for the Flexible Tank at the 460 in. Waste Level for Vertical Excitation at θ=90° and α=0.02.

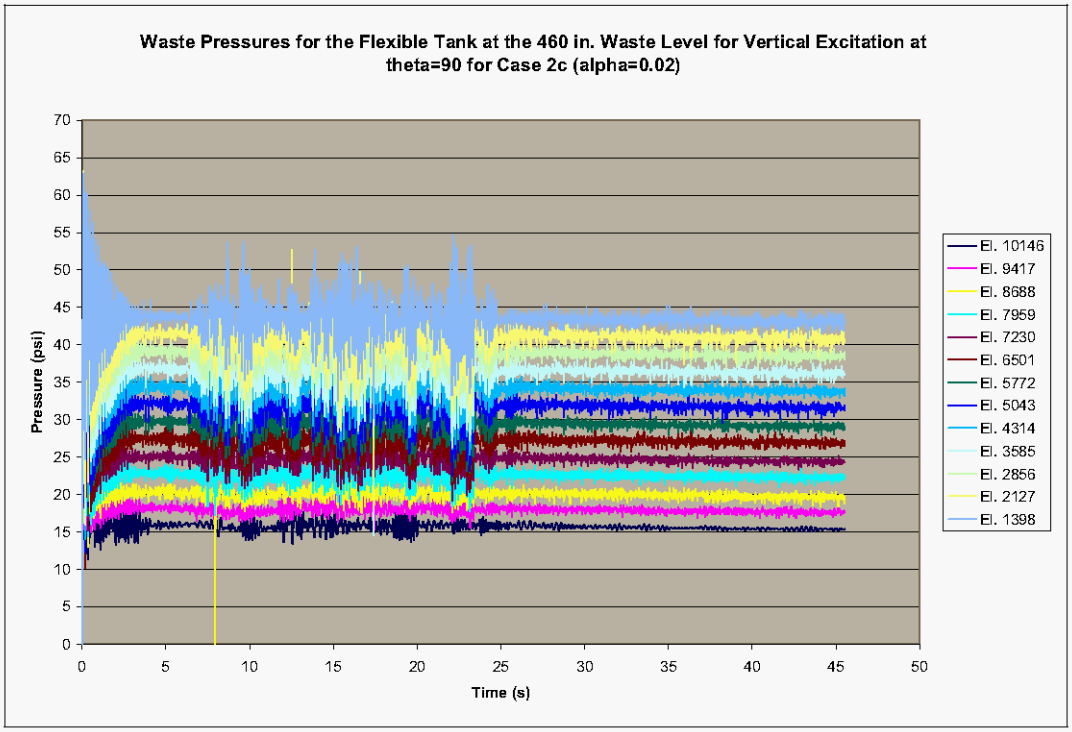

Figure 6-20. Selected Element Waste Pressure for the Flexible Tank at the 460 in. Waste Level for Vertical Excitation at θ=90° and α=0.02.

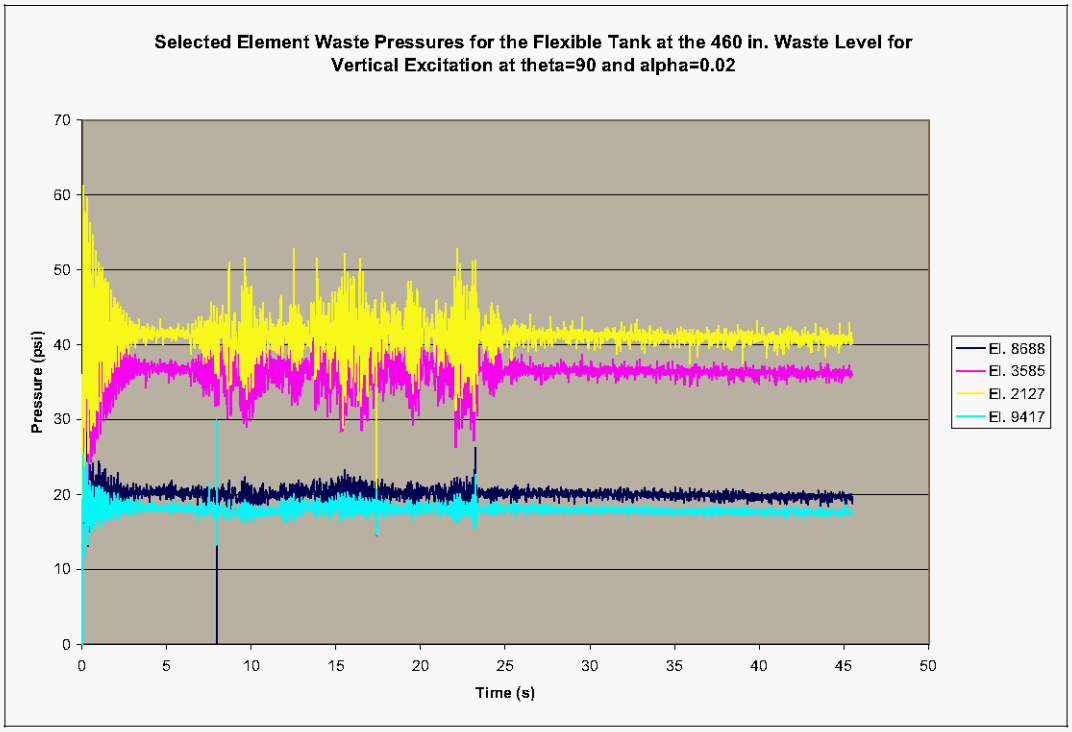

Figure 6-21. Maximum and Minimum Waste Pressures vs. Normalized Waste Height from Tank Bottom for 460 in. Waste Level for Vertical Excitation at θ=0 and α=0.02.

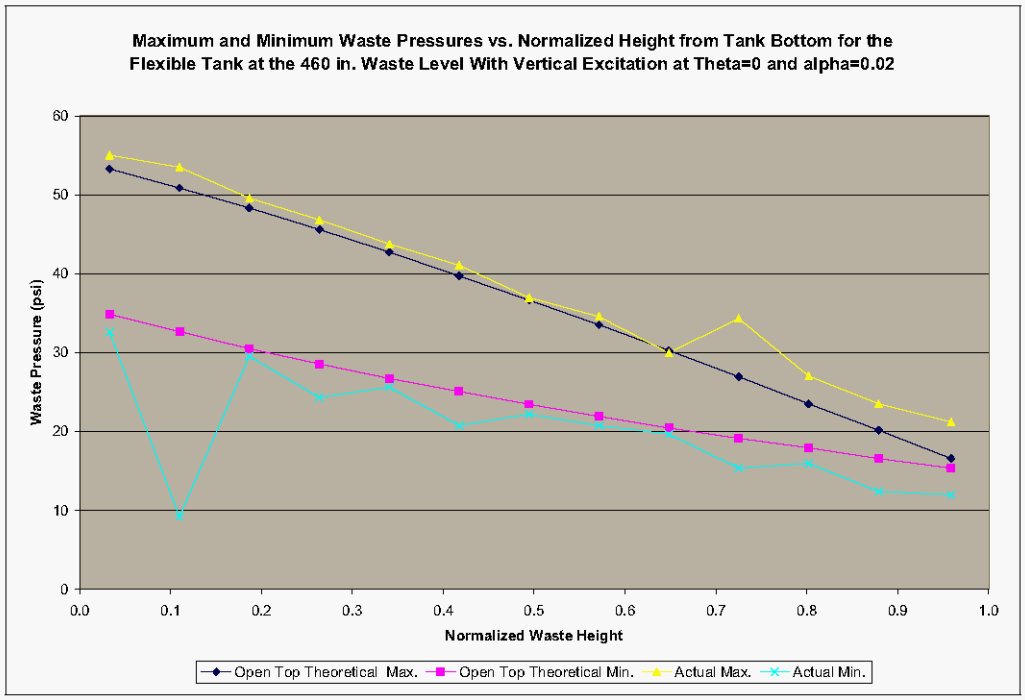

Figure 6-22. Maximum and Minimum Waste Pressures vs. Normalized Waste Height from Tank Bottom for 460 in. Waste Level for Vertical Excitation at θ=45° and α=0.02.

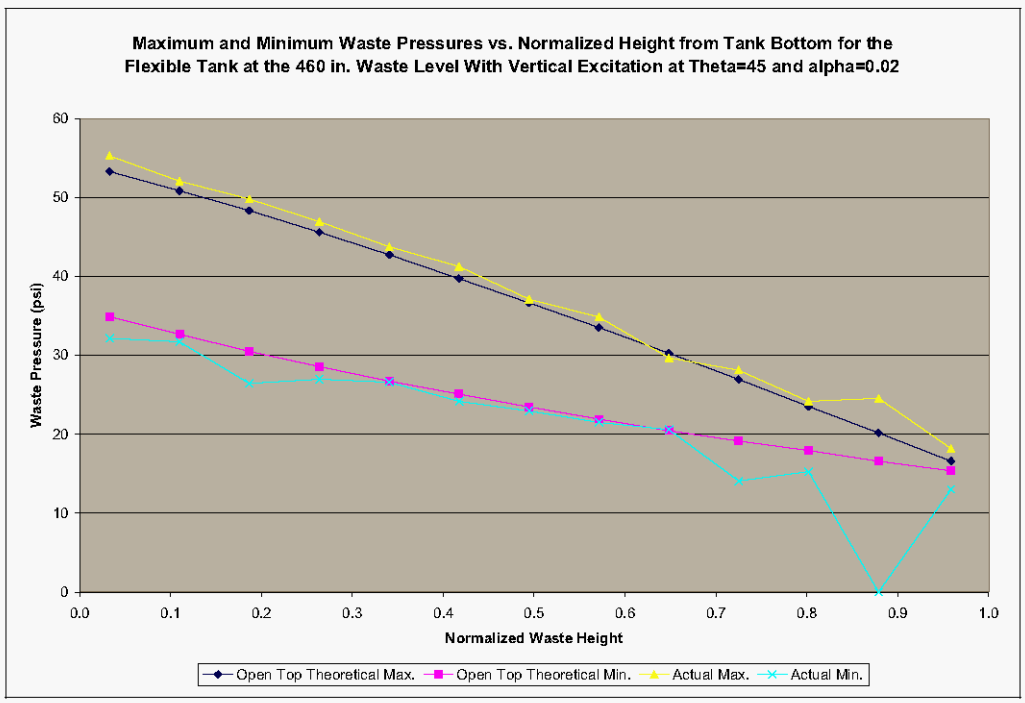

Figure 6-23. Maximum and Minimum Waste Pressures vs. Normalized Waste Height from Tank Bottom for 460 in. Waste Level for Vertical Excitation at θ=90° and α=0.02.

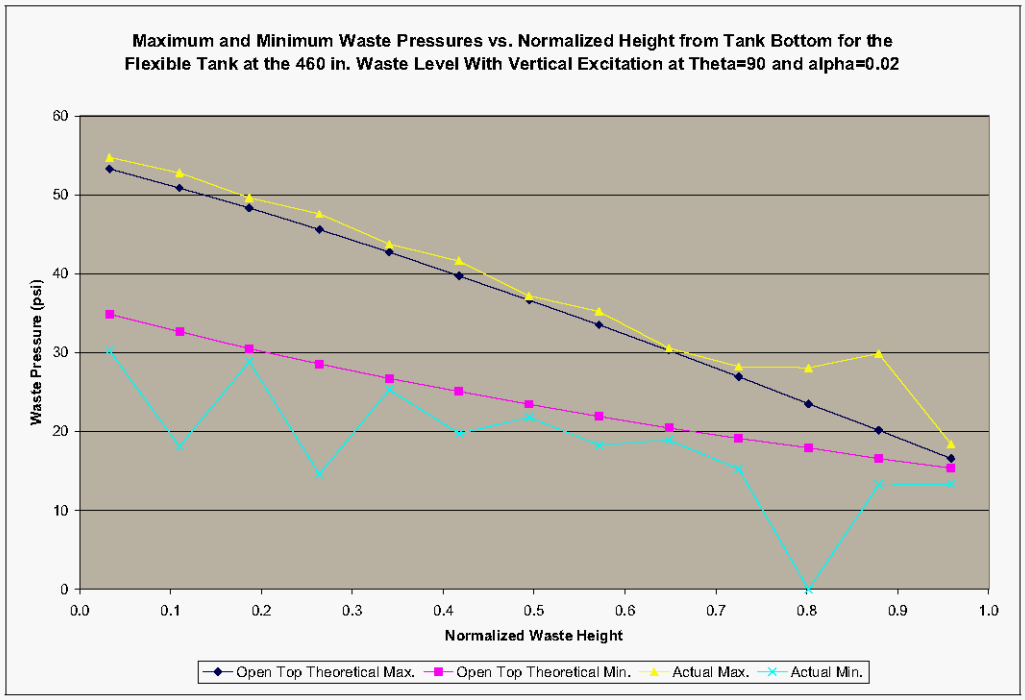

Figure 6-24. Pressure Time History for Bottom Center Waste Element for 460 in. Waste Level and Vertical Excitation for α=0.02.

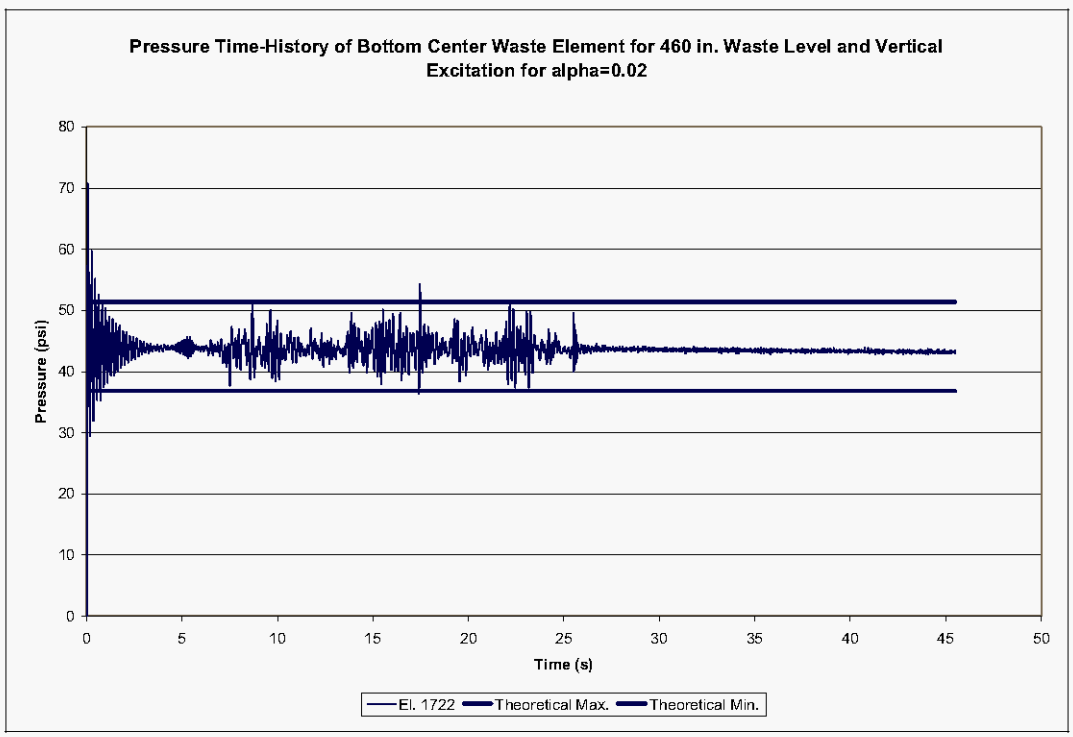

6.3 MAXIMUM SLOSH HEIGHT RESULTS

The time histories of the maximum height of the waste free surface for the simulations at absolute and gage pressure are presented in Figure 6-25. The maximum slosh height predicted for an open tank at the 460 in. waste level is 24.5 in. as shown by the horizontal line in the plot. The maximum value predicted by the Dytran simulation run at absolute pressure is slightly greater than 20 in., and the maximum value predicted for the run at gage pressure is approximately 18 in. Also plotted is the slosh height trace for a rigid tank at the 460 in. waste level run at absolute pressure. The maximum free surface height from that run is just over 21 in. It should not be surprising that the maximum slosh height for the closed tank is less than for the open tank since the presence of the dome should be expected to inhibit the convective response.

The same nonzero slosh heights during gravity loading that were observed in Figure 4-23 show up in Figure 6-25. As remarked in Section 4.3, this may be a limitation with either the slosh height subroutine, or the model discretization.

Figure 6-25. Maximum Slosh Height Time-History for the Flexible Tank at the 460 in. Waste Level for α=0.02.

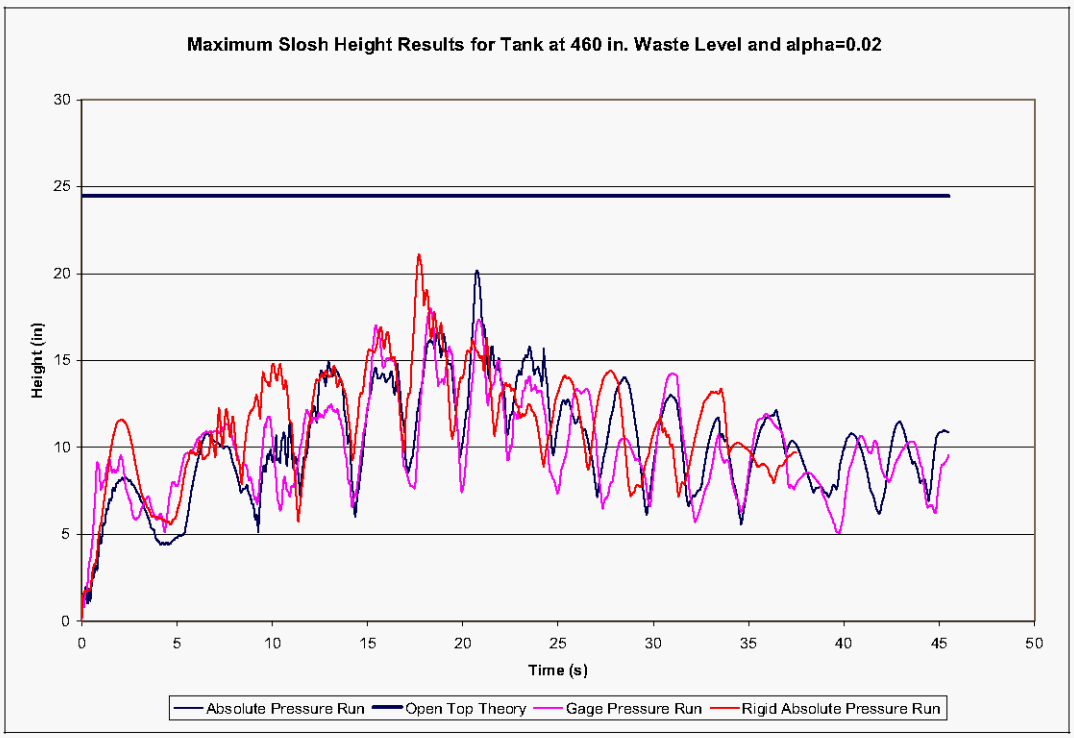

6.4 ELEMENT STRESSES

6.4.1 Horizontal Excitation Run at Absolute Pressure

Mid-plane hoop stresses for the tank shell elements at θ=0, 45, and 90° are presented as Figure 6-26, Figure 6-27, and Figure 6-28, respectively. The general behavior of the hoop stresses is reasonable with the peak stresses generally increasing with waste depth, and decreasing with the angular distance from the plane of excitation in accordance with the waste pressures.

A comparison of the hoop stress to the waste pressures for tank wall element 406 and waste element 9753 is shown as Figure 6-29. Both elements are near the waste free surface at θ=0. Notable in the plot is that the hoop stress does not reflect the spikes in the waste pressure that occur at approximately 14 and 36 s. Similar behavior is displayed in Figure 5-38 for the 422 in. waste level.

Figure 6-26. Mid-Plane Hoop Stress for the Flexible Tank at the 460 in. Waste Level at θ=0 and alpha=0.02 Run at Absolute Pressure.

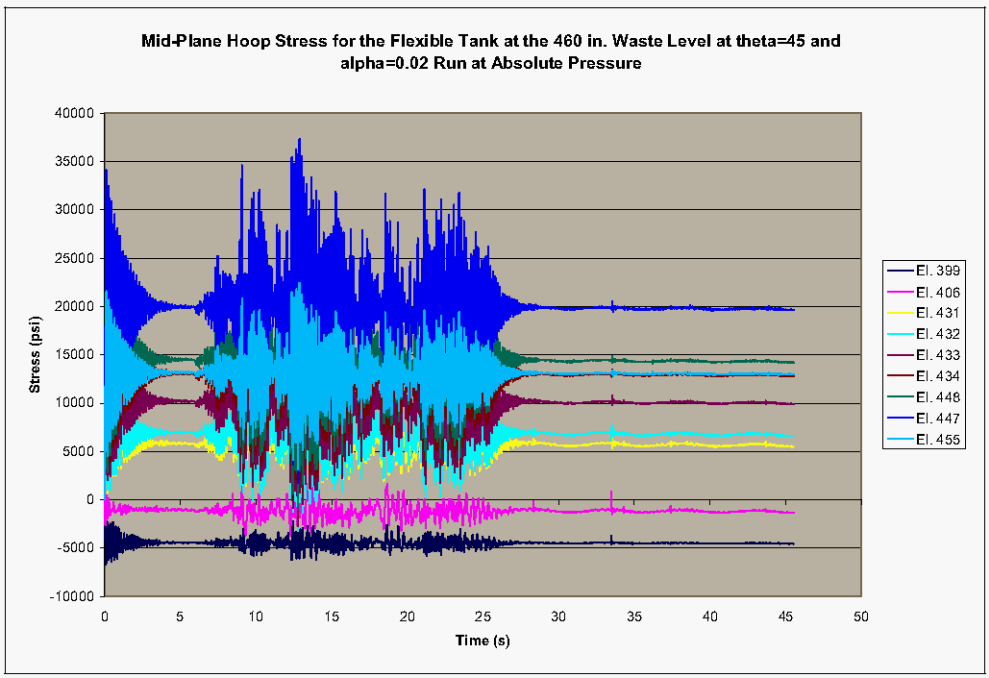

Figure 6-27. Mid-Plane Hoop Stress for the Flexible Tank at the 460 in. Waste Level at θ=45° and alpha=0.02 Run at Absolute Pressure.

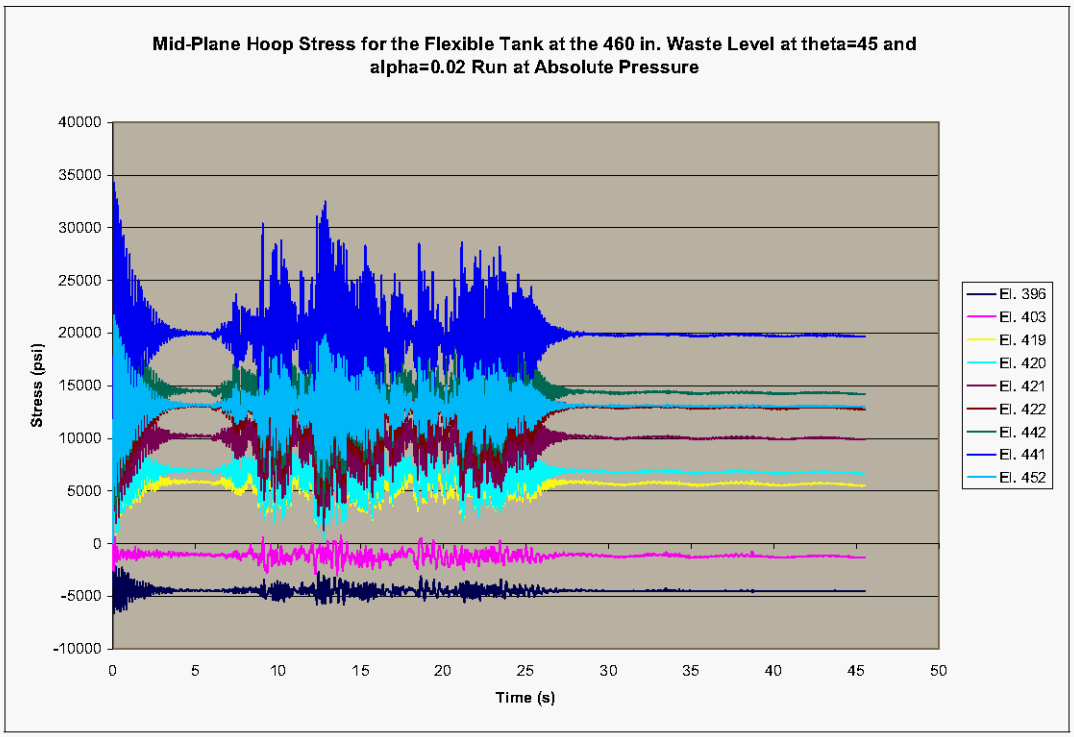

Figure 6-28. Mid-Plane Hoop Stress for the Flexible Tank at the 460 in. Waste Level at θ=90° and alpha=0.02 Run at Absolute Pressure.

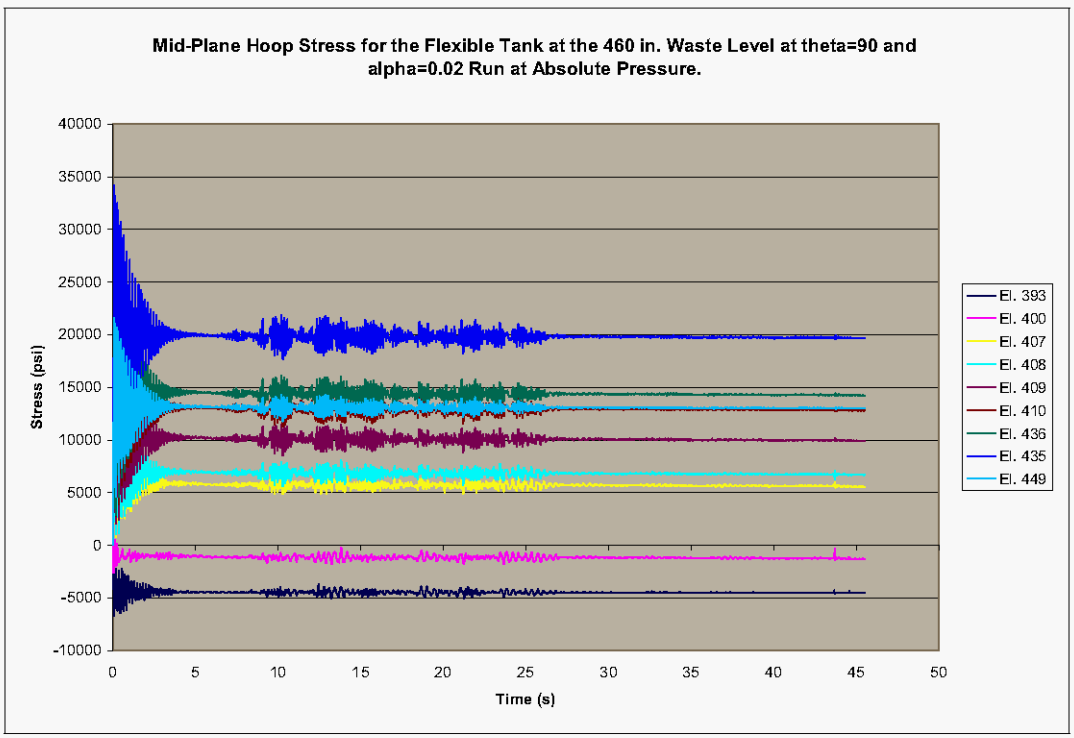

Figure 6-29. Comparison of Waste Pressure to Tank Wall Hoop Stress for the Flexible Tank at the 460 in. Waste Level at Absolute Pressure for Waste Element 9753 and Tank Wall Element 406 Near the Free Surface at θ=0.

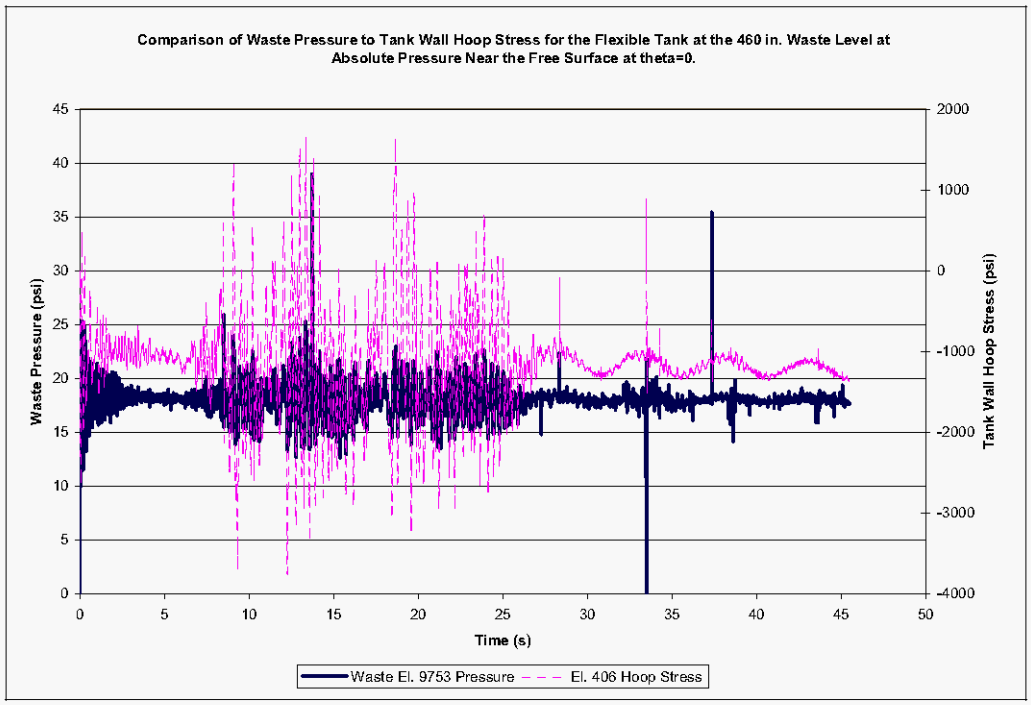

Figure 6-30. Comparison of Waste Pressure to Tank Wall Hoop Stress for the Flexible Tank at the 422 in. Waste Level at Absolute Pressure for Waste Element 9024 and Tank Wall Element 431 Near the Free Surface at θ=0.

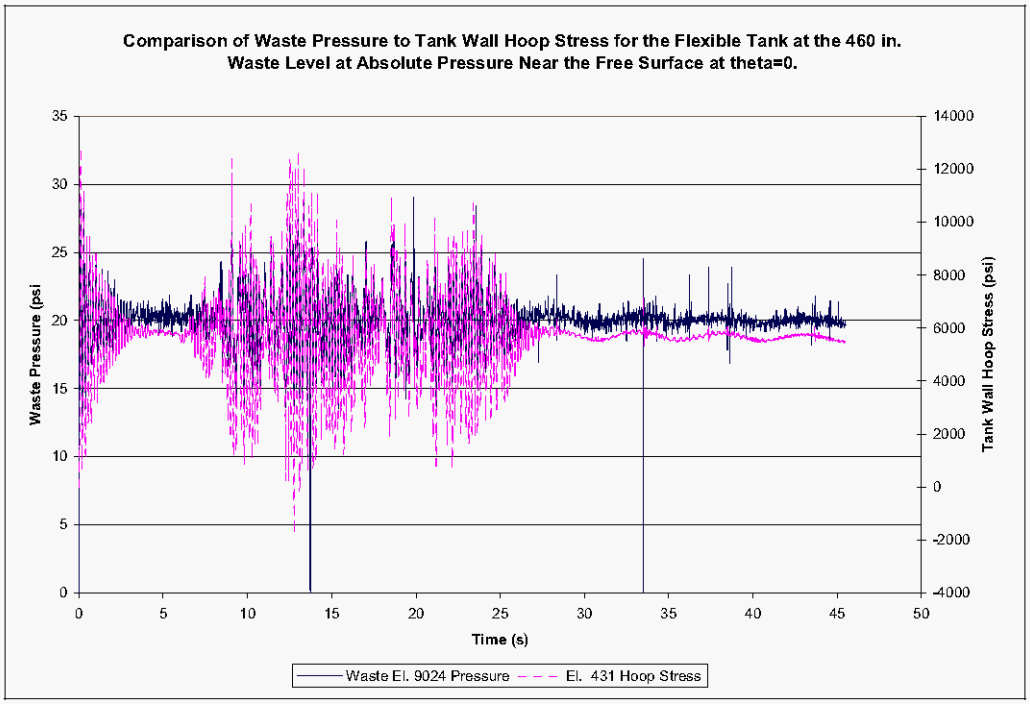

6.4.2 Vertical Excitation Run at Absolute Pressure

Mid-plane hoop stresses for tank shell elements located at θ=0, 45, and 90° are shown in Figure 6-31, Figure 6-32, and Figure 6-33. The general behavior of the hoop stresses is reasonable with similar values and distributions at θ=0, 45, and 90° as expected. A slight downward drift is apparent in the stress that has been observed earlier for the vertical runs. Because of the isolated pressure spikes at waste elements near the free surface shown in Figure 6-18 and Figure 6-20 at the θ=45, and 90° locations, comparisons between the waste pressure and the hoop stress in the adjacent tank wall element are shown in Figure 6-34 and Figure 6-35. In the vertical run, the hoop stress does not follow the pattern of the waste pressure as well as in the horizontal run.

In Figure 6-34, the downward spike in the waste pressure is not reflected in the hoop stress of the adjacent element, but the upward spike in waste pressure shown in Figure 6-35 at approximately 8 s for element 9417 is reflected as a concomitant increase in hoop stress in tank wall element 400. However, magnitude of hoop stress in element 400 is low even with the isolated spike.

Figure 6-31. Mid-Plane Hoop Stress for the Flexible Tank at the 460 in. Waste Level for Vertical Excitation at θ=0 and alpha=0.02 Run at Absolute Pressure.

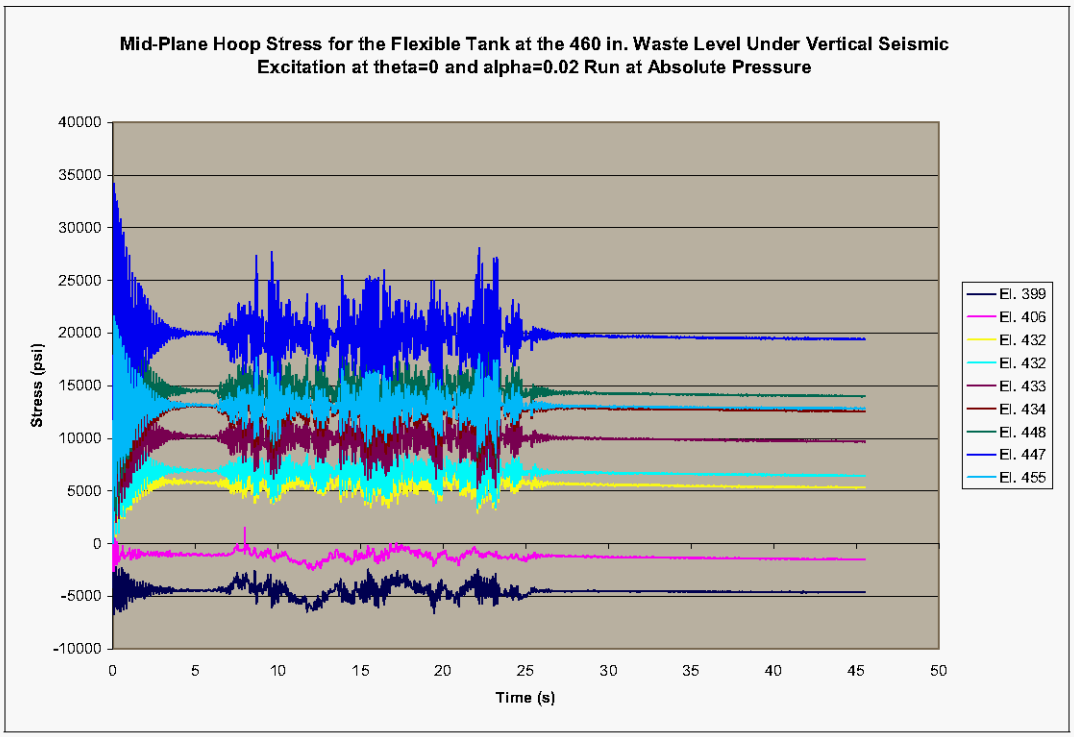

Figure 6-32. Mid-Plane Hoop Stress for the Flexible Tank at the 460 in. Waste Level for Vertical Excitation at θ=45° and alpha=0.02 Run at Absolute Pressure.

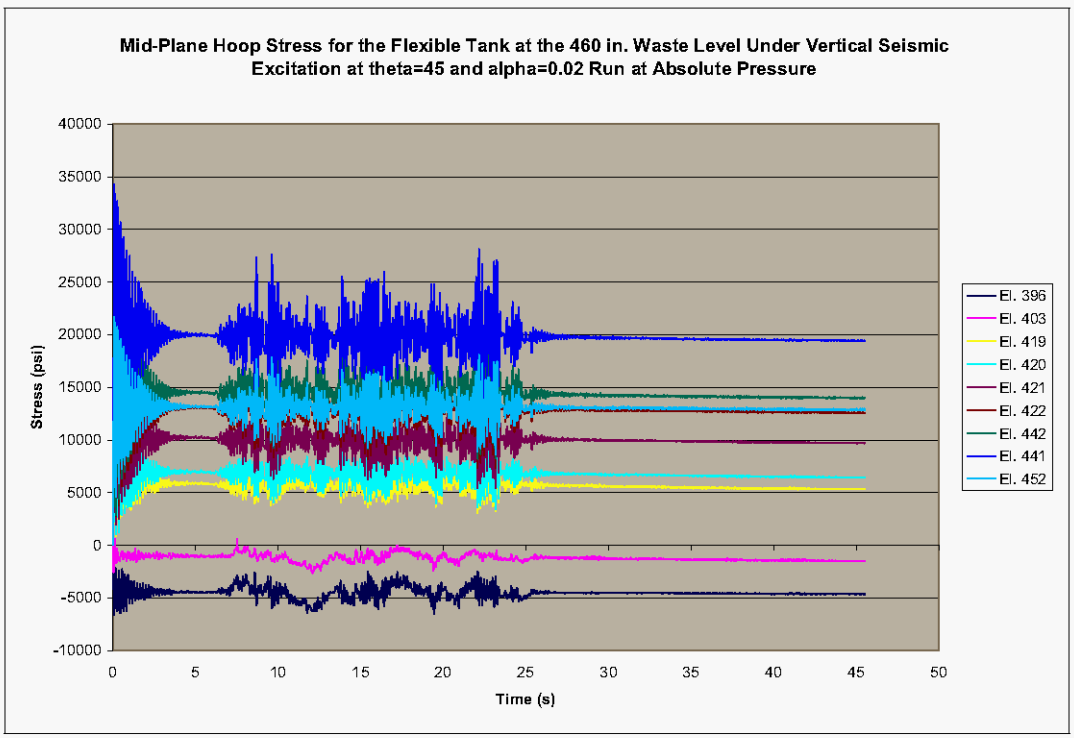

Figure 6-33. Mid-Plane Hoop Stress for the Flexible Tank at the 460 in. Waste Level for Vertical Excitation at θ=90° and alpha=0.02 Run at Absolute Pressure.

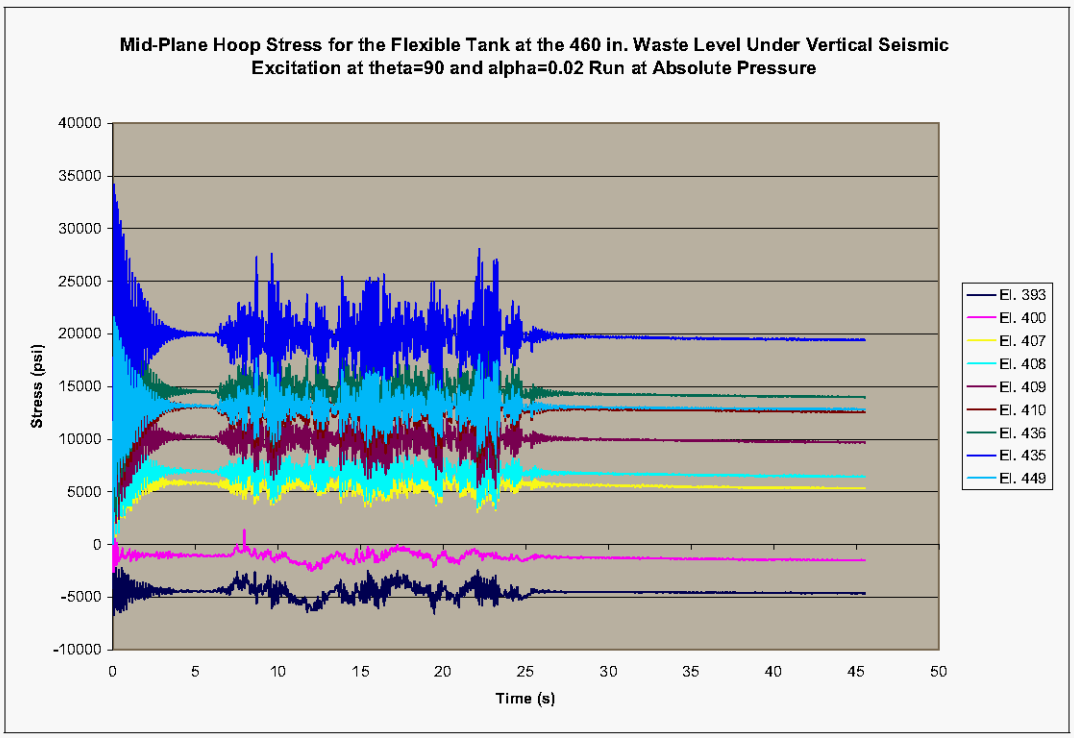

Figure 6-34. Comparison of Waste Pressure to Tank Wall Hoop Stress for the Flexible Tank at the 460 in. Waste Level Under Vertical Excitation at Absolute Pressure Near the Free Surface at θ=45°.

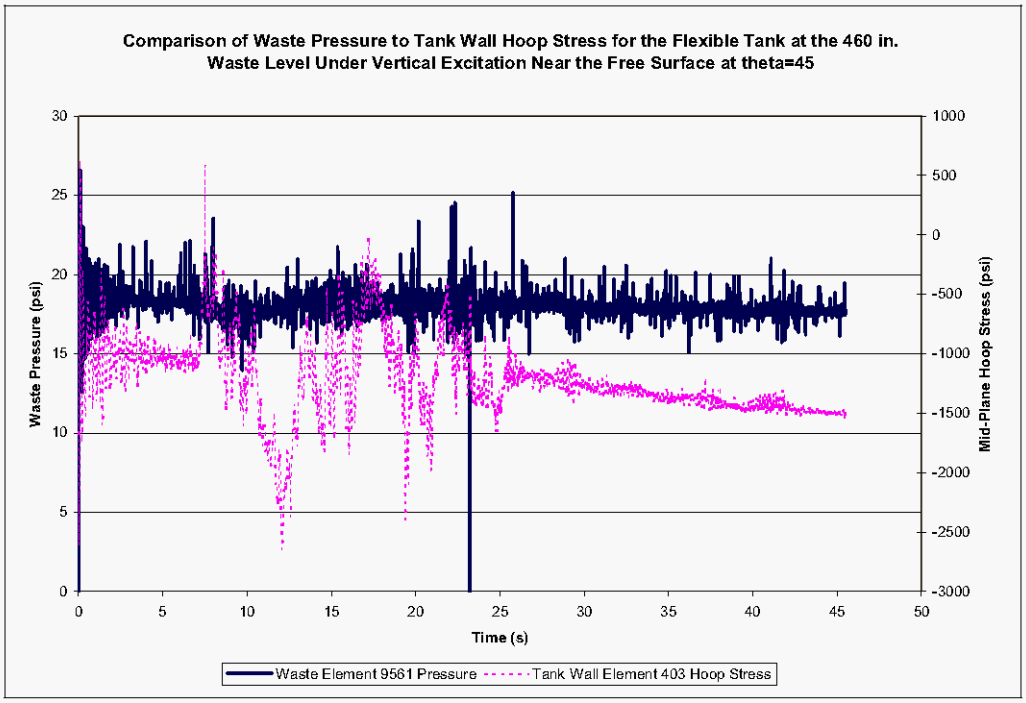

Figure 6-35. Comparison of Waste Pressure to Tank Wall Hoop Stress for the Flexible Tank at the 460 in. Waste Level Under Vertical Excitation at Absolute Pressure Near the Free Surface at θ=90°.

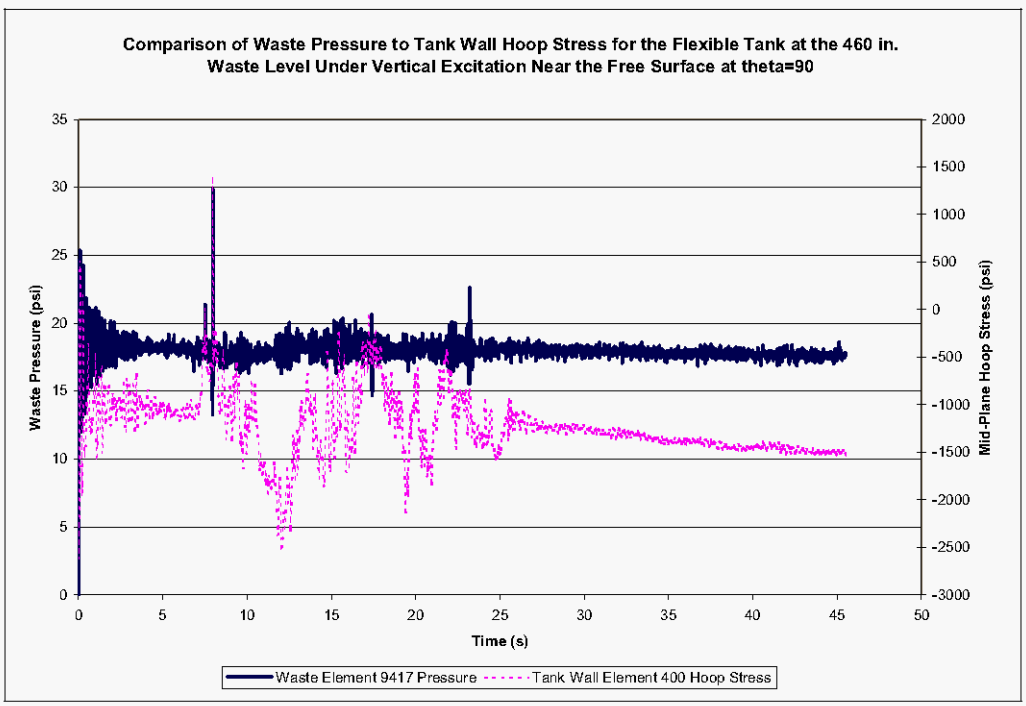

7.0 ANSYS TO DYTRAN COMPARISONS

This report has presented the results of a series of Dytran analyses of simplified primary tank models. A parallel study was conducted using the finite element code ANSYS, and the results of that study are documented in a companion report (Carpenter and Abatt 2006). The goal of the two studies was to evaluate the capabilities and limitations of each code for performing fluid-structure interaction analysis of a DST primary tank. Although the investigations are documented in separate repots, selected results are compared directly in the following sections.

As described in the companion report documenting the ANSYS analyses, the two waste levels of interest are 422 in. and 460 in. The Dytran analyses were performed at these two waste levels. Due to modeling limitations, the lower waste level was modeled in ANSYS as 424 in. At the higher waste level, the ANSYS models were performed at 460 in. for horizontal runs and 452 in. for vertical runs. In the comparison plots to follow, the configurations are generically referred to as the 422 and 460 in. levels, but the actual waste levels used for the ANSYS analyses are as described above. Thus, slight inherent differences exist in some of the solutions due to the difference in waste levels. The theoretical values shown in the plots are for the intended waste levels of 422 and 460 in.

7.1 FREQUENCIES AND SLOSH HEIGHTS

A summary of fundamental frequencies and maximum slosh heights predicted by both ANSYS and Dytran appears as Table 7-1. Both ANSYS and Dytran predict fundamental frequencies that agree well with theory, although Dytran agrees better with theoretical values, particularly for predicting the breathing mode frequencies. It is clear that the ANSYS model is deficient in its ability to predict meaningful slosh heights.

Table 7-1. Comparison of ANSYS and Dytran Frequencies and Maximum Slosh Heights.

Configuration	First Convective Mode Frequency (Hz)			Impulsive Mode Frequency (Hz)			Breathing Mode Frequency (Hz)			Maximum Slosh Height (in)		
	Theory	Dytran	ANSYS	Theory	Dytran	ANSYS	Theory	Dytran	ANSYS	Theory	Dytran	ANSYS
Rigid 422	0.19	0.19	0.184[2]	Rigid	Rigid	Rigid	Rigid	Rigid	Rigid	23.7	25.4	8
Rigid 460[1]	0.2	0.2	0.192	Rigid	Rigid	Rigid	Rigid	Rigid	Rigid	24.5	21.1	8
Flexible 422	0.19	0.19	0.184[3]	7.0	6.85	7.5[2]	6.1	6.0	6.6[2]	23.7	24.5	8
Flexible 460[1]	0.2	0.2	0.192[3]	6.5	6.4	6.6[4]	5.5	5.5	5.7	24.5	20.1	8

[1]Theoretical solutions for the 460 in. waste level are based on an open tank with vertical walls and a hinged top boundary condition.
[2]Based on 424 in. waste level
[3]Convective frequency response based on rigid tank.
[4]Based on 452 in. waste level.

7.2 HYDRODYNAMIC FORCES

Comparisons between the overall reaction forces predicted by ANSYS and Dytran for the flexible tank models are presented in this section. In order to match the Dytran data to the ANSYS data, time scales were shifted as appropriate and the Dytran data was

reversed in sign. The correct signs for the reactions are those predicted by Dytran since the ANSYS data was a result of nodal force post-processing. The results are presented for comparison, but if a physical interpretation of the reaction force is desired, the signs should be reversed from those shown in the plots. For example, in Figure 7-4, the static portion of the vertical reaction force is a downward force due to gravity, and the peak dynamic component of the reaction force occurs in the same direction as the waste weight.

A comparison of the overall horizontal reaction force due to horizontal seismic excitation for the flexible tank at the 422 in. waste level is shown in Figure 7-1. The general agreement between the two responses is good with the peak reaction force predicted by ANSYS slightly higher (that is, conservative) relative to that predicted by Dytran. The comparison of vertical responses to vertical input shown in Figure 7-2 also shows similar signals, and again, the peak response from ANSYS is slightly conservative relative the Dytran prediction.

A comparison of the total horizontal reaction force for horizontal seismic excitation of the flexible tank at the 460 in. waste level is shown as Figure 7-3. Once again, the responses are very similar and the peak reaction force predicted by ANSYS is slightly greater than the peak reaction force predicted by Dytran. Figure 7-4 shows the comparison of the total vertical reaction forces for vertical seismic input for the flexible tank at the 460 in. waste level. This time, although the responses are similar, the higher peak response is predicted by Dytran rather than ANSYS. A review of Figure 6-5 also shows that both models predict a higher peak vertical force than would be expected from the corresponding open top theoretical solution.

Comparison of the reaction forces from the ANSYS and Dytran models shows that the responses from the models are similar with ANSYS generally being conservative relative to Dytran. Both models predict responses that are in good agreement with theoretical solutions. In terms of global reactions on the primary tank, both ANSYS and Dytran appear capable of providing good results. In particular, since the loads into the j-bolts connecting the primary tank to the concrete dome are driven by the overall forces on the primary tank, it appears that a global ANSYS model is sufficient for analysis of the j-bolts and that any sub-model of the primary tank need not contain the j-bolts.

Figure 7-1. Comparison of ANSYS and Dytran Total Horizontal Reaction Forces for the Flexible Tank at the 422 in. Waste Level Under Horizontal Seismic Excitation.

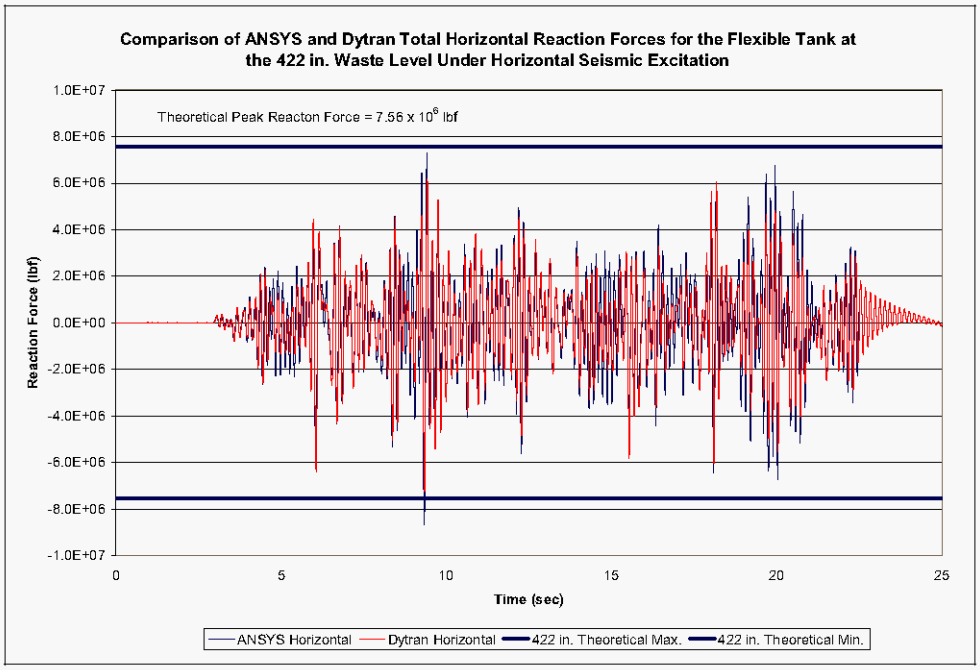

Figure 7-2. Comparison of ANSYS and Dytran Total Vertical Reaction Forces for the Flexible Tank at the 422 in. Waste Level Under Vertical Seismic Excitation.

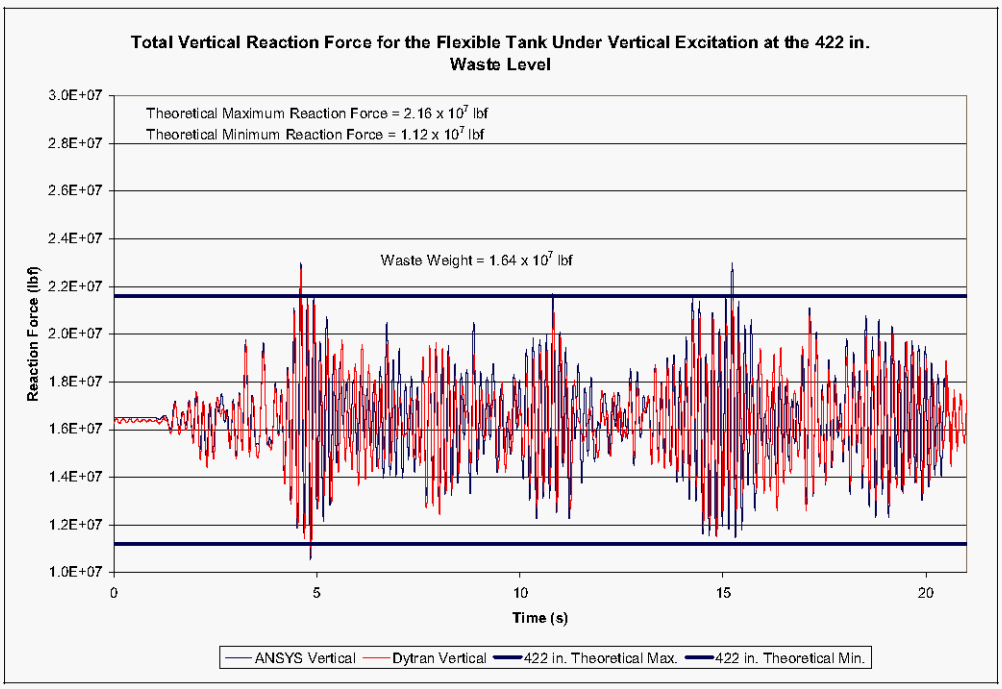

Figure 7-3. Comparison of ANSYS and Dytran Total Horizontal Reaction Forces for the Flexible Tank at the 460 in. Waste Level Under Horizontal Seismic Excitation.

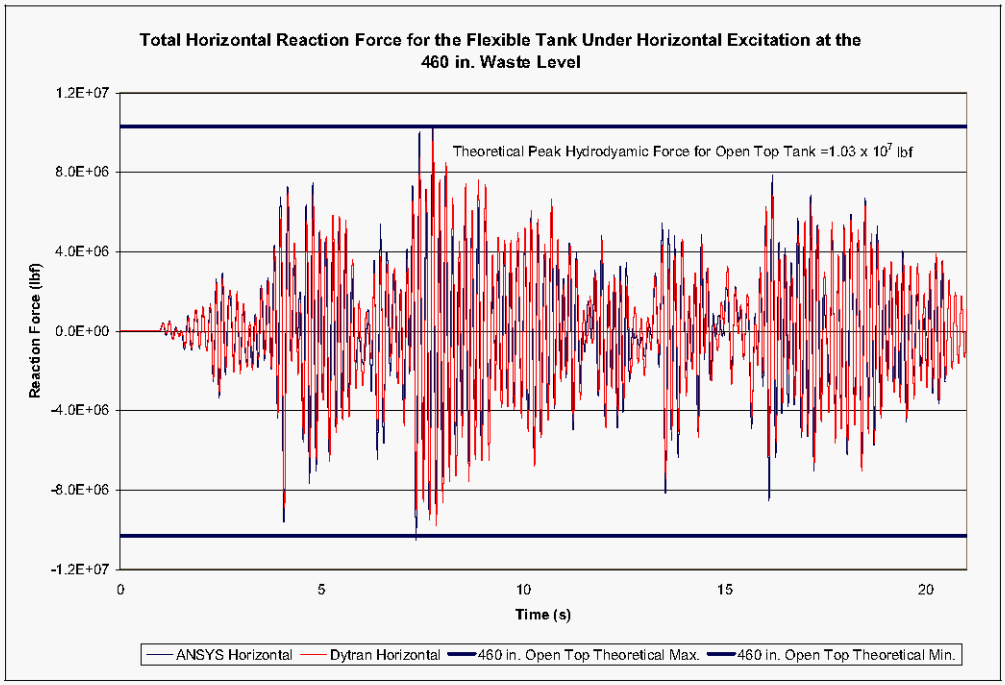

Figure 7-4. Comparison of ANSYS and Dytran Total Vertical Reaction Forces for the Flexible Tank at the 460 in. Waste Level Under Vertical Seismic Excitation.

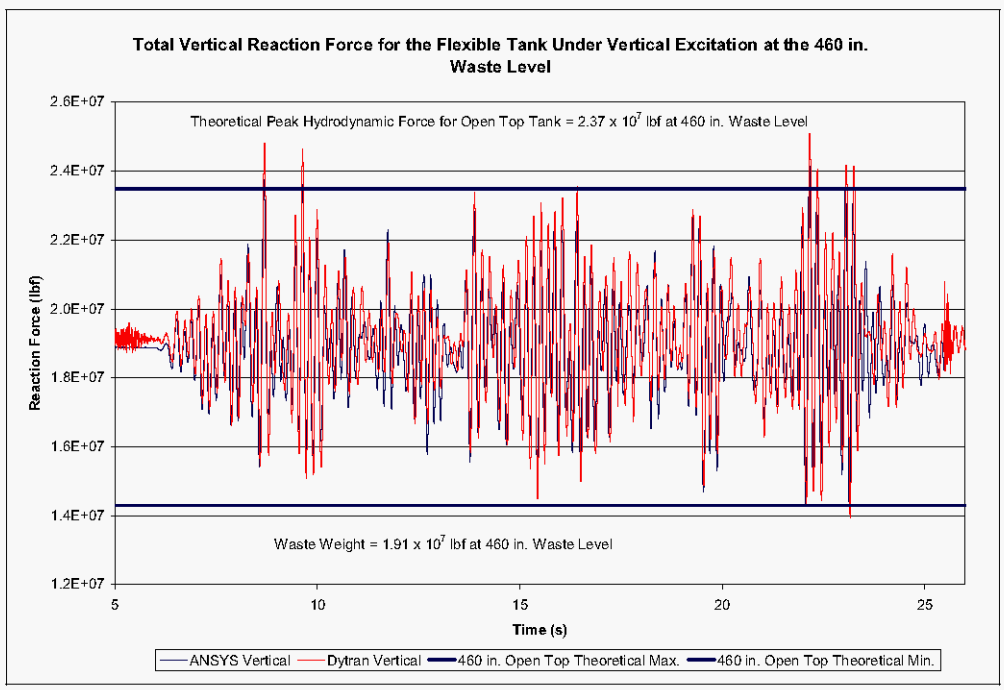

7.3 WASTE PRESSURES

Direct comparisons of waste pressures predicted by ANSYS and Dytran are presented in this section. To be consistent with the pressures reported by ANSYS, the Dyran pressures have been shifted down by 14.7 lbf/in^2, since the ANSYS simulations were run at gage pressure and the Dytran simulations were performed at absolute pressure. The ANSYS and Dytran model meshes were not identical, so comparisons are made for waste elements at similar elevations. All comparisons were made for elements along the plane of excitation (θ=0). The waste element numbers, centroidal elevations, and theoretical hydrostatic pressures are summarized in Table 7-2. The element numbers for ANSYS are actually contact element numbers between the waste and the primary tank, since these are the elements used to report the waste pressures from ANSYS.

Waste element pressures at the 422 in. waste level are presented as Figure 7-5 and Figure 7-6. A comparison of waste pressures near the top and bottom of the tank is shown in Figure 7-5 and a comparison of waste pressures approximately 2/3 the way up the waste is shown in Figure 7-6. Both plots show reasonably good agreement with the dynamic pressures reported by ANSYS tending to run slightly higher than those from Dytran except at a few isolated peaks near the waste surface in Figure 7-5. The plots also show that in the upper portion of the waste, the low-frequency convective response is more pronounced in ANSYS than in Dytran.

Wastes pressures from the simulations at the 460 in. waste level are shown in Figure 7-7 and Figure 7-8. The responses are again similar, but at the bottom of the waste, the peak pressures reported by Dytran exceed those reported by ANSYS. In the upper portion of the waste, the peak pressures from ANSYS are greater than the peak pressures from Dytran. The convective response is also less apparent in the ANSYS simulation at the 460 in. waste level than at the 422 in. waste level.

Table 7-2. Summary of Centroidal Elevations for ANSYS and Dytran Selected Waste Elements at θ=0.

ANSYS Element No.	Centroidal Elevation from Tank Bottom (in.)	Theoretical Hydrostatic Pressure (psi)	Dytran Element No.	Centroidal Elevation from Tank Bottom (in.)	Theoretical Hydrostatic Pressure (psi)*
422 in. Waste Level					
5521	401.9	1.4	9753	404.3	1.1
5581	291.8	8.1	7566	298.2	7.6
5721	54.5	22.7	2463	50.5	22.8
460 in. Waste Level					
5511	438.3	1.4	10482	441.0	1.3
5831	291.8	11.1	7566	298.2	10.7
5971	54.5	26.8	2463	50.5	27.1

*Dytran waste pressures have been shifted down by 14.7 lbf/in^2 to be consistent with ANSYS.

Figure 7-5. Comparison of ANSYS and Dytran Waste Pressures for the Flexible Tank at the 422 in. Waste Level Under Horizontal Excitation – Waste Elements Near Tank Top and Bottom at θ=0.

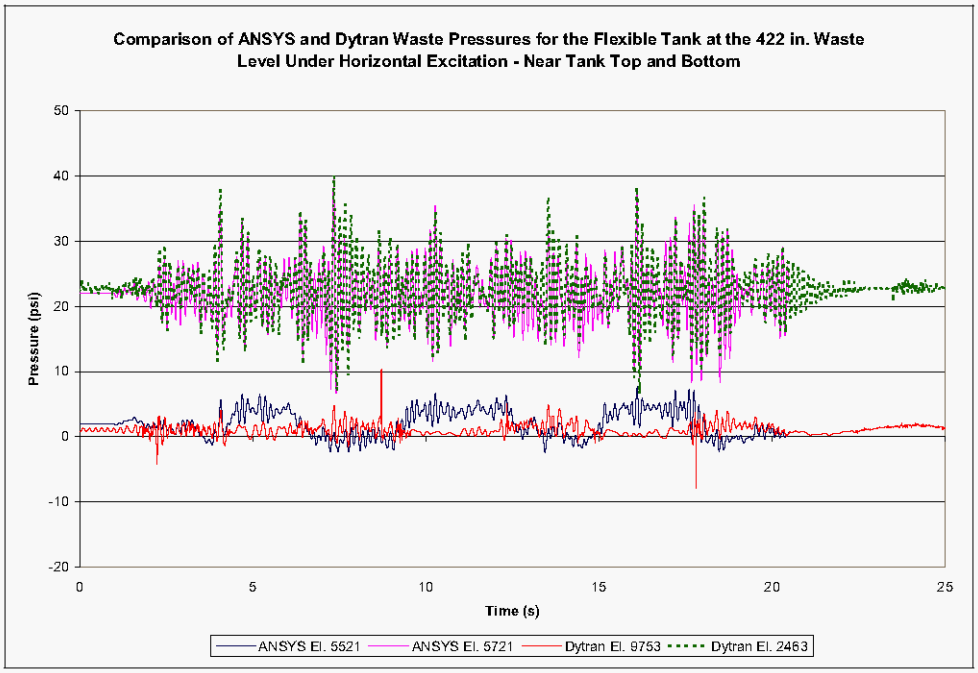

Figure 7-6. Comparison of ANSYS and Dytran Waste Pressures for the Flexible Tank at the 422 in. Waste Level Under Horizontal Excitation – Waste Elements at Elevation 292 in. Above Tank Bottom at θ=0.

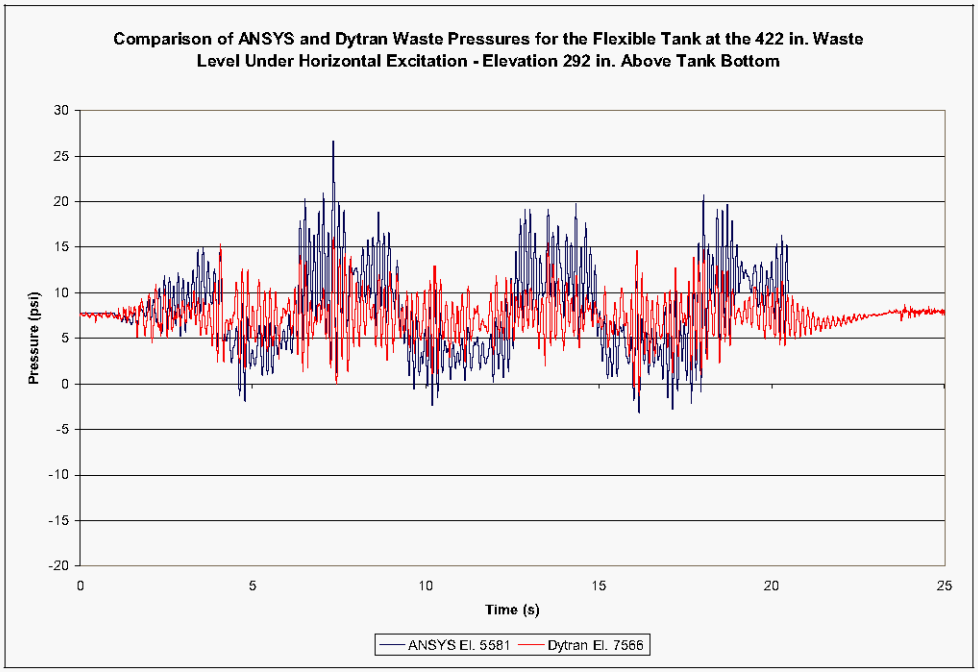

Figure 7-7. Comparison of ANSYS and Dytran Waste Pressures for the Flexible Tank at the 460 in. Waste Level Under Horizontal Excitation – Waste Elements Near Tank Top and Bottom at θ=0.

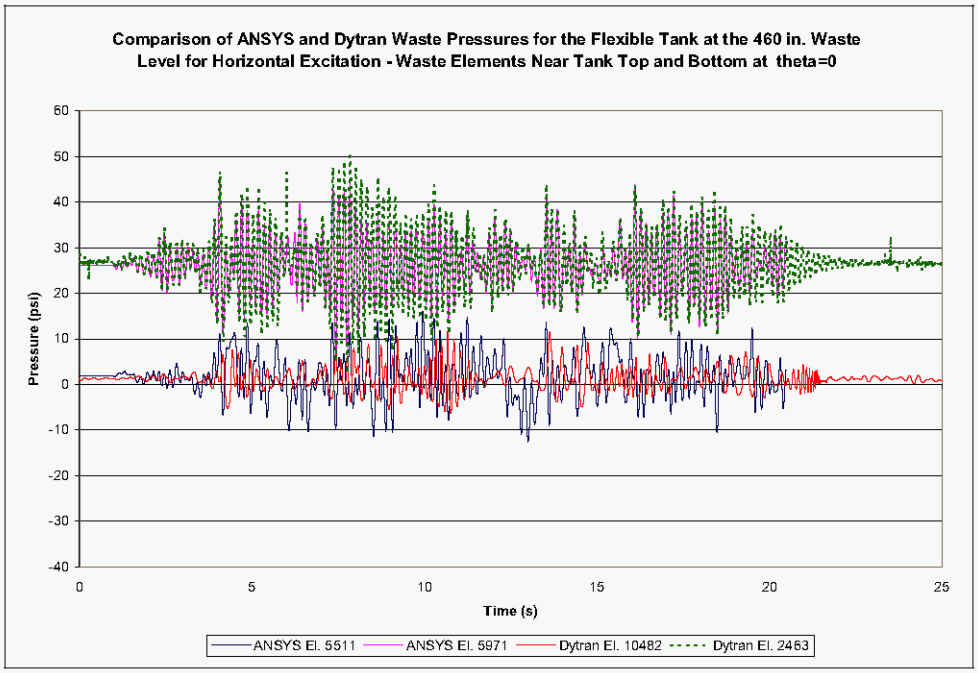

Figure 7-8. Comparison of ANSYS and Dytran Waste Pressures for the Flexible Tank at the 460 in. Waste Level Under Horizontal Excitation – Waste Elements at Elevation 292 in. Above Tank Bottom at θ=0.

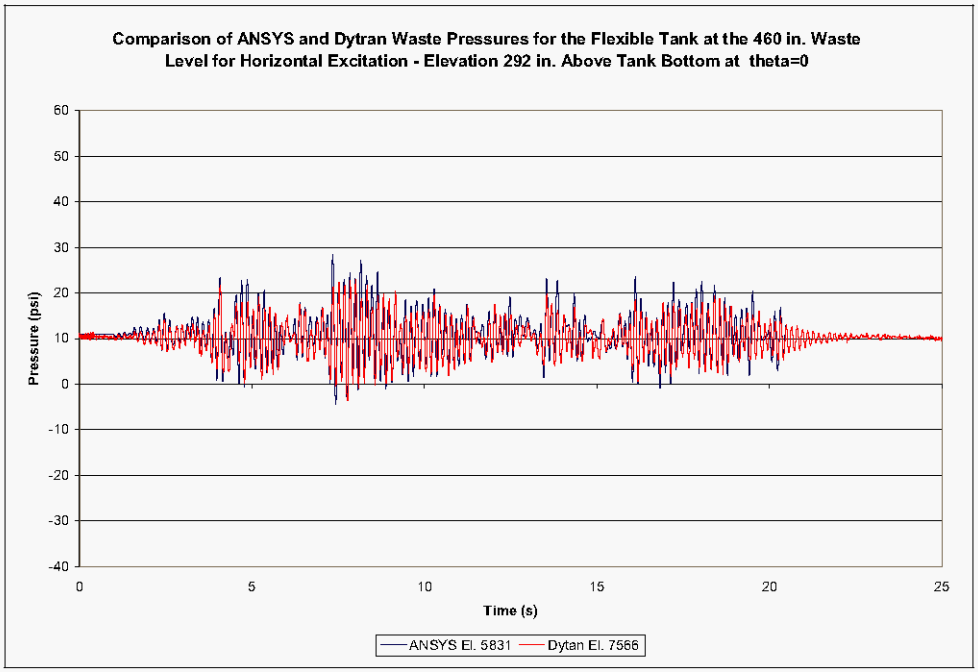

7.4 ELEMENT STRESSES

Direct comparisons of element mid-wall hoop stresses predicted by ANSYS and Dytran are presented in this section. The ANSYS and Dytran model meshes were not identical, so comparisons are made for tank wall elements at elevations as close as possible. However, the difference in mesh resolutions and the local modeling of the tank knuckle region is expected to cause differences in the reported stresses even at similar elevations. All comparisons were made for elements along the plane of excitation (θ=0). The tank wall element numbers and centroidal elevations are summarized in Table 7-3.

Mid-wall hoop stresses at the 422 in. waste level are presented for tank elements near the waste free surface, approximately 2/3 of the way up from the tank bottom, and near the tank bottom in Figure 7-9, Figure 7-10, and Figure 7-11, respectively. The static portion of the hoop stresses shown in Figure 7-9 differ by approximately 1,000 lbf/in^2, even though the element elevations are nearly the same as shown in Table 7-3. According to Figure 7-5, the waste pressures adjacent to these elements are nearly the same, so apparently the difference in stresses is due to a combination of the difference in mesh resolution and the difference in how the two codes transmit the waste pressures into the structure. Interestingly, whereas the convective response was more pronounced in the waste pressures predicted by ANSYS at this elevation, the convective response is more apparent in the stresses predicted by Dytran. This may be due to the difference in the Lagrangian vs. Eulerian formulation of the waste elements.

At the 292 in. elevation, and at the bottom, the responses are similar with ANSYS predicting a slightly higher stresses at the 292 in. level, and Dytran predicting a slightly higher stresses near the tank bottom. The differences near the tank bottom may be due partly to the difference in the details of the mesh in the tank knuckle region and partly due to the more than nine inch difference in the elevation of the wall element centroids.

Table 7-3. Summary of Centroidal Elevations for Tank Wall Elements at θ=0.

ANSYS Element No.	Centroidal Elevation from Tank Bottom (in.)	Dytran Element No.	Centroidal Elevation from Tank Bottom (in.)
961	438.3	399	441.8
981	401.9	406	402.9
1041	291.8	432	292.77
1181	54.5	447	63.9

Figure 7-9. Comparison of ANSYS and Dytran Mid-Plane Hoop Stress at Primary Tank Wall Element Near the Waste Free Surface for the Flexible Tank at the 422 in. Waste Level for Horizontal Excitation and θ=0.

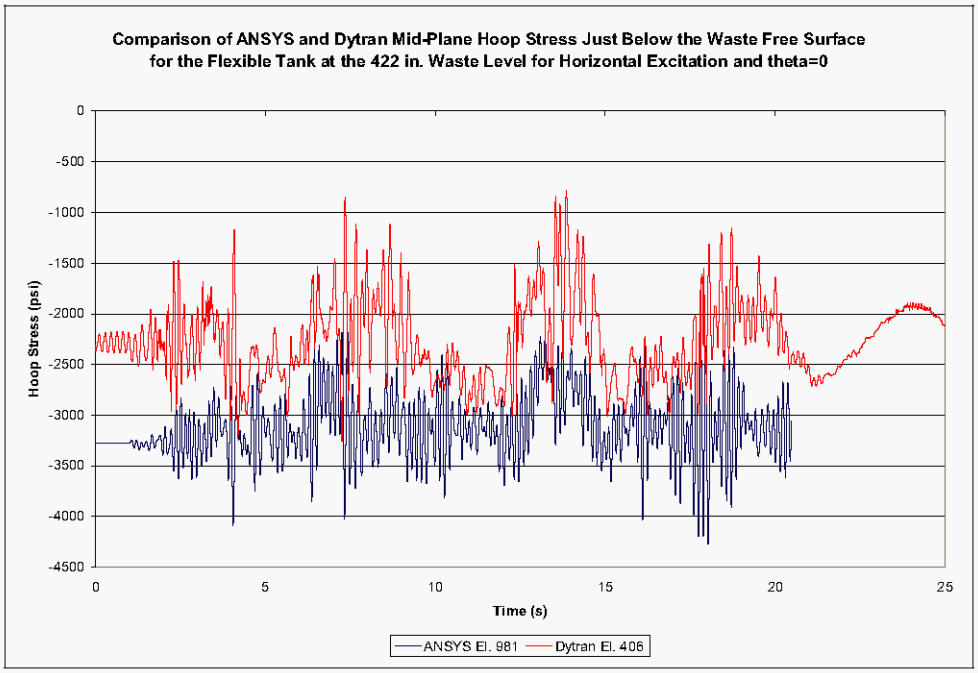

Figure 7-10. Comparison of ANSYS and Dytran Mid-Plane Hoop Stress at an Elevation of 292 in. from the Tank Bottom for the Flexible Tank at the 422 in. Waste Level for Horizontal Excitation and θ=0.

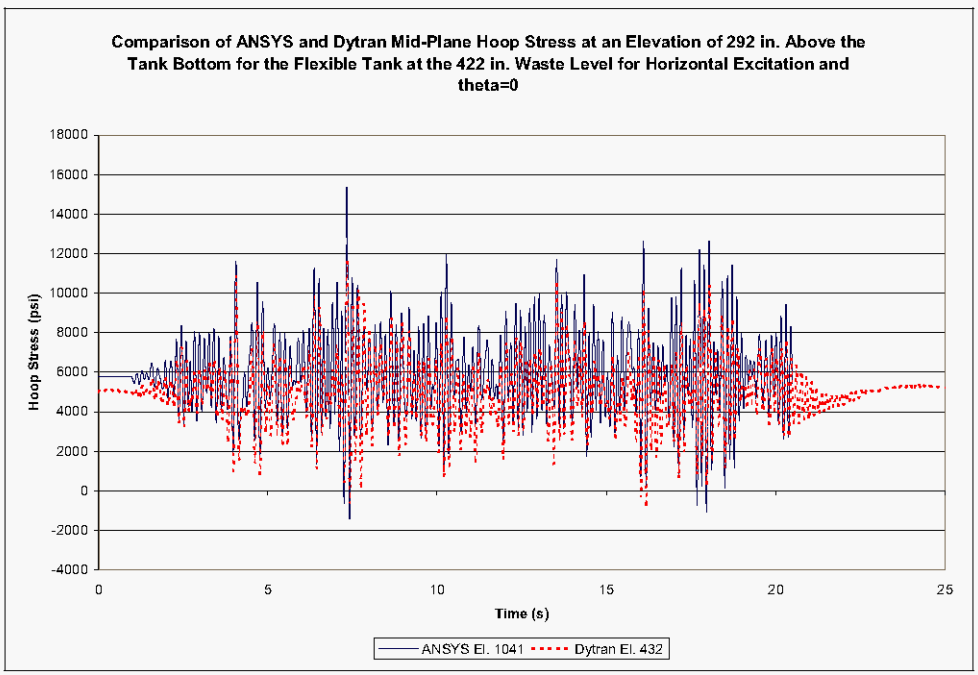

Figure 7-11. Comparison of ANSYS and Dytran Mid-Plane Hoop Stress at Primary Tank Wall Element Near the Tank Bottom for the Flexible Tank at the 422 in. Waste Level for Horizontal Excitation and θ=0.

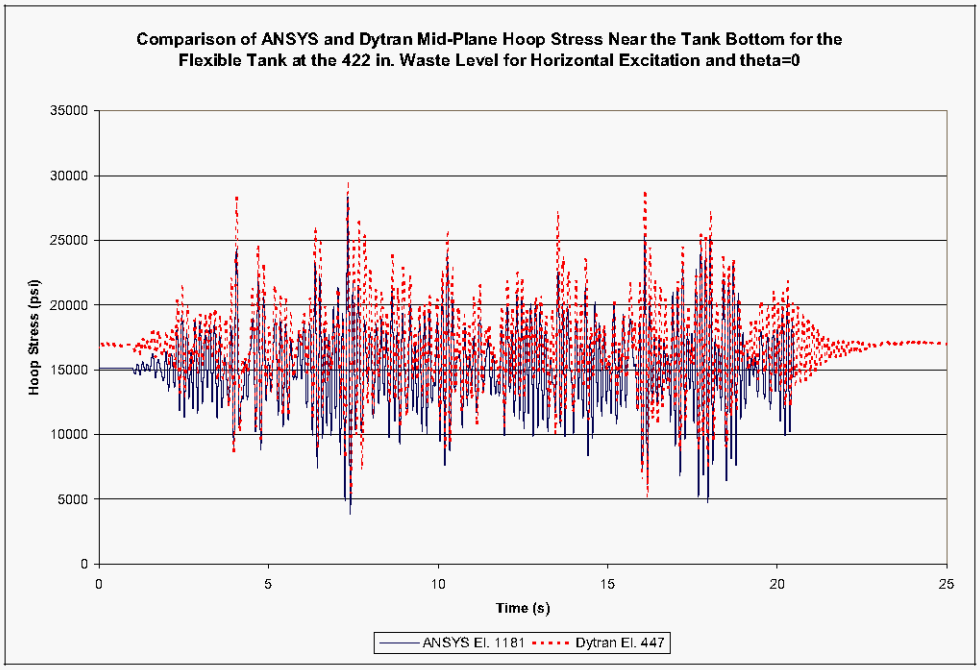

Figure 7-12. Comparison of ANSYS and Dytran Mid-Plane Hoop Stress at Primary Tank Wall Element Near the Waste Free Surface for the Flexible Tank at the 460 in. Waste Level for Horizontal Excitation and θ=0.

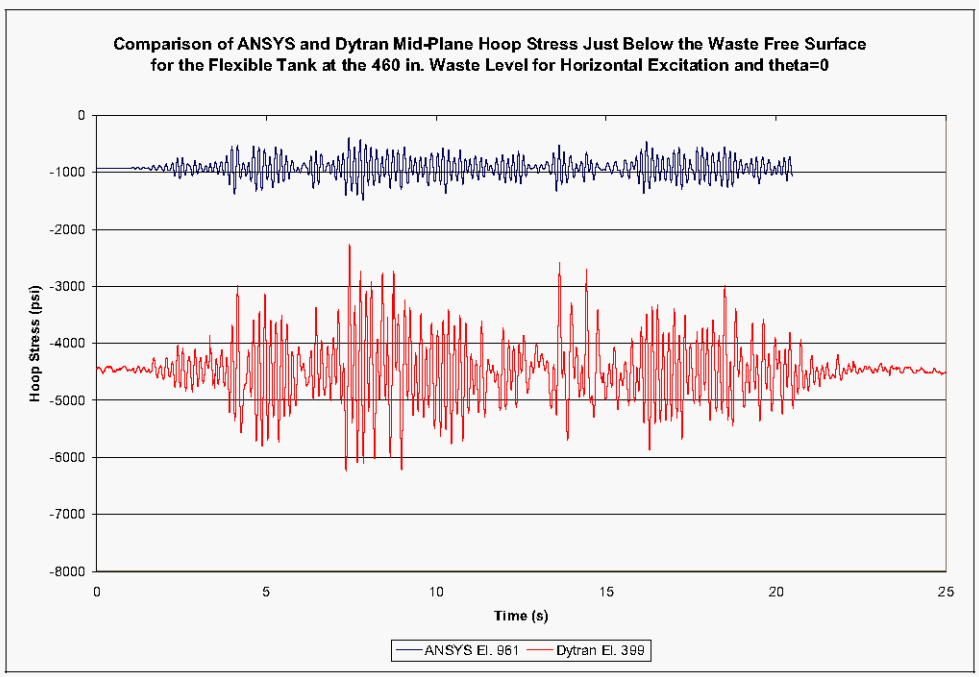

Figure 7-13. Comparison of ANSYS and Dytran Mid-Plane Hoop Stress at an Elevation of 292 in. from the Tank Bottom for the Flexible Tank at the 460 in. Waste Level for Horizontal Excitation and θ=0.

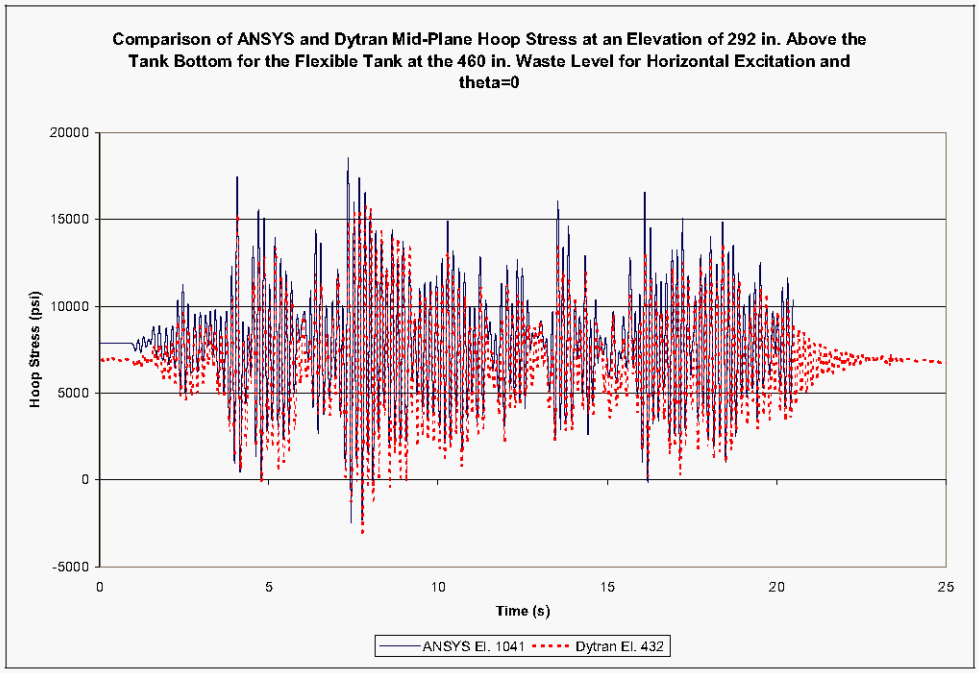

Figure 7-14. Comparison of ANSYS and Dytran Mid-Plane Hoop Stress at Primary Tank Wall Element Near the Tank Bottom for the Flexible Tank at the 460 in. Waste Level for Horizontal Excitation and θ=0.

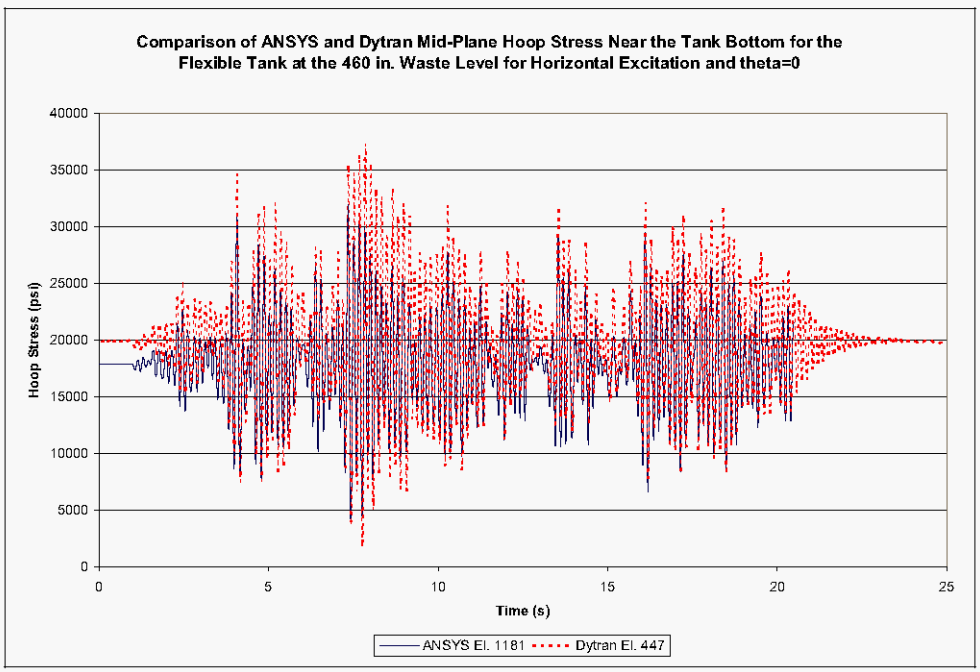

8.0 REFERENCES

Abatt, F.G., B.G. Carpenter, C.A. Hendrix , 2006, *Establishment of Methodology for Time Domain Soil-Structure Interaction Analysis of a Hanford Double Shell Tank*, M&D-2008-004-RPT-01, Rev. 0, Prepared by M&D Professional Services, Inc. for Pacific Northwest National Laboratory, Richland, Washington.

BNL 1995, *Seismic Design and Evaluation Guidelines for the Department of Energy High-Level Waste Storage Tanks and Appurtenances*, Report No. 52361, October 1995, Engineering Research and Applications Division, Department of Advanced Technology, Brookhaven National Laboratory, Associated Universities, Inc., Upton, New York.

Carpenter, B.G., and F.G. Abatt, 2006, *ANSYS Benchmark Analysis of Seismically Induced Fluid-Structure Interaction in a Hanford Double Shell Primary Tank*, M&D-2008-004-RPT-02, Rev. 0, Prepared by M&D Professional Services, Inc. for Pacific Northwest National Laboratory, Richland, Washington.

Carpenter, B.G., C.A. Hendrix, and F.G. Abatt, 2006, *ANSYS Soil-Structure Interaction Analysis of a Hanford Double Shell Tank*, M&D-2008-004-CALC-01, Rev. 0, Prepared by M&D Professional Services, Inc. for Pacific Northwest National Laboratory, Richland, Washington.

Clough, R.W. and J. Penzien, 1975, *Dynamics of Structures*, McGraw-Hill Book Company, New York, New York.

DOE-STD-1020-2002, January 2002, *Natural Phenomenon Hazards Design and Evaluation Criteria for Department of Energy Facilities*, U.S. Department of Energy, Washington, D.C.

Hanford Drawing H-2-64449, Rev. 6, Tank Elevation and Details, Bldg. No. 241-AY.

Kurihara, et al. 1992, *Sloshing Impact Pressure in Roofed Tanks*, PVP-Vo.232, Fluid Structure Vibration and Sloshing, ASME 1992.

M&D, 2005, *DYTRAN 2006 Development Version Verification of M&D Workstation Kingair*, M&D-V&V-DYT-2006DV-001 R0, M&D Professional Services, Inc., Richland, Washington.

MSC 2005a, *MSC.Dytran 2005 Theory Manual, Version 2005*, MSC Software Corporation, Santa Ana, California.

MSC 2005b, *MSC.Dytran Reference Manual, Version 2005*, MSC Software Corporation, Santa Ana, California.

Rinker, M.W., J.E. Deibler, K.I. Johnson, S.P. Pilli, C.E. Guzman-Leong, and O.D. Mullen, 2004, *Hanford Double-Shell Tank Thermal and Seismic Project – Thermal and Operating Loads Analysis*, RPP-RPT-23308, Rev. 0, Pacific Northwest National Laboratory, Richland, Washington.

APPENDIX A

Description of Input and Results Files

Table A-1. Description of Input and Results Files

File Extension	Typical File Name	Description
.db	Rigid_422.db	Patran database file used for model creation. The Dytran input files are created by translating this file to Dytran input file format within Patran.
.dat	alpha_02_abs.dat	Main Dytran input file. Required bulk data files are called from this file
.bdf	Flex_422_horiz.bdf	Dytran bulk data file containing node and element information. This file is called by the main input file and is common to a given tank configuration (rigid or flexible) and waste level. Total of four files.
.bdf	DomeTH.bdf	Dytran bulk data file containing the seismic time history. Two files – one for horizontal excitation and one for vertical excitation (Vert_TH.bdf).
.xls	Results_422_Flex_Horizontal_alpha02_ABS.xls	Excel spreadsheet containing results from a given run. In the example at left, the results are for the flexible tank at the 422 in. waste level with horizontal excitation run at absolute pressure with a damping parameter of 0.02.

APPENDIX B

Theoretical Solutions

41 pages including cover sheet

Prepared by: F. G. Abatt
M&D Professional Services
8/10/05
Rev. 1

Theoretical Fluid Response Calculations for Rigid Primary Tank at 422 in. Waste Level

Checked by: B.G. Carpenter
M&D Professional Services
2/1/06

$H_l := 422 \cdot in$ Baseline waste level

$H_t := 460 \cdot in$ Height to primary tank tangent line

$\frac{H_l}{H_t} = 0.92$ Ratio of waste height to tank height

$g := 386.4 \cdot \frac{in}{sec^2}$

$R := 450 \cdot in$ Tank radius

$\frac{H_l}{R} = 0.94$ Ratio of waste height to tank radius

$i := 0..2$

$\lambda := \begin{pmatrix} 1.841 \\ 5.331 \\ 8.536 \end{pmatrix}$ Bessel function roots

$\theta := \begin{pmatrix} 0 \cdot deg \\ 45 \cdot deg \\ 90 \cdot deg \end{pmatrix}$ Circumferential location of waste elements for which pressures are reported

Convective Frequencies

$fcon_i := \frac{1}{2 \cdot \pi} \cdot \left[\sqrt{\left[\lambda_i \left[\frac{g}{R} \cdot \tanh\left[\lambda_i \cdot \left(\frac{H_l}{R} \right) \right] \right] \right]} \right]$ Eqn. 4.14 BNL 1995

$fcon = \begin{pmatrix} 0.19 \\ 0.34 \\ 0.43 \end{pmatrix} Hz$ First three convective frequencies

$\rho_l := 1.59 \cdot 10^{-4} \cdot \frac{lbf \cdot sec^2}{in^4}$ waste density - specific gravity = 1.7

Prepared by: F. G. Abatt
M&D Professional Services
8/10/05
Rev. 1

Theoretical Fluid Response Calculations for Rigid Primary Tank at 422 in. Waste Level

Checked by: B.G. Carpenter
M&D Professional Services
2/1/06

Determine Convective Pressures on the Tank Wall:

$$z := \begin{pmatrix} 15\cdot in \\ 50.5\cdot in \\ 85.8\cdot in \\ 121.2\cdot in \\ 156.6\cdot in \\ 192.0\cdot in \\ 227.4\cdot in \\ 262.8\cdot in \\ 298.2\cdot in \\ 333.5\cdot in \\ 368.9\cdot in \\ 404.3\cdot in \end{pmatrix}$$

Vertical location of Euler element centroids at which pressures are reported.

$$\eta_l := \frac{z}{H_l}$$

Ratio of tank wall vertical location to waste height for waste element centroids.

$\eta_l =$

	0
0	0.04
1	0.12
2	0.2
3	0.29
4	0.37
5	0.45
6	0.54
7	0.62
8	0.71
9	0.79
10	0.87
11	0.96

Prepared by: F. G. Abatt
M&D Professional Services
8/10/05
Rev. 1

Theoretical Fluid Response Calculations for Rigid Primary Tank at 422 in. Waste Level

Checked by: B.G. Carpenter
M&D Professional Services
2/1/06

Determine convective coefficients as a function of dimensionless height per Eqn. 4.4 BNL 1995

$$con_0(\eta_l) := \left[\frac{2}{(\lambda_{0,})^2 - 1} \cdot \frac{\cosh\left[\lambda_0 \cdot \left(\frac{H_l}{R}\right) \cdot \eta_l\right]}{\cosh\left[\lambda_0 \cdot \left(\frac{H_l}{R}\right)\right]} \right]$$

$$con_1(\eta_l) := \left[\frac{2}{(\lambda_{1,})^2 - 1} \cdot \frac{\cosh\left[\lambda_1 \cdot \left(\frac{H_l}{R}\right) \cdot \eta_l\right]}{\cosh\left[\lambda_1 \cdot \left(\frac{H_l}{R}\right)\right]} \right]$$

$$con_2(\eta_l) := \left[\frac{2}{(\lambda_{2,})^2 - 1} \cdot \frac{\cosh\left[\lambda_2 \cdot \left(\frac{H_l}{R}\right) \cdot \eta_l\right]}{\cosh\left[\lambda_2 \cdot \left(\frac{H_l}{R}\right)\right]} \right]$$

$con_0(\eta_l) =$

	0
0	0.29
1	0.29
2	0.31
3	0.32
4	0.35
5	0.38
6	0.42
7	0.47
8	0.53
9	0.6
10	0.68
11	0.78

$con_1(\eta_l) =$

	0
0	$9.99 \cdot 10^{-4}$
1	$1.16 \cdot 10^{-3}$
2	$1.54 \cdot 10^{-3}$
3	$2.18 \cdot 10^{-3}$
4	$3.22 \cdot 10^{-3}$
5	$4.83 \cdot 10^{-3}$
6	$7.31 \cdot 10^{-3}$
7	0.01
8	0.02
9	0.03
10	0.04
11	0.06

$con_2(\eta_l) =$

	0
0	$1.93 \cdot 10^{-5}$
1	$2.78 \cdot 10^{-5}$
2	$4.91 \cdot 10^{-5}$
3	$9.35 \cdot 10^{-5}$
4	$1.82 \cdot 10^{-4}$
5	$3.55 \cdot 10^{-4}$
6	$6.94 \cdot 10^{-4}$
7	$1.36 \cdot 10^{-3}$
8	$2.66 \cdot 10^{-3}$
9	$5.19 \cdot 10^{-3}$
10	0.01
11	0.02

Prepared by: F. G. Abatt
M&D Professional Services
8/10/05
Rev. 1

Theoretical Fluid Response Calculations for Rigid Primary Tank at 422 in. Waste Level

Checked by: B.G. Carpenter
M&D Professional Services
2/1/06

Impulsive pressure coefficient as a function of dimensionless wall height

$c_i(\eta_1) := 1 - con_0(\eta_1) - con_1(\eta_1) - con_2(\eta_1)$ Eqn. 4.7 BNL 1995

$c_i(\eta_1) =$

	0
0	0.71
1	0.7
2	0.69
3	0.67
4	0.65
5	0.61
6	0.57
7	0.52
8	0.45
9	0.37
10	0.27
11	0.14

Calculate maximum values of dynamic wall pressures from spectral acceleration of dome input TH.

Consider the first three convective mode spectral accelerations for the 0.5% damped spectrum

$SA_{c0} := 0.062 \cdot g$ $SA_{c0} = 23.96 \frac{in}{sec^2}$ Figure 2-21 of main report

$SA_{c1} := 0.108 \cdot g$ $SA_{c1} = 41.73 \frac{in}{sec^2}$

$SA_{c2} := 0.163 \cdot g$ $SA_{c2} = 62.98 \frac{in}{sec^2}$

Associate the impulsive mode with the ZPA, since the tank is rigid.

$PGA := 0.276 \cdot g$ $PGA = 106.65 \frac{in}{sec^2}$ ANSYS dome RS from Spectr - Figure 2-19 of main report.

Prepared by: F. G. Abatt
M&D Professional Services
8/10/05
Rev. 1

Theoretical Fluid Response Calculations for Rigid Primary Tank at 422 in. Waste Level

Checked by: B.G. Carpenter
M&D Professional Services
2/1/06

$$p_{maxconv}(\eta_1,\theta) := \left[\sqrt{\left(con_0(\eta_1)\cdot SA_{c0}\right)^2 + \left(con_1(\eta_1)\cdot SA_{c1}\right)^2 + \left(con_2(\eta_1)\cdot SA_{c2}\right)^2}\right]\cdot\left(\rho_l\cdot R\cdot\cos(\theta\cdot deg)\right)$$

$$p_{maximpulsive}(\eta_1,\theta) := \left[\sqrt{\left[c_i(\eta_1)\cdot(PGA)\right]^2}\right]\cdot\left(\rho_l\cdot R\cdot\cos(\theta\cdot deg)\right)$$

$$p_{max}(\eta_1,\theta) := \left[\sqrt{\left[\left(c_i(\eta_1)\right)\cdot(PGA)\right]^2 + \left(con_0(\eta_1)\cdot SA_{c0}\right)^2 + \left(con_1(\eta_1)\cdot SA_{c1}\right)^2 + \left(con_2(\eta_1)\cdot SA_{c2}\right)^2}\right]\cdot\left(\rho_l\cdot R\cdot\cos(\theta\cdot deg)\right)$$

Eqn. 4.24 BNL 1995

$p_{maximpulsive}(\eta_1,0) =$ $\frac{lbf}{in^2}$

	0
0	5.42
1	5.37
2	5.28
3	5.13
4	4.93
5	4.67
6	4.34
7	3.93
8	3.43
9	2.8
10	2.03
11	1.06

Maximum impulsive dynamic pressures at theta = 0.

$p_{maxconv}(\eta_1,0) =$ $\frac{lbf}{in^2}$

	0
0	0.5
1	0.51
2	0.53
3	0.56
4	0.6
5	0.66
6	0.73
7	0.81
8	0.91
9	1.03
10	1.18
11	1.36

Maximum convective dynamic pressures at theta = 0.

Prepared by: F. G. Abatt
M&D Professional Services
8/10/05
Rev. 1

Theoretical Fluid Response Calculations for Rigid Primary Tank at 422 in. Waste Level

Checked by: B.G. Carpenter
M&D Professional Services
2/1/06

$p_{max}(\eta_1, 0) =$

	0
0	5.44
1	5.39
2	5.3
3	5.16
4	4.97
5	4.72
6	4.4
7	4.01
8	3.55
9	2.99
10	2.35
11	1.72

$\frac{lbf}{in^2}$

Maximum total dynamic pressure at theta = 0.

$p_{max}(\eta_1, 45) =$

	0
0	3.85
1	3.81
2	3.75
3	3.65
4	3.51
5	3.34
6	3.11
7	2.84
8	2.51
9	2.11
10	1.66
11	1.22

$\frac{lbf}{in^2}$

Maximum total dynamic pressure at theta = 45 degrees.

$p_{max}(\eta_1, 90) =$

	0
0	0
1	0
2	0
3	0
4	0
5	0
6	0
7	0
8	0
9	0
10	0
11	0

$\frac{lbf}{in^2}$

Maximum total dynamic pressure at theta = 90 degrees.

Prepared by: F. G. Abatt
M&D Professional Services
8/10/05
Rev. 1

Theoretical Fluid Response Calculations for Rigid Primary Tank at 422 in. Waste Level

Checked by: B.G. Carpenter
M&D Professional Services
2/1/06

Calculate Maximum Slosh Height:

$$conmax := \begin{pmatrix} 0.837 \\ 0.073 \\ 0.028 \end{pmatrix}$$ Maximum value of convective coefficients at η_l=1

$$h_{maxslosh} := R \cdot \sqrt{\left(conmax_0 \cdot \frac{SA_{c0}}{g}\right)^2 + \left(conmax_1 \cdot \frac{SA_{c1}}{g}\right)^2 + \left(conmax_2 \cdot \frac{SA_{c2}}{g}\right)^2}$$ Eqn. 4.60 BNL 1995

$h_{maxslosh} = 23.71\,in$ Maximum theoretical slosh height

Calculate Maximum Total Hydrodynamic Force:

The maximum hydrodynamic force induced on the tank wall is given by Eqn. 4.31 of BNL 1995 with the instantaneous accelerations replaced by the maximum spectral accelerations. First determine the effective impulsive and convective masses.

$m_{lapprox} := \pi \cdot R^2 \cdot H_l \cdot \rho_l$ $m_{lapprox} = 4.27 \times 10^4 \frac{lbf \cdot sec^2}{in}$ Total waste mass based on circular cylinder approximation.

$m_l := 4.23 \cdot 10^4 \cdot \frac{lbf \cdot sec^2}{in}$ Actual waste mass reported by Dytran model.

$$m_{c0} := \left[\frac{2}{\lambda_0 \cdot \left[\left(\lambda_0\right)^2 - 1\right] \cdot \left(\frac{H_l}{R}\right)}\right] \cdot \tanh\left[\lambda_0 \cdot \left(\frac{H_l}{R}\right)\right] \cdot m_l$$

$m_{c0} = 1.93 \times 10^4 \frac{lbf \cdot sec^2}{in}$ First mode convective mass

$$m_{c1} := \left[\frac{2}{\lambda_1 \cdot \left[\left(\lambda_1\right)^2 - 1\right] \cdot \left(\frac{H_l}{R}\right)}\right] \cdot \tanh\left[\lambda_1 \cdot \left(\frac{H_l}{R}\right)\right] \cdot m_l$$ Second mode convective mass

Prepared by: F. G. Abatt
M&D Professional Services
8/10/05
Rev. 1

Theoretical Fluid Response Calculations for Rigid Primary Tank at 422 in. Waste Level

Checked by: B.G. Carpenter
M&D Professional Services
2/1/06

$$m_{c1} = 617.11 \frac{lbf \cdot sec^2}{in}$$

$$m_{c2} := \left[\frac{2}{\lambda_2 \cdot \left[\left(\lambda_2 \right)^2 - 1 \right] \cdot \left(\frac{H_l}{R} \right)} \right] \cdot \tanh\left[\lambda_2 \cdot \left(\frac{H_l}{R} \right) \right] \cdot m_l$$ Third mode convective mass

$$m_{c2} = 147.06 \frac{lbf \cdot sec^2}{in}$$

$$m_i := m_l - \left(m_{c0} + m_{c1} + m_{c2} \right)$$ Impulsive mass

$$m_i = 2.23 \times 10^4 \frac{lbf \cdot sec^2}{in}$$

$$F_{max} := m_i \cdot PGA + m_{c0} \cdot SA_{c0} + m_{c1} \cdot SA_{c1} + m_{c2} \cdot SA_{c2}$$ Eqn. 4.31 BNL 1995

$$F_{max} = 2.87 \times 10^6 lbf$$ Conservative estimate of maximum hydrodynamic force

The above expression is a conservative estimate because it assumes that the peak impulsive and convective forces occur simultaneously. A less conservative estimate can be made via a square-root-sum-of-the-squares (SRSS) combination.

$$F_{srss} := \sqrt{\left(m_i \cdot PGA \right)^2 + \left(m_{c0} \cdot SA_{c0} \right)^2 + \left(m_{c1} \cdot SA_{c1} \right)^2 + \left(m_{c2} \cdot SA_{c2} \right)^2}$$ Eqn. 4.31 BNL 1995

$$F_{srss} = 2.42 \times 10^6 lbf$$ SRSS estimate of peak hydrodynamic force

$$F_{conmax} := \sqrt{\left(m_{c0} \cdot SA_{c0} \right)^2 + \left(m_{c1} \cdot SA_{c1} \right)^2 + \left(m_{c2} \cdot SA_{c2} \right)^2}$$

$$F_{conmax} = 4.62 \times 10^5 lbf$$ Peak hydrodynamic force due to convective response - shows up in free oscillations.

Prepared by: F. G. Abatt
M&D Professional Services
8/10/05
Rev. 1

Theoretical Fluid Response
Calculations for Rigid Primary Tank
at 422 in. Waste Level

Checked by: B.G. Carpenter
M&D Professional Services
2/1/06

Consider Vertical Excitation:

For a rigid tank, the period of the breathing mode is zero and the associated spectral acceleration is the vertical ZPA.

$ZPA_{vert} := 0.12 \cdot g$ ANSYS Haunch RS from Spectr - see also Figure 2-16 of main report.

The maximum wall pressure as a function of the dimensionless vertical distance is given by

$$p_{maxv}(\eta_l) := (0.8) \cdot \left(\cos\left(\frac{\pi}{2} \cdot \eta_l\right)\right) \cdot (\rho_l \cdot H_l \cdot ZPA_{vert})$$ Eqn. 4.52 BNL 1995

$p_{maxv}(\eta_l) =$

	0
0	2.49
1	2.45
2	2.36
3	2.24
4	2.08
5	1.88
6	1.65
7	1.39
8	1.11
9	0.81
10	0.49
11	0.16

$\frac{lbf}{in^2}$

The maximum base pressure and force are given by

$p_{maxbasevert} := \rho_l \cdot H_l \cdot ZPA_{vert}$ $p_{maxbasevert} = 3.11 \frac{lbf}{in^2}$ Eqn. 4.55 BNL 1995

$F_{maxbasevert} := m_l \cdot ZPA_{vert}$ $F_{maxbasevert} = 1.96 \times 10^6 lbf$ Eqn. 4.57 BNL 1995

Prepared by: F. G. Abatt
M&D Professional Services
8/17/05
Rev. 1

Theoretical Fluid Response Calculations for Rigid Primary Tank at 460 in. Waste Level - Dytran Configuration

Checked by: B.G. Carpenter
M&D Professional Services
2/1/06

$H_l := 460.0 \cdot in$ Baseline waste level

$H_t := 460.0 \cdot in$ Height to primary tank tangent line

$\frac{H_l}{H_t} = 1$ Ratio of waste height to tank height

$g := 386.4 \cdot \frac{in}{sec^2}$

$R := 450 \cdot in$ Tank radius

$\frac{H_l}{R} = 1.02$ Ratio of waste height to tank radius

$i := 0..2$

$\lambda := \begin{pmatrix} 1.841 \\ 5.331 \\ 8.536 \end{pmatrix}$ Bessel function roots

$\theta := \begin{pmatrix} 0 \cdot deg \\ 45 \cdot deg \\ 90 \cdot deg \end{pmatrix}$ Circumferential location of waste elements for which pressures are reported

Convective Frequencies

$fcon_i := \frac{1}{2 \cdot \pi} \cdot \left[\sqrt{\left[\lambda_i \left[\frac{g}{R} \cdot \tanh\left[\lambda_i \cdot \left(\frac{H_l}{R} \right) \right] \right] \right]} \right]$ Eqn. 4.14 BNL 1995

$fcon = \begin{pmatrix} 0.2 \\ 0.34 \\ 0.43 \end{pmatrix} Hz$ First three convective frequencies

$\rho_l := 1.71 \cdot 10^{-4} \cdot \frac{lbf \cdot sec^2}{in^4}$ waste density - specific gravity = 1.83

Prepared by: F. G. Abatt
M&D Professional Services
8/17/05
Rev. 1

Checked by: B.G. Carpenter
M&D Professional Services
2/1/06

Determine Convective Pressures on the Tank Wall:

$$z := \begin{pmatrix} 15\cdot in \\ 50.5\cdot in \\ 85.8\cdot in \\ 121.2\cdot in \\ 156.6\cdot in \\ 192.0\cdot in \\ 227.4\cdot in \\ 262.8\cdot in \\ 298.2\cdot in \\ 333.5\cdot in \\ 368.9\cdot in \\ 404.3\cdot in \\ 441\cdot in \end{pmatrix}$$

Vertical location of Euler element centroids at which pressures are reported.

$$\eta_l := \frac{z}{H_l}$$

Ratio of tank wall vertical location to waste height for waste element centroids.

$\eta_l =$

	0
0	0.03
1	0.11
2	0.19
3	0.26
4	0.34
5	0.42
6	0.49
7	0.57
8	0.65
9	0.73
10	0.8
11	0.88
12	0.96

Prepared by: F. G. Abatt
M&D Professional Services
8/17/05
Rev. 1

Theoretical Fluid Response Calculations for Rigid Primary Tank at 460 in. Waste Level - Dytran Configuration

Checked by: B.G. Carpenter
M&D Professional Services
2/1/06

Determine convective coefficients as a function of dimensionless height per BNL 1995 Eqn. 4.4

$$con_0(\eta_l) := \left[\frac{2}{\left(\lambda_{0,}\right)^2 - 1} \cdot \frac{\cosh\left[\lambda_0 \cdot \left(\frac{H_l}{R}\right) \cdot \eta_l\right]}{\cosh\left[\lambda_0 \cdot \left(\frac{H_l}{R}\right)\right]} \right]$$

$$con_1(\eta_l) := \left[\frac{2}{\left(\lambda_{1,}\right)^2 - 1} \cdot \frac{\cosh\left[\lambda_1 \cdot \left(\frac{H_l}{R}\right) \cdot \eta_l\right]}{\cosh\left[\lambda_1 \cdot \left(\frac{H_l}{R}\right)\right]} \right]$$

$$con_2(\eta_l) := \left[\frac{2}{\left(\lambda_{2,}\right)^2 - 1} \cdot \frac{\cosh\left[\lambda_2 \cdot \left(\frac{H_l}{R}\right) \cdot \eta_l\right]}{\cosh\left[\lambda_2 \cdot \left(\frac{H_l}{R}\right)\right]} \right]$$

$con_0(\eta_l) =$

	0
0	0.25
1	0.25
2	0.26
3	0.28
4	0.3
5	0.33
6	0.37
7	0.41
8	0.46
9	0.52
10	0.59
11	0.68
12	0.78

$con_1(\eta_l) =$

	0
0	$6.37 \cdot 10^{-4}$
1	$7.43 \cdot 10^{-4}$
2	$9.8 \cdot 10^{-4}$
3	$1.39 \cdot 10^{-3}$
4	$2.05 \cdot 10^{-3}$
5	$3.08 \cdot 10^{-3}$
6	$4.66 \cdot 10^{-3}$
7	$7.07 \cdot 10^{-3}$
8	0.01
9	0.02
10	0.02
11	0.04
12	0.06

$con_2(\eta_l) =$

	0
0	$9.41 \cdot 10^{-6}$
1	$1.35 \cdot 10^{-5}$
2	$2.39 \cdot 10^{-5}$
3	$4.55 \cdot 10^{-5}$
4	$8.84 \cdot 10^{-5}$
5	$1.73 \cdot 10^{-4}$
6	$3.38 \cdot 10^{-4}$
7	$6.61 \cdot 10^{-4}$
8	$1.29 \cdot 10^{-3}$
9	$2.53 \cdot 10^{-3}$
10	$4.94 \cdot 10^{-3}$
11	$9.68 \cdot 10^{-3}$
12	0.02

Prepared by: F. G. Abatt
M&D Professional Services
8/17/05
Rev. 1

Theoretical Fluid Response Calculations for Rigid Primary Tank at 460 in. Waste Level - Dytran Configuration

Checked by: B.G. Carpenter
M&D Professional Services
2/1/06

Impulsive pressure coefficient as a function of dimensionless wall height

$c_i(\eta_1) := 1 - con_0(\eta_1) - con_1(\eta_1) - con_2(\eta_1)$ Eqn. 4.7 BNL 1995

$c_i(\eta_1) =$

	0
0	0.75
1	0.74
2	0.73
3	0.72
4	0.7
5	0.67
6	0.63
7	0.58
8	0.53
9	0.46
10	0.38
11	0.28
12	0.14

Calculate maximum values of dynamic wall pressures from spectral acceleration of dome input TH.

Consider the first three convective mode spectral accelerations for the 0.5% damped spectrum

$SA_{c0} := 0.064 \cdot g$ $SA_{c0} = 24.73 \frac{in}{sec^2}$ Figure 2-21 of main report

$SA_{c1} := 0.108 \cdot g$ $SA_{c1} = 41.73 \frac{in}{sec^2}$

$SA_{c2} := 0.163 \cdot g$ $SA_{c2} = 62.98 \frac{in}{sec^2}$

Associate the impulsive mode with the ZPA, since the tank is rigid.

$PGA := 0.276 \cdot g$ $PGA = 106.65 \frac{in}{sec^2}$ ANSYS dome RS from Spectr - Figures 2-15 and 2-19 of main report.

Prepared by: F. G. Abatt
M&D Professional Services
8/17/05
Rev. 1

Theoretical Fluid Response Calculations for Rigid Primary Tank at 460 in. Waste Level - Dytran Configuration

Checked by: B.G. Carpenter
M&D Professional Services
2/1/06

$$p_{maxconv}(\eta_1,\theta) := \left[\sqrt{\left(con_0(\eta_1)\cdot SA_{c0}\right)^2 + \left(con_1(\eta_1)\cdot SA_{c1}\right)^2 + \left(con_2(\eta_1)\cdot SA_{c2}\right)^2}\right]\cdot\left(\rho_1\cdot R\cdot\cos(\theta\cdot deg)\right)$$

$$p_{maximpulsive}(\eta_1,\theta) := \left[\sqrt{\left[c_i(\eta_1)\cdot(PGA)\right]^2}\right]\cdot\left(\rho_1\cdot R\cdot\cos(\theta\cdot deg)\right)$$

$$p_{max}(\eta_1,\theta) := \left[\sqrt{\left[\left(c_i(\eta_1)\right)\cdot(PGA)\right]^2 + \left(con_0(\eta_1)\cdot SA_{c0}\right)^2 + \left(con_1(\eta_1)\cdot SA_{c1}\right)^2 + \left(con_2(\eta_1)\cdot SA_{c2}\right)^2}\right]\cdot\left(\rho_1\cdot R\cdot\cos(\theta\cdot deg)\right)$$

Eqn. 4.24 BNL 1995

$p_{maximpulsive}(\eta_1,0) =$ $\frac{lbf}{in^2}$

	0
0	6.15
1	6.11
2	6.03
3	5.89
4	5.71
5	5.47
6	5.17
7	4.8
8	4.34
9	3.79
10	3.11
11	2.28
12	1.19

Maximum impulsive dynamic pressures at theta = 0.

$p_{maxconv}(\eta_1,0) =$ $\frac{lbf}{in^2}$

	0
0	0.48
1	0.48
2	0.5
3	0.53
4	0.57
5	0.63
6	0.69
7	0.78
8	0.87
9	0.99
10	1.13
11	1.29
12	1.49

Maximum convective dynamic pressures at theta = 0.

Prepared by: F. G. Abatt
M&D Professional Services
8/17/05
Rev. 1

Theoretical Fluid Response Calculations for Rigid Primary Tank at 460 in. Waste Level - Dytran Configuration

Checked by: B.G. Carpenter
M&D Professional Services
2/1/06

$p_{max}(\eta_1, 0) =$

	0
0	6.17
1	6.13
2	6.05
3	5.92
4	5.74
5	5.51
6	5.22
7	4.86
8	4.43
9	3.92
10	3.31
11	2.62
12	1.91

$\frac{lbf}{in^2}$

Maximum total dynamic pressure at theta = 0.

$p_{max}(\eta_1, 45) =$

	0
0	4.36
1	4.34
2	4.28
3	4.18
4	4.06
5	3.89
6	3.69
7	3.44
8	3.13
9	2.77
10	2.34
11	1.85
12	1.35

$\frac{lbf}{in^2}$

Maximum total dynamic pressure at theta = 45 degrees.

$p_{max}(\eta_1, 90) =$

	0
0	0
1	0
2	0
3	0
4	0
5	0
6	0
7	0
8	0
9	0
10	0
11	0
12	0

$\frac{lbf}{in^2}$

Maximum total dynamic pressure at theta = 90 degrees.

Prepared by: F. G. Abatt
M&D Professional Services
8/17/05
Rev. 1

Theoretical Fluid Response Calculations for Rigid Primary Tank at 460 in. Waste Level - Dytran Configuration

Checked by: B.G. Carpenter
M&D Professional Services
2/1/06

Calculate Maximum Slosh Height:

$$conmax := \begin{pmatrix} 0.837 \\ 0.073 \\ 0.028 \end{pmatrix}$$ Maximum value of convective coefficients at η_l=1

$$h_{maxslosh} := R \cdot \sqrt{\left(conmax_0 \cdot \frac{SA_{c0}}{g}\right)^2 + \left(conmax_1 \cdot \frac{SA_{c1}}{g}\right)^2 + \left(conmax_2 \cdot \frac{SA_{c2}}{g}\right)^2}$$ Eqn. 4.60 BNL 1995

$h_{maxslosh} = 24.45\,in$ Maximum theoretical slosh height

Calculate Maximum Total Hydrodynamic Force:

The maximum hydrodynamic force induced on the tank wall is given by Eqn. 4.31 of BNL 1995 with the instantaneous accelerations replaced by the maximum spectral accelerations. First determine the effective impulsive and convective masses.

$m_{lapprox} := \pi \cdot R^2 \cdot H_l \cdot \rho_l$ $m_{lapprox} = 5 \times 10^4 \frac{lbf \cdot sec^2}{in}$ Total waste mass based on circular cylinder approximation.

$m_l := 4.95 \cdot 10^4 \cdot \frac{lbf \cdot sec^2}{in}$ Actual waste mass reported by Dytran model.

$$m_{c0} := \left[\frac{2}{\lambda_0 \cdot \left[\left(\lambda_0\right)^2 - 1\right] \cdot \left(\frac{H_l}{R}\right)}\right] \cdot \tanh\left[\lambda_0 \cdot \left(\frac{H_l}{R}\right)\right] \cdot m_l$$ Eqn. 4.32 BNL 1995

$m_{c0} = 2.1 \times 10^4 \frac{lbf \cdot sec^2}{in}$ First mode convective mass

$$m_{c1} := \left[\frac{2}{\lambda_1 \cdot \left[\left(\lambda_1\right)^2 - 1\right] \cdot \left(\frac{H_l}{R}\right)}\right] \cdot \tanh\left[\lambda_1 \cdot \left(\frac{H_l}{R}\right)\right] \cdot m_l$$ Second mode convective mass

Prepared by: F. G. Abatt
M&D Professional Services
8/17/05
Rev. 1

Theoretical Fluid Response Calculations for Rigid Primary Tank at 460 in. Waste Level - Dytran Configuration

Checked by: B.G. Carpenter
M&D Professional Services
2/1/06

$$m_{c1} = 662.53 \frac{lbf \cdot sec^2}{in}$$

$$m_{c2} := \left[\frac{2}{\lambda_2 \cdot \left[\left(\lambda_2 \right)^2 - 1 \right] \cdot \left(\frac{H_l}{R} \right)} \right] \cdot \tanh\left[\lambda_2 \cdot \left(\frac{H_l}{R} \right) \right] \cdot m_l$$ Third mode convective mass

$$m_{c2} = 157.88 \frac{lbf \cdot sec^2}{in}$$

$m_i := m_l - (m_{c0} + m_{c1} + m_{c2})$ Impulsive mass Eqn. 4.33 BNL 1995

$$m_i = 2.77 \times 10^4 \frac{lbf \cdot sec^2}{in}$$

$F_{max} := m_i \cdot PGA + m_{c0} \cdot SA_{c0} + m_{c1} \cdot SA_{c1} + m_{c2} \cdot SA_{c2}$ Eqn. 4.31 BNL 1995

$F_{max} = 3.51 \times 10^6 lbf$ Conservative estimate of maximum hydrodynamic force

The above expression is a conservative estimate because it assumes that the peak impulsive and convective forces occur simultaneously. A less conservative estimate can be made via a square-root-sum-of-the-squares (SRSS) combination.

$$F_{srss} := \sqrt{(m_i \cdot PGA)^2 + (m_{c0} \cdot SA_{c0})^2 + (m_{c1} \cdot SA_{c1})^2 + (m_{c2} \cdot SA_{c2})^2}$$ Eqn. 4.31 BNL 1995 - SRSS

$F_{srss} = 3 \times 10^6 lbf$ SRSS estimate of peak hydrodynamic force

$$F_{conmax} := \sqrt{(m_{c0} \cdot SA_{c0})^2 + (m_{c1} \cdot SA_{c1})^2 + (m_{c2} \cdot SA_{c2})^2}$$

$F_{conmax} = 5.21 \times 10^5 lbf$ Peak hydrodynamic force due to convective response - shows up in free oscillations.

Prepared by: F. G. Abatt
M&D Professional Services
8/17/05
Rev. 1

Theoretical Fluid Response Calculations for Rigid Primary Tank at 460 in. Waste Level - Dytran Configuration

Checked by: B.G. Carpenter
M&D Professional Services
2/1/06

Consider Vertical Excitation:

For a rigid tank, the period of the breathing mode is zero and the associated spectral acceleration is the vertical ZPA.

$ZPA_{vert} := 0.12 \cdot g$ ANSYS Haunch RS from Spectr - see also Figure 2-16 of main report.

The maximum wall pressure as a function of the dimensionless vertical distance is given by

$$p_{maxv}(\eta_l) := (0.8) \cdot \left(\cos\left(\frac{\pi}{2} \cdot \eta_l \right) \right) \cdot (\rho_l \cdot H_l \cdot ZPA_{vert})$$ Eqn. 4.52 BNL 1995

$p_{maxv}(\eta_l) =$

	0
0	2.91
1	2.87
2	2.79
3	2.67
4	2.51
5	2.31
6	2.08
7	1.82
8	1.53
9	1.22
10	0.89
11	0.55
12	0.19

$\frac{lbf}{in^2}$

The maximum base pressure and force are given by

$p_{maxbasevert} := \rho_l \cdot H_l \cdot ZPA_{vert}$ $p_{maxbasevert} = 3.65 \frac{lbf}{in^2}$ Eqn. 4.55 BNL 1995

$F_{maxbasevert} := m_l \cdot ZPA_{vert}$ $F_{maxbasevert} = 2.3 \times 10^6 lbf$ Eqn. 4.57 BNL 1995

Reference:

BNL 1995, *Seismic Design and Evaluation Guidelines for the Department of Energy High-Level Waste Storage Tanks and Appurtenances*, BNL 52361, Rev. 10/95, Brookhaven National Laboratory, Upton, New York.

Prepared by: F. G. Abatt
M&D Professional Services
8/31/05
Rev. 2

Theoretical Fluid Response for Simplified AY Flexible Wall Tank at 422 in. Waste Level

Checked by: B.G. Carpenter
M&D Professional Services
2/1/06

$H_l := 422 \cdot in$ Baseline waste level

$H_t := 460 \cdot in$ Height to primary tank tangent line

$\frac{H_l}{H_t} = 0.92$ Ratio of waste height to tank height

$g := 386.4 \cdot \frac{in}{sec^2}$

$R := 450 \cdot in$ Tank radius

$\frac{H_l}{R} = 0.94$ Ratio of waste height to tank radius

$i := 0..2$

$\lambda := \begin{pmatrix} 1.841 \\ 5.331 \\ 8.536 \end{pmatrix}$ Bessel function roots

$\theta := \begin{pmatrix} 0 \cdot deg \\ 45 \cdot deg \\ 90 \cdot deg \end{pmatrix}$ Circumferential location of waste elements for which pressures are reported

Convective Frequencies

$fcon_i := \frac{1}{2 \cdot \pi} \cdot \left[\sqrt{\left[\lambda_i \left[\frac{g}{R} \cdot \tanh\left[\lambda_i \cdot \left(\frac{H_l}{R} \right) \right] \right] \right]} \right]$ Eqn. 4.14 BNL 1995

$fcon = \begin{pmatrix} 0.19 \\ 0.34 \\ 0.43 \end{pmatrix} Hz$ First three convective frequencies

$\rho_l := 1.59 \cdot 10^{-4} \cdot \frac{lbf \cdot sec^2}{in^4}$ waste density - specific gravity = 1.7

Prepared by: F. G. Abatt
M&D Professional Services
8/31/05
Rev. 2

Theoretical Fluid Response for Simplified AY Flexible Wall Tank at 422 in. Waste Level

Checked by: B.G. Carpenter
M&D Professional Services
2/1/06

Calculation of Impulsive Frequency:

$\rho_t := 7.35 \cdot 10^{-4} \cdot \frac{lbf \cdot sec^2}{in^4}$ Steel density

$t_{tw} := 0.65 \cdot in$ Average thickness of AY over lower 2/3.

$E_t := 29 \cdot 10^6 \cdot \frac{lbf}{in^2}$ Elastic modulus for steel

$C_{iref} := 0.102$ Table 4.4 of BNL 1995

$C_i := C_{iref} \cdot \sqrt{127 \cdot \frac{\left(\frac{t_{tw}}{R}\right)}{\left(\frac{\rho_l}{\rho_t}\right)}}$ Eqn. 4.18 BNL 1995

$C_i = 0.09$ Impulsive coefficient for frequency calculation

$f_i := \frac{1}{2 \cdot \pi} \cdot \frac{C_i}{H_l} \cdot \sqrt{\frac{E_t}{\rho_t}}$ $f_i = 7.04\,Hz$ Eqn. 4.16 BNL 1995

Determine Convective Pressures on the Tank Wall:

$$z := \begin{pmatrix} 15 \cdot in \\ 50.5 \cdot in \\ 85.8 \cdot in \\ 121.2 \cdot in \\ 156.6 \cdot in \\ 192.0 \cdot in \\ 227.4 \cdot in \\ 262.8 \cdot in \\ 298.2 \cdot in \\ 333.5 \cdot in \\ 368.9 \cdot in \\ 404.3 \cdot in \end{pmatrix}$$

Vertical location of Euler element centroids at which pressures are reported.

Prepared by: F. G. Abatt
M&D Professional Services
8/31/05
Rev. 2

Theoretical Fluid Response for Simplified AY Flexible Wall Tank at 422 in. Waste Level

Checked by: B.G. Carpenter
M&D Professional Services
2/1/06

$\eta_l := \frac{z}{H_l}$ Ratio of tank wall vertical location to waste height for waste element centroids.

$\eta_l =$

	0
0	0.04
1	0.12
2	0.2
3	0.29
4	0.37
5	0.45
6	0.54
7	0.62
8	0.71
9	0.79
10	0.87
11	0.96

Determine convective coefficients as a function of dimensionless height per BNL 1995 Eqn. 4.4

$$con_0(\eta_l) := \left[\frac{2}{\left(\lambda_{0,}\right)^2 - 1} \cdot \frac{\cosh\left[\lambda_0 \cdot \left(\frac{H_l}{R}\right) \cdot \eta_l\right]}{\cosh\left[\lambda_0 \cdot \left(\frac{H_l}{R}\right)\right]} \right]$$

$$con_1(\eta_l) := \left[\frac{2}{\left(\lambda_{1,}\right)^2 - 1} \cdot \frac{\cosh\left[\lambda_1 \cdot \left(\frac{H_l}{R}\right) \cdot \eta_l\right]}{\cosh\left[\lambda_1 \cdot \left(\frac{H_l}{R}\right)\right]} \right]$$

$$con_2(\eta_l) := \left[\frac{2}{\left(\lambda_{2,}\right)^2 - 1} \cdot \frac{\cosh\left[\lambda_2 \cdot \left(\frac{H_l}{R}\right) \cdot \eta_l\right]}{\cosh\left[\lambda_2 \cdot \left(\frac{H_l}{R}\right)\right]} \right]$$

Prepared by: F. G. Abatt
M&D Professional Services
8/31/05
Rev. 2

Theoretical Fluid Response for Simplified AY Flexible Wall Tank at 422 in. Waste Level

Checked by: B.G. Carpenter
M&D Professional Services
2/1/06

$con_0(\eta_1) =$

	0
0	0.29
1	0.29
2	0.31
3	0.32
4	0.35
5	0.38
6	0.42
7	0.47
8	0.53
9	0.6
10	0.68
11	0.78

$con_1(\eta_1) =$

	0
0	$9.99 \cdot 10^{-4}$
1	$1.16 \cdot 10^{-3}$
2	$1.54 \cdot 10^{-3}$
3	$2.18 \cdot 10^{-3}$
4	$3.22 \cdot 10^{-3}$
5	$4.83 \cdot 10^{-3}$
6	$7.31 \cdot 10^{-3}$
7	0.01
8	0.02
9	0.03
10	0.04
11	0.06

$con_2(\eta_1) =$

	0
0	$1.93 \cdot 10^{-5}$
1	$2.78 \cdot 10^{-5}$
2	$4.91 \cdot 10^{-5}$
3	$9.35 \cdot 10^{-5}$
4	$1.82 \cdot 10^{-4}$
5	$3.55 \cdot 10^{-4}$
6	$6.94 \cdot 10^{-4}$
7	$1.36 \cdot 10^{-3}$
8	$2.66 \cdot 10^{-3}$
9	$5.19 \cdot 10^{-3}$
10	0.01
11	0.02

Impulsive pressure coefficient as a function of dimensionless wall height

$$c_i(\eta_1) := 1 - con_0(\eta_1) - con_1(\eta_1) - con_2(\eta_1)$$

Eqn. 4.7 BNL 1995

$c_i(\eta_1) =$

	0
0	0.71
1	0.7
2	0.69
3	0.67
4	0.65
5	0.61
6	0.57
7	0.52
8	0.45
9	0.37
10	0.27
11	0.14

Prepared by: F. G. Abatt M&D Professional Services 8/31/05 Rev. 2	Theoretical Fluid Response for Simplified AY Flexible Wall Tank at 422 in. Waste Level	Checked by: B.G. Carpenter M&D Professional Services 2/1/06

Calculate maximum values of dynamic wall pressures from spectral acceleration of dome input TH.

Consider the first three convective modes

$SA_{c0} := 0.062 \cdot g$ $\quad SA_{c0} = 23.96 \frac{in}{sec^2}$

$SA_{c1} := 0.108 \cdot g$ $\quad SA_{c1} = 41.73 \frac{in}{sec^2}$ 0.5% Dome RS from Spectr - see Figure 2-21 of main report.

$SA_{c2} := 0.163 \cdot g$ $\quad SA_{c2} = 62.98 \frac{in}{sec^2}$

Determine the spectral acceleration for the impulsive mode.

$SA_i := 0.876 \cdot g$ $\quad SA_i = 338.49 \frac{in}{sec^2}$ 4% Dome RS from Spectr - see Figure 2-19 of main report.

$$p_{maxconv}(\eta_1, \theta) := \left[\sqrt{\left(con_0(\eta_1) \cdot SA_{c0}\right)^2 + \left(con_1(\eta_1) \cdot SA_{c1}\right)^2 + \left(con_2(\eta_1) \cdot SA_{c2}\right)^2}\right] \cdot \left(\rho_1 \cdot R \cdot \cos(\theta \cdot deg)\right)$$

$$p_{maximpulsive}(\eta_1, \theta) := \left[\sqrt{\left[c_i(\eta_1) \cdot \left(SA_i\right)\right]^2}\right] \cdot \left(\rho_1 \cdot R \cdot \cos(\theta \cdot deg)\right)$$

$$p_{max}(\eta_1, \theta) := \left[\sqrt{\left[\left(c_i(\eta_1)\right) \cdot \left(SA_i\right)\right]^2 + \left(con_0(\eta_1) \cdot SA_{c0}\right)^2 + \left(con_1(\eta_1) \cdot SA_{c1}\right)^2 + \left(con_2(\eta_1) \cdot SA_{c2}\right)^2}\right] \cdot \left(\rho_1 \cdot R \cdot \cos(\theta \cdot deg)\right)$$

Eqn. 4.24 BNL 1995

Prepared by: F. G. Abatt
M&D Professional Services
8/31/05
Rev. 2

Theoretical Fluid Response for Simplified AY Flexible Wall Tank at 422 in. Waste Level

Checked by: B.G. Carpenter
M&D Professional Services
2/1/06

$p_{maximpulsive}(\eta_1, 0) =$ $\frac{lbf}{in^2}$

	0
0	17.19
1	17.05
2	16.75
3	16.29
4	15.66
5	14.83
6	13.78
7	12.48
8	10.87
9	8.9
10	6.44
11	3.36

Maximum impulsive dynamic pressures at theta = 0.

$p_{maxconv}(\eta_1, 0) =$ $\frac{lbf}{in^2}$

	0
0	0.5
1	0.51
2	0.53
3	0.56
4	0.6
5	0.66
6	0.73
7	0.81
8	0.91
9	1.03
10	1.18
11	1.36

Maximum convective dynamic pressures at theta = 0.

$p_{max}(\eta_1, 0) =$ $\frac{lbf}{in^2}$

	0
0	17.2
1	17.06
2	16.76
3	16.3
4	15.67
5	14.84
6	13.8
7	12.51
8	10.91
9	8.96
10	6.55
11	3.62

Maximum total dynamic pressure at theta = 0.

Prepared by: F. G. Abatt
M&D Professional Services
8/31/05
Rev. 2

Theoretical Fluid Response for Simplified AY Flexible Wall Tank at 422 in. Waste Level

Checked by: B.G. Carpenter
M&D Professional Services
2/1/06

$p_{max}(\eta_l, 45) =$

	0
0	12.16
1	12.06
2	11.85
3	11.53
4	11.08
5	10.5
6	9.76
7	8.84
8	7.71
9	6.33
10	4.63
11	2.56

$\frac{lbf}{in^2}$

Maximum total dynamic pressure at theta = 45 degrees.

$p_{max}(\eta_l, 90) =$

	0
0	0
1	0
2	0
3	0
4	0
5	0
6	0
7	0
8	0
9	0
10	0
11	0

$\frac{lbf}{in^2}$

Maximum total dynamic pressure at theta = 90 degrees.

Calculate Maximum Slosh Height:

$$conmax := \begin{pmatrix} 0.837 \\ 0.073 \\ 0.028 \end{pmatrix}$$

Maximum value of convective coefficients at η_l=1

$$h_{maxslosh} := R \cdot \sqrt{\left(conmax_0 \cdot \frac{SA_{c0}}{g}\right)^2 + \left(conmax_1 \cdot \frac{SA_{c1}}{g}\right)^2 + \left(conmax_2 \cdot \frac{SA_{c2}}{g}\right)^2}$$

Eqn. 4.60 BNL 1995

$h_{maxslosh} = 23.71\,in$

Prepared by: F. G. Abatt
M&D Professional Services
8/31/05
Rev. 2

Theoretical Fluid Response for Simplified AY Flexible Wall Tank at 422 in. Waste Level

Checked by: B.G. Carpenter
M&D Professional Services
2/1/06

Calculate Maximum Total Hydrodynamic Force:

The maximum hydrodynamic force induced on the tank wall is given by Eqn. 4.31 of BNL 1995 with the instantaneous accelerations replaced by the maximum spectral accelerations. First determine the effective impulsive and convective masses.

$m_{lapprox} := \pi \cdot R^2 \cdot H_l \cdot \rho_l$ $\quad m_{lapprox} = 4.27 \times 10^4 \frac{lbf \cdot sec^2}{in}$ Total waste mass base on circular cylinder approximation.

$m_l := 4.23 \times 10^4 \cdot \frac{lbf \cdot sec^2}{in}$ Actual waste mass reported by Dytran model.

$$m_{c0} := \left[\frac{2}{\lambda_0 \cdot \left[\left(\lambda_0\right)^2 - 1\right] \cdot \left(\frac{H_l}{R}\right)}\right] \cdot \tanh\left[\lambda_0 \cdot \left(\frac{H_l}{R}\right)\right] \cdot m_l$$ First mode convective mass - Eqn. 4.32 BNL 1995

$m_{c0} = 1.93 \times 10^4 \frac{lbf \cdot sec^2}{in}$

$$m_{c1} := \left[\frac{2}{\lambda_1 \cdot \left[\left(\lambda_1\right)^2 - 1\right] \cdot \left(\frac{H_l}{R}\right)}\right] \cdot \tanh\left[\lambda_1 \cdot \left(\frac{H_l}{R}\right)\right] \cdot m_l$$ Second mode convective mass

$m_{c1} = 617.11 \frac{lbf \cdot sec^2}{in}$

$$m_{c2} := \left[\frac{2}{\lambda_2 \cdot \left[\left(\lambda_2\right)^2 - 1\right] \cdot \left(\frac{H_l}{R}\right)}\right] \cdot \tanh\left[\lambda_2 \cdot \left(\frac{H_l}{R}\right)\right] \cdot m_l$$ Third mode convective mass

$m_{c2} = 147.06 \frac{lbf \cdot sec^2}{in}$

$m_i := m_l - (m_{c0} + m_{c1} + m_{c2})$ Impulsive mass Eqn. 4.33 BNL 1995

$m_i = 2.23 \times 10^4 \frac{lbf \cdot sec^2}{in}$

Prepared by: F. G. Abatt
M&D Professional Services
8/31/05
Rev. 2

Theoretical Fluid Response for Simplified AY Flexible Wall Tank at 422 in. Waste Level

Checked by: B.G. Carpenter
M&D Professional Services
2/1/06

$F_{max} := m_i \cdot SA_i + m_{c0} \cdot SA_{c0} + m_{c1} \cdot SA_{c1} + m_{c2} \cdot SA_{c2}$ Eqn. 4.31 BNL 1995

$F_{max} = 8.04 \times 10^6 \text{ lbf}$ Conservative estimate of maximum hydrodynamic force

The above expression is a conservative estimate because it assumes that the peak impulsive and convective forces occur simultaneously. A less conservative estimate can be made via a square-root-sum-of-the-squares (SRSS) combination.

$F_{srss} := \sqrt{(m_i \cdot SA_i)^2 + (m_{c0} \cdot SA_{c0})^2 + (m_{c1} \cdot SA_{c1})^2 + (m_{c2} \cdot SA_{c2})^2}$ Eqn. 4.31 BNL 1995 - SRSS

$F_{srss} = 7.56 \times 10^6 \text{ lbf}$ SRSS estimate of peak hydrodynamic force

$F_{con} := \sqrt{(m_{c0} \cdot SA_{c0})^2 + (m_{c1} \cdot SA_{c1})^2 + (m_{c2} \cdot SA_{c2})^2}$

$F_{con} = 4.62 \times 10^5 \text{ lbf}$ Peak hydrodynamic force due to convective effects only

Consider Vertical Excitation:

Calculate the axisymmetric breathing mode frequency for the tank

$C_{vref} := 0.088$ Table 4.17 BNL 1995

$C_v := C_{vref} \cdot \sqrt{127 \cdot \frac{\left(\frac{t_{tw}}{R}\right)}{\left(\frac{\rho_l}{\rho_t}\right)}}$ $C_v = 0.081$

$f_v := \frac{1}{2 \cdot \pi} \cdot \frac{C_v}{H_l} \cdot \sqrt{\frac{E_t}{\rho_t}}$ $f_v = 6.07 \text{ Hz}$ Eqn. 4.53 BNL 1995

$S_{Av} := 0.53 \cdot g$ $S_{Av} = 204.79 \frac{\text{in}}{\text{sec}^2}$ Vert. Haunch 4 % RS from Spectr - see Figure 2-19 of main report.

The maximum dynamic wall pressure as a function of the dimensionless vertical distance is given by

$p_{maxv}(\eta_l) := (0.8) \cdot \left(\cos\left(\frac{\pi}{2} \cdot \eta_l\right)\right) \cdot (\rho_l \cdot H_l \cdot S_{Av})$ Eqn. 4.52 BNL 1995

Prepared by: F. G. Abatt
M&D Professional Services
8/31/05
Rev. 2

Theoretical Fluid Response for Simplified AY Flexible Wall Tank at 422 in. Waste Level

Checked by: B.G. Carpenter
M&D Professional Services
2/1/06

$p_{maxv}(\eta_l) =$

	0
0	10.98
1	10.8
2	10.44
3	9.89
4	9.18
5	8.3
6	7.28
7	6.14
8	4.89
9	3.56
10	2.16
11	0.72

$\frac{lbf}{in^2}$

$c_{oprimeouter} := 0.28$ $c_{oprimecenter} := 0.54$ Estimated from Figure 4.7 BNL 1995

$c_{vprimeouter} := 0.72$ $c_{vprimecenter} := 0.46$

$PGA_{vert} := 0.12 \cdot g$ Figure 2-16 of main report.

The maximum base pressures at the outer and center elements are given by

$p_{maxbasevertouter} := c_{oprimeouter} \cdot \rho_l \cdot H_l \cdot PGA_{vert} + c_{vprimeouter} \cdot (\rho_l \cdot H_l) \cdot S_{Av}$ Eqn. 4.55 BNL 1995

$p_{maxbasevertcenter} := c_{oprimecenter} \cdot \rho_l \cdot H_l \cdot PGA_{vert} + c_{vprimecenter} \cdot (\rho_l \cdot H_l) \cdot S_{Av}$

$p_{maxbasevertouter} = 10.76 \frac{lbf}{in^2}$

$p_{maxbasevertcenter} = 8 \frac{lbf}{in^2}$

Determine the maximum vertical force on the base

$m_0 := 0.402 \cdot m_l$ Component of waste mass particpating in the motion of the tank base

$m_v := 0.598 \cdot m_l$ Component of waste mass particpating in the motion of the tank wall

BNL Table 4.17

$$F_{maxbasevert} := \sqrt{\left(m_0 \cdot PGA_{vert}\right)^2 + \left(m_v \cdot S_{Av}\right)^2}$$

Eqn. 4.57 BNL 1995 modified for maximum response per p. 4-34

$$F_{maxbasevert} = 5.24 \times 10^6 \text{ lbf}$$

$$m_0 = 1.7 \times 10^4 \text{ lbf} \cdot \frac{\text{sec}^2}{\text{in}}$$

$$m_v = 2.53 \times 10^4 \text{ lbf} \cdot \frac{\text{sec}^2}{\text{in}}$$

Reference:

BNL 1995, *Seismic Design and Evaluation Guidelines for the Department of Energy High-Level Waste Storage Tanks and Appurtenances*, BNL 52361, Rev. 10/95, Brookhaven National Laboratory, Upton, New York.

Prepared by: F. G. Abatt
M&D Professional Services
10/05/05
Rev. 2

Theoretical Fluid Response for Simplified AY Flexible Wall Tank at 460 in. Waste Level - Dytran Configuration

Checked by: B.G. Carpenter
M&D Professional Services
2/1/06

$H_l := 460 \cdot in$ Baseline waste level

$H_t := 460 \cdot in$ Height to primary tank tangent line

$\frac{H_l}{H_t} = 1$ Ratio of waste height to tank height

$g := 386.4 \cdot \frac{in}{sec^2}$

$R := 450 \cdot in$ Tank radius

$\frac{H_l}{R} = 1.02$ Ratio of waste height to tank radius

$i := 0..2$

$\lambda := \begin{pmatrix} 1.841 \\ 5.331 \\ 8.536 \end{pmatrix}$ Bessel function roots

$\theta := \begin{pmatrix} 0 \cdot deg \\ 45 \cdot deg \\ 90 \cdot deg \end{pmatrix}$ Circumferential location of waste elements for which pressures are reported

Convective Frequencies

$fcon_i := \frac{1}{2 \cdot \pi} \cdot \left[\sqrt{\left[\lambda_i \left[\frac{g}{R} \cdot \tanh\left[\lambda_i \cdot \left(\frac{H_l}{R} \right) \right] \right] \right]} \right]$ Eqn. 4.14 BNL 1995

$fcon = \begin{pmatrix} 0.2 \\ 0.34 \\ 0.43 \end{pmatrix} Hz$ First three convective frequencies

$\rho_l := 1.71 \cdot 10^{-4} \cdot \frac{lbf \cdot sec^2}{in^4}$ waste density - specific gravity = 1.83

Prepared by: F. G. Abatt
M&D Professional Services
10/05/05
Rev. 2

Checked by: B.G. Carpenter
M&D Professional Services
2/1/06

Calculation of Impulsive Frequency:

$\rho_t := 7.35 \cdot 10^{-4} \cdot \frac{lbf \cdot sec^2}{in^4}$ Steel density

$t_{tw} := 0.65 \cdot in$ Average thickness of AY over lower 2/3.

$E_t := 29 \cdot 10^6 \cdot \frac{lbf}{in^2}$ Elastic modulus for steel

$C_{iref} := 0.1062$ Table 4.4 of BNL 1995

$C_i := C_{iref} \cdot \sqrt{127 \cdot \frac{\left(\frac{t_{tw}}{R}\right)}{\left(\frac{\rho_l}{\rho_t}\right)}}$ Eqn. 4.18 BNL 1995

$C_i = 0.09$ Impulsive coefficient for frequency calculation

$f_i := \frac{1}{2 \cdot \pi} \cdot \frac{C_i}{H_l} \cdot \sqrt{\frac{E_t}{\rho_t}}$ $f_i = 6.48 Hz$ Eqn. 4.16 BNL 1995

Determine Convective Pressures on the Tank Wall:

$$z := \begin{pmatrix} 15.1 \cdot in \\ 50.5 \cdot in \\ 85.8 \cdot in \\ 121.2 \cdot in \\ 156.6 \cdot in \\ 192 \cdot in \\ 227.4 \cdot in \\ 262.8 \cdot in \\ 298.2 \cdot in \\ 333.5 \cdot in \\ 368.9 \cdot in \\ 404.3 \cdot in \\ 441 \cdot in \end{pmatrix}$$

Vertical location of Euler element centroids at which pressures are reported.

Prepared by: F. G. Abatt
M&D Professional Services
10/05/05
Rev. 2

Theoretical Fluid Response for Simplified AY Flexible Wall Tank at 460 in. Waste Level - Dytran Configuration

Checked by: B.G. Carpenter
M&D Professional Services
2/1/06

$\eta_l := \frac{z}{H_l}$ Ratio of tank wall vertical location to waste height for waste element centroids.

$\eta_l =$

	0
0	0.03
1	0.11
2	0.19
3	0.26
4	0.34
5	0.42
6	0.49
7	0.57
8	0.65
9	0.73
10	0.8
11	0.88
12	0.96

Determine convective coefficients as a function of dimensionless height per BNL 1995 Eqn. 4.4

$$con_0(\eta_l) := \left[\frac{2}{\left(\lambda_{0,}\right)^2 - 1} \cdot \frac{\cosh\left[\lambda_0 \cdot \left(\frac{H_l}{R}\right) \cdot \eta_l\right]}{\cosh\left[\lambda_0 \cdot \left(\frac{H_l}{R}\right)\right]} \right]$$

$$con_1(\eta_l) := \left[\frac{2}{\left(\lambda_{1,}\right)^2 - 1} \cdot \frac{\cosh\left[\lambda_1 \cdot \left(\frac{H_l}{R}\right) \cdot \eta_l\right]}{\cosh\left[\lambda_1 \cdot \left(\frac{H_l}{R}\right)\right]} \right]$$

$$con_2(\eta_l) := \left[\frac{2}{\left(\lambda_{2,}\right)^2 - 1} \cdot \frac{\cosh\left[\lambda_2 \cdot \left(\frac{H_l}{R}\right) \cdot \eta_l\right]}{\cosh\left[\lambda_2 \cdot \left(\frac{H_l}{R}\right)\right]} \right]$$

Prepared by: F. G. Abatt
M&D Professional Services
10/05/05
Rev. 2

Theoretical Fluid Response for Simplified AY Flexible Wall Tank at 460 in. Waste Level - Dytran Configuration

Checked by: B.G. Carpenter
M&D Professional Services
2/1/06

$con_0(\eta_1) =$

	0
0	0.25
1	0.25
2	0.26
3	0.28
4	0.3
5	0.33
6	0.37
7	0.41
8	0.46
9	0.52
10	0.59
11	0.68
12	0.78

$con_1(\eta_1) =$

	0
0	$6.37 \cdot 10^{-4}$
1	$7.43 \cdot 10^{-4}$
2	$9.8 \cdot 10^{-4}$
3	$1.39 \cdot 10^{-3}$
4	$2.05 \cdot 10^{-3}$
5	$3.08 \cdot 10^{-3}$
6	$4.66 \cdot 10^{-3}$
7	$7.07 \cdot 10^{-3}$
8	0.01
9	0.02
10	0.02
11	0.04
12	0.06

$con_2(\eta_1) =$

	0
0	$9.41 \cdot 10^{-6}$
1	$1.35 \cdot 10^{-5}$
2	$2.39 \cdot 10^{-5}$
3	$4.55 \cdot 10^{-5}$
4	$8.84 \cdot 10^{-5}$
5	$1.73 \cdot 10^{-4}$
6	$3.38 \cdot 10^{-4}$
7	$6.61 \cdot 10^{-4}$
8	$1.29 \cdot 10^{-3}$
9	$2.53 \cdot 10^{-3}$
10	$4.94 \cdot 10^{-3}$
11	$9.68 \cdot 10^{-3}$
12	0.02

Impulsive pressure coefficient as a function of dimensionless wall height

$$c_i(\eta_1) := 1 - con_0(\eta_1) - con_1(\eta_1) - con_2(\eta_1)$$

Eqn. 4.7 BNL 1995

$c_i(\eta_1) =$

	0
0	0.75
1	0.74
2	0.73
3	0.72
4	0.7
5	0.67
6	0.63
7	0.58
8	0.53
9	0.46
10	0.38
11	0.28
12	0.14

Prepared by: F. G. Abatt M&D Professional Services 10/05/05 Rev. 2	Theoretical Fluid Response for Simplified AY Flexible Wall Tank at 460 in. Waste Level - Dytran Configuration	Checked by: B.G. Carpenter M&D Professional Services 2/1/06

Calculate maximum values of dynamic wall pressures from spectral acceleration of dome input TH.

Consider the first three convective modes

$SA_{c0} := 0.064 \cdot g$ $\quad SA_{c0} = 24.73 \frac{in}{sec^2}$

$SA_{c1} := 0.108 \cdot g$ $\quad SA_{c1} = 41.73 \frac{in}{sec^2}$ 0.5% Dome RS from Spectr - see Figure 2-21 of main report.

$SA_{c2} := 0.163 \cdot g$ $\quad SA_{c2} = 62.98 \frac{in}{sec^2}$

Determine the spectral acceleration for the impulsive mode.

$SA_i := 0.967 \cdot g$ $\quad SA_i = 373.65 \frac{in}{sec^2}$ 4% Dome RS from Spectr - see Figure 2-19 of main report.

$$p_{maxconv}(\eta_l, \theta) := \left[\sqrt{\left(con_0(\eta_l) \cdot SA_{c0}\right)^2 + \left(con_1(\eta_l) \cdot SA_{c1}\right)^2 + \left(con_2(\eta_l) \cdot SA_{c2}\right)^2}\right] \cdot \left(\rho_l \cdot R \cdot \cos(\theta \cdot deg)\right)$$

$$p_{maximpulsive}(\eta_l, \theta) := \left[\sqrt{\left[c_i(\eta_l) \cdot \left(SA_i\right)\right]^2}\right] \cdot \left(\rho_l \cdot R \cdot \cos(\theta \cdot deg)\right)$$

$$p_{max}(\eta_l, \theta) := \left[\sqrt{\left[\left(c_i(\eta_l)\right) \cdot \left(SA_i\right)\right]^2 + \left(con_0(\eta_l) \cdot SA_{c0}\right)^2 + \left(con_1(\eta_l) \cdot SA_{c1}\right)^2 + \left(con_2(\eta_l) \cdot SA_{c2}\right)^2}\right] \cdot \left(\rho_l \cdot R \cdot \cos(\theta \cdot deg)\right)$$

Eqn. 4.24 BNL 1995

Prepared by: F. G. Abatt
M&D Professional Services
10/05/05
Rev. 2

Theoretical Fluid Response for Simplified AY Flexible Wall Tank at 460 in. Waste Level - Dytran Configuration

Checked by: B.G. Carpenter
M&D Professional Services
2/1/06

$p_{maximpulsive}(\eta_1, 0) =$ $\frac{lbf}{in^2}$

	0
0	21.56
1	21.41
2	21.11
3	20.65
4	20
5	19.17
6	18.11
7	16.81
8	15.21
9	13.28
10	10.9
11	7.98
12	4.17

Maximum impulsive dynamic pressures at theta = 0.

$p_{maxconv}(\eta_1, 0) =$ $\frac{lbf}{in^2}$

	0
0	0.48
1	0.48
2	0.5
3	0.53
4	0.57
5	0.63
6	0.69
7	0.78
8	0.87
9	0.99
10	1.13
11	1.29
12	1.49

Maximum convective dynamic pressures at theta = 0.

$p_{max}(\eta_1, 0) =$ $\frac{lbf}{in^2}$

	0
0	21.56
1	21.42
2	21.12
3	20.65
4	20.01
5	19.18
6	18.13
7	16.83
8	15.24
9	13.31
10	10.96
11	8.08
12	4.43

Maximum total dynamic pressure at theta = 0.

Prepared by: F. G. Abatt
M&D Professional Services
10/05/05
Rev. 2

Theoretical Fluid Response for Simplified AY Flexible Wall Tank at 460 in. Waste Level - Dytran Configuration

Checked by: B.G. Carpenter
M&D Professional Services
2/1/06

$p_{max}(\eta_1, 45) =$ (lbf/in^2)

	0
0	15.25
1	15.14
2	14.93
3	14.6
4	14.15
5	13.56
6	12.82
7	11.9
8	10.78
9	9.41
10	7.75
11	5.71
12	3.13

Maximum total dynamic pressure at theta = 45 degrees.

$p_{max}(\eta_1, 90) =$ (lbf/in^2)

	0
0	0
1	0
2	0
3	0
4	0
5	0
6	0
7	0
8	0
9	0
10	0
11	0
12	0

Maximum total dynamic pressure at theta = 90 degrees.

Calculate Maximum Slosh Height:

$$conmax := \begin{pmatrix} 0.837 \\ 0.073 \\ 0.028 \end{pmatrix}$$

Maximum value of convective coefficients at η_l=1

$$h_{maxslosh} := R \cdot \sqrt{\left(conmax_0 \cdot \frac{SA_{c0}}{g}\right)^2 + \left(conmax_1 \cdot \frac{SA_{c1}}{g}\right)^2 + \left(conmax_2 \cdot \frac{SA_{c2}}{g}\right)^2}$$

Eqn. 4.60 BNL 1995

$h_{maxslosh} = 24.45\,in$

Prepared by: F. G. Abatt
M&D Professional Services
10/05/05
Rev. 2

Theoretical Fluid Response for Simplified AY Flexible Wall Tank at 460 in. Waste Level - Dytran Configuration

Checked by: B.G. Carpenter
M&D Professional Services
2/1/06

Calculate Maximum Total Hydrodynamic Force:

The maximum hydrodynamic force induced on the tank wall is given by Eqn. 4.31 of BNL 1995 with the instantaneous accelerations replaced by the maximum spectral accelerations. First determine the effective impulsive and convective masses.

$m_{lapprox} := \pi \cdot R^2 \cdot H_l \cdot \rho_l$ $\quad m_{lapprox} = 5 \times 10^4 \frac{lbf \cdot sec^2}{in}$ Total waste mass base on circular cylinder approximation.

$m_l := 4.95 \times 10^4 \cdot \frac{lbf \cdot sec^2}{in}$ Actual waste mass reported by Dytran model.

$m_{c0} := \left[\frac{2}{\lambda_0 \cdot \left[\left(\lambda_0\right)^2 - 1\right] \cdot \left(\frac{H_l}{R}\right)}\right] \cdot \tanh\left[\lambda_0 \cdot \left(\frac{H_l}{R}\right)\right] \cdot m_l$ First mode convective mass - Eqn. 4.32 BNL 1995

$m_{c0} = 2.1 \times 10^4 \frac{lbf \cdot sec^2}{in}$

$m_{c1} := \left[\frac{2}{\lambda_1 \cdot \left[\left(\lambda_1\right)^2 - 1\right] \cdot \left(\frac{H_l}{R}\right)}\right] \cdot \tanh\left[\lambda_1 \cdot \left(\frac{H_l}{R}\right)\right] \cdot m_l$ Second mode convective mass

$m_{c1} = 662.53 \frac{lbf \cdot sec^2}{in}$

$m_{c2} := \left[\frac{2}{\lambda_2 \cdot \left[\left(\lambda_2\right)^2 - 1\right] \cdot \left(\frac{H_l}{R}\right)}\right] \cdot \tanh\left[\lambda_2 \cdot \left(\frac{H_l}{R}\right)\right] \cdot m_l$ Third mode convective mass

$m_{c2} = 157.88 \frac{lbf \cdot sec^2}{in}$

$m_i := m_l - \left(m_{c0} + m_{c1} + m_{c2}\right)$ Impulsive mass - Eqn. 4.33 BNL 1995

$m_i = 2.77 \times 10^4 \frac{lbf \cdot sec^2}{in}$

$F_{max} := m_i \cdot SA_i + m_{c0} \cdot SA_{c0} + m_{c1} \cdot SA_{c1} + m_{c2} \cdot SA_{c2}$ Eqn. 4.31 BNL 1995

$F_{max} = 1.09 \times 10^7 \text{ lbf}$ Conservative estimate of maximum hydrodynamic force

The above expression is a conservative estimate because it assumes that the peak impulsive and convective forces occur simultaneously. A less conservative estimate can be made via a square-root-sum-of-the-squares (SRSS) combination.

$F_{srss} := \sqrt{(m_i \cdot SA_i)^2 + (m_{c0} \cdot SA_{c0})^2 + (m_{c1} \cdot SA_{c1})^2 + (m_{c2} \cdot SA_{c2})^2}$ Eqn. 4.31 BNL 1995 - SRSS

$F_{srss} = 1.03 \times 10^7 \text{ lbf}$ SRSS estimate of peak hydrodynamic force

$F_{con} := \sqrt{(m_{c0} \cdot SA_{c0})^2 + (m_{c1} \cdot SA_{c1})^2 + (m_{c2} \cdot SA_{c2})^2}$

$F_{con} = 5.21 \times 10^5 \text{ lbf}$ Peak hydrodynamic force due to convective effects only

Consider Vertical Excitation:

Calculate the axisymmetric breathing mode frequency for the tank

$C_{vref} := 0.089$ Table 4.17 BNL 1995

$C_v := C_{vref} \cdot \sqrt{127 \cdot \frac{\left(\frac{t_{tw}}{R}\right)}{\left(\frac{\rho_l}{\rho_t}\right)}}$ $C_v = 0.079$ Eqn. 4.16 BNL 1995

$f_v := \frac{1}{2 \cdot \pi} \cdot \frac{C_v}{H_l} \cdot \sqrt{\frac{E_t}{\rho_t}}$ $f_v = 5.43 \text{ Hz}$ Eqn. 4.53 BNL 1995

$S_{Av} := 0.38 \cdot g$ $S_{Av} = 146.83 \frac{\text{in}}{\text{sec}^2}$ Vert. Haunch 4 % RS from Spectr - see Figure 2-19 of main report.

The maximum dynamic wall pressure as a function of the dimensionless vertical distance is given by

$p_{maxv}(\eta_l) := (0.8) \cdot \left(\cos\left(\frac{\pi}{2} \cdot \eta_l\right)\right) \cdot (\rho_l \cdot H_l \cdot S_{Av})$ Eqn. 4.52 BNL 1995

Prepared by: F. G. Abatt
M&D Professional Services
10/05/05
Rev. 2

Theoretical Fluid Response for Simplified AY Flexible Wall Tank at 460 in. Waste Level - Dytran Configuration

Checked by: B.G. Carpenter
M&D Professional Services
2/1/06

$p_{maxv}(\eta_l) =$

	0
0	9.23
1	9.1
2	8.85
3	8.46
4	7.95
5	7.32
6	6.59
7	5.76
8	4.85
9	3.87
10	2.83
11	1.75
12	0.6

$\frac{lbf}{in^2}$

$c_{oprimeouter} := 0.28$ $c_{oprimecenter} := 0.54$ Estimated from Figure 4.7 BNL 1995

$c_{vprimeouter} := 0.72$ $c_{vprimecenter} := 0.46$

$PGA_{vert} := 0.12 \cdot g$ Figure 2-16 of main report

The maximum base pressures at the outer and center elements are given by

$p_{maxbasevertouter} := c_{oprimeouter} \cdot \rho_l \cdot H_l \cdot PGA_{vert} + c_{vprimeouter} \cdot (\rho_l \cdot H_l) \cdot S_{Av}$ Eqn. 4.55 BNL 1995

$p_{maxbasevertcenter} := c_{oprimecenter} \cdot \rho_l \cdot H_l \cdot PGA_{vert} + c_{vprimecenter} \cdot (\rho_l \cdot H_l) \cdot S_{Av}$

$p_{maxbasevertouter} = 9.34 \frac{lbf}{in^2}$

$p_{maxbasevertcenter} = 7.28 \frac{lbf}{in^2}$

Determine the maximum vertical force on the base

$m_0 := 0.388 \cdot m_l$ Component of waste mass particpating in the motion of the tank base

$m_v := 0.612 \cdot m_l$ Component of waste mass particpating in the motion of the tank wall

BNL Table 4.17

Prepared by: F. G. Abatt
M&D Professional Services
10/05/05
Rev. 2

Theoretical Fluid Response for Simplified AY Flexible Wall Tank at 460 in. Waste Level - Dytran Configuration

Checked by: B.G. Carpenter
M&D Professional Services
2/1/06

$$F_{maxbasevert} := \sqrt{\left(m_0 \cdot PGA_{vert}\right)^2 + \left(m_v \cdot S_{Av}\right)^2}$$

Eqn. 4.57 BNL 1995 modified for maximum response per p. 4-34

$$F_{maxbasevert} = 4.54 \times 10^6 \text{ lbf}$$

$$m_0 = 1.92 \times 10^4 \text{ lbf} \cdot \frac{\text{sec}^2}{\text{in}}$$

$$m_v = 3.03 \times 10^4 \text{ lbf} \cdot \frac{\text{sec}^2}{\text{in}}$$

Reference:

BNL 1995, *Seismic Design and Evaluation Guidelines for the Department of Energy High-Level Waste Storage Tanks and Appurtenances*, BNL 52361, Rev. 10/95, Brookhaven National Laboratory, Upton, New York.